Genetic regulation of secretory granule and exosome biogenesis within *Drosophila* secondary cells

Adam Wells

Wolfson College

University of Oxford

Hilary Term 2024

DPhil in Physiology, Anatomy and Genetics

Supervisor: Clive Wilson

Department of Physiology, Anatomy and Genetics

i: Declaration

The thesis I am submitting is entirely my own work except where otherwise indicated in the text.

ii: Acknowledgements

First of all, I would like to thank my supervisor, Professor Clive Wilson, who has always been proactive, accessible and enthusiastic, and has shared his time with me freely whenever I needed help. I am grateful to have been a part of his laboratory and for the enormous amount I have learnt regarding every aspect of being a researcher.

I would also like to thank the other members of the Wilson laboratory, past and present. In particular, I would like to thank Dr. Pauline Marie, Dr Claudia Mendes and Dr. Preman Singh, all past lab members who were exceptionally helpful and kind and whose previous work I have relied on to carry out my research. Additionally, I would like to thank Dr Mark Wainwright for his wealth of *Drosophila* knowledge. I similarly extend my gratitude to all lab members and collaborators whose work has assisted the results in this thesis and any other publication I am included in. I am also grateful to the staff at Micron, particularly Dr Deirdre Kavanagh, Dr Niloufer Irani who trained me in the theory and practice of microscopy and have always been extremely helpful in any situation. Many thanks also to my sponsors, the Biochemical Society, for their generous financial support and to my mum who may or may not read this but has always been extremely supportive.

I would also like to thank the friends I have met during my PhD including soon to be doctors, Frederik, Madhu, Jason and Samuel. Also, Emma, Sekoah and many others, I am glad to have spent the last three years with you all. Likewise, to my closest friends from before coming to Oxford, James, Cat, Steven, Finn, Eve, Nelly, Owain, Matthew, thank you. Finally, to my partner Emiry, you're the best.

iii: Abstract

Secretory pathways are an essential feature of cell-cell signalling processes, yet many fundamental questions remain unanswered concerning the regulatory mechanisms controlling the biogenesis and maturation of the small secretory compartments generated in most cells. During my thesis work, I have studied the formation of two structures in secretory compartments with important, wide-spread functions in cell signalling, namely secretory granules and exosomes. Secretory granules, also known as dense core granules (DCGs), are insoluble stores of secretory proteins in the regulated secretory pathway. Prominent examples include insulin granules and neuropeptide granules. Exosomes meanwhile are a class of extracellular vesicles (EVs) that form within endosomal compartments, including some that make DCGs. These vesicles take part in a diverse array of signalling events including many linked to cancer, immunity and stress-related pathways. To conduct my research, I utilised the prostate-like secondary cells (SCs) of *Drosophila* accessory glands which represent a novel *in vivo*, secretory epithelial model. SCs possess giant secretory compartments that are labelled by the recycling endosomal marker and small monomeric GTPase Rab11. Importantly, these Rab11-compartments produce both exosomes and DCGs. Alongside the abundant genetic tools available in *Drosophila*, SCs therefore provide an outstanding model for live cell and real-time microscope-based studies of exosome, DCG and secretory compartment biogenesis.

Using new time-lapse imaging techniques that I developed in SCs, I identify a number of changes in Rab labelling occurring on maturing secretory compartments, including a novel Rab6 to Rab11 transition. I also acquire the first views of DCG formation occurring in real time, a process that directly informs our understanding of DCG protein aggregation within secretory compartments. Using SC-specific RNAi expression, I confirm that SC DCGs are controlled by conserved regulators identified in mammals, and by the novel Rab6 to Rab11 transition, which also regulates exosome biogenesis. Building on known links to defective regulated secretion in neurodegenerative disease, I use time-lapse imaging to investigate the effects of neurodegeneration-linked genes on DCG biogenesis mechanisms. Following knockdown of homologues of genes encoding proteins such as the glycolytic enzyme GAPDH2, the extracellular chaperone

HSP90AA1, and Alzheimer's disease- (AD-)associated Amyloid Precursor Protein (APP), or after overexpression of Aβ-42 amyloid mutants, I find that DCG biogenesis mechanisms are interrupted, resulting in defective DCG aggregation and aberrant compartment maturation.

Focusing on Rab11-exosomes, an exosome subtype formed within Rab11-compartments of SCs, which has also been identified in EVs from human cancer cells, I identify several new regulatory mechanisms. Of particular significance, I identify novel exosome-forming, membrane-associated microdomains on the limiting membrane of Rab11-compartments that are E-cadherin/Rab11/Rab19-positive and which recruit members of the essential exosome-forming ESCRT-complex. Further research identifies factors such as the lipid-raft-associated protein Prohibitin 2 (Phb2), the class III PI3-kinase Vps34, and the PI3K/Akt/mTOR pathway as essential regulators of both Rab11-exosome formation and E-cadherin-positive lipid microdomain (ELM) assembly. In addition, inhibition of the Rab11-interacting exocyst complex results in impaired Rab11-compartment secretion and apparently reduced Rab11-exosome formation.

Finally, through knockdown of the ubiquitin-like molecule SUMO and its associated factors, I find evidence that this post-translational modification controls both Rab11-exosome and ELM biogenesis. By examining homologues of SUMO-targeted human Rab11a-exosome proteins, I identify several novel regulators of Rab11-exosome formation, at least one of which, Arc1, an RNA-binding protein, is strongly implicated in AD. Some SUMO-targeted regulators also disrupt DCG biogenesis. I develop a model to explain the connections between ELMs, Rab11-exosomes and DCGs. This model provides a platform for further studies of (i) the potential role of SUMO as a subtype-specific tag for Rab11-exosome cargos at ELMs, (ii) Rab11-exosome biogenesis and function, and (iii) the link between Rab11-exosomes, DCGs and neurodegenerative disease.

iv: List of abbreviations

Abbreviation	*Full reference*
Aβ	Amyloid β-protein
AD	Alzheimer's disease
Alix	ALG-2 interacting protein X
AP-1	Adaptor protein-1
APP	Amyloid-precursor protein
APPL	Amyloid-precursor protein like
Arf	ADP ribosylation factor
Bet3	Blocked early in transport 3
BMP	Bone-morphogenetic protein
CFP	Cyan fluorescent protein
CHGA/B	Chromogranin A/B
Chmp	charged multivesicular body protein
DCG	Dense core granules
dsx	double-sex
Ecad	E-cadherin
EE	Early endosome
ELM	E-cadherin-positive lipid microdomain
ESCRT	Endosomal sorting complex required for transport
esg	escargot
Exo	Exocyst
Flo1/2	Flotillin-1/2
GAPDH2	Glyceraldehyde 3-phosphate dehydrogenase 2
GEF	Guanine nucleotide exchange factor
GFP	Green fluorescent protein
Hrs	Hepatocyte receptor tyrosine kinase substrate
ILV	Intraluminal vesicles
LE	Late endosome
M6P-R	Mannose 6-phosphate receptor

MFAS	Midline fasciclin
MVE	Multivesicular endosome
PC	Prohormone convertase
Phb1/2	Prohibitin-1/2
PI3K	Phosphatidylinositol 3-kinase
PI3P	Phosphatidylinositol 3-phosphate
PIP2	Phosphatidylinositol 4,5-bisphosphate
PIP3	Phosphatidylinositol 3,4,5-triphosphate
PLD	Phospholipase D
Rab	Ras-associated binding
Rab11-FIP	Rab11-family interacting protein
RE	Recycling endosome
RFP	Red fluorescent protein
Sec	Secretory
SNX	Sorting-nexin
SPFH	Stomatin/prohibitin/flotillin/HflK/C
StomL2	Stomatin-Like-2
SUMO	Small Ubiquitin-Like Modifier
TGFBI	Transforming growth factor-beta-induced
TGN	*Trans*-Golgi network
Vps	Vacuolar protein sorting
YFP	Yellow fluorescent protein

v: Table of Contents

Contents

Chapter 1: Introduction and Literature Review

1.1 Introduction

Cell-cell communication is a foundational component of all complex life, allowing cells to detect and respond to changes in their environment. Signalling within and between cells is essential for the proper functioning of physiological processes and in the absence of appropriate signalling pathways, biological processes rapidly become dysregulated. The consequences of such dysregulation can be seen in diseases such as cancers, diabetes, autoimmune conditions and neurodegenerative illnesses which can at some level be viewed as cell-signalling disorders affecting cell growth/survival, hormone signalling, immune activation and homeostatic processes respectively. Cell signalling therefore represents an essential feature of both regular physiology and disease.

Unsurprisingly then, prominent signalling pathways such as the insulin signalling or adrenaline signalling pathways are exceptionally well-studied biology (Chhatar & Lal, 2021; Le et al., 2023), with detailed research produced on all aspects of their biology from the biochemical structures of key molecules to their interactions with other signalling pathways and disease states. However, an often-understudied area of cell-cell signalling pathways is the sorting and packaging of signalling molecules within cells prior to secretion. Secreted signalling factors undergo numerous, stringently regulated steps prior to their secretion which can include quality control steps (Sun &

Brodsky, 2019), proteolytic maturation (Seidah et al., 2013), and numerous forms of packaging into appropriate vesicles or other structures (Campelo et al., 2023; Dixson et al., 2023; Xie et al., 2022). Intracellular regulatory processes add additional layers of complexity to cell signalling pathways and can fundamentally alter the dynamics of signalling molecules, yet they are often among the least well understood aspect of signalling cascades.

I therefore became interested in two prominent examples of intracellular packaging that have immense impacts on cell-cell signalling dynamics and are poorly understood in terms of both mechanisms and regulation. The first was secretory granules, which form as part of the regulated secretory pathway and facilitate the coordinated release of large numbers of signalling molecules. The second was exosomes, a class of extracellular vesicle which forms intracellularly and concentrates specific cargoes into its membrane and lumen.

Secretory granules, otherwise known as dense core granules (DCGs), are an important mechanism for coordinating the release of signalling proteins such as hormones and neuropeptides (Mironov & Arvan, 2008; Russo, 2017; Vazquez-Martinez & Gasman, 2014). In essence, DCGs allow newly synthesised signalling molecules to be stored inertly within a proteinaceous granule inside intracellular, membrane-bound compartments until external stimuli cause that compartment to fuse with the plasma membrane. At this point, granules are thought to dissipate, leading to the release of the individual signalling proteins it is comprised from. DCGs are an integral part of the regulated secretory pathway and contribute to key signalling pathways through the

formation of structures such as insulin granules, chromaffin granules and neuropeptide granules.

By contrast, exosomes are a specialised class of extracellular vesicles that are formed by the inward budding of membranes on intracellular endosomes (Krylova & Feng, 2023; Xie et al., 2022). Crucially, exosomes incorporate thousands of different molecules within their lumen and membrane which, following secretion, allows exosomes to induce complex signalling changes by either interacting with cell-surface receptors or by having their cargoes internalised by cells, typically through endocytosis (Arya et al., 2024). Exosomes are produced by a wide variety of cell types, but current research highlights their role in immune cells, cancer cells and neuronal cells.

Despite the very different nature of DCGs and exosomes, they do share several important qualities. Firstly, both are general signalling structures that are widely utilised and not pathway-specific. Secondly, both are formed within intracellular, membrane-bound compartments and then released in response to external signalling stimuli. And finally, largely because of their origins within intracellular compartments, the formation of both DCGs and exosomes remain poorly documented. Fundamentally, this is because small vesicular structures such as endosomes and secretory compartments cannot be visualised effectively using light microscopy and because specific compartment/vesicle populations cannot be easily isolated from each other. Accordingly, only a limited number of methodologies such as electron microscopy can be used to routinely address questions about the processes occurring inside of compartments.

Therefore, within my PhD I sought to expand our understanding of the basic biology underpinning DCG and exosome biogenesis. To do this, I utilised a novel experimental model within the secondary cells of male *Drosophila* accessory glands that allows for more flexible study of DCGs, exosomes and the secretory compartments they form within. The key feature of *Drosophila* secondary cells that makes this possible is the presence of naturally occurring giant secretory compartments that are thousands of times larger in volume than the secretory compartments of most other *in vivo* cell types. As a result, although biochemical analyses remain impractical, fluorescence microscopy becomes a uniquely viable approach for studying the internal processes occurring within compartments. Of particular interest for my work, secondary cells contain giant Rab11-positive compartments that appear analogous to REs and which form both DCGs and exosomes within their lumen. I therefore used *Drosophila* SCs as a novel model for studying the formation and regulation of DCGs, exosomes and secretory compartments. Before examining the results of my research however, it is important to first review the most current literature that exists regarding each of DCG, exosome and secretory biology

1.2 The regulated secretory pathway and DCGs

1.2.1 Regulated secretion

Eukaryotic cells feature both a constitutive and regulated secretory system. Both systems transport materials from the *trans*-Golgi network (TGN) directly to the plasma membrane but the constitutive secretory pathway does so mostly independently of

most external stimuli whilst the regulated secretory pathway acts in a more tightly regulated manner, dependent on external signalling (Mironov & Arvan, 2008; Ponnambalam & Baldwin, 2003; Stalder & Gershlick, 2020). As a result, materials in the regulated secretory pathway are often retained in cells for long period before being secreted and so must be stored in insoluble secretory granules, also known as dense core granules (DCGs), whilst within cells.

1.2.2 DCG biology

1.2.2.1 Overview of DCGs

First identified through electron microscopy in the 1950s (Siekevitz & Palade, 1958a, 1958b, 1958c), DCGs are a hallmark of the regulated secretory pathway in animals. Fundamentally, DCGs allow soluble proteins to condense into reversible, non-aqueous structures within the confines of a membrane-bound compartment. This condensation enables cells to overcome the osmolarity constraints which would otherwise prevent the packaging of so many soluble proteins into small secretory compartments. DCGs such as insulin granules or neuropeptide granules are therefore an indispensable feature of signalling pathways that require timely or coordinated secretion under specific conditions. Although numerous DCG-dependent signalling cascades have been extensively researched, the study of DCGs within cells has been more limited (Bowman et al., 2009; Campelo et al., 2023; Tanguy et al., 2016). I will therefore review intracellular DCG biology, with a focus on biogenesis mechanisms.

1.2.2.2 DCG cargoes

One fundamental aspect of DCG biology is the protein cargoes that comprise them. Like other secreted factors, DCG cargoes initially form in the ER lumen and are trafficked to the Golgi following folding, glycosylation and quality control steps. Several conserved families of DCG cargoes exist and cargoes often share important qualities that are essential for the process of DCG biogenesis.

One of the most important families of DCG cargo are granins, a conserved family of granule-targeted proteins that make up an essential part of the DCG matrix (Bartolomucci et al., 2011; Huttner et al., 1991) . Insulin granules for example contain no less than five granin family members (Germanos et al., 2021). Interestingly, granins do not necessarily possess well-conserved amino acid sequences or even secondary structure motifs (Bartolomucci et al., 2011). Instead, they are largely defined by intrinsically disordered domains which facilitate flexible protein-protein interactions required for DCG condensate formation. Crucially though, condensation is inducible and only occurs following a fall in pH, a rise in divalent cations and cleavage of granin proproteins (Chanat & Huttner, 1991; Colomer et al., 1996; Huttner et al., 1991). This makes granins essential structural elements and important temporal regulators of DCG condensation. Indeed, granin proteins constitute such a central component of DCG biology that simply expressing granins such as Chromogranin A (CHGA) or Chromogranin B (CHGB) in non-secretory cells is sufficient for those cells to form DCG compartments (Elias et al., 2012; Huh et al., 2003; Montero-Hadjadje et al., 2009).

Regulated secretory compartments also house proteolytic enzymes that play an essential role in DCG biology by cleaving granins and other DCG proproteins into

biologically active forms. The full cast of processing enzymes is not fully established – for example, recent analysis has identified 29 proteases expressed in human brain tissue that are likely to process neuronal granins (Quinn et al., 2021) – however, the most significant proteases for DCG biogenesis are the prohormone convertase (PC) serine endoproteases, PC1/3 and PC2 (Seidah et al., 2013). PC enzymes require acidic pHs and high Ca^{2+} concentrations to function, meaning they first become activated in maturing DCG compartments, slightly prior to DCG formation (Schmidt & Moore, 1995; Shennan et al., 1994). Different PCs are actually activated across a range of pHs and Ca^{2+} concentrations, suggesting that they may act on proproteins sequentially as the compartment matures and lumenal conditions change (Dey et al., 2004). Interestingly, PCs and other types of processing enzyme actually incorporate into the DCG matrix, making them a form of DCG cargo as well as processing enzymes (Parchure et al., 2022).

Finally, DCGs also house a diverse range of other cargoes, with several hundred potential cargoes existing within individual cell types such as neurons (Germanos et al., 2021; Wen G et al., 2021). Indeed, even insulin granules contain between 80 and 130 different identified proteins (Brunner et al., 2007; M. Li et al., 2018). Types of DCG cargo vary greatly, and include digestive enzymes, neuropeptides and hormones. The structure of these proteins is also highly varied, but common features include a requirement for proteolytic cleavage and close association with divalent cations. Well-studied examples include the processing of insulin from proinsulin precursors and formation of Zn^{2+}-stabilised isoline hexamers and growth hormone aggregates (Emdin et al., 1980; Jacob et al., 2016; Nettleton et al., 2000).

1.2.3 DCG biogenesis

1.2.3.1 Introduction to DCG biogenesis

DCG biogenesis oversees the conversion of individual soluble cargoes into a single non-aqueous granule which can be rapidly secreted on demand. DCG-specific regulation begins at the TGN and involves several stages where DCG cargoes are sorted into budding DCG compartments, cargo maturation and finally DCG condensation (Fig. 1.1) (Campelo et al., 2023). DCG structures can form both protein condensates and aggregates, with condensate denoting protein-ion mixtures that readily resolubilise and aggregate referring to structures defined by strong protein-protein interactions like “zipped” β-sheets that may not easily resolubilise (Makin et al., 2005; Parchure et al., 2022; Venko & Žerovnik, 2023). Finally, DCG secretion is triggered by external stimuli. Ultimately, despite decades of research, much debate still exists regarding DCG biogenesis mechanisms.

1.2.3.2 Protein sorting at the TGN

The regulated secretory pathway represents just one of numerous trafficking pathways emanating from the TGN. Given the very different functions and cargoes involved in these various pathways, it is therefore essential for DCG-targeted proteins to be sorted and concentrated appropriately into regulated secretory compartments. However, the mechanisms by which this is achieved remain highly ambiguous and represent one of the greatest sources of debate among researchers in this field.

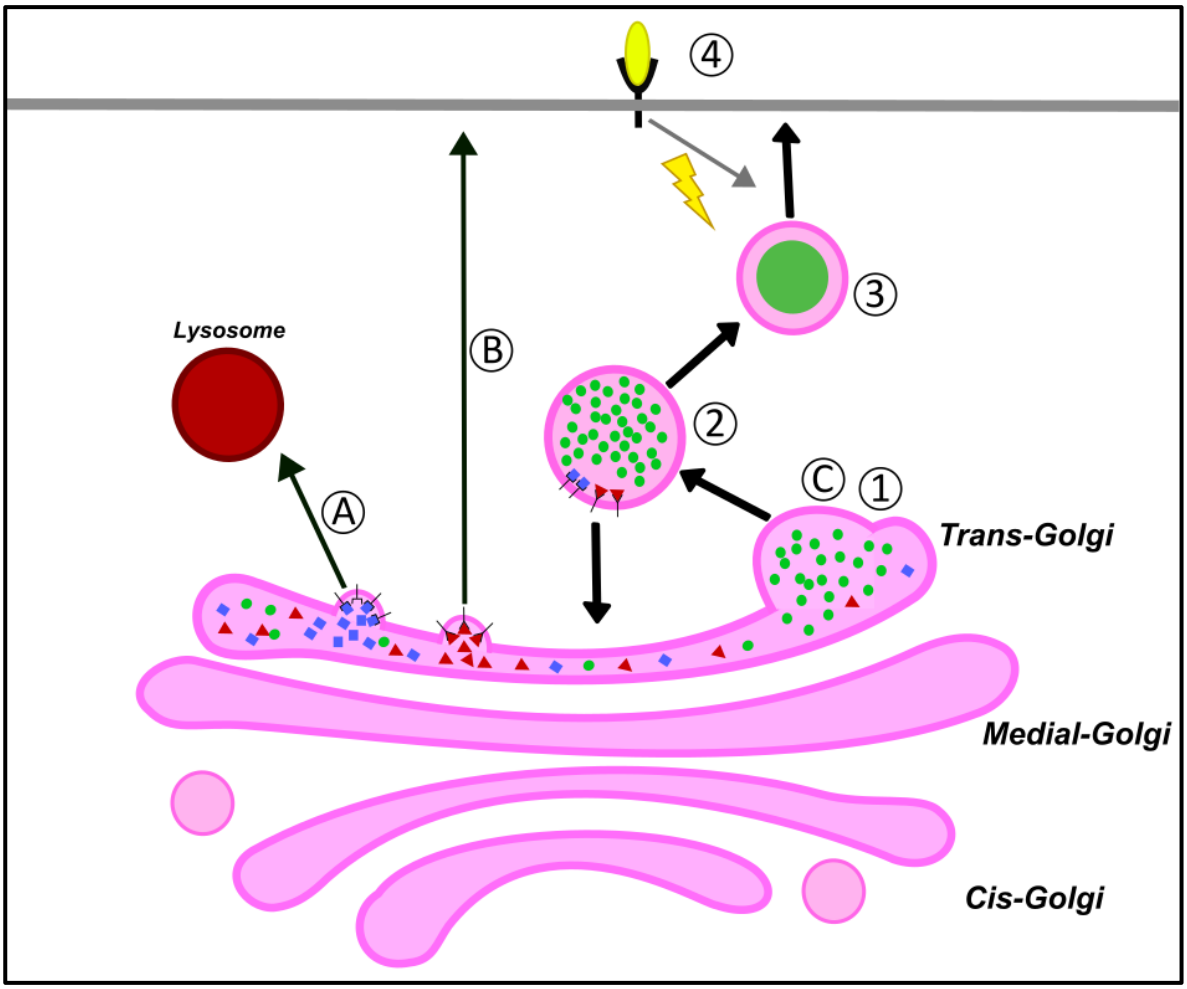

Figure 1.1. Schematic of major trafficking/secretion pathways emanating from the *trans*-Golgi. Following trafficking through the ER and Golgi, soluble cargoes can be sorted into different pathways. Sorting can be receptor-mediated, as in the lysosomal-hydrolase pathway (A) or various constitutive secretory pathways (B). DCGs (C) form through several steps including undefined cargo sorting and vesicle budding mechanisms (1), maturation steps including receptor-mediated removal of missorted proteins (2), and eventual granule condensation (3). DCG release is regulated by external stimuli (4).

Early models of DCG sorting were based on the mannose-6-phosphate receptor (M6P-R) sorting pathway that mediates trafficking of acid hydrolases to lysosomes. In this pathway, the lumenal domains of transmembrane M6P-R act as a receptor for soluble lysosomal hydrolases within the TGN whilst the cytoplasmic face recruits adaptor proteins and clathrin which induce membrane curvature and budding (Braulke & Bonifacino, 2009; Gabel & Foster, 1986). Since the M6P-R pathway was the first soluble-cargo sorting mechanism to be described, it was commonly assumed that other TGN sorting mechanisms utilised similar membrane-bound receptor, adaptor proteins and coat proteins (Arvan & Castle, 1998; Bauerfeind & Huttner, 1993). Broadly speaking, variations of this pathway do appear to be utilised in many secretory processes including constitutive secretion (Ponnambalam & Baldwin, 2003), yet since this model was first postulated in the late 1980's, no receptors and no cognate sorting motifs have been definitively identified that allow efficient sorting of soluble DCG proteins (Campelo et al., 2023; Chung et al., 1989). Indeed, DCG cargo proteins have been found to be quite varied in structure, and evidence from electron microscope studies suggests that the process of ISG budding does not require either adaptor proteins or coat proteins as might be expected for a receptor-based sorting mechanism (Rambourg et al., 1989).

In the absence of these factors then, several competing models have emerged to explain the mechanism of DCG protein sorting. We will explore the major alternative model here, which hypothesizes that DCG proteins can be sorted via protein condensation. Unlike the sorting by receptor-based model which supposes that DCG proteins are concentrated as receptor ligands, the sorting by condensation model (also known as sorting by aggregation) suggests DCG cargoes self-sort in the TGN by

forming a partial protein condensate that concentrates DCG cargoes and excludes proteins from other pathways.

The sorting by condensation model is broadly consistent with observations of TGN compartments and with the biophysical properties of DCG cargo proteins. Explaining this, electron microscope studies of mucous-containing DCGs have shown that DCG proteins are evenly dispersed in the flat cis- and medial-Golgi cisternae, but appear to coalesce into discrete, swollen areas in the TGN (Clermont et al., 1993; Rambourg et al., 1988). This suggests that DCG cargoes can cluster in the TGN and deform the TGN membrane. Because of this, it has also been suggested that large condensates could help induce membrane curvature, removing some need for adaptor and coat proteins in DCG compartment budding.

Additionally, the condensation hypothesis fits fairly well with the physical properties of DCG proteins, which have been shown in cell-free studies to begin aggregating under mildly acidic conditions similar to those in the TGN (Chanat & Huttner, 1991; Colomer et al., 1996). Indeed, it has even been shown that granin proteins can control the sorting and packaging of other DCG proteins into the regulated secretory pathway, likely via condensation-dependent clustering mechanisms. For example, overexpressing CHGA or CHGB in AtT-20 neuroendocrine cells leads to increased sorting of pro-opiomelanocortin into DCGs (Montero-Hadjadje et al., 2009; Natori & Huttner, 1996). Finally, it has been shown that certain cargoes including granins can associate with lipid rafts and other lipid domains (Carmon et al., 2020; Hosaka et al., 2004; C. Zhang et al., 2003). In the case that condensates do form in the TGN, lipid raft

associations would connect condensates to the TGN membrane, thereby linking DCG cargoes to membranes prior to compartment budding and scission.

However, the sorting by condensation model also possesses important limitations. For example, one conceptual issue for this model is the fact that many DCG cargoes exist as prohormones within the TGN and only undergo full proteolytic processing within the DCG compartment (Schmidt & Moore, 1995; Seidah et al., 2013; Shennan et al., 1994). If DCG cargoes have already formed a condensate or solid aggregate whilst still within the TGN lumen, it is not clear whether processing enzymes could effectively access and cleave DCG cargoes later. On the other hand, PCs can still be integrated into DCG condensates after exiting the TGN, although not into aggregates, so it is unclear whether this is a decisive limitation of the condensation model (Parchure et al., 2022).

1.2.3.3 ISG budding from the TGN

Another area of debate in DCG research is the mechanism by which DCG compartments separate from the TGN following cargo sorting. It is fairly well-established that DCG compartment budding does not require adaptor or coat proteins, but to date no other budding mechanism has been firmly established. With that said, certain factors have been implicated in compartment budding. The most fundamental of these is ATP, which was shown early on to be essential for budding and scission (Tooze & Huttner, 1990).

Another implicated factor is Arf1 GTPase, which was shown to enhance the rate of compartment biogenesis by up to two or three times (Y.-G. Chen & Shields, 1996; Faúndez et al., 1997). Likewise, the lipid modifying protein Phospholipase D (PLD) was

also found to contribute to the budding process (Y.-G. Chen et al., 1997; Tanguy et al., 2022). When activated, PLD converts phosphatidyl choline into phosphatidic acid which promotes membrane curvature. This conversion has been suggested to induce DCG compartment budding in itself (Segev, 2009), but recent research has also shown that CHGA preferentially binds to phosphatidic acid species leading to increased membrane curvature and secretory granule biogenesis (Carmon et al., 2020). These pathways are particularly interesting because they offer mechanisms by which membrane curvature can be induced without adaptor or coat proteins. They are also interesting because PLD is known to be activated by small GTPases including Arf1, suggesting that the functions of these two genes in secretory compartment budding may be linked (Cockcroft et al., 1994; Donaldson et al., 1992).

Cholesterol is another lipid implicated in secretory granule budding, although its role is not clear (Tanguy et al., 2016). Cholesterol depletion reversibly inhibits DCG compartment biogenesis, yet this effect may not be specific as it also blocks budding for constitutive secretory vesicles (Y. Wang et al., 2000). On the other hand, elevated cholesterol produces enlarged insulin granules, supporting a role for cholesterol in the budding process (Bogan et al., 2012). This is consistent with the larger idea that cholesterol-rich lipid rafts help to induce membrane budding by connecting DCG cargoes to the wider membrane, possibly allowing large DCG condensates to deform the membrane around themselves (Section 1.2.3.2) (Hosaka et al., 2004; C. Zhang et al., 2003). However, the presence of condensates within the TGN is still debated, meaning the role of cholesterol in the budding process remains unclear.

1.2.3.4 DCG maturation and condensation

Once separated from the TGN, the process of full DCG condensation occurs. This is one of the better understood aspects of DCG biology and involves at least three different processes, namely the removal of missorted proteins, the processing of proproteins, and the influx of stabilising ions.

Examining these processes in turn, the removal of missorted proteins is overseen by the conserved DCG regulators, Arf1, AP-1 and clathrin (Bonnemaison et al., 2013). Arf1 is a small GTPase that localises to the membrane of immature DCG compartments and helps to recruit the AP-1 complex (Austin et al., 2000). The AP-1 complex recognises the cytoplasmic tails of missorted membrane proteins and acts as an adaptor for clathrin which binds and induces strong enough membrane curvature to form clathrin-coated vesicles (Burgess et al., 2011; Klumperman et al., 1998). Over time, this process clusters and extracts essentially all missorted transmembrane proteins as well as any soluble ligands attached to them, leaving a refined population of DCG-specific cargoes. The fate of the removed proteins appears to vary, with some vesicles thought to fuse with the plasma membrane in a form of constitutive-like secretion, whilst other vesicles are recycled to the TGN where they may assist further DCG compartment formation (Bonnemaison et al., 2013; Burgess et al., 2011; Kuliawat & Arvan, 1992).

Alongside protein removal, DCG biogenesis also requires an influx of H^+ ions and divalent cations, most typically Ca^{2+} and Zn^{2+} (Duncan et al., 2003; Lorenson et al., 1983; Tooze, 1998; Winkler & Westhead, 1980; M. M. Wu et al., 2001). Changes in compartment pH are mediated by the conserved V-ATPase proton transport complex (Sun-wada et al., 2006; Tompkins et al., 2002a), whilst various phylogenetically related

ion transporters regulate Zn^{2+} import. The origins of secretory granule Ca^{2+} meanwhile are less clear. Given the high affinity that DCG matrix proteins like granins have for Ca^{2+} ions, it is possible that they simply capture Ca^{2+} ions during their passage through the ER, but it is also possible that an unidentified calcium-transporter exists (Mitchell et al., 2003). Regardless, the overall effect of compartment acidification and ion import is to promote DCG condensation. Divalent Ca^{2+} and Zn^{2+} cations help to organise intermediate structures such as insulin hexamers that promote stable DCG formation whilst low pHs allow acidic matrix proteins such as granins to begin condensation which excludes H_2O molecules (Bartolomucci et al., 2011; Germanos et al., 2021; Huttner et al., 1991; Jacob et al., 2016).

Finally, as briefly discussed in Section 1.2.2.2, many DCG cargoes undergo processing to convert them from proproteins into mature granins, hormones, neuropeptides, etc. This process is essential for both cargo activation and DCG condensation and is overseen by proteolytic enzymes such as PC enzymes whose activity is controlled by Ca^{2+} concentration and compartment acidity, both of which evolve as compartments mature (Schmidt & Moore, 1995; Seidah et al., 2013; Shennan et al., 1994).

1.2.4 DCG biogenesis and disease

Although the process of DCG biogenesis is only partially understood, several recent pieces of evidence suggest that changes or faults in DCG formation might be important for understanding human pathologies. Indeed, given the central role of DCGs in important signalling pathways and their seemingly well-conserved regulatory mechanisms, it seems likely that defects in DCG biogenesis could disrupt signalling

processes and contribute to certain diseases. Supporting this, dysregulation of PC enzymes has been implicated in many human pathologies including cancer, cardiovascular disease, autoimmune diseases and neurodegenerative conditions (Cendron et al., 2023; Salton & Lin, 2013). In addition, a number of granin proteins have been found to regulate the development of diabetes (Herold et al., 2021). Taking CHGB as an example, reducing or eliminating its expression in pancreatic beta cells has been shown to decrease insulin secretion and potentially impair DCG biogenesis, with one study finding a decrease in insulin granule density (Bearrows et al., 2019; Obermüller et al., 2010).

One particularly interesting putative role for DCGs is in neurodegeneration. Neurodegenerative conditions such as Alzheimer's disease (AD) and Parkinson's disease are defined by the extracellular accumulation of proteinaceous β-amyloid which is irreversibly aggregated and induces cytotoxic damage in nearby neurons (C. Wells et al., 2021). In recent years, the regulation and processing of numerous DCG proteins has been implicated in the progression of neurodegenerative diseases. For example, 22 neuronal protease enzymes predicted to be involved in granin processing in the brain were also identified as contributing to dementia onset in patients with AD (Quinn et al., 2021). What's more, the levels of secreted granin products have been found to be significantly altered in patients with neurodegenerative conditions, with Chromogranin A and VGF products found to be significantly elevated and decreased respectively in the brains of AD patients (Quinn et al., 2023). Additionally, in mouse models of Parkinson's disease, significantly fewer DCGs are found in neuron populations, and proteomic analysis of purified neuronal granules found defects in granin-mediated peptide processing (Wen G et al., 2021). One especially interesting

result found that a single nucleotide polymorphism in the DCG cargo brain-derived neurotrophic factor (BDNF) is associated with the onset of AD (Cozza et al., 2008).

The mechanistic link between DCGs and neurodegenerative disease remains unclear, but it is interesting to note the role of DCGs in inducing protein aggregation and amyloid formation in secretory cells such as neurons under normal physiological conditions. The fact that dysregulation of DCG cargoes and their processing enzymes correlates with the development of amyloid-driven neurodegenerative conditions therefore suggests that defects in DCG organisation may lead to the secretion of inappropriate factors which promote extracellular amyloid accumulation. This is an idea that is far from proven, but which informed some of my own investigations into DCG biology.

1.3 The endosomal system

1.3.1 Overview of endosome biology

The primary function of endosomes is to serve as hubs for the sorting of intracellular cargoes such as internalised receptors, nutrient transporters and ligands. The majority of endosomal cargoes derive from endocytosed vesicles which join with the first of three major endosome compartments, the early endosome (EE). From here, cargoes may be directed down one of several minor pathways that deliver molecules to organelles such as the Golgi and nuclear envelope (Buser & Spang, 2023; Chaumet et al., 2015; Marco et al., 2021). However, the majority of cargoes are directed toward two fates, degradation or recycling (Fig. 1.2). Sorting for these fates occurs at EEs, with

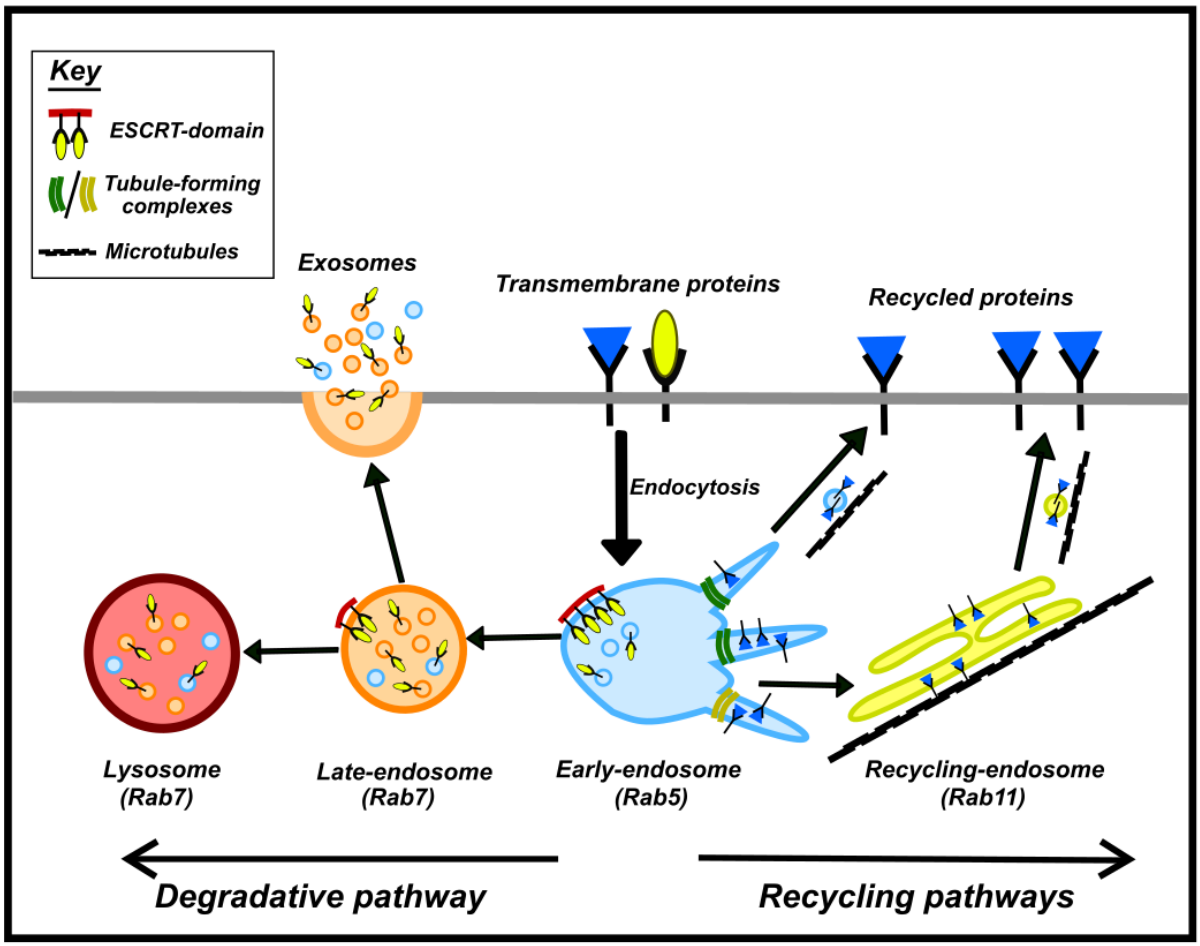

Figure 1.2. Schematic of endocytic trafficking. Endocytosed membrane proteins are trafficked to early endosomes and sorted into degradative or recycling pathways. Cargo sorting in the degradative pathway is mediated by vacuolar, ESCRT-domains that produce ILVs whilst cargo recycling depends on tubular, recycling domains. Vacuolar regions develop into late endosomes which typically fuse with lysosomes, leading to cargo degradation. However, late-endosomes can also be secreted, leading to release of ILVs as exosomes. Tubular domains can recycle cargoes directly back to the plasma membrane or can direct cargoes to recycling endosomes which then migrate and fuse with plasma membranes.

degradative cargoes trafficked to late endosomes (LEs) and eventually lysosomes, whilst recycling cargoes are returned either directly from EEs to the plasma membrane, or returned via a slower recycling endosome (RE) route. (Hu et al., 2015; O'Sullivan & Lindsay, 2020).

Endosomes play an essential role in regulating the distribution of key molecules and the availability of nutrients (Gilleron et al., 2019; Naslavsky & Caplan, 2018), meaning endosomes must respond adaptably to cellular requirements. For example, endosomal trafficking of hyperactivated receptors to lysosomes can specifically potentiate overactivated pathways (Marchese et al., 2008), whilst elevated endolysosomal trafficking in response to nutrient deprivation replenish global essential nutrient levels (MacDonald et al., 2015). Endosomes therefore provide a dynamic balance between cargo recycling and degradation, with each of EEs, LEs and REs playing specific roles in this process.

1.3.2 Early endosomes

Early endosomes (EEs) exist at the centre of endosomal trafficking and are the major site of cargo entry into the endosomal system. Their gross structure is formed by the fusion of endocytosed vesicles (Rizzoli et al., 2006), meaning they contain an eclectic mixture of cargoes which must then be sorted into the degradative and recycling pathways. To facilitate this sorting, the limiting membrane of EEs is characterised by the coexistence of distinct membrane microdomains required for cargo sorting to specific pathways (Norris & Grant, 2020).

One prominent constituent of EE microdomains is the charged lipid phosphatidylinositol 3-phosphate (PI3P), which is produced by Vps34 following its activation by the EE marker Rab5 GTPase (Buckles et al., 2020; Gillooly et al., 2000). PI3P is required for the recruitment of specific proteins possessing Phox (PX) domains and Fab1P, YOTB, Vac1p, and EEA1 (FYVE) domains (Chandra et al., 2019; Kutateladze, 2006). Members of the Rab family of small GTPases also play an important role in recruiting and activating specific factors in each pathway, with specific microdomains known to be marked by Rab4, Rab7, Rab11, Rab14 and possibly Rab3 (Diaz-Rohrer et al., 2023; Proikas-Cezanne et al., 2006; Sönnichsen et al., 2000).

Broadly speaking, EEs are divided between two domains, vacuolar domains that organise cargoes for the degradative pathway and tubular domains that contribute to different recycling pathways. Vacuolar domains are broadly spherical and include most of the aqueous lumen of EEs, whilst tubular domains account for much of surface area. The membrane of vacuolar domains are defined by the ESCRT-complex, a membrane remodelling complex which clusters transmembrane cargoes and packages them into intraluminal vesicles (ILVs) within the lumen of EEs and LEs (Henne et al., 2011). Incidentally, ILVs are precursors of exosomes (Juan & Fürthauer, 2018), and so the mechanism of ESCRT-dependent ILV biogenesis will be reviewed in detail in Section 1.4.3.1. Of note here, ESCRT proteins are recruited to endosomes by monoubiquitinated transmembrane proteins (Hirano et al., 2006). The ultimate result of ESCRT activity is the concentration of specific cargoes into ILVs which are then accessible to lysosomal hydrolases. Since cargo ubiquitination varies in response to stimuli like nutrient availability, this pathway acts as an important regulator of nutrient availability (Gilleron et al., 2019; MacDonald et al., 2015).

In comparison to the invagination of membranes in vacuolar domains, tubular domains project into the cytosol and can be formed by several methods, most of which depend on the retromer or retromer-related complexes such as Retriever (Chen et al., 2019; Gershlick & Lucas, 2017). The retromer is a conserved protein complex consisting of a cargo-sorting complex (CSC) trimer containing Vps35, Vps26 and Vps29 and a SNX-BAR dimer containing SNX1/2 with SNX5/6 (Seaman, 2021; Tu & Seaman, 2021). In higher eukaryotes the SNX-BAR dimer is not included in the term retromer. In the traditional view, the CSC trimer is responsible for recognising recycling cargoes whilst SNX-BAR dimers polymerise and induce tubule formation through amphipathic, membrane deforming BAR domains (van Weering et al., 2010). However, more recent evidence indicates that, particularly in higher eukaryotes, each of the CSC and SNX-BAR dimer can mediate cargo-selection and tubule formation independently (Cui et al., 2018; Kovtun et al., 2018; Kvainickas et al., 2017; Simonetti et al., 2017). Once formed, tubules can form vesicles that recycle materials in the fast-recycling and retrograde recycling pathways, or they can undergo scission from EEs to create RE compartments.

The establishment of retromer-dependent microdomains is regulated by several factors including PI3P and Rab7 (Rojas et al., 2008; van Weering et al., 2010). Interestingly, the retromer complex also plays a role in restricting ESCRT microdomain proliferation through the recruitment of Hsc70 and its cochaperone RME-8 and, in the absence of either RME-8 or SNX1, degradative ESCRT microdomains are found to over-assemble on endosome surfaces and drive inappropriate sorting of recycling cargoes to the degradative pathway (Norris et al., 2017). As such, the retromer plays an essential role in mediating endosomal trafficking and cargo sorting and mutations in

retromer components such as Vps35 are often associated with diseases thought to result from endosomal trafficking defects including neurodegenerative illnesses and cancer (Sassone et al., 2021; Sullivan et al., 2011; Yu et al., 2023).

1.3.3 Late endosomes

Late endosomes (LEs) form as a direct continuation of EEs, which gradually mature and take on new characteristics over time (Borchers et al., 2023; Poteryaev et al., 2010). One part of this process is a refinement in cargoes which occurs through the concentration of LE cargoes in vacuolar domains or ILVs and the separation of recycling cargoes through recycling vesicles and endosomes. These processes occur in EEs but are continued in LEs. As examples, both the ESCRT and retromer complexes continue to operate on LEs, whilst other pathways such as a Rab3-dependent recycling pathway appear to be LE-specific and further refine cargo populations (Diaz-Rohrer et al., 2023; Juan & Fürthauer, 2018; Rojas et al., 2008).

Compartment identifiers also evolve as endosomes develop, with the resulting LE effectively coming to resemble an intermediate structure between EEs and the lysosome (Hu et al., 2015). Exemplifying this, during maturation, the EE marker Rab5 is gradually displaced by Rab7 (Borchers et al., 2023; Poteryaev et al., 2010), a marker which compartments will retain even after their fusion with lysosomes. Similarly, LEs become enriched in lysosome-related factors such as the transmembrane marker LAMP1 and lipid species such as LBPA which are also a hallmark of lysosomes (Falcón-Pérez et al., 2005; Matsuo et al., 2004). Indeed, the study of LEs is actually significantly

complicated by the fact that LEs possess very few exclusive molecular markers (Scott et al., 2014).

Finally, as EEs develop into LEs, the lumenal pH falls, from pH ~6.2 in EEs to ~5.7 in LEs (L. Ma et al., 2017). This increase in acidity is mediated by the highly conserved V-ATPase proton pump complex and is more specifically regulated by an increase in the ratio of V_1 to V_0 V-ATPase subcomplexes in endosome membranes as compartments mature (Lafourcade et al., 2008). The lower pH of LEs allows them to fuse with lysosomes without disrupting the acidic microenvironment required for acid hydrolases.

Ultimately, most late endosomal compartments undergo fusion with lysosomes, a process that requires Rab7, Rab2, the multimeric protein complex HOPS and the R-SNARE VAMP7 amongst other factors (Lund et al., 2018; Pryor et al., 2004; Schleinitz et al., 2023). This fusion leads to the complete degradation of cargoes to provide new essential nutrients for cells. However, in many cases LEs can instead be directed to fuse with plasma membranes. This results in the extracellular release of ILVs as exosomes, which can then act as potent signalling factors. The mechanisms regulating the fate of LEs are of great interest to researchers yet they generally remain quite ambiguous. Factors such as Rab27, Rab35 and the SNAREs syntaxin-4, SNAP-23, and VAMP7 are each known to support fusion with the plasma membrane (Hsu et al., 2010; C. Liu et al., 2023; Ostrowski et al., 2010), whilst the fate of individual LEs appears to correlate with membrane cholesterol content (Abdullah et al., 2021; Möbius et al., 2003). Overall however, this remains a fairly poorly defined process in endosomal and exosomal biology.

1.3.4 Recycling endosomes

Recycling endosomes (REs) are tubular structures that concentrate in the perinuclear space, nearby the microtubule-organising centre (MTOC). They are associated with Rab11, Rab8 and Rab22 and are an essential feature of the slow recycling pathway (Grant & Donaldson, 2009). REs are generally thought to arise from scission of tubular recycling domains on EEs which can be formed by retromer-dependent pathways (Section 1.3.2), or a Rab22a-dependent pathway (Kong et al., 2023; Shakya et al., 2018). This pathway sees Rab22a form a complex with biogenesis of lysosome-related organelles complex (BLOC) proteins BLOC1 and BLOC2, as well as the kinesin motor protein KIF13A. This complex then facilitates tubule formation and potentially scission as well as transport to the MTOC. It is also possible that multiple RE subpopulations exist, with REs labelled by Rab11a and Rab8a possessing distinct cargoes and potentially regulatory mechanisms (Goldenring, 2015).

Tubule scission mechanisms are not yet clearly understood, though it was recently shown that scission requires the membrane curvature-inducing proteins LITAF and CDIP1 (Wunderley et al., 2021). Scission is also widely thought to require membrane constriction by actin filaments as well as participation of microtubule filaments (Norris & Grant, 2020; Simonetti & Cullen, 2019). Supporting this, actin polymerisation, the microtubule severing protein Spastin and the kinesin motor protein KIF13A are all required for effective recycling and tubule scission (Allison et al., 2013; Delevoye et al., 2014; Weigert et al., 2004). Additionally, both the actin-binding protein Annexin A2 (AnxA2) and the actin-nucleating/cross-linking complex Arp2/3 appear to localise to tubule stems and support scission (Delevoye et al., 2016). This AnxA2-dependent,

Arp2/3-dependent pathway also requires upstream BLOC1 and KIF13A activity, suggesting that the Rab22a/BLOC1/BLOC2 complex contribute to this process. Likewise, BLOC1 and Arp2/3 are known to interact with the WASH complex which concentrates at sites of tubule scission, suggesting it may have a role in this system (Rowland et al., 2014; Ryder et al., 2013; Simonetti & Cullen, 2019).

Following their formation, REs retain tubular or vesicular structures that are enriched in a diverse set of recycling cargoes. These tubules/vesicles gradually migrate to the plasma membrane, with transport mediated by Rab11-family interacting proteins (Rab11-FIPs), a family of cytoskeleton-adaptor proteins which interact with Rab11 (Horgan & McCaffrey, 2009; Machesky, 2019). Upon arrival at the cell periphery, RE tubules/vesicles fuse with the plasma membrane in an exocyst dependent manner (Guichard et al., 2010; Langevin et al., 2005; Oztan et al., 2007), thereby fully recycling membrane linked materials to the plasma membrane and secreting soluble contents.

Overall, REs play important roles in cellular homeostasis. The precise trafficking of tubule and vesicle transport appears to be significant in recycling trafficking specificity, with REs playing an important role in polarised transport and delivery of specific materials to various junctions (Chalmers & Whitley, 2012; Jing & Prekeris, 2009; B. X. Li et al., 2007; Lock & Stow, 2005). REs also mediate significant cancer-related processes (D'Agostino et al., 2019; Ferro et al., 2021; Khan & Steeg, 2021). Broadly speaking, REs support recycling activity that prevents the degradation and loss of important tumour suppressor proteins. As an example, internalisation and degradation of the cell-adhesion molecule E-cadherin plays an important role in cancer metastasis which is ameliorated by Rab11-dependent trafficking through the RE (Lock & Stow, 2005;

Mendonsa et al., 2018). Additionally, in recent research produced in collaboration with the Wilson laboratory that has directly informed my own research within this thesis, it has also been shown that Rab11-positive REs act as novel sites of exosome biogenesis in human cancer cells (Fan et al., 2020). These exosomes were further demonstrated to induce pro-cancer signalling pathways, providing a fascinating case study for examining novel exosome and RE biology in the context of cancer signalling.

1.4 Exosome biology

1.4.1 Outline of exosome signalling

Exosomes are a class of extracellular vesicle that function in a wide variety of biological signalling processes. They were first identified through electron microscope studies of reticulocyte maturation where they were suggested to represent a novel form of waste disposal (Harding et al., 1983; Pan & Johnstone, 1983). Since then however, it has become clear that exosomes play a central role in cell-cell signalling processes including immunomodulation (Buzas, 2023), cancer signalling (Tai et al., 2018), and neurodegenerative disease progression (Xiao et al., 2017).

Since the details of exosome biology are reviewed excellently elsewhere (Arya et al., 2024; Juan & Fürthauer, 2018; Krylova & Feng, 2023), the basic exosome signalling pathway will be outlined fairly briefly. Exosomes are originally formed as intraluminal vesicles (ILVs) within the lumen of multi-vesicular endosomes (MVEs) through the inward budding of endosome membranes. During budding, a variety of cargo molecules from the cytosol and endosome membrane are sorted into exosomes,

including transmembrane receptors, soluble enzymes, specific lipids and even nucleic acids molecules such as miRNAs and mRNAs that are specifically concentrated in exosomes (Valadi et al., 2007). Exosomes may contain thousands of different cargo molecules and, ultimately, it is these cargo molecules that allow exosomes to propagate complex, specific signalling changes.

Exosomes are released from “donor cells” when MVEs fuse with the plasma membrane. Secretion allows exosomes to come into contact with “recipient cells” which exosomes can interact with based on their protein corona, inducing signalling changes through either cell-surface interactions or cargo internalisation, generally via endocytosis. It is generally assumed that many exosomes act on recipient cells in close proximity to the donor cell, but exosomes have also been shown to act across large distances (Corrigan et al., 2014; Rohrer et al., 2019).

Although the basic outline of exosome signalling is relatively straightforward, our overall understanding of exosomes remains very limited. This is largely due to technical constraints, with exosomes being too small to examine in detail using light microscopy, and too similar in size and chemical composition to effectively isolate from other EV populations. As such, many details of exosome signalling remain unclear, particularly in terms of intracellular events.

1.4.2 Exosome signalling mechanisms

1.4.2.1 Cell-surface interactions

The protein corona of exosomes is comprised from transmembrane proteins inherent to exosomes themselves and from other factors that those membrane proteins recruit (Heidarzadeh et al., 2023). Corona proteins play several important roles in exosome signalling, most directly, by binding proteins on the surface of recipient cells. This directly stimulates specific signalling pathways in a variety of ways, including classical receptor-ligand interactions, adhesion-molecule dimerization and potentially even novel, non-canonical signalling pathways as seen in other EV populations (Abusamra et al., 2005; M. K. S. Tang et al., 2018; Q. Wang & Lu, 2017). Cell-surface interactions also facilitate exosome internalisation and play a determining role in exosome-specificity through recipient cell-targeting (He et al., 2022; Sancho-Albero et al., 2019; Viñas et al., 2018). As examples, the *Drosophila* protein Sas appears to be packaged into EVs and then promote their targeting to cells expressing the Ptp10D receptor, for which Sas is a ligand (Lee et al., 2023). Similarly, cancer cell exosomes housing syndecan are specifically internalised by recipient cells displaying similar heparan sulphate proteoglycans with which they can interact (Christianson et al., 2013).

1.4.2.2 Cargo internalisation

Exosome internalisation can occur in two ways, exosome fusion with the plasma membrane or endocytic internalisation of the entire exosome paired with subsequent cargo uncoating through fusion with endosomal membranes. Through these pathways, exosomes are effectively able to transplant signalling molecules such as receptors,

enzymes, ncRNAs and mRNAs from donor cells to recipient cells (de Godoy et al., 2018; Subra et al., 2010; Valadi et al., 2007). This allows for novel forms of cell regulation, including the translation of non-native mRNAs, the silencing of native gene expression, and even the delivery of cell-type specific protein isoforms to different cell types.

Although exosome fusion has been observed to occur in dendritic cells and tumour cells, our current understanding of this process remains very limited and the factors mediating potential membrane fusion events are unknown (Montecalvo et al., 2012; Y. Zheng et al., 2019). Because of this, the general relevance of fusion in most exosome signalling pathways is disputed, though it has been suggested that the acidic microenvironment of tumours might make exosome fusion more common amongst cancer cells due to increased membrane rigidity (Gurung et al., 2021; Parolini et al., 2009).

In comparison to exosome fusion, the mechanisms regulating exosome internalisation are significantly better studied. Internalisation occurs when receptors attached to exosomes become endocytosed and then trafficked to EEs. The primary mechanism for exosome internalisation appears to be clathrin-mediated endocytosis, which facilitates exosome uptake in epithelial cells, neural cells and macrophages amongst many others (Feng et al., 2010; Gonda et al., 2019; Guan et al., 2014; Yoon et al., 2020). Upon arrival in EEs, exosomes can be directed down several routes, the best established which is the LE/lysosomal pathway (C. Chen et al., 2018).

Ultimately, many exosomes appear to be trafficked to lysosomes and degraded, but exosomes may still stimulate signalling changes during trafficking. Exemplifying this,

exosomes housing TGFβ-1 attached to pH sensitive surface proteins have been found to induce a migratory phenotype in human mesenchymal stem cells (MSCs) upon entry into acidic endosomal compartments (Shelke et al., 2019). However, exosomes can also evade degradation and unload their cargoes into the recipient cell cytoplasm, often through virus-like mechanisms. For example, exosomes can be targeted to CD81 positive compartments in contact with plasma membrane, just as HIV-1 particles are (Izquierdo-Useros et al., 2009), or can fuse with the anionic lipid LBPA to escape LEs just as enveloped viruses do (Zhenlan et al., 2018). Interestingly, exosome uncoating in LEs appears to be pH dependent, with endosome neutralisation blocking cargo release into the cytoplasm (Joshi et al., 2020).

1.4.2.3 Role of exosome signalling

Although the effects of exosome signalling are highly diverse, certain trends have become clear over decades of study. One of the most significant is the protective, pro-survival effect of many exosomes. As examples, MSC-derived exosomes protect recipient cells from apoptosis caused by hypoxia, oxidative stress, cisplatin exposure via both miRNA144 and Hsp70 action (Z. Liu et al., 2019; Park et al., 2021; Wen et al., 2020). They can also alleviate amyloid-β-induced oxidative stress through direct delivery of catalase to neurons (de Godoy et al., 2018). Exosomes can assist recovery from physical or ischaemic injuries (J. H. Huang et al., 2023; Y. Jiang et al., 2020; Viñas et al., 2018; H. Xu et al., 2020), and can even provide protection beyond their immediate recipient cells, for example by promoting angiogenesis in oxygen-deprived regions (Babaei & Rezaie, 2021; Kang et al., 2019; Moeinabadi-Bidgoli et al., 2023).

Related to these protective, pro-survival effects, exosomes also act as important regulators of cancer signalling. Indeed, exosomes modulate virtually every stage of cancer progression from pre-metastatic niche formation and metastasis (Guo et al., 2019; Yang et al., 2021; Yuan et al., 2021), to cell migration (Harris et al., 2015; Matsumoto et al., 2020) and survival/apoptosis (Ham et al., 2018; Hosseini-Beheshti et al., 2016; J. Huang et al., 2019). Exosomes have also been found to promote oxygen and nutrient supply to tumours through angiogenesis (Mao et al., 2019; Miaomiao et al., 2023; X. Zheng et al., 2021), and to promote aggressive cell proliferation through changes in glycolysis and the cell cycle (J. Huang et al., 2019; Matsumoto et al., 2020; Nie et al., 2020). Interestingly, exosomes have also been reported with anti-tumour activities, often by promoting anti-cancer immune cell responses (Aqil & Gupta, 2022; Romagnoli et al., 2015; Zitvogel et al., 1998).

In addition to cancer, exosomes have been implicated in pathologies as diverse as autoimmune disorders (Miao et al., 2021; Zou et al., 2021) and cardiovascular disease (Jadli et al., 2021; Reiss et al., 2023; Z. Zhang et al., 2023). However, one of their most interesting roles is in neurodegenerative illnesses where exosomes exacerbate neurodegeneration by acting as vehicles for amyloidogenic proteins and promoting their uptake by neurons (Emmanouilidou et al., 2010; Laulagnier et al., 2018; Rajendran et al., 2006; Xiao et al., 2017). Exosomes have also been shown to accelerate protein aggregation, and negatively impact neuronal survival (Emmanouilidou et al., 2010; Grey et al., 2015).

Interestingly, the role of exosomes in neurodegenerative disease is closely tied to endosome dysregulation in donor cells (Izco et al., 2022). For example, depleting

neurons of the early endosomal lipid phosphatidylinositol-3-phosphate results in increased trafficking of amyloid precursor protein (APP) on exosomes (Miranda et al., 2018). Likewise, inhibition of the retromer complex significantly increases trafficking of APP and presenilin fragments (Sullivan et al., 2011), whilst exosomes taken from the brains of induced-tauopathy mice house significantly greater amounts of Tau protein and induce seeding of Tau aggregates (Polanco et al., 2016). These results suggest a pivotal role for exosomes within neurodegenerative diseases which are characterised by widespread endosome dysregulation (Malik et al., 2019). Understanding this role, however, requires far greater understanding of exosome regulation within endosomes.

1.4.3 Exosome biogenesis

Current research indicates that several exosome-forming pathways exist, which are generally separated into ESCRT-dependent and ESCRT-independent. Each of these pathways mediates ILV budding, scission and cargo loading, though through quite different means.

1.4.3.1 The classical ESCRT-dependent exosome biogenesis

As implied by the name, the ESCRT-dependent pathway relies on the highly conserved ESCRT protein complex to induce exosome biogenesis. ILV formation begins when monoubiquitinated transmembrane proteins on the surface of endosomes recruit ESCRT-0 proteins Hrs and STAM (Hirano et al., 2006; Mizuno et al., 2003). Interestingly, cargoes that lack their own ubiquitin tags can still be sorted via associations with ubiquitinated tetraspan transmembrane proteins such as yeast Cos proteins and

mammalian tetraspanins (MacDonald et al., 2015). ESCRT-0-cargo interactions are stabilised by phosphatidyl-inositol 3-phosphate (Raiborg et al., 2001), and allow ESCRT-0 proteins to further recruit the ESCRT-I and ESCRT-II complexes as well as clathrin. This dynamic clathrin-ESCRT complex serves three purposes. Firstly, it clusters large numbers of cargo proteins into defined microdomains, possibly supported by tetraspan-lipid associations (Norris & Grant, 2020; Raiborg et al., 2006; Trajkovic et al., 2008). Secondly, it recruits initial ESCRT-III proteins and associated factors (Christ et al., 2016; McCullough et al., 2018). Thirdly, it passively produces slight membrane deformation through protein crowding (Liese et al., 2020). This slight deformation is important as it facilitates full ILV budding through the polymerisation of ESCRT-III proteins.

The ESCRT-III complex is comprised of four "core" subunits, Vps20 (CHMP6), Snf7 (CHMP4), Vps24 (CHMP3), and Vps2 (CHMP2) in yeast and (mammals) respectively. Of these, Vps20 is recruited first, followed by repeating polymerisation of Snf7-Vps2-Vps24 driven by the ATPase Vps4 (Henne et al., 2011; Pfitzner et al., 2020). This polymerisation produces a downward tilting spiral filament that pushes into the membrane, providing the force required for ILV budding. Additionally, accessory factors such as ALG-2 interacting protein X (ALIX) stabilise the filament and recruit deubiquitinating enzymes to remove monoubiquitin tags (Luhtala & Odorizzi, 2004; Odorizzi et al., 2003). As the ESCRT-III spiral develops, the core ESCRT-III subunits can be substituted for the "accessory" ESCRT-III proteins Did2 and Ist1 to create a steeper tilt and promote scission (Pfitzner et al., 2020). The overall product of the ESCRT-dependent pathway is a fully formed ILV enriched in cargoes that were sorted based on monoubiquitin tags.

1.4.3.2 Other biogenesis pathways

Although the classical ESCRT-dependent pathway is considered to be the major exosome-forming pathway in most cells, a number of other pathways also oversee exosome formation. The best understood is the ALIX-syndecan-syntenin pathway, which sees the accessory ESCRT protein ALIX bind to Syntenin and thereby recruit the proteoglycan Syndecan (Baietti et al., 2012; Odorizzi et al., 2003). ALIX also directly recruits the ESCRT-III protein Chmp4 to membranes without assistance from earlier ESCRT complexes, though with help from the late endosomal lipid LBPA (Ghossoub et al., 2014; Katoh et al., 2003; Larios et al., 2020; Matsuo et al., 2004). From here, ESCRT-III polymerisation occurs as normal to drive ILV formation whilst Syndecan mediates cargo selection through the interactions of its heparan sulphate sidechains with various receptors and cell adhesion molecules (Abrami et al., 2013; Imjeti et al., 2017; Poulain & Yost, 2015). Interestingly, cargo recruitment and clustering is further regulated by heparanase enzymes (David & Zimmermann, 2016).

Additionally, although only recently described and minimally studied at present, recent work in the Wilson laboratory has also defined a novel ESCRT-dependent pathway that appears to be conserved in *Drosophila* and humans (Fan et al., 2020). This pathway requires all four core ESCRT-complexes yet unlike the classical ESCRT-dependent pathway, it acts at Rab11-positive REs and specifically requires accessory ESCRT-III proteins (Marie et al., 2023). As a result, the regulation of this novel exosome population is a major focus of this thesis.

Finally, although it is particularly poorly understood at present, an entirely ESCRT-independent ILV biogenesis mechanism also exists, as demonstrated by continued ILV

biogenesis in yeast MVEs even following simultaneous inhibition of all four ESCRT complexes (Stuffers et al., 2009). Work in recent years has begun to identify regulators of this pathway. One significant player is the sphingolipid ceramide, which is formed by neutral sphingomyelinases in response to stress and is able to produce negative membrane curvature (Nikolova-Karakashian & Rozenova, 2010; Trajkovic et al., 2008). Recent work has also implicated Rab31 as a cofactor for ceramide at endosomal lipid rafts enriched in Flotillin1 and Flotillin 2 (D. Wei et al., 2021). In addition, other studies have found that proteins such as CD9, CD63, CD82 and ApoE integrate into ESCRT-independent ILVs and contribute to the sorting of proteins such as PMEL and β-catenin (Chairoungdua et al., 2010; van Niel et al., 2011, 2015).

1.4.3.3 Limitations of biogenesis models

Despite recent advances in the study of exosome biogenesis pathways, several important questions remain unanswered. For example, it remains unclear what the functional difference between exosomes formed by different pathways is. It has been suggested that the ALIX-syntenin-syndecan pathway is particularly relevant in cancer cells (Fares et al., 2017), and indeed cancer cell exosomes do require recipient cell-surface proteoglycans to be internalised (Christianson et al., 2013). However, the role of the ALIX-syntenin-syndecan pathway in normal physiology is not so obvious, and likewise no defined functions have been established for the other ESCRT-dependent and ESCRT-independent pathways.

It is also unclear how much overlap exists between different pathways in terms of machinery, regulators and cargoes. As an example, the accessory ESCRT-III ALIX

functions in both the classical ESCRT-dependent and ALIX-dependent pathways and can recruit syntenin and syndecan in both (Henne et al., 2011). What's more, despite functioning independently of ESCRT-I and ESCRT-II complexes, the ALIX-syntenin-syndecan pathway does seem to be assisted by the ESCRT-I and ESCRT-II proteins TSG101 and Vps22 (Baietti et al., 2012). Similarly, both ESCRT-dependent and -independent exosomes appears to be regulated by Rab27a, whilst cargoes such as the tetraspanin CD63 has identified on ESCRT-independent and ESCRT-dependent exosomes in different systems (Bobrie et al., 2012; Corrigan et al., 2014; van Niel et al., 2011). Overall, large gaps in our knowledge of ILV-forming pathways persist that make it difficult to understand their role in cells.

1.4.3.4 Biogenesis and exosome heterogeneity

A defining feature of exosome biology is their heterogeneity. Exosome secretions often contain thousands of different signalling cargoes, and different exosomes can vary greatly in terms of size, lipid composition, cargo molecules and signalling effects even when produced by the same cell-type (J. Li et al., 2023; Xie et al., 2022). Crucially, changes in characteristic like cargo composition often appear to be coordinated shifts, involving dozens or hundreds of cargo molecules with shared functions in specific pathways. As examples, heat shock in the sea cucumber *Apostichopus japonicus* produces exosomes with cargo profiles significantly enriched in DNA repair factors (Huo et al., 2023), whilst inflammatory stresses induce human pancreatic cells to secrete exosomes enriched in factors regulating pro-survival PI3K/Akt and MAPK signalling (Saravanan et al., 2019). These changes demonstrate a sophisticated and

adaptable regulatory mechanism for exosome cargo selection, yet it is not generally clear how these changes are accomplished or even how information from wider signalling cascades interacts with biogenesis pathways.

The best current models of exosome signalling regulation suggest that specific exosome subtypes are produced and released in response to different signalling stimuli. These different subtypes are presumed to have distinct biogenesis mechanisms, regulatory pathways, cargo profiles and signalling outcomes. This model has gained support in recent years with findings that individual cell types like human colon carcinoma cells can produce multiple exosome populations with non-overlapping cargo groupings (Tauro et al., 2013). Additionally, vesicles separated based on size or density have also been shown to produce groupings of exosomes with different cargo compositions and signalling effects (Willms et al., 2016; H. Zheng et al., 2020).

Important pieces of evidence are also beginning to be acquired regarding the regulation of exosome subtypes. Spectral analysis of exosomes from multiple cell lines found that diverse sets of exosomes clustered into 4 groupings, regardless of origin cells, indicating that a fairly small number exosome subtypes may be shared by different cell-types (Smith et al., 2015). Discrete exosome-subtype have also been indicated to be shared by evolutionarily distant organisms such as humans and *Drosophila* (Fan et al., 2020; Marie et al., 2023) and even some specific signalling pathways are now being implicated in subtype-specific control, such as NF-κβ signalling which promotes ESCRT-independent but not ESCRT-dependent exosome secretion (Singh et al., 2023).

1.5 Limitations in current secretory biology research

In each of the systems outlined above – i.e. the regulated secretory, endosomal and exosomal systems – research efforts have been complicated by the fact that only a limited number of experimental techniques exist that can be used to investigate fundamental aspects of their biology. Fundamentally, this is a result of the small, vesicular nature of these systems and the heterogeneity inherent to each. For example, due to the small size of endosomes (~100-500nm diameter, (Klumperman & Raposo, 2014)), DCG compartments (~350-450nm average diameter, (Hammel et al., 2010; Lehane, 1988)), and exosome vesicles (30-150nm diameter (Kowal et al., 2014)), light microscopy generally cannot be used to investigate events occurring on or within them and electron microscopy is often used instead (Campelo et al., 2023; Chuo et al., 2018). Similarly, the overlapping chemical compositions of structures such as different endosome populations and exosome subtypes means that biochemically isolating specific compartment or vesicle populations is exceptionally difficult (Campelo et al., 2023; J. Chen et al., 2022; Naslavsky & Caplan, 2018). Density gradients can often enrich structures of interest, but can rarely purify them entirely. Indeed, despite recent advances, even isolating exosomes from other populations of EVs remains labour intensive despite larger differences in size, composition and origins (J. Chen et al., 2022; Gao et al., 2023; Patel et al., 2019; Welsh et al., 2024). As a result, many forms of biochemical analysis remain impractical for studying regulated secretory compartments, endosomes and exosomes. These experimental limitations manifest in an inability to investigate important aspects of these systems' basic biology, especially within less pliable *in vivo* systems. Of particular significance for

researchers, many of the mechanisms controlling DCG and exosome biogenesis remain only partially understood, despite their central role in DCG and exosome signalling pathways.

1.6 The Drosophila *secondary cell model*

Because of the limitations faced by secretory compartment research in most experimental systems, I elected to conduct my research in the secondary cells (SCs) of male *Drosophila* accessory glands which have recently been developed as a model *in vivo* system for studying secretory compartment biology (C. Wilson et al., 2017). The accessory gland is an important reproductive structure in males that stores seminal fluid prior to mating (Kalb et al., 1993). The accessory gland is formed of two symmetrical arms which are connected to an ejaculatory duct, producing an overall Y-shaped structure. The accessory glands arms are comprised of two major secretory cell types which produce important seminal fluid proteins that promote male fertility and sexual competitiveness (P. S. Chen et al., 1988; Herndon et al., 1997; Wolfner, 1997). These two cell-types are the main cells, which constitute >96% of cells and prostate-like secondary cells which represent ~4% of accessory gland epithelia cells (Chapman & Davies, 2004; Kalb et al., 1993; C. Wilson et al., 2017). Although there are many fewer SCs than main cells, they still play an important role in reproductive success and have evolved as a highly specialised secretory cell-type. In particular, secondary cells possess uniquely large regulated secretory compartments which

contain DCGs and are labelled by the RE marker Rab11 (Prince et al., 2019; Redhai et al., 2016; C. Wilson et al., 2017).

Interestingly, these DCG compartments also contain Rab11-labelled ILVs which are then secreted as exosomes and transferred to females during mating where they take part in the post-mating response (PMR) (Corrigan et al., 2014; Marie et al., 2023). The PMR is induced in females by male seminal fluid factors and causes changes in female physiology and behaviour that promote male sexual competitiveness such as increased egg-laying (P. S. Chen et al., 1988), increased feeding (Carvalho et al., 2006), decreased immune responses (Fedorka et al., 2007), and decreased remating receptivity (Manning, 1962). Rab11-exosomes are specifically required to induce changes in remating behaviour and this involvement represents a relatively rare example of a well-defined *in vivo* exosome signalling pathway (Corrigan et al., 2014; Marie et al., 2023). Importantly, Rab11a-positive compartments in human cancer cells also appear to form Rab11a-exosomes which share important regulatory features with *Drosophila* Rab11-exosomes such as being formed in Rab11-positive compartments and specifically requiring accessory ESCRT-III proteins for their biogenesis (Fan et al., 2020; Marie et al., 2023). Interestingly, within at least human cells, Rab11a-exosomes possess cargo profiles and pro-cancer signalling effects that are distinct from LE-derived exosomes, indicating that Rab11-exosomes possess unique biogenesis and cargo-loading mechanisms that may be relevant for understanding cancer-related exosome signalling pathways (Fan et al., 2020).

The unique biology of SCs provides numerous advantages when studying secretory biology. Primarily, since SC DCG compartments are thousands of times larger than

equivalent structures in other cell-types, light microscopy becomes a practical approach for examining the internal processes in DCG- and exosome-forming compartments (Corrigan et al., 2014; Marie et al., 2023; Prince et al., 2019). Not only is light microscopy less time- and resource-intensive than electron microscopy, thereby allowing greater sample sizes and faster experiment turnover, but it also facilitates live-cell imaging, time-lapse imaging and colocalisation experiments in a way that is simply not possible with electron microscopy. Furthermore, for exosome study in particular, the role of SC-derived exosomes in the female PMR represent one of only a few *in vivo* exosome signalling cascades that can be practically examined (Xie et al., 2022). In combination with the general advantages of working in *Drosophila* – e.g. the short generation time, easy handling, and advanced genetic toolsets available (Tolwinski, 2017; R.-G. Xu et al., 2019) – SCs provide an ideal model for microscope-based investigations of DCG and exosome biology.

1.7 Research goals

Based on my particular interests in exosome and DCG biology, I utilised the powerful genetic tools available in *Drosophila* to study the factors regulating DCG and exosome biogenesis in the giant secretory compartments of SCs. In particular, I employed the UAS/GAL4/GAL80 temperature sensitive system to induce a range of SC-specific genetic manipulations such as RNAi expressions in SCs that could specifically report on the effects of markers for these biogenesis pathways (McGuire et al., 2003; R.-G. Xu et al., 2019). Since the SC system is still a fairly new experimental model, core aspects

of its secretory biology remained unknown. As such, I sought to firstly conduct a detailed characterisation of SC secretory compartments and then to explore the specific regulation of DCG biogenesis and Rab11-exosome biogenesis.

In particular, I looked to examine the mechanisms controlling exosome subtype-specific biogenesis for the Rab11-exosome subtype, which is produced both in *Drosophila* SCs and human cancer cells (Fan et al., 2020). SCs presented an exceptional *ex vivo* model for research into subtype-specific regulation of exosome biogenesis and exosome biology more generally.

With this in mind, I had the following core goals for my research:

1) To detail essential secretory pathway trafficking events preceding DCG and exosome biogenesis;
2) To study the mechanisms controlling DCG biogenesis in SCs;
3) To study the mechanisms controlling subtype-specific exosome biogenesis in SCs;
4) To examine links between these structures and important pathologies such as cancer and neurodegenerative disease;
5) If possible, to develop new methods/tools that could be used in the study of SC biology.

Chapter 2: Materials and Methods

2.1 Fly stocks

Genotype	Name in text	Source	Stock number
w^{1118}; +; dsx-GAL4	dsx-Gal4	(Rideout et al., 2010)	N/A
w^{1118}; P{tub-GAL80^{ts}}; +	tub-Gal80^{ts}	BDSC	7108
w^{1118}; P{tub-GAL80^{ts}}; dsx-GAL4	"Driver line"	Dr C. Mendes	N/A
w; esg-GAL4 tub-GAL80^{ts} UAS-FLP/CyO; UAS-GFP$_{nls}$ actin > FRT > CD2 > FRT > GAL4/TM6	esgF/Ots	(Jiang et al., 2009)	N/A
w^{1118}; P{ry$^{TRiP.HMS02827}$};+	Control RNAi	BDSC	44106
w^{1118}; +; TI{TI}Rab1^{EYFP}	YFP-Rab1	BDSC(Dunst et al., 2015)	62539
w^{1118}; TI{TI}Rab2^{EYFP};+	YFP-Rab2	BDSC(Dunst et al., 2015)	62540
w^{1118}; TI{TI}Rab6^{CFP}; +	CFP-Rab6	S. Eaton and F. Karch	N/A
w^{1118}; P{tub-GAL80^{ts}}, TI{TI}Rab6^{CFP}; dsx-GAL4	CFP-Rab6 background	Recombined in Wilson lab	N/A
w^{1118}; +; TI{TI}Rab7^{EYFP}	YFP-Rab7	BDSC(Dunst et al., 2015)	62545
w^{1118}; P{tub-GAL80^{ts}}; dsx-GAL4, TI{TI}Rab7^{EYFP}	YFP-Rab7 background	Recombined in Wilson lab	N/A
w^{1118}; +; TI{TI}Rab11^{EYFP}	YFP-Rab11	BDSC (Dunst et al., 2015)	62549
w^{1118}; P{tub-GAL80^{ts}}; dsx-GAL4, TI{TI}Rab11^{EYFP}	YFP-Rab11 background	Recombined in Wilson lab	N/A
w^{1118}; +; TI{TI}Rab19^{EYFP}	YFP-Rab19	BDSC (Dunst et al., 2015)	62552
w^{1118}; P{tub-GAL80^{ts}}; dsx-GAL4, TI{TI}Rab19^{EYFP}	YFP-Rab19 background	Recombined in Wilson lab	N/A

w^{1118}; +; GFP-mfas$^{MI11275\text{-}GFSTF.2}$	GFP-MFAS	BDSC	63204
w^{1118}; P{tub-GAL80^{ts}}; dsx-GAL4, GFP-mfas$^{MI11275\text{-}GFSTF.2}$	GFP-MFAS background	Recombined in Wilson lab	N/A
w[*]; TI{T-STEP.TagRFP-T}Vps35[KI]	Vps35-RFP	BDSC	66527
w^{1118}; +; P{UAS-GFP.GPI}	GFP-GPI	(Greco et al., 2001)	N/A
w^{1118}; P{tub-GAL80^{ts}}; dsx-GAL4, P{UAS-GFP.GPI}	GFP-GPI background	Recombined in Wilson lab	N/A
w^{1118}; +; P{Arf1^{GD12522}}	Arf1-RNAi#1	VDRC	23082
w^{1118}; P{Arf1^{KK101396}} ; +	Arf1-RNAi#2	VDRC	103572
w^{1118}; +; P{AP-1γ$^{TRiP.JF02684}$};	AP-1γ-RNAi	BDSC	27533
w^{1118}; +; P{AP-1μ^{GD14206}}	AP-1μ-RNAi	VDRC	24017
w^{1118}; P{AP-1σ^{KK108869}}; +	AP-1σ-RNAi	VDRC	107322
w^{1118}; +; P{Rab6$^{TRiP.HMS01486}$}	Rab6-RNAi#1	BDSC	35744
w^{1118}; +; P{Rab6$^{TRiP.JF02640}$}	Rab6-RNAi#2	BDSC	27490
w^{1118}; +; P{Rab11$^{TRiP.JF02812}$}	Rab11-RNAi#1	BDSC	27730
w^{1118}; P{Rab11^{KK108297}}; +	Rab11-RNAi#2	VDRC	108382
w^{1118};+; P{APPL^{GD3170}}	APL-RNAi	VDRC	42673
y, v;+; P{GAPDH2$^{TRiP.JF02072}$}	GAPDH2-RNAi	BDSC	26302
y, w^{1118};; UAS-Aβ$_{42}^{D694N\text{-}Iowa}$	Aβ42$_{Iowa}$	BDSC	33779
w^{1118}; UAS-Aβ$_{42}^{E693Q\text{-}Dutch}$	Aβ42$_{Ducth}$	BDSC	33775
y^1 sc^* v^1 sev^{21}; P{Bet3$^{TRiP.HMS01764}$}	Bet3-RNAi	BDSC	38302
w^{1118}; P{Chmp5^{KK109120}}; +	Chmp5-RNAi#1	VDRC	*101422*
w^{1118}; +; P{Chmp5^{GD10565}}	Chmp5-RNAi#2	VDRC	*25990*
y^1 v^1; P{Hrs$^{TRiP.JF02860}$ }	Hrs-RNAi	BDSC	28026
w; P{w^+, UAS-Dad}	UAS-Dad	(Tsuneizumi et al., 1997)	N/A
w;ubi-DE-Cadherin-tagRFP, P{tub-GAL80^{ts}}; dsx-GAL4	Ecad-RFP	(Michel et al., 2011)	N/A
w; UAS-GFP-Hrs/Xa	Hrs-GFP	(Marie et al., 2023)	N/A
y^1 v^1; +; P{ Ecad$^{TRiP.JF02769}$}	Ecad-RNAi#1	BDSC	27689
y^1 v^1; P{ Ecad^{KK103334}};+	Ecad-RNAi#2	VDRC	103962
w^{1118}; P{Rab19^{KK107774}};+	Rab19-RNAi#1	VDRC	103653
y^1 sc^* v^1 sev^{21}; +; P{Rab19$^{TRiP.HMS00592}$}	Rab19-RNAi#2	BDSC	34607
w^{1118}; +; P{Nuf$^{TRiP.HMS02713}$}	Nuf-RNAi	BDSC	17279
y^1 sc^* v^1; +; P{Rip11$^{TRiP.HMS01792}$}	Rip11-RNAi	BDSC	38325
y^1 w; +; nuf$^{MI09643\text{-}GFSTF.2}$*	Nuf-GFP	BDSC	61802

y¹ v¹; +; P{ Sec6$^{TRiP.JF02623}$}	Sec6-RNAi	BDSC	27314
y¹ sc v¹ sev²¹; +; P{Sec8$^{TRiP.HMC04748}$}*	Sec8-RNAi	BDSC	57441
w^{1118}; +; P{Sec15^{GD12109}}	Sec15-RNAi	VDRC	35161
y¹ sc v¹ sev²¹; +; P{Exo70$^{TRiP.GLC01851}$}*	Exo70-RNAi	BDSC	55234
y¹ v¹; +; P{Exo84$^{TRiP.JF03139}$}	Exo84-RNAi	BDSC	28712
y¹ sc v¹ sev²¹; +; P{Rala$^{TRiP.HMS01365}$}*	Rala-RNAi	BDSC	34375
w; P{UAS-Rala^{S25N}}2; +*	Rala-DN	BDSC	32094
y¹ v¹; +; P{Magi$^{TRiP.JF01798}$}	Magi-RNAi#1	BDSC	25792
y¹ sc v¹ sev²¹; +; P{Magi$^{TRiP.GL00180}$}*	Magi-RNAi#2	BDSC	35279
y¹ sc v¹ sev²¹; P{Flo1$^{TRiP.GL00609}$};+*	Flo1-RNAi	BDSC	36649
y¹ sc v¹ sev²¹; P{Flo2$^{TRiP.GLC01829}$};+*	Flo2-RNAi	BDSC	55212
y¹ v¹; P{Mec2$^{TRiP.HMJ23038}$};+	Mec2-RNAi	BDSC	61259
y¹ sc v¹ sev²¹; +; P{Phb1$^{TRiP.HMS00399}$}*	Phb1-RNAi	BDSC	32404
y¹ v¹; P{Phb2$^{TRiP.HMS02001}$};+	Phb2-RNAi	BDSC	40835
w^{1118}; +; P{StomL2^{KK109375}}	StomL2-RNAi	VDRC	110562
y¹ sc v¹ sev²¹; +; P{Vps34$^{TRiP.HMS00261}$}*	Vps34-RNAi#1	BDSC	33384
y¹ sc v¹ sev²¹; +; P{Vps34$^{TRiP.GL00175}$}*	Vps34-RNAi#2	BDSC	36056
w^{1118}; +; P{InR^{GD104}}	InR-RNAi	VDRC	991
W; +; P[w+;UAS-InR^{wt}]	UAS-InR	(Brogiolo et al., 2001)	N/A
w^{1118}; +; P{Dp110^{GD11228}}	Dp110-RNAi#1	VDRC	38985
y¹ v¹; +; P{Magi$^{TRiP.HMC02413}$}	Dp110-RNAi#2	BDSC	44491
W; P{w+; UAS-DPTEN FF20.2}; +	UAS-PTEN#1	(Goberdhan et al., 1999)	N/A
W; P{w+; UAS-DPTEN FF20.5}; +	UAS-PTEN#2	(Goberdhan et al., 1999)	N/A
w^{1118}; +; P{PTEN^{GD13500}}	PTEN-RNAi#1	VDRC	35731
w^{1118}; P{PTEN^{KK109278}}; +	PTEN-RNAi#2	VDRC	101475
y¹ v¹; +; P{Akt$^{TRiP.HMS00007}$}	Akt-RNAi	BDSC	33615
y¹ v¹; +; P{raptor$^{TRiP.JF01088}$}	raptor-RNAi#1	BDSC	31529
y¹ v¹; P{raptor$^{TRiP.HMS02306}$}; +	raptor-RNAi#2	BDSC	41912
y¹ sc v¹ sev²¹; +; P{SUMO$^{TRiP.HMS01540}$}*	SUMO-RNAi#1	BDSC	36125
y¹ v¹; +; P{SUMO$^{TRiP.JF02869}$}	SUMO-RNAi#2	BDSC	28034
w^{1118}; P{SUMO^{KK101786}}; +	SUMO-RNAi#3	VDRC	105980
y¹ v¹; +; P{lwr$^{TRiP.JF01386}$}	lwr-RNAi	BDSC	31396
w; P{UAS-lwr.DN}3, P{ActGFP}JMR2; +*	lwr-DN	BDSC	9318
w^{1118}; +; P{PTEN^{GD7581}}	Ulp1-RNAi	VDRC	31744
y¹ v¹; +; P{Su(var)2-10$^{TRiP.JF03384}$}	Su(var)2-10-RNAi#1	BDSC	29448

$y^1\ v^1;\ +;\ P\{Su(var)2\text{-}10^{TRiP.JF01408}\}$	Su(var)2-10-RNAi#2	BDSC	31623
$y^1\ v^1;\ +;\ P\{tna^{TRiP.JF02907}\}$	tna-RNAi#1	BDSC	28070
$y^1\ v^1;\ +;\ P\{tna^{TRiP.JF02536}\}$	tna-RNAi#2	BDSC	29372
$y^1\ sc^*\ v^1\ sev^{21};\ P\{Ald1^{TRiP.HMC06146}\};\ +$	Ald1-RNAi#1	BDSC	65884
$w^{1118};\ P\{Ald1^{KK107680}\};\ +$	Ald1-RNAi#2	VDRC	101339
$w^{1118};\ P\{dlp^{KK107351}\};\ +$	dlp-RNAi	VDRC	100268
$w^{1118};\ P\{Emp^{GD3569}\};\ +$	Emp-RNAi#1	VDRC	12232
$y^1\ sc^*\ v^1\ sev^{21};\ P\{Emp^{TRiP.HMS02195}\};\ +$	Emp-RNAi#2	BDSC	40947
$w^{1118};\ P\{Hrb87F^{KK108162}\};\ +$	Hrb87F-RNAi	VDRC	100732
$w^{1118};\ +;\ P\{Rbp1^{GD9289}\}$	Rbp1-RNAi#1	VDRC	21083
$y^1\ sc^*\ v^1\ sev^{21};\ P\{Rbp1^{TRiP.HMC03902}\};\ +$	Rbp1-RNAi#2	BDSC	55688
$w^{1118};\ P\{Set^{KK107410}\};\ +$	Set-RNAi	VDRC	108987
$w^{1118};\ P\{Arc1^{KK115868}\};\ +$	Arc1-RNAi#1	VDRC	109141
$w^{1118};\ +;\ P\{Arc1^{GD16710}\}$	Arc1-RNAi#2	VDRC	48131
$y^1\ v^1;\ +;\ P\{Fs(2)Ket^{TRiP.JF01755}\}$	Fs(2)Ket-RNAi#1	BDSC	31242
$w^{1118};\ P\{Fs(2)Ket^{KK112702}\};\ +$	Fs(2)Ket-RNAi#2	VDRC	107662
$w^{1118};\ +;\ P\{Hsp83^{GD1202}\}$	Hsp83-RNAi#1	VDRC	7716
$w^{1118};\ P\{Hsp83^{KK101256}\};\ +$	Hsp83-RNAi#2	VDRC	108568
$w^{1118};\ +;\ P\{PromL^{GD2271}\}$	PromL-RNAi#1	VDRC	51957
$w^{1118};\ P\{PromL^{KK103090}\};\ +$	PromL-RNAi#2	VDRC	102612
$w^{1118};\ P\{Rap1^{KK107785}\};\ +$	Rap1-RNAi#1	VDRC	110757
$w^{1118};\ +;\ P\{Rap1^{GD9686}\}$	Rap1-RNAi#2	VDRC	33437
$y^1\ sc^*\ v^1\ sev^{21};\ +;\ P\{Rac1^{TRiP.HMS01258}\}$	Rac1-RNAi	BDSC	34910
$w^{1118};\ P\{Hrb98DE^{GD14939}\};\ +$	Hrb98DE-RNAi	VDRC	29523
$w^{1118};\ P\{Hsc\text{-}70\text{-}4^{KK108223}\};\ +$	Hsc-70-4-RNAi#1	VDRC	101734
$w^{1118};\ +;\ P\{Hsc\text{-}70\text{-}4^{GD11264}\}$	Hsc-70-4-RNAi#2	VDRC	26465
$w^{1118};\ P\{Nlp^{GD12319}\};\ +$	Nlp-RNAi#1	VDRC	22623
$y^1\ sc^*\ v^1\ sev^{21};\ +;\ P\{Nlp^{TRiP.HMS00556}\}$	Nlp-RNAi#2	BDSC	33688
$y^1\ sc^*\ v^1\ sev^{21};\ +;\ P\{Pyk^{TRiP.GL00099}\}$	Pyk-RNAi#1	BDSC	35218
$w^{1118};\ P\{Pyk^{GD16178}\};\ +$	Pyk-RNAi#2	VDRC	49533
$w^{1118};\ P\{Rac2^{GD13964}\};\ +$	Rac2-RNAi#1	VDRC	28926
$w^{1118};\ +;\ P\{Rac2^{GD17536}\}$	Rac2-RNAi#2	VDRC	50349
$w^*;\ P\{UAS\text{-}GFP\text{-}dlp.E\}3$	dlp-GFP	BDSC	94556

w; +; UAS-dARC1-GFP	Arc1-GFP	(Montana & Littleton, 2006)	N/A
w; +; UAS-darc1-UGR-GFP	Arc1-UGR-GFP	(Ashley et al., 2018)	N/A

Table 2.1, List of all *Drosophila* stocks used to produce the data shown in this thesis. The genotype, in text name, source (either the relevant public stock centre or original publication) and stock number (if appropriate) are shown. Stocks were sourced from two public stock centres, Bloomington *Drosophila* Stock Centre (BDSC) (Ni et al., 2009) and Vienna *Drosophila* Resource Centre (VDRC) (Dietzl et al., 2007).

2.2 Fly husbandry

All flies were housed in either plastic vials or plastic bottles containing a cornmeal-agar-glucose mixture. This food mixture was made from mixing, per litre of water, 93 g D- (+)-glucose (Sigma-Aldrich®) 75 g cornmeal (BTP Drewitt), 31.5 g inactivated yeast (Lallemand Baking), 12.5 g agar (F Gutkind & Co. Ltd), 8.6 g potassium sodium tartrate tetrahydrate (Sigma-Aldrich®), 2.5 g methyl 4-hydroxybenzoate dissolved in 12 ml ethanol (Sigma-Aldrich®) and 0.7 g calcium chloride dihydrate (Sigma-Aldrich®). Stock lines were typically kept at 19°C when not being amplified. Older bottles being used for virgin fly collection and experimental crosses were stored at 25°C to increase the rate of development of the flies. Stock lines were transferred into new vials/bottles with fresh food medium after 1-2 generations had eclosed (typically 2-4 weeks). Flies used in experimental crosses was transferred into new vials with fresh food medium every

4-6 days to prevent them from mating with their offspring which eclose as adults after 10-11 days at 25°C.

Virgin female flies which were used to create experimental crosses were collected in the mornings from older bottles. Putative virgins were selected and moved into new vials in small groups (typically < 8 individuals). These putative virgins were then stored for at least 4 days at 19°C and checked for larvae before being used in experiments.

2.3 Control of transgene expression in SCs

Secondary cell-specific expression of transgenes was achieved using the GAL4-GAL80^{ts}-UAS regulatory system (Fig. 2.1). In this system, the GAL4 transcription driver binds to UAS promoter sequences and induces transcription unless blocked by GAL80^{ts}, a temperature sensitive inhibitor of GAL4. At temperatures below 29°C, GAL80^{ts} inhibits GAL4 activity, blocking UAS-transgene expression. At temperatures above 29°C, temperature-sensitive GAL80 fails to function and UAS-transgenes are highly transcribed.

In all microscope-based experiments, SC-specific transgene expression was achieved by placing *GAL4* under the control of *dsx* regulatory sequences, with *dsx* being highly expressed specifically in SCs within the accessory gland. In physiological assays examining the effects of Rab11-exosome signalling on female remating behaviour, SC-specific transgene expression was instead achieved using the esgF/Ots transgene combination (H. Jiang et al., 2009), which permits SC-specific, UAS-mediated gene expression within male reproductive systems. By placing *GAL4* under either of these regulatory sequences and *GAL80^{ts}* under universally expressed *ubi* regulatory

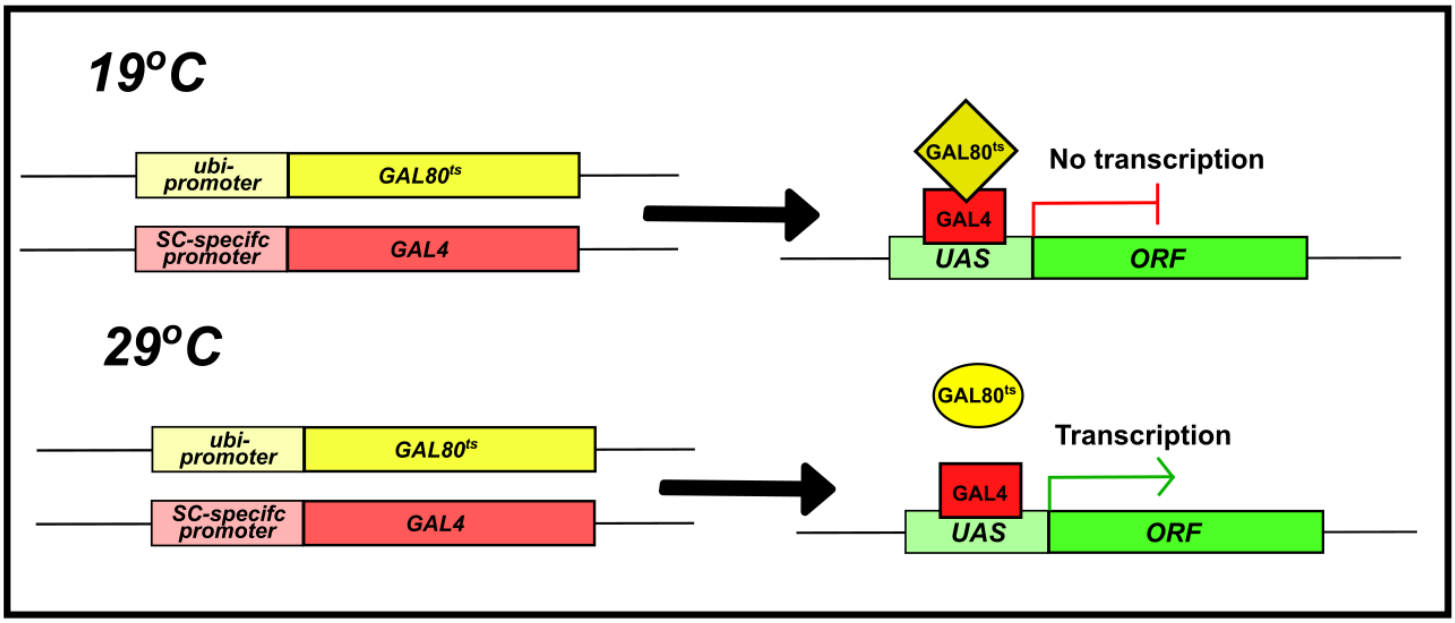

Figure 2.1. Schematic of UAS/GAL4/GAL80^{ts} expression system. At restrictive temperatures (19C) GAL80^{ts} protein binds to and inhibits GAL4 activity, preventing transcription. At permissive temperatures (29C) GAL80^{ts} fails to inhibit GAL4, leading to transcription of genes under UAS-control.

sequences, strong SC-specific expression of UAS-transgenes was achieved on demand by shifting individuals to a 29°C environment.

Adult male offspring were collected on the day they eclosed and, unless otherwise stated, moved to a 29°C incubator for 6 days post-eclosion to induce SC-specific UAS-transgene expression. In the case of timelapse imaging experiments, incubation at 29°C could vary from 5-7 days post-eclosion. Previous studies have indicated that incubation at 29°C for this period does not affect SC morphology or block male fertility (Corrigan et al., 2014; Fan et al., 2020; Marie et al., 2023), findings I confirmed by showing that the numbers and organisation of specific secretory compartment populations are unaffected by temperature (Appendix 8.1).

2.4 Remating assays

To investigate the effects of different regulators on Rab11-exosome signalling *in vivo,* SC-specific, UAS-mediated transgene expression was induced in virgin male flies carrying the esgF/Ots transgene combination by shifting them to a 29°C environment for 6 days post-eclosion (H. Jiang et al., 2009). Males were then separated, placed into a vial containing a single virgin female of the w^{118} genotype and incubated overnight to allow mating. After 24 hours, females were separated into individual vials and kept at 19°C whilst males were returned to a 29°C environment for another 24-hour period with new virgin w^{118} females. This was repeated until males had mated with three virgin females for three separate 24-hour periods. After three matings, males were discarded. Mated females were flipped into fresh vials after 3 days, and old vials were

kept to check for larvae so that successful mating could be confirmed. Once in the new vials, mated females were introduced to individual Canton S males that were 4–8 days old for a 1-hour period each day. During this time, vials were kept at room temperature and without disturbance, though they were observed so that any mating events could be recorded. If mating occurred within that 1-hour period, this was recorded and the relevant vial was discarded. If no mating occurred, then the female flies were again separated without anaesthesia into individual vials and kept for repeat experiments the next day. In cases where females died or escaped before remating, the date of their loss was recorded.

2.5 Dissection and mounting

To prepare accessory glands for live-cell imaging, glands were dissected out of males into chilled PBS. If lysosomes were visualised, then these accessory glands were incubated with either 500nM Lysotracker Red DN-99 (Invitrogen) or 500nM LysoSensor Yellow/Blue DND-160 (Invitrogen) for 5 minutes on ice and washed again with chilled PBS. Glands were then mounted in a small drop of PBS between two coverslips (thickness No. 1.5H, Marienfeld-Superior) supported by a custom-made metal mount. Finally, after mounting, filter paper was used to draw off excess PBS until glands were slightly flattened against the glass.

For time-lapse imaging experiments, dissection and mounting proceeded as described above. However, separating oil was used to create a circle into which the glands were mounted in a drop of PBS. This ring of oil prevented evaporation of PBS

over the course of time-lapse experiments and so kept glands from dehydrating and being crushed between the coverslips.

2.6 Live cell microscopy

Following dissection and mounting, accessory glands were visualised using the DeltaVision Elite inverted wide-field fluorescence microscope (GE Healthcare Life Sciences). Live SCs were analysed using both fluorescence and differential interference contrast (DIC) microscopy which allowed us to determine the localisation of specific molecules and assess the overall organisation of SCs. In all cases, SCs were viewed at 1000X magnification using a 100x objective lens (Olympus UPlanSApo NA 1.4; oil objective) with immersion oil with refractive index of 1.514 (Cargille labs) and an EMCCD Evolve-512 camera. Imaging was carried out at ~18°C. For experiments other than time-lapse imaging, Z-stacks with 0.3 µm spacing between slices were obtained for three SCs per gland, with ≥10 glands typically being imaged and analysed per genotype. All image files used the maximum pixel density (512 x 512 pixels) and were saved as 16-bit files.

To avoid selection bias, the SCs chosen for imaging were always the group of three SCs closest to the tip of an accessory gland arm which could fit into a single frame and therefore be imaged together in apical cross-section. This had the added benefit of reducing photobleaching and the duration of live-cell imaging experiments. When no group of three SCs was close enough to be imaged together, a Z-stack was obtained of the two SCs closest to the tip of an accessory gland arm which could be imaged

together, and another Z-stack was obtained of the single SC closest to the tip of the other accessory gland arm.

2.7 Time-lapse imaging

The imaging parameters for time-lapse experiments varied depending on the fluorophores used and the biological process that was being tracked. Imaging still utilised 1000X magnification, however, to minimise photobleaching and phototoxicity, lower laser intensities were employed and spacing between Z-stacks slices was increased from 0.3 µm to 0.5-1 µm. In certain experiments such as those imaging the Rab6 to Rab11 transition, Z-stacks were not acquired and only a single representative plane was imaged at each timepoint. Likewise, the frequency of sampling varied between experiments with the gaps between timepoints ranging from 1 minute to 14 minutes. Beyond 14 minutes the motion of compartments became difficult to accurately track.

By their nature, our timelapse experiments were more time and resource intensive than our other live-cell imaging experiments. The data they produced was also less suited to quantification since timelapse experiments were typically used to view the processes occurring in just a single secretory compartment over time. As a result, it was generally not feasible to subject the results of timelapse imaging experiments to the same statistical analyses we used for other live-cell imaging experiments. To ensure our observations were representative however, a minimum of 3 timelapse imaging experiments with consistent findings were required. These experiments were

required to be carried out using accessory glands from ≥3 individuals dissected and imaged in separate experiments.

2.8 Deconvolution

Deconvolution was carried out using Resolve 3D-constrained iterative deconvolution algorithm within SoftWoRx 5.5 Software (GE Healthcare Life Sciences) to improve the signal:noise ratio in images prior to analysis. Images from non-time-lapse experiments were saved as 16-bit images, but the final results of time-lapse deconvolution were saved as 32-bit floating point images.

Unless otherwise stated, all display images included in this thesis were produced using single representative, deconvolved Z-slices from the relevant genotype. The exceptions to this are:

1) Panels displaying time-lapse imaging experiments where no Z-stack was acquired and deconvolution was not carried out.
2) Panels displaying time-lapse imaging experiments of DCG biogenesis where, to best show all the materials in compartments of interest, z-projections were used that include fluorescent signal from every z-slice within the bounds of the relevant compartment. In these cases, a single representative slice from the DIC channel is still used, taken from the centre of the compartment of interest.

2.9 Analysis on Fiji/ImageJ

After Z-stacks had been acquired from live-cell imaging, the organisation of SCs was assessed using the Fiji/ImageJ software. Most forms of analysis were done by visually examining the data and taking quantitative measurements of features within SCs. Whenever data was analysed visually, certain steps were taken to limit the effects of biases on the results. Firstly, data from numerous genotypes (typically 5-8 genotypes) was collected together and anonymised before analysis. The only genotypes for which this was not the case were *Arf1*, *AP1*, *Rab6* and *Rab11* knockdown data shown in chapter 4. Secondly, guidelines were created for each type of measurement which were applied equally to all relevant analyses (Appendix 8.2).

2.10 Statistical analysis

All statistical analyses were carried out using the GraphPad Prism software. Wherever relevant, statistical analyses were performed using non-parametric tests. Genotypes from remating analyses were compared using the Gehan-Breslow-Wilcoxon test. Where only two datasets were assessed, i.e. one control and one experimental group, statistical significance was determined using the Mann-Whitney test. Where >2 datasets were analysed together, statistical significance was determined using the Kruskal-Wallis test followed by Dunn's multiple comparisons post hoc test with a Bonferroni correction of P values for Type 1 errors. The results of each experimental genotype was compared to results from a control group.

Within this thesis, groupings of datasets that were analysed together have sometimes been divided between multiple figures to maintain clarity when presenting data. However, statistical significance was always determined for the entire grouping at once, with a single control genotype compared pairwise to all other experimental genotypes. As such, the following pairs or trios of graphs display the same control dataset:

4.8C and 6.5G; 4.8E and 5.10K 5.1F and 5.2C; 5.1G and 5.2D; 5.7D and 6.4G; 5.7E and 5.12E; 5.8E and 5.9D; 5.8G and 5.9E; 5.11E, 5.13C and 5.16F; 5.11F, 5.13D and 5.16G; 6.2D-F and 6.3D-F; 6.5 H,I and J.

Chapter 3: Organisation and maturation of SC secretory compartments

3.1 Introduction and aims

3.1.1 Aims

Although the *Drosophila* SC model has been used in several studies and shows great promise as a model for understanding secretory compartment biology, it is still a relatively new experimental model and has not yet been fully characterised in terms of the different types of secretory compartment present or their behaviour. This posed a number of interesting questions, as these are features that are also only partially described in other secretory cell types where technical limitations have made it significantly more difficult to investigate aspects like compartment identity and maturation. I therefore had two initial aims:

1) To produce a more detailed characterisation of SC biology, with a particular focus on the number and identity of different large compartments;
2) To identify key trafficking changes that occurred in SCs in the lead up to major events such as DCG and exosome biogenesis.

3.1.2 Previous work on secretory compartment markers in SCs

One of the main guides for this research was previous work carried out in the SC system which I looked to expand on. Collaborative work with our group led by Dr E. Prince showed that large secretory compartments in SCs are marked by several members of the Rab family of GTPase proteins (Prince et al., 2019), a conserved family of trafficking regulators that act in endosomal and secretory pathways (Homma et al., 2021; Jin et al., 2021; Pylypenko et al., 2018). In particular, Rab6, Rab11 and Rab19 were found to be important markers of large secretory compartments in SCs (Prince et al., 2019).

Rab6 is a well-established Golgi marker and in fact represents the most abundant small GTPase associated with the Golgi apparatus (Gilchrist et al., 2006). Rab6 has been reported to be associated with all parts of the Golgi apparatus and is required for numerous intra-Golgi trafficking pathways, including medial-trans Golgi anterograde trafficking and rapid retrograde pathways that enable effective endosome-ER trafficking (Dickson et al., 2020; Goud et al., 2018; Kawamura et al., 2014; White et al., 1999). However, Rab6 is specifically enriched within the TGN where it mediates anterograde trafficking toward endosomes and apical secretory pathways (Dunst et al., 2015; Iwanami et al., 2016; Satoh et al., 2016). Within this context, Rab6 has been implicated in DCG biogenesis in several different systems including mammalian cell lines and *Drosophila* salivary glands, although the mechanisms by which it promotes DCG biogenesis are not well characterised (C. Ma & Brill, 2021; Miserey-Lenkei et al., 2010).

In contrast to Rab6, Rab11 is primarily associated with REs (Kelly et al., 2012; Naslavsky & Caplan, 2018). Rab11 plays a role in many cellular and developmental processes, including maintenance of endosome homeostasis, establishment of cell polarity, recycling of plasma membrane proteins and apical secretion (Jing & Prekeris, 2009; Kelly et al., 2012; B. X. Li et al., 2007; Zulkefli et al., 2019). Of particular interest for my research, in addition to its role in the REs, Rab11 is also one of several endosomal Rabs associated with matured DCG compartments (Sugawara et al., 2009a). Indeed, Rab11 was found to regulate secretory granule size through an as yet undefined maturation mechanism (Neuman et al., 2021).

Finally, Rab19 is a poorly studied Rab that is derived from an ancestral Rab1 duplication and which is structurally related to mammalian Rab19 and Rab43 (Gillingham et al., 2014). Rab43 is the better studied of these and localises to the Golgi apparatus, particularly the medial-Golgi where it regulates the sorting of specific membrane proteins (Cox et al., 2016; Goud et al., 2018). Rab19 meanwhile localises to vesicles near the apical membrane, with mammalian Rab19 implicated in cortical remodelling and *Drosophila* Rab19 suggested to function in apical secretion (Dunst et al., 2015; Jewett et al., 2021; Prince et al., 2019).

In addition to these three markers of large secretory compartments in *Drosophila* SCs, unpublished preliminary images by Dr B. Kroeger indicated that populations of small SC compartments were labelled by Rab1 and Rab2 (Kroeger, 2017). Both Rab1 and Rab2 are markers of the ER and Golgi which function in pre-Golgi maturation and ER-Golgi trafficking (Alvarez et al., 2003; Galea & Simpson, 2015; Saraste, 2016). Rab1 and Rab2 have also both been linked to the process of DCG biogenesis, with Rab2 being

indirectly linked via the role of two Rab2-interacting proteins in DCG compartment maturation, whilst Rab1 has been more directly tied to the process via its colocalisation with Rab6 on maturing secretory granule-compartments and its role in driving secretory granule growth alongside Rab11 (Ailion et al., 2014; C. Ma & Brill, 2021; Neuman et al., 2021).

Building on these previous findings, my initial aim was to gain deeper insights into the specific localisation and function of each of these Rab GTPases in SCs. Although imaging of Rabs in SCs had been conducted previously, in particular by Prince et al., this imaging was primarily conducted in fixed cells using *Drosophila* lines expressing YFP-Rabs from the endogenous *Rab* locus, meaning that compartment morphology was not ideally preserved and that the overlap between Rab markers could not be readily assessed (Prince et al., 2019). As such, in my experiments, a mix of YFP-Rab and CFP-Rab fusion proteins under endogenous promoter control were employed so that the extent of overlap between alternatively labelled Rabs could be determined. Live-cell imaging was also utilised to better preserve SC architecture and to allow for the possibility of time-lapse imaging which could provide unique insights into the dynamics of Rab protein associations with compartments and intra-compartmental processes.

3.2 Results

3.2.1 Rab6, Rab11 and Rab19 mark distinct but overlapping populations of large secretory compartments in SCs

By examining endogenously expressed, fluorescently tagged *Rab* lines on their own and then in combination with each other, I aimed to understand the relative distribution of each marker in live SCs *ex vivo*. I began by characterising the distribution of different Rab proteins on large secretory compartments (Fig. 3.1). In control and fluorescently tagged Rab backgrounds, the acidic compartment dye LysoTracker Red stained 6.5 ± 1.7 (mean ± SD) large compartments and could either label the entire volume of compartments or could label acidic domains within compartments. No acidic-compartments were labelled by the Rab6, Rab11 or Rab19 gene traps, fitting with the accepted understanding of lysosomal compartments as being primarily labelled by Rab7. SCs in all genetic backgrounds also contained 11.0 ± 2.2 large DCG compartments and 2.7 ± 2.0 large compartments that had no DCG.

DCG compartments were not stained by LysoTracker Red and, as previously reported, DCG compartments could be labelled by any of Rab6, Rab11 or Rab19 (Fig. 3.1A-C). SCs contained 7.2 ± 1.9 large non-acidic compartments labelled by CFP-Rab6, including every non-DCG compartment (Fig. 3.1A). 14.7 ± 3.3 large non-acidic compartments were labelled by YFP-Rab11, and just 3.7 ± 1.3 were labelled entirely by YFP-Rab19 (Fig. 3.1D, results produced in collaboration with Dr C. Mendes).

Examining the distribution of the Rab proteins more closely, YFP-Rab11 and YFP-Rab19 were notable for their mostly selective labelling of DCG compartments, with 76.7 ±

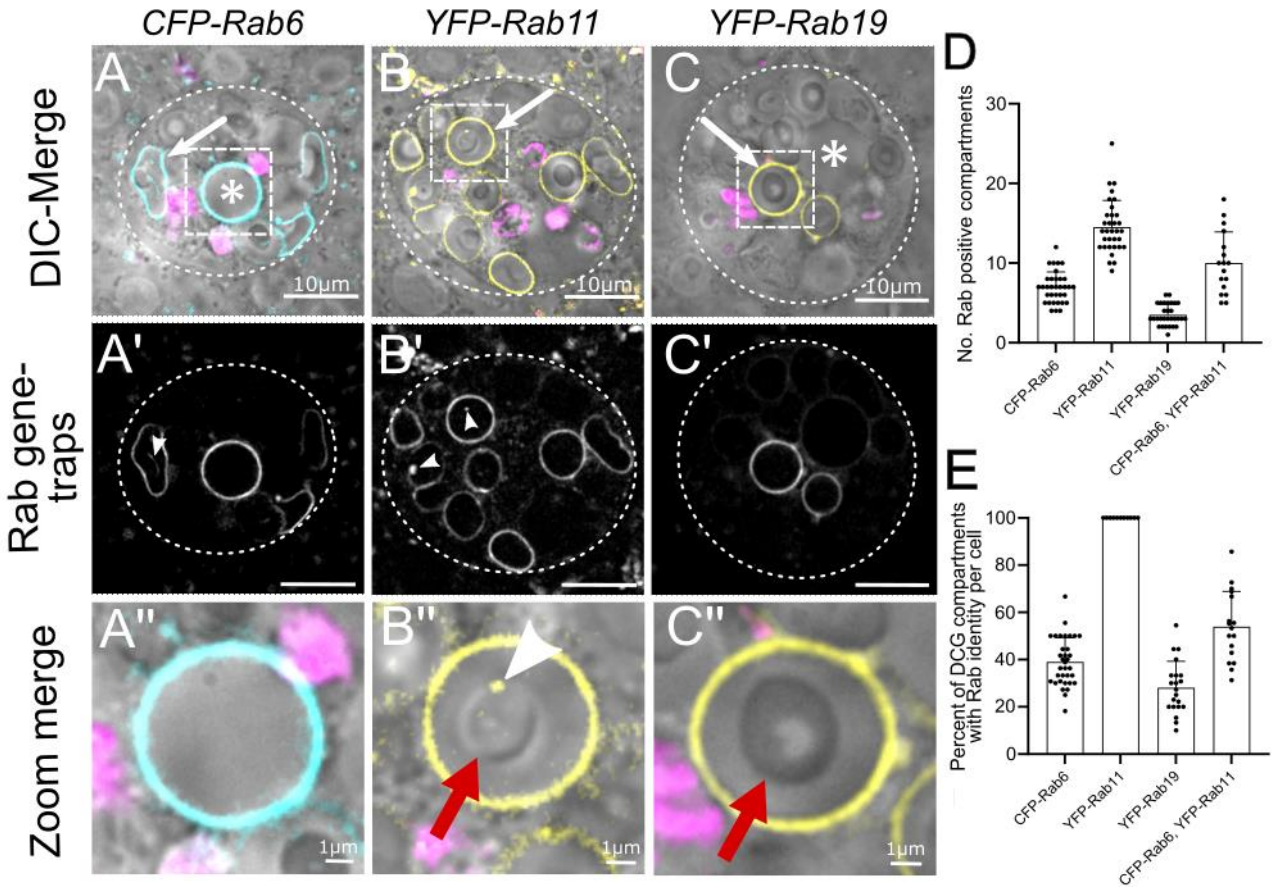

Figure 3.1. Rab6, Rab11 and Rab19 label discrete populations of large secretory compartments in SCs - (**A-C**) Wide-field fluorescence images of SCs expressing *CFP-Rab6* (**A**), *YFP-Rab11* (**B**), or *YFP-Rab19* (**C**). In multicoloured images, Rab11 and Rab19 are shown in yellow, Rab6 in cyan, LysoTracker Red in magenta and DIC images in grayscale. Representative Rab-labelled DCG compartments are indicated by white arrows, non-DCG compartments are indicated by asterixis. Rab6 was found to label all compartments without DCGs (e.g. **A"**) as well as some compartments with DCGs. Rab11 and Rab19 primarily labelled compartments with DCGs (**B"**-**C"**, red arrows indicate DCGs). Rab11 compartments often also housed Rab11-positive ILVs (**B"**, white arrowhead indicates ILVs). SCs boundaries marked by dashed circles (**D**) Bar charts showing number of non-acidic compartments labelled by Rab6, Rab11, Rab19, and Rab6+Rab11. (**E**) Bar charts showing percent of DCG compartments labelled by Rab6, Rab11, Rab19, and Rab6+Rab11. Notably, 100% of DCG compartments were labelled by Rab11. For D-E, bars show mean ± n = 17 to 34 for all genotypes.

12.7% of Rab11-positive compartments and 84.3 ± 16.4% of Rab19-positive compartments containing DCGs. In terms of the proportion of total DCG compartments labelled by each Rab gene trap though, every DCG-containing compartment or 100.0 ± 0.0% of DCG compartments were labelled by YFP-Rab11, whilst just 28.1 ± 10.9% were labelled by YFP-Rab19 (Fig. 3.1E, results produced in collaboration with Dr C. Mendes). In keeping with previous results, these experiments highlighted that Rab11 marks all DCG compartments as well as a few non-DCG compartments whilst Rab19 appears to mark a subset of DCG compartments and occasional non-DCG compartments, marking approximately one non-DCG compartment per 2-3 SCs (Prince et al., 2019). From these findings, I concluded that Rab11 and Rab19 colocalise on the membranes of DCG compartments marked by Rab19.

In contrast to Rab11 and Rab19, Rab6 labelled a significant number of non-DCG compartments. Just 39.0 ± 10.1% of total DCG compartments were labelled by CFP-Rab6, but every large non-DCG compartment was labelled (Fig. 3.1E).

In each tagged Rab genetic background, it was also common to see fluorescent puncta within the lumen of non-acidic compartments (e.g. arrowheads in Fig. 3.1B). Based on previous work in the *Drosophila* SC system which demonstrated that SCs secrete exosomes, these puncta were deemed to represent intraluminal vesicles (ILVs) that incorporate a small proportion of the fluorescent Rabs during their internalisation, though other ILVs may also have been present that were not labelled by Rabs (Corrigan et al., 2014; Fan et al., 2020; Marie et al., 2023). 57.8 ± 12.9% of Rab11-compartments contained Rab11-positive ILVs and 68.9 ± 8.4% of Rab6-compartments contained

Rab6-positive ILVs. Across all genetic backgrounds, it was also notable that ILVs were closely associated with the boundaries of DCGs. Indeed, ILVs were often seen clustering near DCGs and marking extended tracts along the DCG edge (Fig. 3.2A and B, arrows). Rab6- and Rab11-positive ILVs were also observed to aggregate into bridge-like structures which frequently spanned from compartment limiting membranes to the boundary of DCGs (Fig. 3.2A and B, arrowheads).

To investigate this apparent association between DCGs and ILVs further, I compared the prevalence of ILVs in Rab6-positive compartments that did and did not contain DCGs. In compartments with DCGs, 82.6 ± 9.9 % also contained Rab6-positive ILVs. By contrast, the vast majority of non-DCG compartments contained no ILVs, with only 4.8 ± 19.8% containing ILVs overall (Fig. 3.2C). This again highlighted an unexpected association between DCGs and exosomes and suggests that the biogenesis of both structures might be linked.

To better understand the role of each compartment label, the degree of overlap between different Rab markers was assessed. YFP-Rab11 and YFP-Rab19 had already been determined to colocalise on DCG compartments labelled by YFP-Rab19, so to examine the extent of colocalization between Rab6 and both of Rab11 and Rab19, *CFP-Rab6* was expressed alongside either *YFP-Rab11* Fig. 3.3A,B) or *YFP-Rab19* in SCs (Fig. 3.3C,D). From these experiments, it was evident that significant overlap exists in the distribution of Rab6 and Rab11, whilst overlap is very limited between Rab6 and Rab19. 10.2 ± 3.8 compartments were marked by both Rab11 and Rab6 in SCs (i.e. approximately two thirds of Rab11 compartments). with the vast majority of co-labelled compartments containing DCGs. Interestingly, Rab11 was typically only

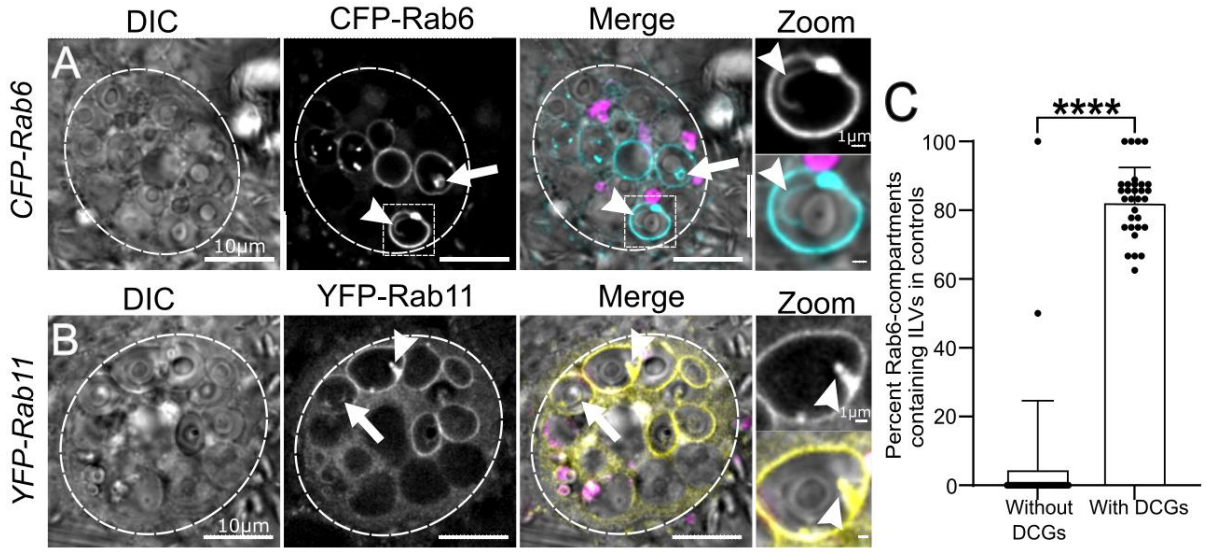

Figure 3.2. Rab6-positive and Rab11-positive compartments produce ILVs that associate with DCGs and form bridge-like structures. (**A-B**) Wide-field fluorescence images of SCs expressing *CFP-Rab6* (**A**) or *YFP-Rab11* (**B**). In multicoloured images, Rab11 is shown in yellow, Rab6 in cyan, LysoTracker Red in magenta and DIC images in grayscale. Both Rab6- and Rab11-positive compartments produce ILVs with noteworthy characteristics: Firstly, ILVs can be labelled by both of Rab6 and Rab11; Secondly, ILVs are frequently found to associate with the surface of DCGs (examples indicated by white arrows); Finally, groups of both Rab6-ILVs and Rab11-ILVs form bridge-like structures which can extend from the limiting membrane of compartments to the surface of DCGs across several micrometres (examples indicated by white arrowheads, see zoom images). SCs boundaries marked by dashed circles. (**C**) Bar charts showing percent of Rab6-compartments with and without DCGs that contain ILVs. Notably, ILVs appear to form preferentially within compartments that also contain DCGs. For graph, n=31 and P<0.0001:****

present on a minority of non-DCG compartments marked by Rab6.

CFP-Rab6- and YFP-Rab11-labelled ILVs were also observed to coexist in many compartments, with Rab6-positive ILVs often observed within Rab11- and Rab19-positive compartments (Fig. 3.3B,D). Indeed, in compartments labelled by both Rab6 and Rab11, Rab6-ILVs and Rab11-ILVs were even seen to cooperatively form bridge-like structures as described earlier (Fig. 3.3A). In this context, the two varieties of ILVs could either colocalise or remain spatially segregated. The close cooperation between these two groups may suggest that the differently labelled vesicles are functionally similar "species" of ILV which possess different Rab labelling.

In comparison to Rab6-Rab11 colocalisation, no examples were found of compartments marked by CFP-Rab6 whose membranes were also labelled wholly by YFP-Rab19. However, on compartments labelled by CFP-Rab6, including those that did not contain DCGs, a small proportion of the limiting membrane was often co-labelled by YFP-Rab19 though the function of these microdomains was not immediately apparent (Fig. 3.3C,D).

In summary, Rab6, Rab11 and Rab19 marked the highly enlarged secretory compartments found in SCs. Rab6 labelled all large non-acidic compartments that did not contain DCGs, whilst Rab11 marked all the compartments that did. There was also significant overlap between these two markers, with Rab6 and Rab11 often colocalising on DCG compartments and on sporadic non-DCG compartments. Rab19 marked a subset of DCG compartments that was distinct from the subset of Rab6-labelled compartments, yet also formed microdomains on Rab6-positive compartments. This high degree of overlap between Rab markers perhaps helps to

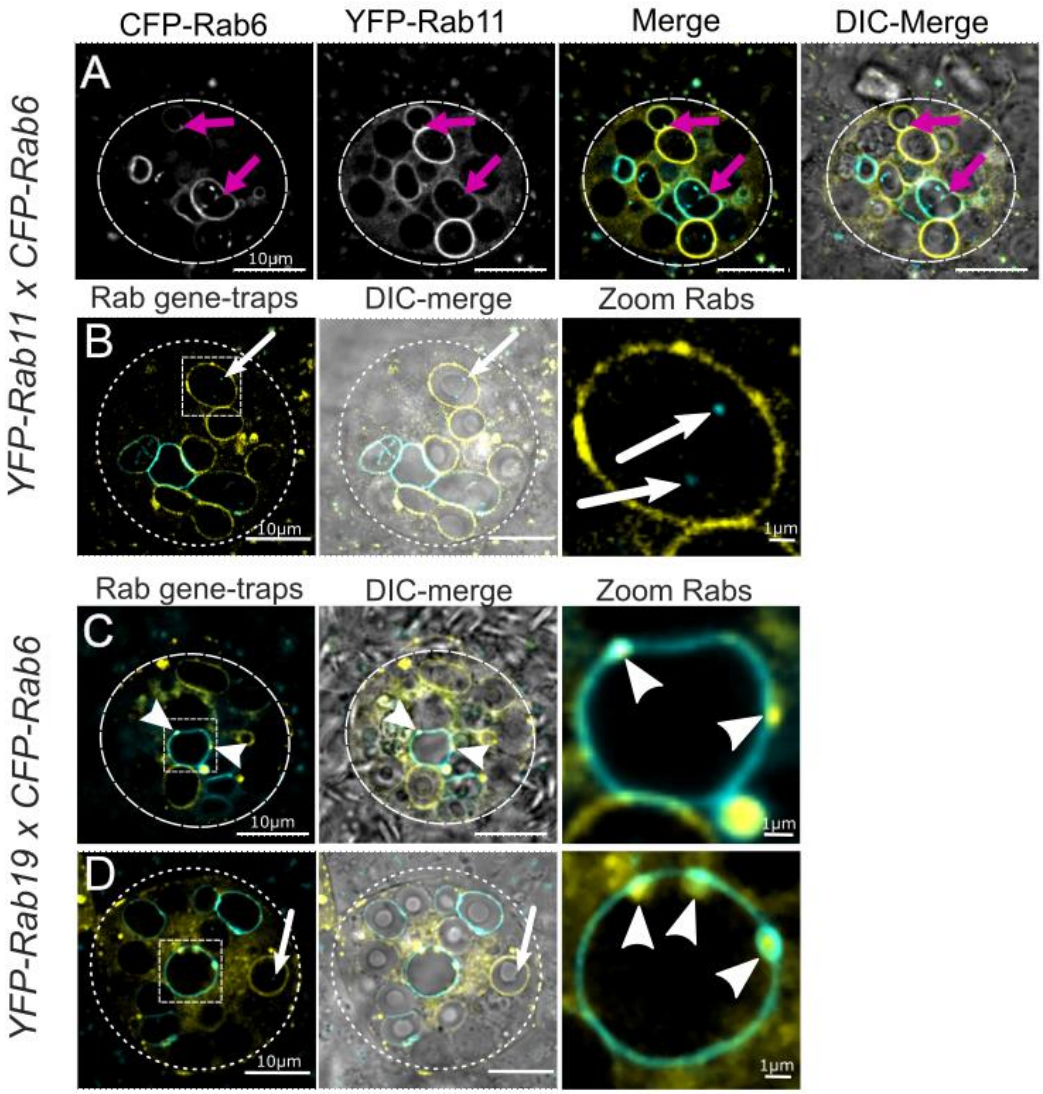

Figure 3.3. Rab6 and Rab11 overlap on the surface of certain compartments whilst Rab19 labels microdomains on Rab6-compartments. (**A-D**) Wide-field fluorescence images of SCs expressing *CFP-Rab6* alongside *YFP-Rab11* (**A,B**) or *YFP-Rab19* (**C,D**). In multicoloured images, Rab11 and Rab19 are shown in yellow, Rab6 in cyan and DIC images in grayscale. Images in **B** and **D** were acquired by Dr. Mendes. (**A**) Rab6 and Rab11 overlap on the membranes of specific compartments (e.g. magenta arrows). In these compartments, Rab6- and Rab11-ILVs can also be seen forming jointly labelled ILV bridges (e.g. magenta arrows). (**B**) Rab6-labelled ILVs (white arrows) can be located within Rab11-compartments. (**C**,**D**) Rab19 and Rab6 do not appear to co-label compartments though Rab19 does label microdomains located on compartments otherwise labelled by Rab6. White arrowheads indicate Rab19-microdomains, white arrows indicate Rab6-labelled ILVs within a Rab19-positive compartment. SCs boundaries marked by dashed circles.

explain the large admixture of Rab-labelled ILVs across compartments, with ILVs marked by specific Rabs frequently found in compartments labelled by other Rabs.

3.2.2 Rab1 and Rab2 mark smaller compartments which surround Rab6-positive compartments.

To examine the localisation of Rab1 and Rab2 in SCs, *YFP-Rab1* and *YFP-Rab2* under endogenous promoter control were visualised, first individually and then alongside CFP-Rab6. When expressed alone in live cells, YFP-Rab1 and YFP-Rab2 were each observed to mark a large number of small, centrally located compartments in SCs (Fig. 3.4A,B), a position previously thought to be occupied by the Golgi apparatus (Prince et al., 2019). The extent of Rab2 labelling on compartments appeared to be slightly less than that of Rab1, but their localisation was otherwise very similar, as would be expected for two Golgi markers.

When *CFP-Rab6* was expressed, the small compartments labelled by YFP-Rab1 and YFP-Rab2 were often found in close proximity to Rab6-positive compartments (Fig. 3.4C,D). Indeed, small Rab1 and Rab2 compartments frequently surrounded the core-less compartments marked by Rab6. This association was not evident for compartments not labelled by Rab6 but is consistent with the idea that Rab6 compartments are formed at the surface of the *TGN*.

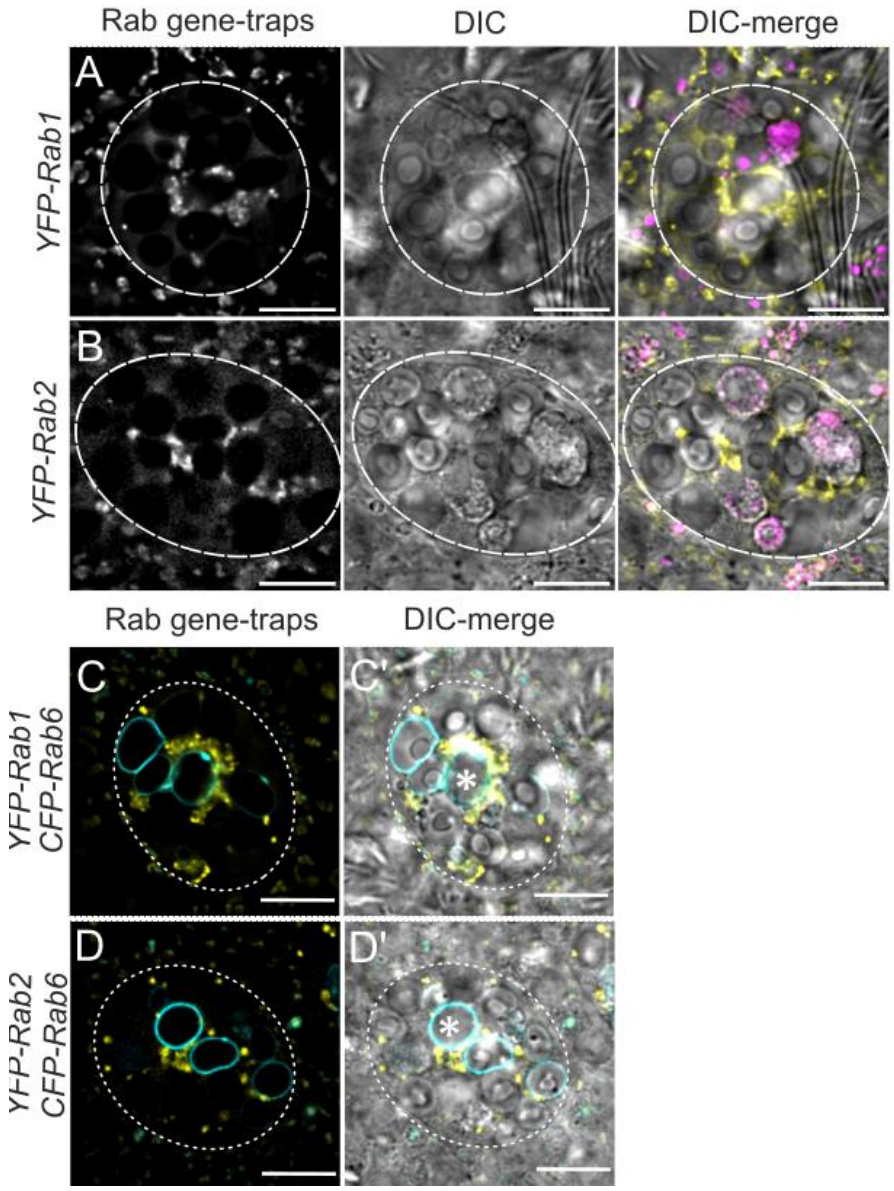

Figure 3.4. Rab1 and Rab2 label populations of small vesicles adjacent to Rab6-positive compartments. (**A-D**) Wide-field fluorescence images of SCs expressing *YFP-Rab1* (**A**), *YFP-Rab2* (**B**), and *CFP-Rab6* with *YFP-Rab1* (**C**), or *YFP-Rab2* (**D**). In multicoloured images Rab1 and Rab2 are shown in yellow, Rab6 in cyan, LysoTracker Red in magenta and DIC images in grayscale. Rab1 and Rab2 are seen in SCs to label clusters of small compartments that are often located centrally within the cell (**A**, **B**). These small Rab1- and Rab2-positive compartments also appear to exist in close proximity to larger Rab6-positive compartments (**C**, **D**). SCs boundaries marked by dashed circles, Scale bars: 10μm. Asterisks indicate non-DCG Rab6-compartments.

3.2.3 *Constructing a timeline of secretory compartment maturation events*

The distributions of different Rab-labelled compartments in *Drosophila* SCs highlighted the apparent interconnectedness of different markers, compartments and structures. Of particular interest were:

1. The colocalisation of different Rab markers on compartments, especially Rab6 and Rab11;
2. The association of small Rab1-/Rab2-positive compartments with Rab6-positive ones;
3. The presence of Rab-labelled ILVs in compartments that were not labelled by that Rab;

When viewed together, these observations suggest a dynamic, interrelated system of trafficking exists within SCs. I therefore hypothesised that these observations were best explained by compartments progressively converting between differently labelled compartment types. With this hypothesis in mind, I decided to take advantage of the unique biology of SCs by observing them using time-lapse imaging. This would provide direct evidence of any trafficking and interconversion events between compartment types and would enable additional insights into compartment dynamics that would not be possible using other approaches. I therefore worked to develop new time-lapse imaging protocols for use in the accessory gland and applied them to understanding the relationships between different compartments.

3.2.4 Small Rab1-positive compartments are the precursors of large Rab6-positive core-less compartments

To begin to understand the connections between secretory compartments in SCs, the relationship between small Rab1-positive compartments and the larger Rab6-positive compartments they contact was investigated. Since Rab1 is typically associated with endoplasmic reticulum exit sites as well as Golgi stacks, and Rab6 is associated with the *trans*-Golgi network (Miserey-Lenkei et al., 2010), I hypothesised that small Rab1-positive compartments might contribute to the development of Rab6-positive compartments. This could occur either through trafficking between these compartments (as has been suggested to occur via the ER-Golgi intermediate compartment) or by Rab1-positive compartments maturing into Rab6-positive compartments a phenomenon that has been observed in yeast (Thomas et al., 2021).

Through time-lapse imaging of SCs that were expressing both *YFP-Rab1* and *CFP-Rab6*, I demonstrated that Rab1-positive compartments directly transition into Rab6-positive ones over time (Fig. 3.5). In the Figure 3.5 example, a small Rab1-labelled compartments with a diameter of approximately 0.5 µm was seen to increase in size until it reached ~3 µm in diameter (Fig. 3.5A-C). Simultaneously, the Rab1 on the compartment's membrane was gradually displaced by Rab6. Eventually, over the course of 30 to 60 minutes, this process resulted in the biogenesis of a large Rab6-positive compartment that did not contain a DCG (Fig. 3.5D). In addition, the continued tracking of this compartment demonstrated that after formation, the non-DCG compartment could contract in volume again and then form a DCG (Fig. 3.5E). These

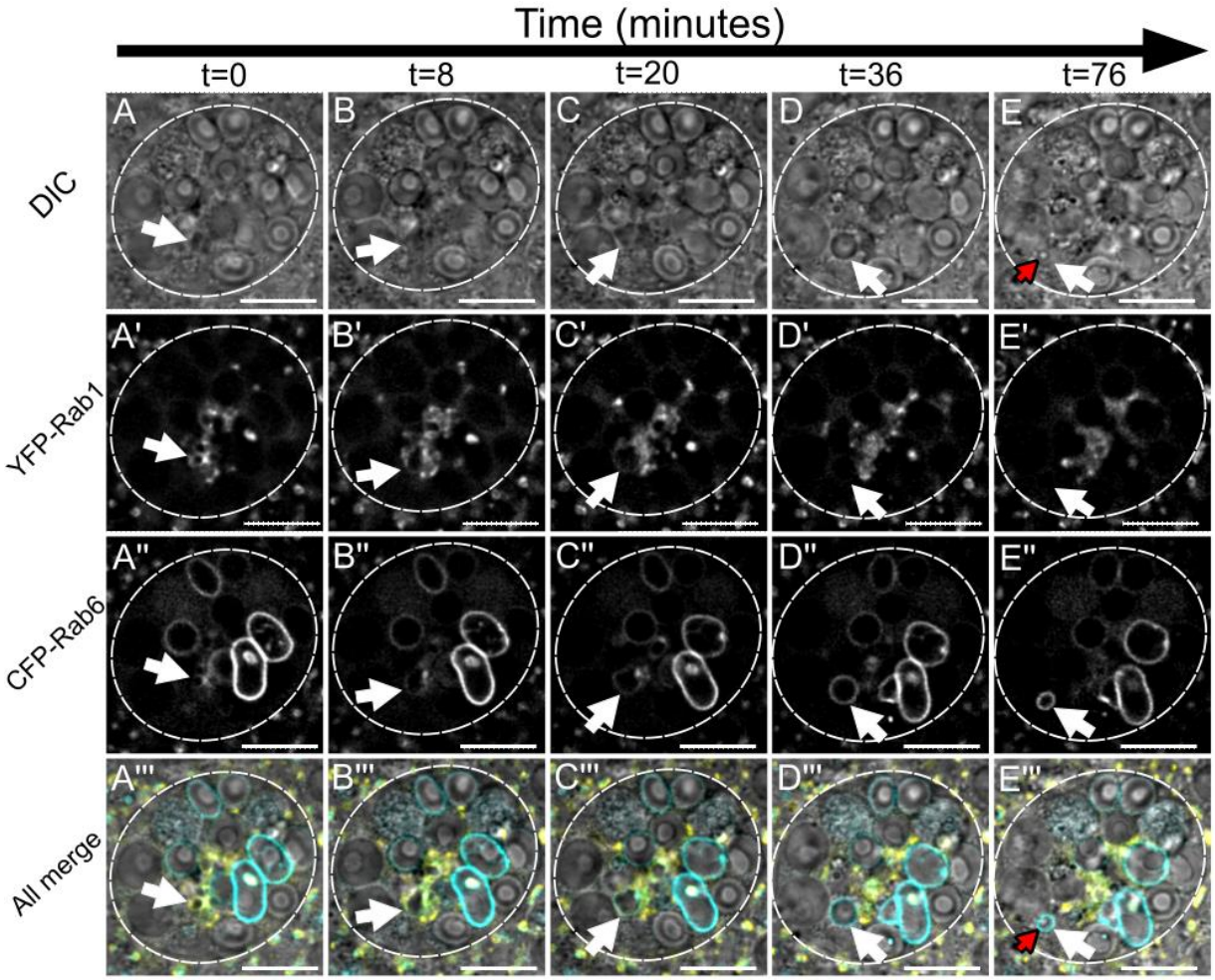

Figure 3.5. Small Rab1-labelled compartments directly transition into large Rab6-labelled compartments. Time-lapse imaging of SCs expressing *CFP-Rab6* and *YFP-Rab1* at five timepoints (**A**-**E**). In multicoloured images, Rab1 is shown in yellow, Rab6 in cyan and DIC images in grayscale. White arrows highlight an initial small Rab1-compartment that gradually swells in size and loses its Rab1-positive identity (**A**-**D**). Concurrently, this compartment acquire greater Rab6-labelling, eventually resulting in a large Rab6-compartment lacking a DCG (**A**-**D**). This process takes approximately 36 minutes. After this though, the same compartment contracts in size and develops a small DCG, highlighted by the red arrow (**E**). Small Rab1-positive compartments therefore seem to transition into larger Rab6-positive compartments which can in turn form DCGs. SCs boundaries marked by dashed circles, Scale bars: 10µm.

time-lapse imaging experiments therefore demonstrate that Rab1-positive compartments are the direct precursors of Rab6-positive compartments, and that these non-DCG Rab6-positive compartments eventually develop into the DCG compartments observed in SCs.

Following these experiments, I conducted further time-lapse imaging to better understand the mechanisms which allow small Rab1-positive compartments to grow so large and so rapidly. I found that compartments which were jointly labelled by Rab1 and Rab6 are able to increase their volume by fusing together (Fig. 3.6). Since the larger Rab6-positive compartments at later stages do not appear to be capable of homotypic fusion, these results suggest that Rab1 is essential for enabling fusion events to occur, possibly in combination with Rab6.

3.2.5 A Rab6 to Rab11 transition accompanies DCG formation in SCs

Having observed that Rab6-positive compartments are capable of forming DCGs, and having shown that Rab11 labels all DCG compartments and significantly overlaps with Rab6 on some compartment membranes, I investigated the hypothesis that non-DCG Rab6-compartments are the precursors of Rab11-positive DCG compartments. To do this, time-lapse imaging of SCs expressing both *CFP-Rab6* and *YFP-Rab11* was conducted.

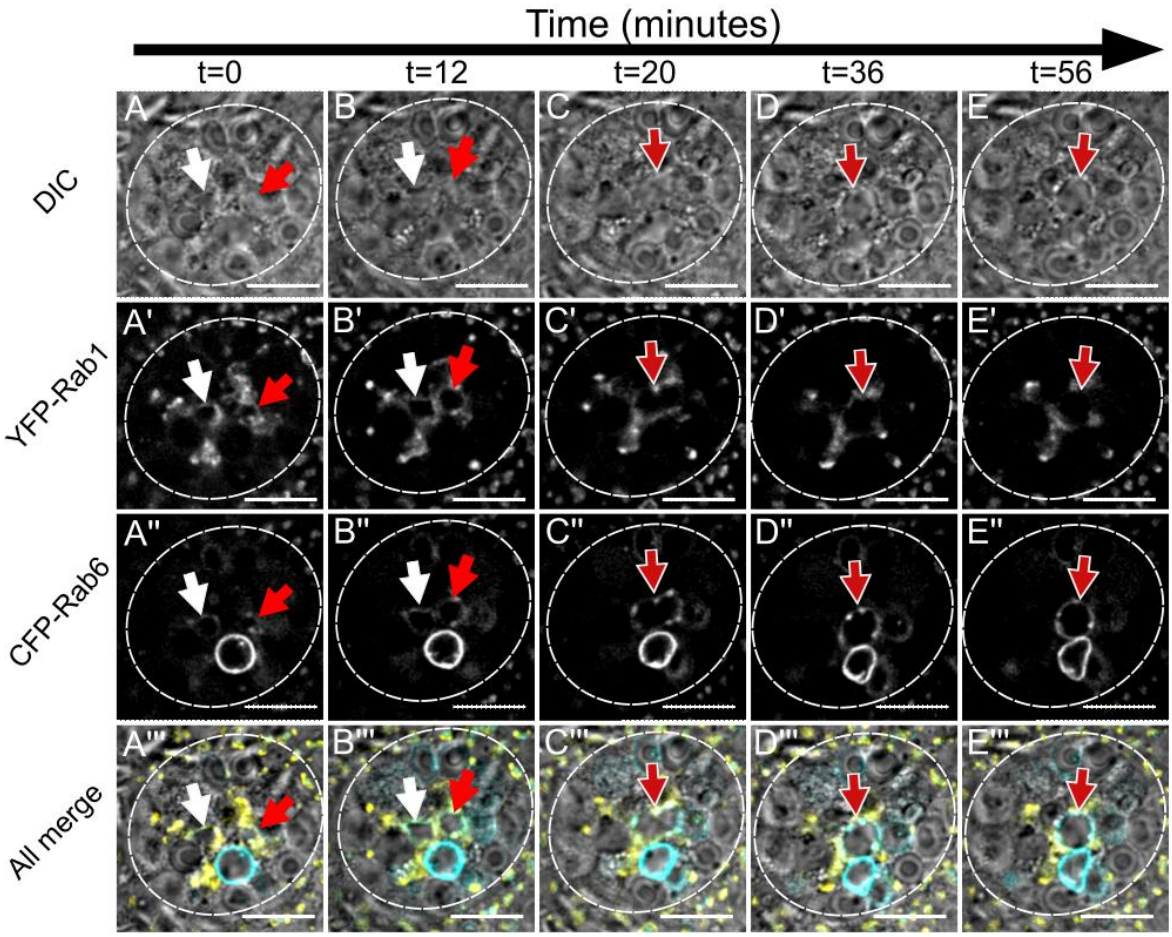

Figure 3.6. Rab1-Rab6 co-labelled compartments undergo homotypic fusion. Time-lapse imaging of SCs expressing *CFP-Rab6* and *YFP-Rab1* at five timepoints (**A**-**E**). In multicoloured images Rab1 is shown in yellow, Rab6 in cyan and DIC images in grayscale. Separate white or red arrows track individual Rab1-/Rab6-positive compartments that are mid-transition and already enlarged compared to typical Rab1-positive compartments (**A**). When these compartments come into contact they fuse into a single compartment (**C**-**D**). Both compartments also progressively lose Rab1-labelling and acquire stronger Rab6-labelling, resulting in a large Rab6-positive non-DCG compartment without Rab1-identity (**E**). Rab6-compartments therefore seem to form via a Rab1 to Rab6 transition that involves homotypic fusion of smaller precursor compartments. SCs boundaries marked by dashed circles, Scale bars: 10μm.

These experiments clearly demonstrated that a Rab6 to Rab11 transition does occur on the membranes of maturing secretory compartments, and that this transition coincides with the onset of DCG and exosome biogenesis (Fig. 3.7 and Fig. 3.8). Previous studies have shown that SCs produce a new DCG compartment every 4-6 h (Redhai et al., 2016), and my results indicated that the full transition lasts in excess of 8 hours. Within this transition process, several stages could be observed which are linked to a number of important changes in maturing secretory compartments.

For example, in the representative examples displayed in Figure 3.7 and 3.8, large, centrally located compartments were initially observed marked only by Rab6 and lacking a DCG (Fig. 3.7A and Fig. 3.8A). Subsequently however, Rab11 began to be recruited to limiting membranes and compartments contracted slightly in volume (Fig. 3.7B and Fig. 3.8B). This contraction coincided with the beginning of ILV biogenesis and transient concentrations of Rab6 at compartment membranes. Within a few minutes of these events, DCGs were formed within the compartmental lumen (Fig. 3.7C). DCG formation occurred rapidly and was generally completed within 20 minutes. An interesting feature of compartments at this stage was that ILVs marked by CFP-Rab6 and YFP-Rab11 were closely associated with the developing DCGs. However, a detailed view of DCG biogenesis was not possible using DIC microscopy alone without an appropriate DCG marker. From this point, developing compartments contained both DCGs and ILVs, but were still predominantly labelled by Rab6 as Rab11 remained at relatively low levels on compartment membranes. As the compartments continue to mature however, Rab11 was increasingly recruited whilst Rab6 was gradually lost (Fig. 3.7D-F and Fig. 3.8C).

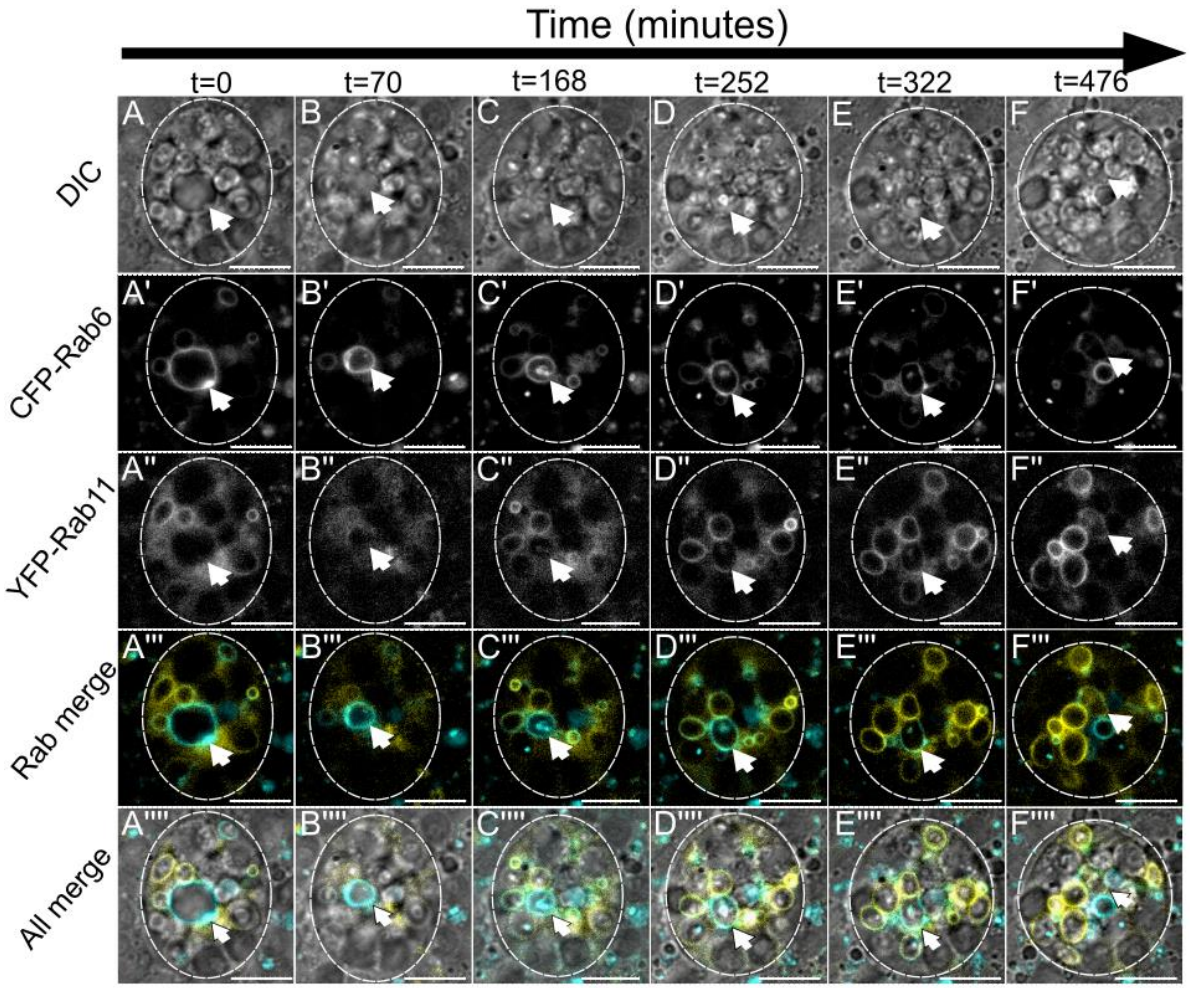

Figure 3.7. DCG and exosome biogenesis are associated with a novel Rab6 to Rab11 transition on compartments. Time-lapse imaging of SCs expressing *CFP-Rab6* and *YFP-Rab11* (**A**-**F**). In multicoloured images Rab11 is shown in yellow, Rab6 in cyan and DIC images in grayscale. White arrows highlight an initial Rab6-compartment that lacks a DCG and Rab11-labelling (**A**). Over time, this compartment contracts in size and gradually acquires faint Rab11-identity (**B**-**D**). Simultaneously, ILV biogenesis (**B**) and DCG biogenesis (**C**) occur within this compartment, with both structures seen to closely associate following biogenesis (**D**). Over several more hours, the compartment continues to lose Rab6-identity and acquire stronger Rab11-identity (**D**-**F**). Overall, a novel Rab6 to Rab11 transition occurs on compartments that coincides with ILV and DCG biogenesis. SCs boundaries marked by dashed circles, Scale bars: 10μm.

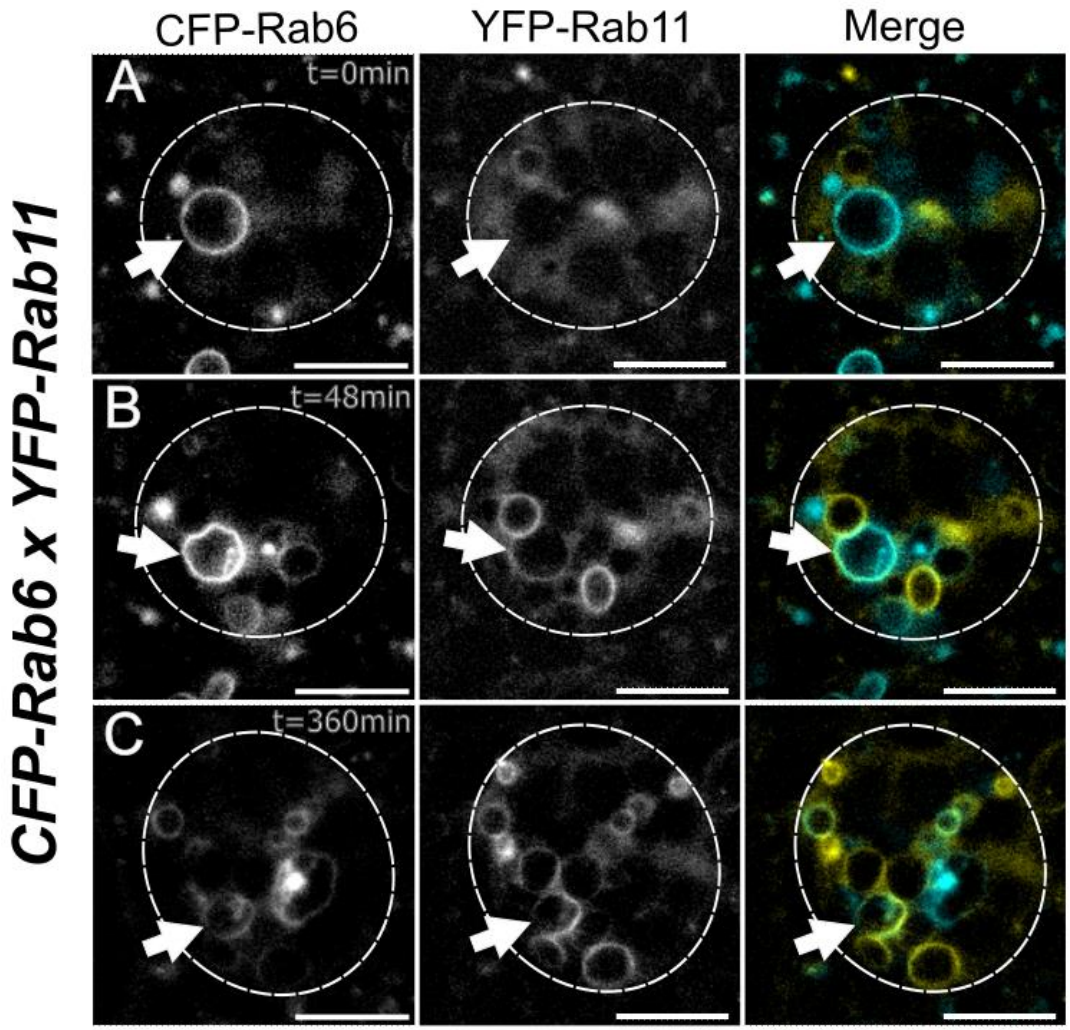

Figure 3.8. Stages of Rab6 to Rab11 transition on secretory compartments. Time-lapse imaging of SCs expressing *CFP-Rab6* and *YFP-Rab11* (A-C). In multicoloured images Rab11 is shown in yellow and Rab6 in cyan. White arrows highlight an initial Rab6-compartment (**A**). >1 hour after imaging begins, this compartment acquires faint Rab11-labelling and contracts slightly in size (**B**). These events coincide with ILV biogenesis within the compartment (**B**). Over approximately 5 more hours, this compartment loses most of its initial Rab6-labelling and develops into a compartment predominantly labelled by Rab11, containing Rab6 and Rab11 ILVs. SC boundaries marked by dashed circles, Scale bars: 10µm.

Based on broader imaging of Rab11 compartments, this process eventually results in DCG compartments that are labelled solely by Rab11 but may still contain Rab6-positive ILV puncta (e.g. Fig. 3.3A,C).

3.2.6 DCGs coalesce via a novel mechanism that can be visualised using GFP-mfas

Given the difficulty of imaging DCGs in most other experimental models, the large DCGs found in SCs presented a promising route to gain new insights into DCG biogenesis. I therefore adapted the time-lapse imaging protocols developed for imaging Rab transitions to study the process of granule biogenesis in real time. To better visualise DCGs during biogenesis, Midline fasciclin (MFAS) was utilised. MFAS is a *Drosophila* homologue of the amyloidogenic human protein TGF-β-induced (TGFBI), which is highly expressed in SCs (Immarigeon et al., 2021). Crucially, work primarily by Dr Preman Singh in the Wilson laboratory had shown that it is a major component of SC DCGs and that protein expressed from a GFP-tagged *mfas* gene trap (BDSC-#63204, (w^{1118}*; +; GFP-mfas*$^{MI11275\text{-}GFSTF.2}$)) specifically localises to DCGs without affecting the organisation of compartments or DCGs (P. Singh, 2023). Building on these findings, I therefore conducted time-lapse imaging of DCG biogenesis in SCs expressing *GFP-mfas*.

By tracking compartments over time, I was able to obtain the first views of DCG biogenesis occurring in real time recorded within any system (e.g. Fig. 3.9). At the start of DCG biogenesis, diffuse GFP-MFAS was present at low levels within a large core-less

compartment that aligns with compartments previously identified as immature Rab6-positive compartments (Fig. 3.9B). However, as the compartment underwent contraction (an event that coincides with the early recruitment of Rab11 to compartment membranes), the diffuse GFP signal within the lumen became increasingly bright (Fig. 3.9C). This increase in GFP signal might be explained by a concentration of soluble GFP-MFAS proteins as the compartment contracts, or it may also reflect the continual delivery of MFAS to maturing compartments over time. Regardless, as GFP-MFAS continued to concentrate in the compartment lumen, a critical point appeared to be reached which induced the spontaneous condensation/aggregation of MFAS into multiple “solid” mini-cores which formed throughout the compartment simultaneously (Fig. 3.9D,E). These mini-core were highly mobile and when two fragments came into contact, they proceeded to merge together, forming larger cores (Fig. 3.9F-H). Potentially dozens of fusion events occurred, and over a period of around 15 minutes, the vast majority of core fragments collided and coalesced into just a few large aggregates located centrally within the compartment lumen (Fig. 3.9H). These typically then proceed to form a single DCG (not imaged in this case due to the compartment migrating out of view of the microscope frame).

Notably, a second similar mechanism was also observed in several cases that appears to occur at a similar rate to the pathway described above (Fig. 3.10). In this alternative mechanism, diffuse mfas-GFP was still seen to concentrate in compartments just prior to biogenesis (Fig. 3.10A-C). However, rather than condensing into numerous mini-cores as seen in the first mechanism, soluble GFP-MFAS in this pathway was

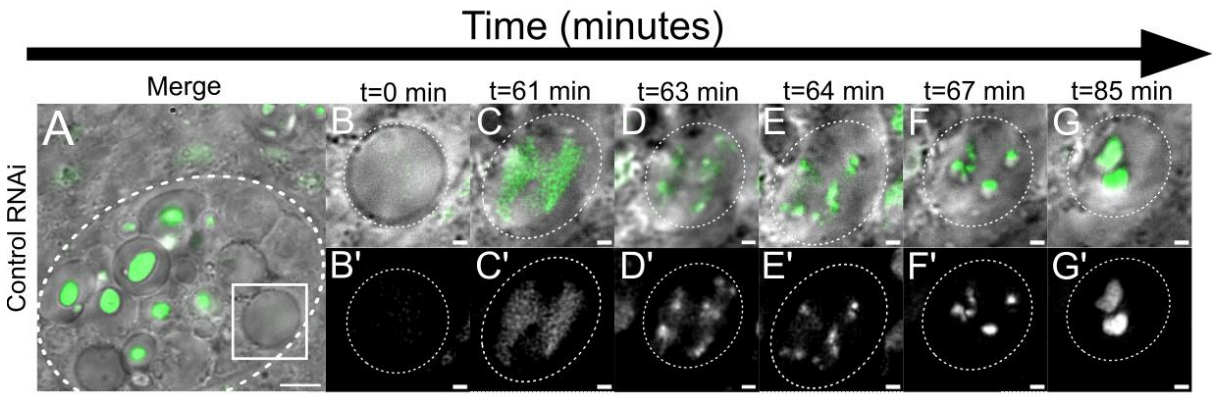

Figure 3.9. DCGs form via a novel mechanism of mini-core fusion in *Drosophila* SCs. Time-lapse imaging of SCs expressing *GFP-mfas* (A-G). In multicoloured images MFAS is shown in green and DIC images in grayscale. Initially, a large non-DCG compartment is seen near the periphery of a SC containing minimal MFAS (**A**-**B**). Over approximately 1 hour though, MFAS is seen to concentrate within the lumen of this compartment in a relatively diffuse manner (**C**). Then, within just 2-3 minutes, the MFAS within this compartment concentrates into a few point-like aggregates termed "mini-cores" (**D**-**E**). Over the next 10-20 minutes, the majority of these mini-cores proceed to collide and fuse together into two large DCGs (**F**-**G**). Typically SCs produce just one DCG per compartment, though occasionally two or more are seen. Overall, DCG biogenesis can occur through a novel process involving homotypic fusion of numerous, simultaneously condensing mini-cores. (A) SCs or (B-G) compartment boundaries marked by dashed circles, Scale bars: (A) 5μm, (B-G) 1μm.

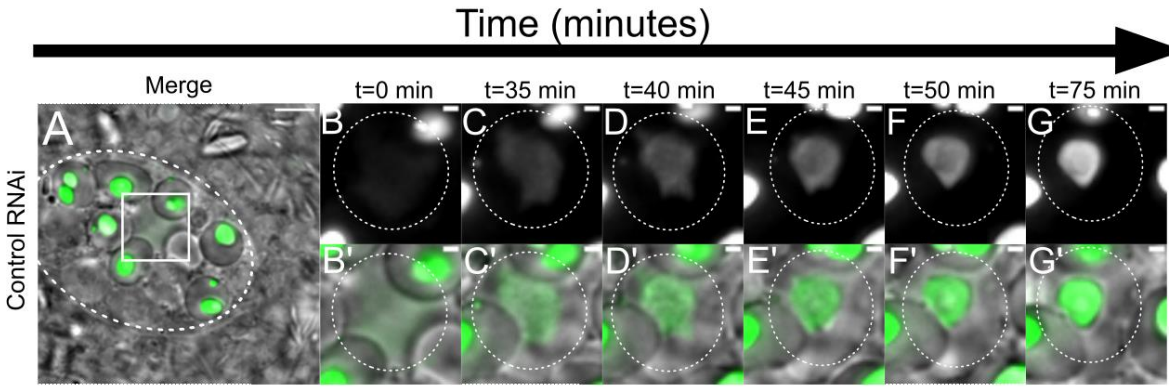

Figure 3.10. DCG biogenesis can also occur via gradual consolidation of diffuse MFAS into a large DCG. Time-lapse imaging of SCs expressing *GFP-mfas* (**A**-**G**). In multicoloured images MFAS is shown in green and DIC images in grayscale. Initially, a large non-DCG compartment is seen containing minimal MFAS (**A**-**B**). Across approximately 35 minutes MFAS is seen to concentrate within the lumen of this compartment in a relatively diffuse manner (**C**). Over the next 5-15 minutes however, MFAS is seen to progressively concentrate in centre of this compartment without any obvious mini-core formation (**D**-**F**). This results in fairly well defined DCG that is discernible through both MFAS fluorescence and DIC microscopy after around 15 minutes (**F**). Across a further 25 minutes, this DCG continues to accumulate brighter MFAS signal (**G**). (**A**) SCs or (**B**-**G**) compartment boundaries marked by dashed circles, Scale bars: (**A**) 5µm, (**B**-**G**) 1µm.

observed to pool in the centre of compartments and then consolidate gradually into a single granule (Fig. 3.10 D-F). This pathway for DCG biogenesis also appeared to occur over a 15-20 minute timeframe following the first signs of MFAS aggregation.

Overall, these two mechanisms appear to be very similar variants of a single pathway. Indeed, the core difference between these pathways was a slight variation in the timing of protein condensation from solution. In the first mechanism, aggregation seems to occur at a point when MFAS proteins are spread diffusely throughout the compartment, including at the limiting membrane. In the second mechanism, soluble MFAS proteins appear to have already collected near the compartment centre in a semi-organised structure by the time protein aggregation occurs.

3.2.7 Rab19 is a transient marker of DCG compartments

Earlier findings described in section 3.2.1 showed that Rab19 and Rab11 coexist on the surface of some DCG compartments. However, it was not clear why Rab19 only marked some DCG compartments or what functionally differentiated those compartments. Since Rab19 did not overlap with Rab6-compartments which represent immature precursors of DCG compartments, one possibility was that Rab19 labelled more mature DCG compartments that had fully undergone the Rab6 to Rab11 transition. Therefore, to evaluate this hypothesis and to analyse the dynamics of Rab19 on DCG compartments, time-lapse imaging of SCs expressing the *YFP-Rab19* fusion-construct was carried out.

Through these time-lapse imaging experiments, I showed that Rab19 displays quite unique dynamics on SC compartments (Fig. 3.11). Demonstrating this, Rab19 was found to be recruited to unlabelled DCG compartments over a relatively short period, reaching maximal levels of Rab19-labelling in <20 minutes (Fig. 3.11A-C). Rab19 was then seen to persist stably on DCG compartments for a variable period between 15 and >90 minutes (Fig. 3.11C-D). Most exceptionally however, when departing from compartment membranes, Rab19 underwent an extremely rapid dissociation, being almost completely removed from compartment membranes over the course of just 2-8 minutes, usually equivalent to only one or two frames of time-lapse imaging (Fig. 3.11D-E).

Given the striking speed of Rab19's dissociation, I conducted further time-lapse imaging of this process (Fig. 3.12). In the example shown in Figure 3.12, two compartments were found to be strongly labelled by YFP-Rab19 at the beginning of time-lapse imaging, a labelling they maintained at fairly constant levels for ≃25 minutes (Fig. 3.12A-B). However, in the space of just 4 minutes, Rab19 was found to completely depart from the membrane of one compartment (Fig. 3.12B-C, white arrow). Immediately following Rab19's departure, no changes were observed in the compartments structure or organisation. Another 4 minutes later, however, the DCG resident in the compartment rapidly dissipated (Fig. 3.12D). Shortly after this, the YFP-Rab19 labelling present on the second compartment was also seen to depart from the limiting membrane with no immediate effect on DCG or compartment organisation (Fig. 3.12D-E, magenta arrow).

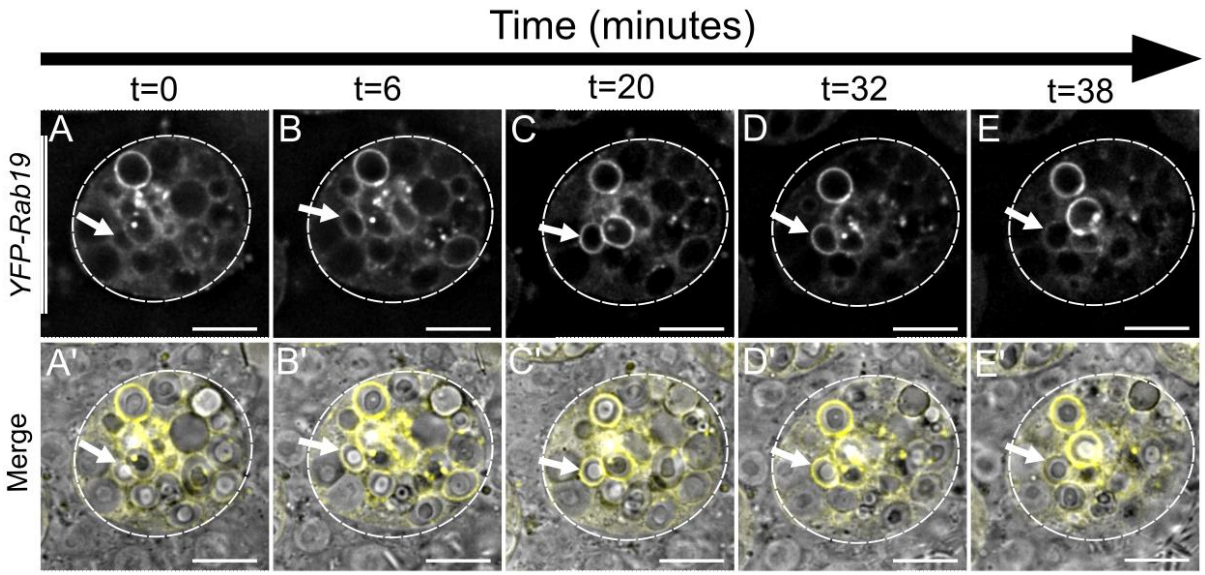

Figure 3.11. Rab19 is recruited and removed from compartments in a relatively fast cycle. Time-lapse imaging of SCs expressing *YFP-Rab19* (A-E). In multicoloured images Rab19 is shown in yellow and DIC images in grayscale. White arrows track a DCG compartment that initially lacks strong Rab19-labelling (**A**). Fairly quickly though, i.e. within 20 minutes, this compartment acquires strong Rab19-labelling (**B-C**) that then plateaus in intensity for approximately another 12 minutes (**D**). Finally, across the space of another 6 minutes, this compartment loses most detectable Rab19-labelling (**E**). Overall, compartments appear able to obtain and then lose Rab19-identity fairly rapidly. In this case, the acquisition and loss of Rab19-identity did not coincide with any detectable changes in the compartment, its DCG or ILVs. SC boundaries marked by dashed circles, Scale bars: 10µm

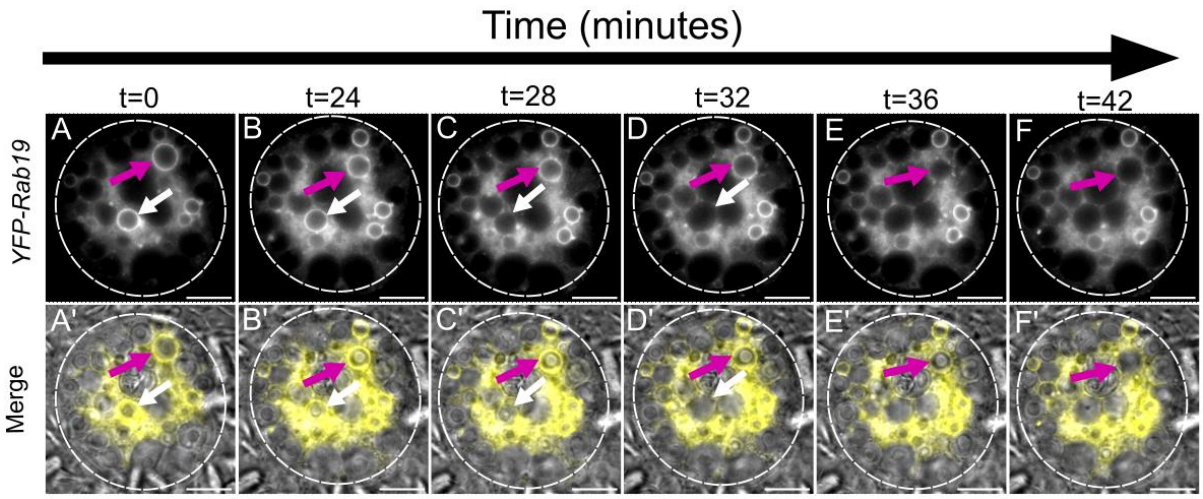

Figure 3.12. Rab19 removal from compartment membranes is frequently associated with a loss of DCGs shortly afterwards. Time-lapse imaging of SCs expressing *YFP-Rab19* (A-E). In multicoloured images Rab19 is shown in yellow and DIC images in grayscale. White and magenta arrows track two individual Rab19-compartment that are initially both labelled by Rab19 (**A**). Both compartments maintain this identity for the first 24 minutes of imaging (**B**), however, in the space of just 4-8 minutes the compartment labelled by the white arrow loses both its Rab19-identity (**C**) and its DCG (**D**). Shortly afterwards, the second compartment, marked by the magenta arrow, also loses its Rab19 identity (**E**) and its DCG (**F**). Therefore, the loss of Rab19-identity appears to be associated with the subsequent loss of DCGs in at least some cases. From these results it is not clear whether the DCG of these compartments is lost due to secretion of the DCG or some form of DCG degradation. SC boundaries marked by dashed circles, Scale bars: 10μm

After 6 minutes, however, the DCG of this compartment was also lost, just as observed in the first compartment (Fig. 3.12F). This change in DCGs following Rab19 dissociation was very intriguing but did not occur consistently in all cases. In the compartment tracked in Fig. 3.11, for example, the DCG persisted until the end of the time-lapse experiment, i.e. for at least 30 minutes after Rab19 departed from the membrane.

These observations highlighted certain attributes of Rab19's behaviour and suggested some possible functions. For example, the fact that Rab19 associated with compartments that have already produced the crucial signalling structures of DCGs and ILVs suggested that Rab19 most likely functions in processes towards the end of a secretory compartment's lifecycle. This hypothesis was supported by the apparent release or degradation of DCGs observed shortly after Rab19's departure and by suggestions from previous studies that Rab19 functions in apical secretion (Dunst et al., 2015). Other characteristics of Rab19 dynamics such as its comparatively quick recruitment phase, its highly variable duration on compartments, and its exceptionally fast loss from membranes also suggested that Rab19 activity may act as an effector for specific, transient signalling operating prior to secretion.

3.2.8 The retromer component Vps35 colocalises with Rab19 on terminal compartments

Vps35 is an essential component of the cargo selective complex, a trimer complex that is vital for retromer function on endosomes. Mutations in Vps35 and the wider retromer complex are associated with late-onset Parkinson's disease as well as some forms of

cancer (Sassone et al., 2021; Yu et al., 2023; Q. Zhou et al., 2023). Given this and given the essential function of the retromer complex in endosome trafficking, the localisation of Vps35 and the retromer complex was investigated through live-cell imaging of SCs expressing *Vps35-RFP* under endogenous promoter control in the YFP-Rab11 background.

Vps35-RFP localised to 1.2 ± 0.83 Rab11-positive DCG compartments and labelled the entirety of those compartment's limiting membranes (Fig. 3.13A). This finding was interesting as it is reminiscent of Rab19's distribution in SCs. It was also interesting because Vps35 is generally recruited to membranes by Rab7, a protein which was found to partially colocalise with Rab19 in fixed SCs (Prince et al., 2019; Rojas et al., 2008). Therefore, the distribution of Vps35-RFP and each of YFP-Rab19 and YFP-Rab7 was examined (Fig. 3.13B,C). Similarly to Rab19 which was earlier found to label 3.7 ± 1.3 compartments in live SCs, Rab7 labelled 3.1 ± 1.3 DCG compartments as well as a 4.2 ± 2.8 acidic compartments. Likewise, Vps35-RFP was found to exclusively label compartments that were also marked by YFP-Rab19 and YFP-Rab7 in their respective backgrounds, with no examples found of Vps35 labelling compartments that were not Rab19-positive and Rab7-positive.

To gain further insights into retromer dynamics in SCs, time-lapse imaging of SCs expressing *YFP-Rab19* and *Vps35-RFP* simultaneously was carried out. As found in live-cell imaging and shown in the example of Figure 3.14, time-lapse imaging showed that Vps35-RFP was present exclusively on a subset of YFP-Rab19 labelled compartments. These two markers were found to stably persist on compartments for

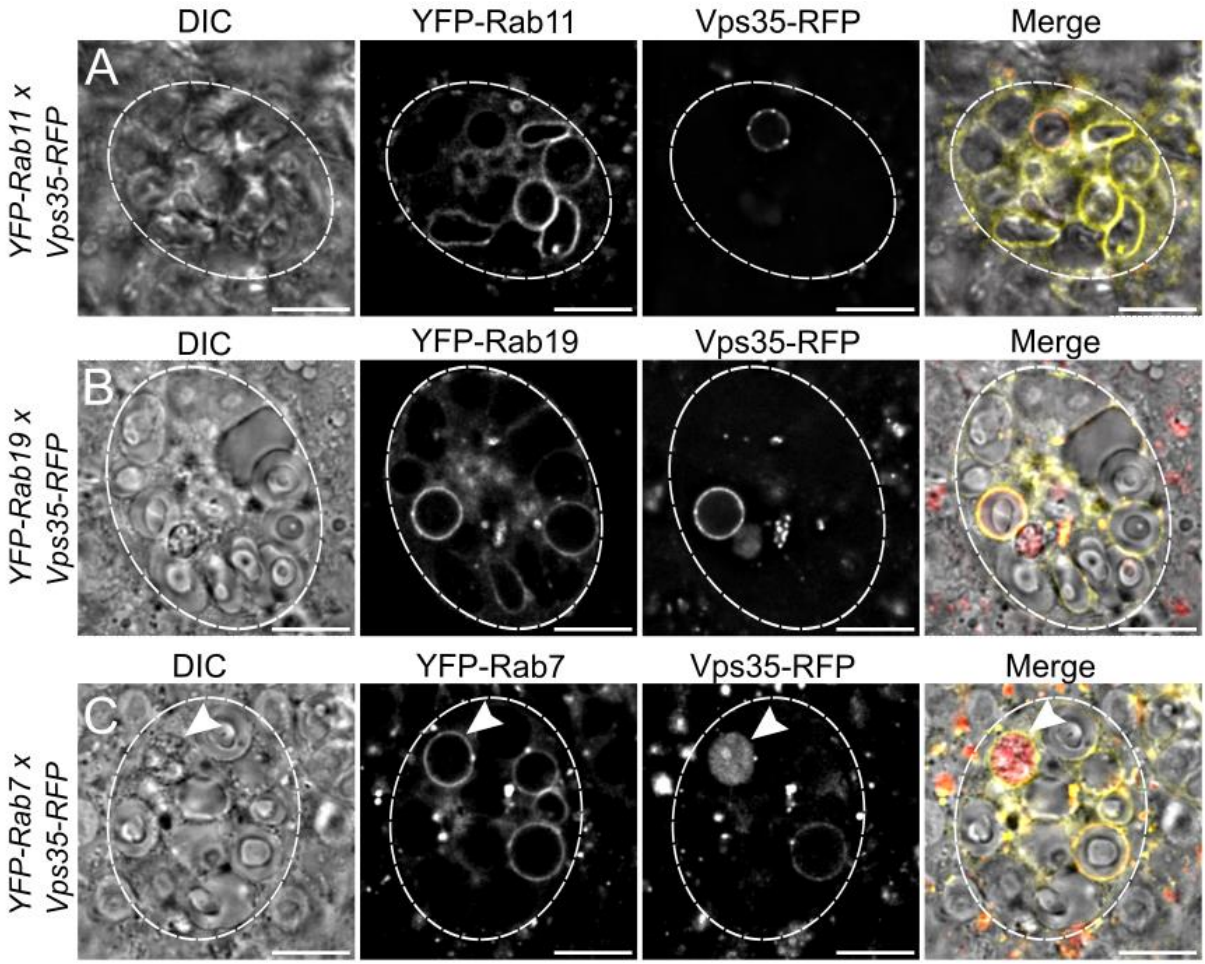

Figure 3.13. The retromer component Vps35 colocalises with a subset of Rab11, Rab19 and Rab7 compartments in SCs. (**A-C**) Wide-field fluorescence images of SCs expressing *Vps35-RFP* together with *YFP-Rab11* (**A**), *YFP-Rab19* (**B**), or *YFP-Rab7* (**C**). In multicoloured images Rab7, Rab11 and Rab19 are shown in yellow, Vps35 in red and DIC images in grayscale. White arrowheads in C highlight a lysosomal compartment with high lumenal RFP concentration. In all three backgrounds, Vps35 was found to label 1-2 compartments per cell. Interestingly, these compartments were also always labelled by Rab11, Rab19 and Rab7 in their respective backgrounds. This indicated that Rab11, Rab19 and Rab7 coexist on specific subsets of DCG compartments. SC boundaries marked by dashed circles, Scale bars: 10µm

an extended period, ~25 minutes in this case (Fig. 3.14A,B). However, when YFP-Rab19 dissociated from the limiting membrane of compartments, Vps35-RFP was initially retained on the compartment's surface (Fig. 3.14C). 3 minutes later however, Vps35-RFP rapidly departed from the membrane, an event that coincided exactly with the loss of the compartment's DCG (Fig. 3.14D). This finding fitted well with my previous observations of Rab19's dynamics on SCs and suggested that a subset of Rab19-compartments labelled by Vps35 and Rab7 represent fully mature DCG compartments which then proceed to lose their DCG either through secretion or degradation.

3.2.9 Vps35-labelled terminal compartments are capable of lysosomal fusion or extracellular release of compartments

Having identified Vps35 as a label of terminal compartments, it was still unclear what exactly was happening to the contents of terminal compartments such as DCGs and exosomes. The two primary explanations for their fate were their release to the extracellular space or their degradation within a lysosome depending on whether the Vps35-labelled compartment fused with the plasma membrane or lysosomes. To distinguish between these possibilities, further time-lapse imaging of *Vps35-RFP*-expressing SCs stained using the acidic compartment dye LysoTracker Yellow/Blue was conducted, indicating that Vps35 labels compartments in both pathways (Fig. 3.15 and Fig. 3.16).

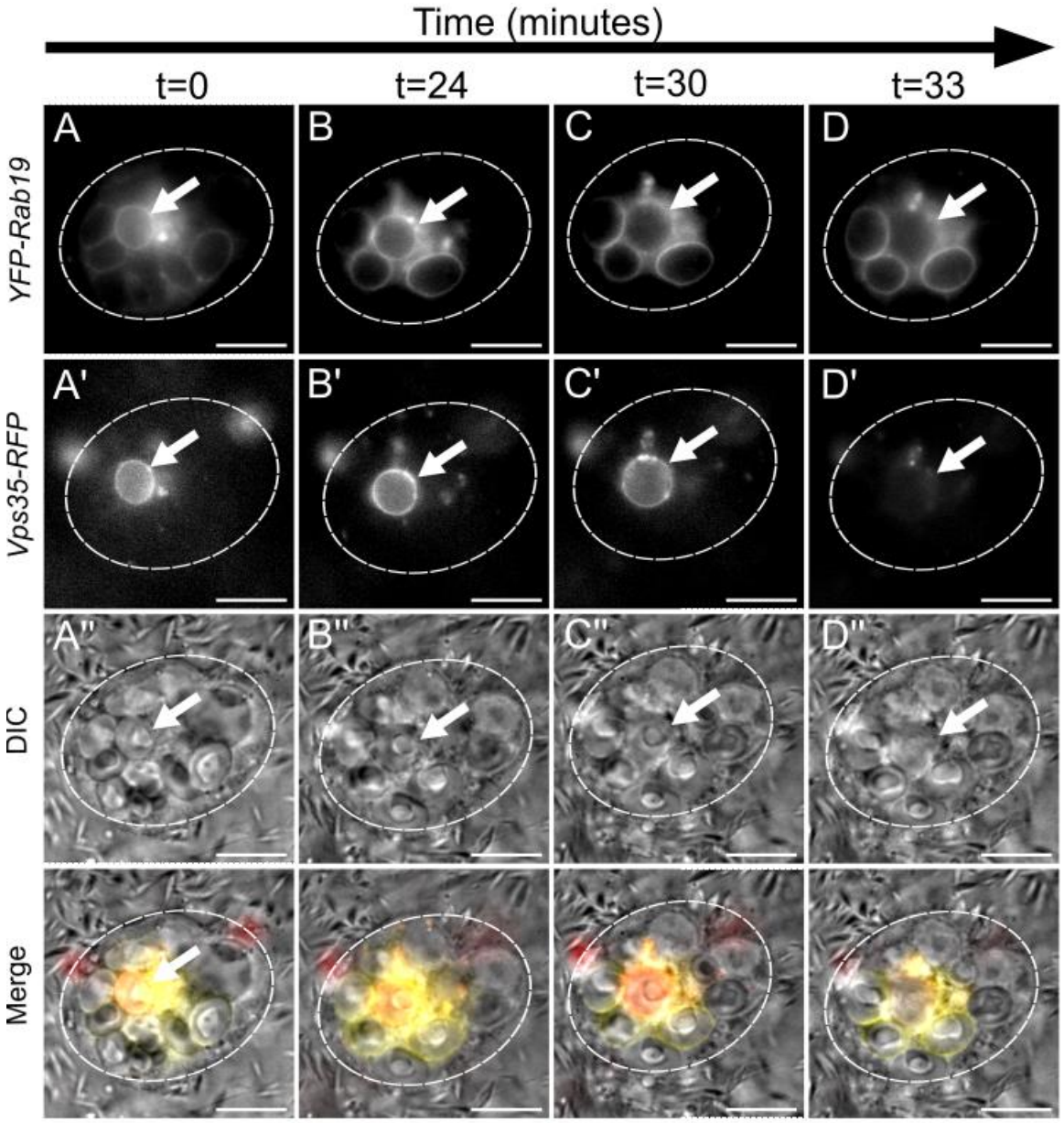

Figure 3.14. Vps35 is briefly retained on mature DCG compartments after Rab19 dissociation. Time-lapse imaging of SCs expressing *YFP-Rab19* and *Vps35-RFP* (A-E). In multicoloured images Rab19 is shown in yellow, Vps35 in red and DIC images in grayscale. White arrows track a Vps35-/Rab19-positive compartment that initially contains a DCG (**A**). Both Rab19 and Vps35 are retained on compartments for ~24 minutes after imaging begins (**B**). However, after a further 6 minutes, Rab19 is lost from the compartment membrane (**C**). After a further 3 minutes, Vps35 is also lost from the compartment (**D**), an event which precisely coincides with the loss the DCG. Alongside earlier findings, loss of Rab19 and Vps35 from compartments appears to be associated with the loss of DCGs. SC boundaries marked by dashed circles, Scale bars: 10μm

In Figure 3.15, a compartment is tracked that undergoes lysosomal fusion. At the beginning of this experiment, the compartment was labelled by Vps35-RFP, contained a DCG and was not in particularly close proximity to any acidic compartments (Fig. 3.15A, white arrow). However, a small acidic compartment was present several micrometres closer to the basal membrane and could be seen when the imaged Z-stacks were viewed as a single 2D projection (Fig. 3.15A''', magenta arrow). Over the next ~20 minutes however, this acidic compartment migrated closer to the Vps35-RFP labelled compartment (Fig. 3.15B). Then, within the same frame, three events were seen to simultaneously occur (Fig. 3.15C). Firstly, Vps35 was seen to depart from the compartment membrane. Secondly, the DCG within this compartment became visibly disrupted and finally, the small acidic compartment fused with the main compartment, which then became less intensely stained by the LysoTracker Yellow/Blue dye (Fig. 3.15C). From this point forwards, the tracked compartment was seen to house acidic domains labelled by LysoTracker Yellow/Blue (Fig. 3.15D).

In Figure 3.16, a broadly similar process was observed apparently showing extracellular secretion. Beginning with a Vps35-RFP labelled DCG compartment, Vps35 was seen to persist on the compartment for ~10 minutes (Fig. 3.16A,B). Vps35 then rapidly departed from the compartment membrane, resulting in the loss of the DCG (Fig. 3.16C). In contrast to the previous experiment however, no acidic compartment fusion was observed, and the compartment was seen to persist as a discrete structure in the SC for at least 30 more minutes without any acidic staining (Fig. 3.16D). It may also be that the compartment remained connected to the plasma membrane for this time, though this has currently not been possible to test.

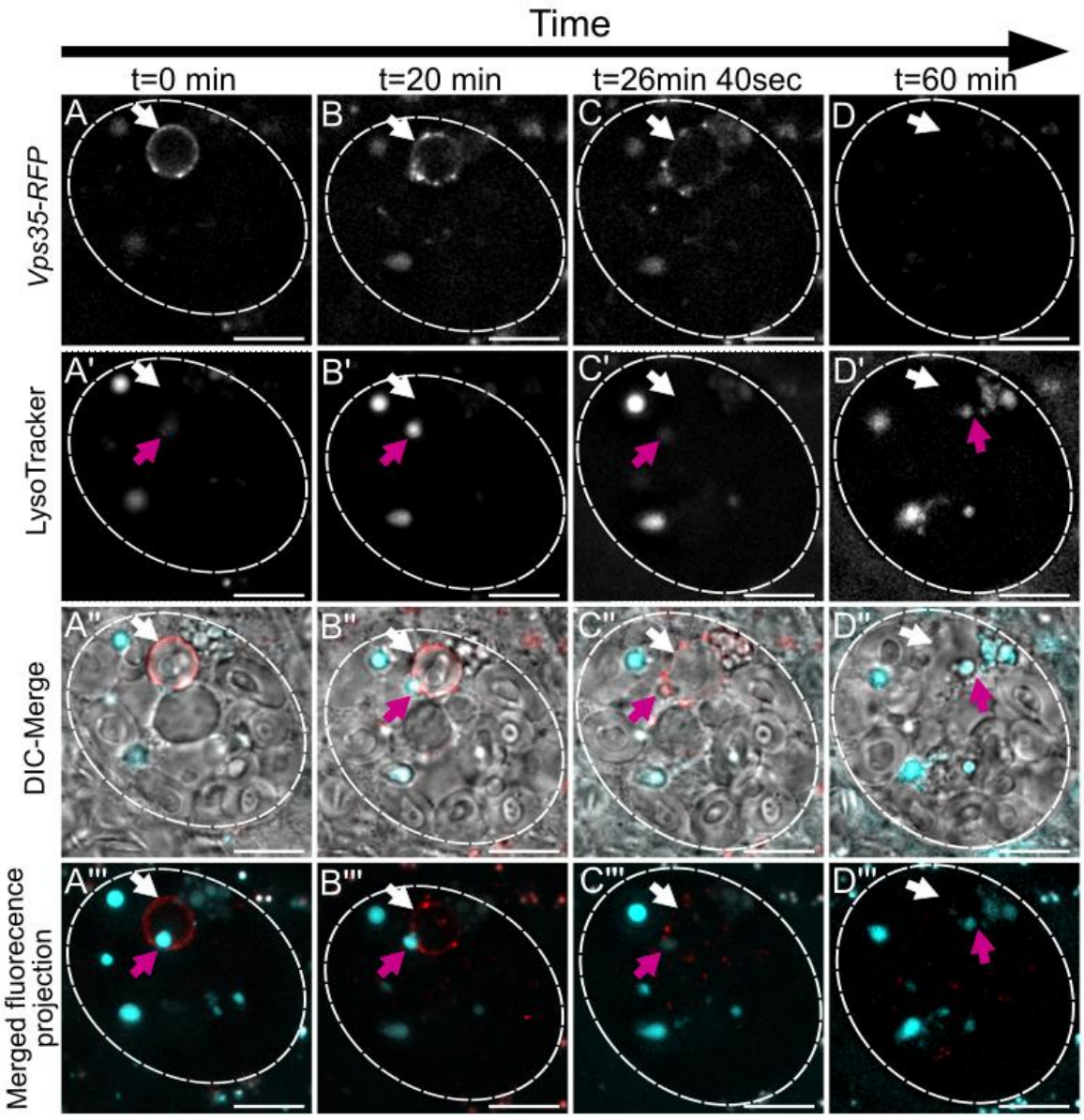

Figure 3.15. Small acidic compartments can fuse with Vps35-positive secretory compartments, leading to the dissociation of DCGs. Time-lapse imaging of SCs expressing *Vps35-RFP* (A-E). In multicoloured images Vps35 is shown in red, LysoTracker Yellow/Blue is shown in cyan and DIC images in grayscale. White arrows track a Vps35-positive compartment whilst magenta arrows track a small lysosomal compartment. Initially, the Vps35-positive compartment is separated from the lysosomal compartment by several micrometres in the Z-axis (**A**, compare the single Z-slice in **A'** to the projection in **A'''**). However, across 20-25 minutes, these two

compartments come together (**B,** compare **B'** to **B'''**). Shortly after this, the Vps35-positive compartment rapidly loses its Vps35-labelling (**C**), fuses with the lysosomal compartment (**C'**) and loses its DCG (**C''**), all within the same imaging frame. From this point forwards, the residual compartment can be seen within the SC with internal acidic domains for at least 30-40 more minutes (**D**). In this case, loss of Vps35 appears to coincide with lysosomal fusion and DCG degradation. SC boundaries marked by dashed circles, Scale bars: 10µm

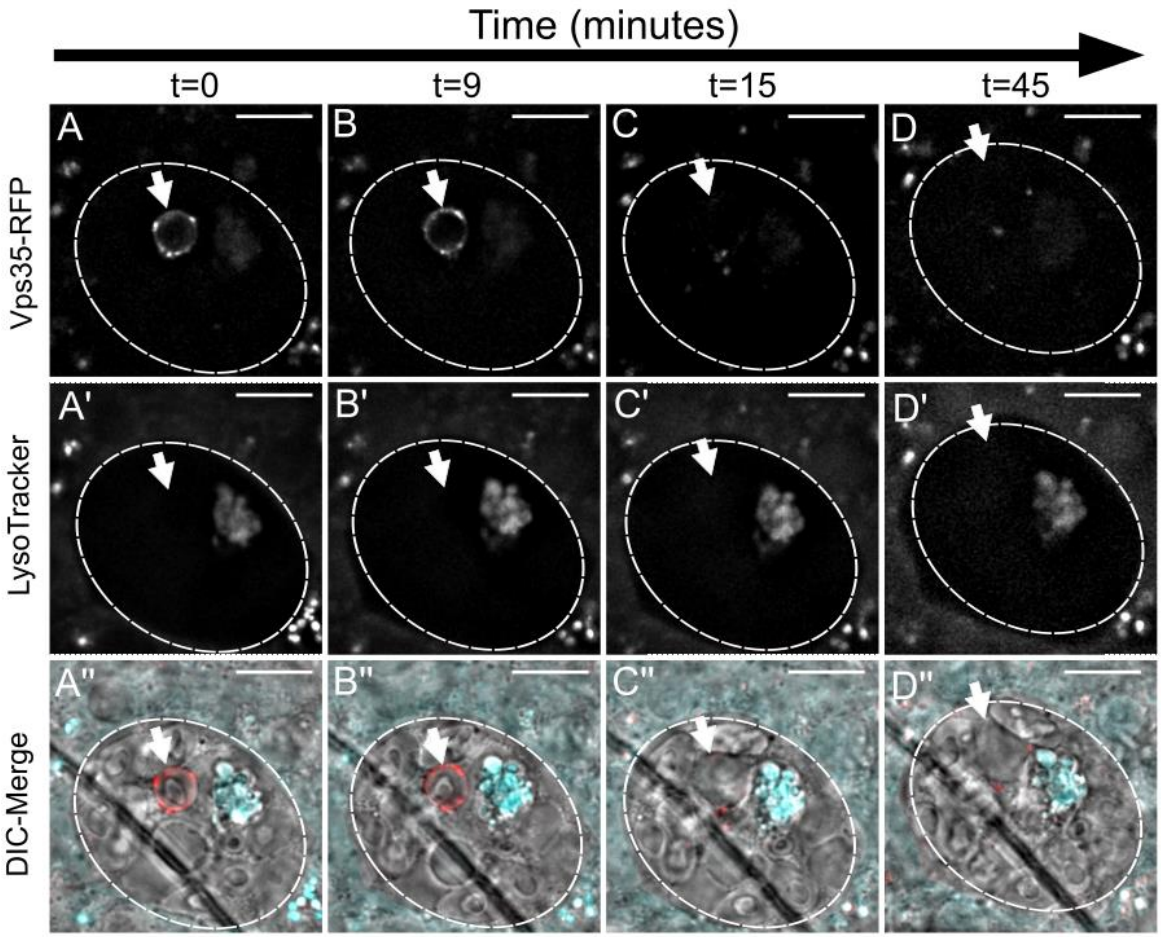

Figure 3.16. Vps35-positive secretory compartments can release their contents extracellularly and then persist as empty compartments in SCs. Time-lapse imaging of SCs expressing *Vps35-RFP* (**A**-**E**). In multicoloured images Vps35 is shown in red, LysoTracker Yellow/Blue is shown in cyan and DIC images in grayscale. White arrows track a Vps35-positive compartment that initially contains a DCG (**C**). After a short time, Vps35 is lost from the surface of this compartment and the DCG disappears from the lumen (**B-C**). However, no lysosomal fusion event is seen to occur, and no acidic domains are seen within the compartment across 30 minutes of further observation (**D**). Since lysosomes are not involved in this process, Vps35 also appears to be associated with DCG compartments that are about to undergo secretion or partial secretion. SC boundaries marked by dashed circles, Scale bars: 10μm

3.3 Discussion

Through the use of live-cell imaging and the development of new time-lapse imaging protocols, I have produced a detailed characterisation of SC secretory compartments and have identified novel processes occurring during secretory compartment maturation. As part of this, I have outlined a series of Rab to Rab transitions that characterise the different stages of secretory compartment development and which seem likely to regulate important processes such as DCG biogenesis and compartment secretion. Most significantly, I identified a novel Rab6 to Rab11 transition occurring on large secretory compartments that coincides with DCG and exosome biogenesis. Furthermore, I also provided the first real-time view of DCG biogenesis produced in any system, a process which involves physiological protein condensation/aggregation. Finally, through further time-lapse imaging, I have provided novel insights into the role of Rab19, Rab7 and Vps35 on late-stage secretory compartments, including potential functions in compartment secretion and degradation.

3.3.1 Secretory compartment maturation – Core findings

Overall, my results highlight the dynamic nature of secretory compartment identity and maturation in SCs. Throughout the work, direct and indirect demonstrations of Rab markers colocalising on compartments were made, and through careful observation as well as novel time-lapse experimentation, new insights were gained showing how Rab labelling reflects different stages of secretory compartment maturation. For

example, it was demonstrated that Rab6 is a marker of large DCG precursor compartments and confirmed that Rab11 is a label of all large DCG compartments.

Among the most interesting of my findings was the direct demonstration of a Rab1 to Rab6 transition being present in *Drosophila* as large secretory compartments are produced via novel homotypic fusion events. This process appears to be similar to transitions recorded in yeast (Thomas et al., 2021), though the process has not previously been viewed in such detail and the role of fusion events has also not been described to my knowledge.

Another novel finding was the demonstration of a previously unknown Rab6 to Rab11 transition occurring on secretory compartments. Of particular note was the timing of this transition, as it starts just as exosomes and DCGs begin to form within the secretory compartment lumen, suggesting that Rab11 may play a role in the initiation biogenesis events.

Finally, the insights gained into the dynamics of Rab19 mark a new set of contributions to the study of this minimally researched protein. My findings reinforce the suggestion of Rab19 functioning in apical secretion and highlight its novel dynamics in comparison to the other Rab markers investigated here. The results also highlight an unexpected association with the retromer component Vps35 and confirm its colocalisation with Rab7 in live SCs.

3.3.2 Secretory compartment maturation – Discussion

Of the factors and processes investigated here, the role of the Rab6 to Rab11 transition, the role of Rab19 on apical compartments and the role of Vps35/Rab7 on terminal compartments warrant particular attention and further research. Since the Rab6 to Rab11 transition is examined more closely in the next chapter, I will focus here on the functions of Rab19, Vps35 and Rab7. Rab19 appears in two contexts on SC compartments, firstly on small microdomains which will also be examined in subsequent chapters, and later around the entire membrane of some apical compartments. From my experiments, it was not possible to discern specific morphological changes that were associated with compartments following the recruitment of Rab19 as it was for Rab6 or Rab11. This presumably reflects the fact that the changes Rab19 mediates are not visible structural changes, but changes in effector activity, protein recruitment and lumenal microenvironment. Given more time to conduct this research, it would be informative to undertake analyses of factors such as Rab19's binding partners. The accessory gland model is not ideal for biochemical investigations, so plated S2 cells may act as a better model system to assess the molecular interactions with Rab19. To obtain the greatest insights into the underlying biology, it would also be beneficial investigate the localisation of important Rab19 binding partners in SCs and to disrupt their function, potentially through use of SC-specific RNAi expression.

Likewise, my investigation into Vps35 and Rab7 on mature apical secretory compartments also offers avenues for further research. One particularly significant question that remains unanswered is how the fate of SC compartments is determined,

i.e. what signalling cascades regulate the choice between lysosomal degradation and extracellular release for each compartment. Although Vps35 is closely associated with compartments at the time this choice is made, it does not alone appear to regulate the fate of compartments, as it is seen to label these compartments regardless of their ultimate fate. Additionally, although not shown here, inducing SC-specific Vps35 knockdown for 6-days produced no significant changes in SC compartment organisation as might have been expected if either degradation or extracellular release had been blocked, if it is assumed that the cell cannot invoke compensatory mechanisms to adjust to any change.

My findings also suggest more attention should be given to Rab7 as a critical factor labelling mature DCG compartments. Indeed, there are parallels between these compartments and the LEs which Rab7 is generally associated with. As examples, both compartment types associate with Rab7, both are forms of multi-vesicular bodies (MVBs) which can release exosomes extracellularly, and both are capable of fusion with either lysosomes or the plasma membrane. In the better-studied LE, Rab7 is essential for fusion with the lysosome, but not with the plasma membrane (Bröcker et al., 2012; Bucci et al., 2000). In HeLa cells, inhibition of Rab7 using shRNA actually has no impact on exosome secretion, indicating that fusion with the plasma membrane does not require Rab7 (Ostrowski et al., 2010). Instead, that same study found that two Rab27 isoforms were responsible for MVB fusion with the plasma membrane. Interestingly, when imaging a YFP-Rab27 fusion expressed from the endogenous *Rab27* locus in *Drosophila* SCs, I found that the architecture of SCs was severely disrupted, with many more, smaller secretory compartments being present than in control cells. This result could be explained by the idea that Rab27 is required for MVB

docking and fusion with the plasma membrane, and that this function is disrupted by expression of the *YFP-Rab27* protein, leading to an accumulation of secretory compartments that cannot fuse with the plasma membrane. Although there has not been time to properly explore these hypotheses, the initial observations are consistent with a model where Rab7 mediates MVB fusion with acidic compartments, whilst Rab27 mediates fusion with the plasma membrane. These incidental observations also suggest that the *Drosophila* accessory gland could be an ideal *in vivo* model to investigate the mechanisms of both exosome secretion and crinophagy, the process by which redundant secretory granules fuse with LEs/lysosomes to degrade their contents (Csizmadia & Juhász, 2020; Szenci et al., 2023). Although it has not been a focus of my own research, my observations here do align with current models of crinophagy in *Drosophila* which indicate that Rab2 and Rab7 are required for the process, alongside numerous other factors (Csizmadia et al., 2017). Since crinophagy represents one of the least well understood autophagy pathways, the large size of SC DCGs and lysosomes would appear to provide an excellent model for examining the mechanisms underlying this process.

3.3.3 DCG biogenesis mechanisms – Core findings

The other key result from the experiments described here was the first direct observation of DCG biogenesis. Because of the small size of DCG compartments in most systems, the events involved in DCG biogenesis have remained difficult to assess until now. For this reason, the demonstration that DCG biogenesis can be observed in real-time, *ex vivo* opens many new avenues for investigating the mechanisms involved

in this process. Of particular note is the finding that DCGs can form from smaller protein aggregates which undergo multiple fusion events with each other. Likewise, the rapid timescale of such a large aggregation event is also of special interest, as was the finding of a second biogenesis mechanism involving the gradual assembly of just one single protein aggregate which becomes the DCG.

These early findings provide many avenues to explore in terms of understanding DCG biogenesis regulation. In later chapters I will explore the role of proteins involved in amyloid regulation and neurodegenerative illnesses in this process, but for now I will discuss other areas that would be beneficial to study based on my results.

3.3.4 DCG biogenesis mechanisms – Discussion and future directions

One interesting aspect of DCG biogenesis observed through real-time imaging was the fact that diffuse GFP-MFAS appears to accumulate for ~1 hour before the first signs of actual aggregation occur. This raises the question of how MFAS is trafficking into these compartments and concentrating within them. One explanation would be that a constant quantity of MFAS is present from the time when each large Rab6-positive DCG precursor compartment is formed, and that the contraction observed in compartment size following Rab11 recruitment leads to GFP-MFAS signal becoming more intense. This hypothesis is broadly consistent with current models of immature secretory vesicle maturation via vesicle remodelling, which state that clathrin-coated vesicles bud off from immature secretory vesicles, removing excess membrane and

factors not required for DCG maturation (Austin et al., 2000; Klumperman et al., 1998). Indeed, in time-lapse experiments of CFP-Rab6-labelled compartments, membranous Rab6-positive structures were frequently observed forming on the outside of compartments during the contraction process. It is feasible that these structures represent the clathrin-coated trafficking vesicles which then take part in constitutive secretion processes.

Overall then, it seems likely that compartment contraction leads to the concentration of DCG proteins in the compartment, but this does not preclude the possibility that additional DCG proteins like MFAS or other factors involved in protein aggregation are also delivered to compartments by small vesicles prior to DCG biogenesis. If we assume that the fundamental processes controlling DCG biogenesis are evolutionarily conserved, an idea for which I will provide evidence in the next chapter, discerning the mechanisms involved in this stage of DCG biogenesis in SCs would be helpful for understanding the requirements for DCG biogenesis in other contexts. As such, greater attention should be given to the fate of apparent vesicular structures observed forming on the outside of compartments during contraction. Additionally, some effort should be made to understand the mechanism of their formation. For example, removal of missorted proteins from immature secretory compartments normally requires clathrin-coated vesicles, so confirming whether clathrin plays a role in DCG biogenesis and compartment contraction would help in dissecting this process and understanding its relation to similar processes in other systems. Previous experiments in the SC system have indicated that clathrin can bind in a punctate manner to secretory compartments, but since clathrin is also recruited in other processes such

as ESCRT-dependent ILV-biogenesis, more direct experiments will be required to examine this possibility (Kroeger, 2017; Raiborg et al., 2006).

Another interesting feature of DCG biogenesis was the simultaneous appearance of numerous, small, spatially separated aggregates. Their simultaneous formation suggests that the initial protein aggregation event occurs when some threshold in the local microenvironment has been reached. Precisely what this threshold is, however, and how it is regulated in SCs requires further investigation. Possible candidates for this environmental factor could include compartmental pH or the concentration of divalent ions such as Zn^{2+}, both of which are factors known to assist the condensation of secretory granules such as insulin granules (Jacob et al., 2016; Nettleton et al., 2000; Sun-wada et al., 2006). In *Drosophila*, zinc import through the ZnT35C transporter is required for lysosome-related storage granule biogenesis, whilst the phylogenetically related ZnT-8 transporter is required for appropriate insulin granule secretion in mice (Pound et al., 2009; Tejeda-Guzmán et al., 2018). Likewise, compartment acidification by the V-ATPase complex is required for several steps of secretory granule biogenesis including prohormone processing prior to biogenesis (Rhodes et al., 1987; Tompkins et al., 2002b). Perhaps surprisingly then, in experiments not included here, I observed no changes in DCG biogenesis following knockdown of either *ZnT35C* or components of the V-ATPase complex despite these genes being among the most highly expressed genes in SCs (Immarigeon et al., 2021). These results may be best explained by inefficient RNAi knockdown during experiments, but it may also indicate that these transporters are not essential for granule biogenesis in SCs. Explaining this, SCs may have compensatory mechanisms for Zn^{2+} and H^{+} ion import. Alternatively, Zn^{2+} and H^{+} ions may simply not be determining factors in DCG protein aggregation. Instead, the

concentration of MFAS protein itself, which is essential for DCG biogenesis (Singh et al., 2024), or the presence of another protein factor could control the onset of DCG aggregation. For example, GAPDH2 knockdown in SCs is known to disrupt both DCG aggregation and ILV biogenesis and so may play a role in the early stages of DCG formation (Dar et al., 2021). Distinguishing between these possibilities will be important for properly understanding the formation and behaviour of DCGs.

Chapter 4: Molecular control of DCG and exosome biogenesis in SCs

4.1 Introduction and aims

4.1.1 Aims

In the previous chapter, I produced a detailed characterisation of SCs and the major processes that occur in secretory compartments from the time they first form to the time they are released. To develop this work, I next began to investigate how some of the important processes that I had identified are regulated and what their functions are within the regulated secretory pathway of SCs. I also sought to establish how representative the processes occurring in SCs are of wider secretory systems, particularly those in mammals, by assessing the functions of known mammalian regulators in SCs. Throughout this, I gave particular attention to the novel Rab6 to Rab11 transition and DCG biogenesis. As such, my general aims were to:

1) Establish the role of conserved regulators in SC processes;
2) Establish the function of the novel Rab6 to Rab11 transition identified in SCs;
3) Identify novel mechanisms regulating DCG biogenesis;
4) Examine links between DCG biogenesis and neurodegenerative disease.

4.1.2 Previous work on DCG biogenesis

As discussed in Chapter 1 (Section 1.2.3), many questions remain concerning the details of DCG biogenesis, with multiple, often mutually exclusive, hypotheses competing to explain the mechanisms of important steps such as cargo selection, packaging and trafficking. What is more, the specifics of DCG-forming pathways seem to vary to some extent between different organisms and even different cell types, as seen by the fact that the use of reducing agents to disrupt the disulphide bridge domain of CHGB caused it to be missorted in rat adrenal P12 cells but not pituitary GH4C1 cells (Glombik et al., 1999; Taupenot et al., 2002).

Despite this, some important aspects of DCG biogenesis are both well-documented and seemingly well-conserved in DCG formation across evolution. Among the best studied of these are Arf1 and AP-1 which have been found to be essential for different DCG biogenesis events across many taxonomic groups. Arf1 and AP-1 function cooperatively in DCG compartment maturation, with Arf1 GTPase acting alongside transmembrane proteins to recruit the AP-1 complex to the cytosolic face of secretory compartment membranes (Austin et al., 2000; Bonnemaison et al., 2013; Burgess et al., 2011). AP-1 in turn recruits clathrin coat proteins to the compartment surface, thereby inducing vesicle budding and scission. This pathway is essential for extracting missorted proteins from regulated secretory compartments and recycling important factors back to the TGN. Inhibition of this pathway has even been found to lead to a complete loss of secretory granules in *Drosophila* salivary glands (Burgess et al., 2011). Interestingly, Arf1 but not AP-1 has also been implicated in the budding of

immature secretory compartments from the TGN, although no definitive mechanism for this process has been defined (Y.-G. Chen & Shields, 1996; Faúndez et al., 1997).

Previous work within the *Drosophila* SC model has also developed our knowledge of DCG biogenesis. For example, research led by Dr S. Redhai has shown that SC DCGs act as stores for DPP, the fly homologue of Bone Morphogenetic Protein (BMP) (Redhai et al., 2016). Following DCG secretion, secreted DPP acts via autocrine signalling to stimulate replenishment of DCG compartments within SCs. Furthermore, DCG biogenesis and maturation has also been shown to depend on the glycolytic protein GAPDH2 and on the membrane deforming ESCRT complex (Dar et al., 2021; Marie et al., 2023). Although the mechanisms regulating these effects are unclear, knockdown of either of *GAPDH2* or ESCRT proteins either inhibited DCG formation or significantly increased defects in DCG structure.

Additionally, from experiments outlined in Chapter 3, it was shown that DCG biogenesis occurs shortly after the onset of a novel Rab6 to Rab11 transition on regulated secretory compartment membranes (Section 3.2.5). It was also shown that SC DCGs form via one of two mechanisms. Specifically, DCGs can either form through the rapid fusion of numerous mini-cores, or they can form via the direct condensation of DCG cargoes into a single DCG (Section 3.2.6)

Finally, several studies in recent years have also found links between DCG protein dysregulation and certain pathologies (summarised in Section 1.2.4). Of particular interest to us were the links to neurodegenerative conditions such as Alzheimer's and Parkinson's disease. For example, specific granins and putative granin-cleaving proteases were found to be present at altered levels in the brains of AD patients (Quinn

et al., 2021, 2023), whilst significant defects in granin-mediated processing of DCG proteins have been found in mouse models of Parkinson's disease (Wen G et al., 2021). Given the abundance of structures such as neuropeptide granules within the brain and the role that protein aggregation plays in both neurodegenerative disease and certain granules, we became interested in the hypothesis that faults in DCG biogenesis could induce or exacerbate neurodegeneration-associated protein aggregation.

Overall then, I aimed to expand on my previous findings by dissecting the mechanisms regulating secretory compartment biology prior to and during DCG biogenesis. To do this, I used the UAS/GAL4/GAL80^{ts} expression system to induce SC-specific expression of relevant transgenes, often RNAi transcripts, within SCs. To assess the function of regulatory genes at different stages of the process, the same genes were often subjected to RNAi-induced knockdown in SCs of different genetic backgrounds, i.e. expressing different fluorescent fusion-proteins such as YFP-Rab1, CFP-Rab6 or YFP-Rab11. Time-lapse imaging has shown these labels mark different stages of secretory compartment maturation (Sections 3.2.4 and 3.2.5). Alongside use of GFP-MFAS, a DCG-specific marker, and GFP-GPI which labels non-acidic compartment membranes and DCGs, the combined use of these different markers allows for unmatched resolution of the different stages of DCG biogenesis and maturation.

4.2 Results

4.2.1 DCG biogenesis in SCs is controlled by the conserved secretory granule regulators Arf1 and AP-1

To test the hypothesis that the large DCGs in SCs are regulated by conserved pathways, I assessed the function of two trafficking regulators, Arf1 and the AP-1 complex, which both possess conserved functions in DCG biogenesis. To control for off-target effects, two independent RNAis were used to knockdown *Arf1* and one RNAi was used for each of the three *Drosophila AP-1* subunits, *AP-1-γ*, *AP-1-μ* and *AP-1-σ*. Although previous electron microscopy studies have indicated that DCGs are not membrane bound (Fan et al., 2020), DCGs can be labelled with a GPI-anchored form of GFP for reasons that remain uncertain. In my own experiments therefore, I used GFP-GPI expressed under UAS-control to mark maturing DCGs in live cells (Fig. 4.1A).

Analysis of DCGs through both GFP-GPI fluorescence and DIC microscopy showed that the number of DCGs is severely reduced following knockdown of *Arf1* (Fig. 4.1B,F) or any of the three AP-1 subunits, *AP-1γ*, *AP-1μ* and *AP-1σ*, although only the *AP-1γ* knockdown produced as strong a phenotype as seen in the Arf1 knockdowns *(*Fig. 4.1C-F). Nevertheless, the average number of DCG's present in all AP-1 knockdowns was reduced by at least two thirds compared to controls, and SCs were frequently found containing no DCGs at all across all *Arf1* and AP-1 knockdowns.

Following all *Arf1* and AP-1 knockdowns, the number of large non-acidic compartments (i.e. large secretory compartments) was also significantly reduced (Fig. 4.1A-E and Fig. 4.1G). Indeed, the average number of non-acidic compartments *was* reduced by approximately half in the least severe *AP-1σ* genotype and by approximately

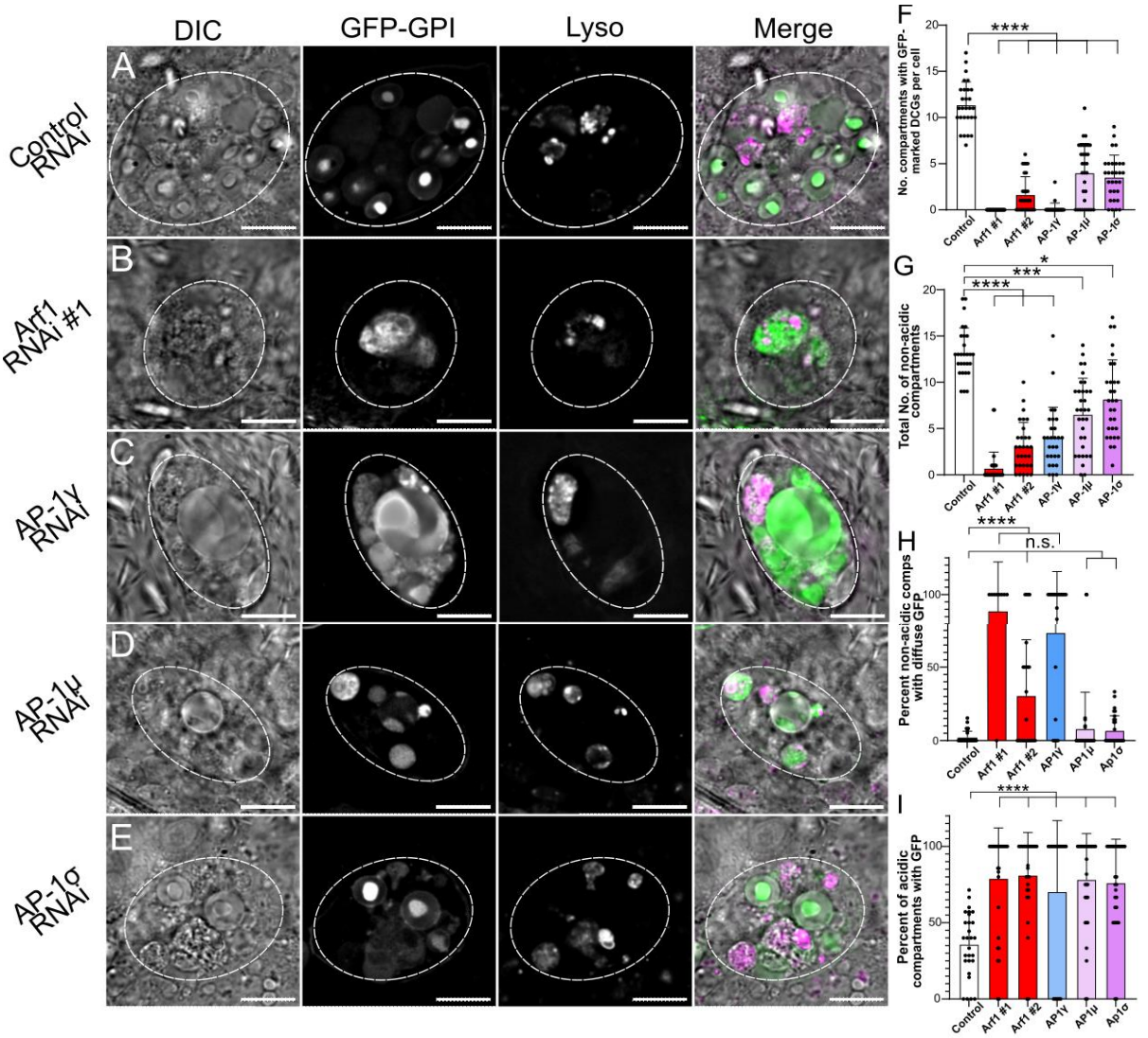

Figure 4.1. Arf1 and the AP-1 complex regulate DCG biogenesis in SCs. (**A-E**) Wide-field fluorescence images of SCs expressing *GFP-GPI* together with a control RNAi (**A**), *Arf1*-targeting RNAi (**B**), *AP-1γ*-targeting RNAi (**C**), *AP-1μ*-targeting RNAi (**D**), or *AP-1σ*-targeting RNAi (**E**). In multicoloured images GFP-GPI is shown in green, LysoTracker Red in magenta and DIC images in grayscale. Overall, expression of any *Arf1* or AP-1 RNAi severely disrupts secretory compartment and DCG organisation (**A-E**). Specifically, knockdown of *Arf1* and AP-1 subunits significantly reduces the numbers of GFP-GPI-marked DCGs (**F**) and the overall number of non-acidic compartments (**G**) in SCs. Additionally, *Arf1* and AP-1 knockdowns increase the proportion of non-acidic compartments in which GFP-GPI is spread diffusely throughout compartments

without concentrating into DCGs (**H**). Likewise, knockdowns significantly increase the proportion of acidic compartments in which GFP signal remains unquenched (**I**). Overall, *Arf1* and AP-1 knockdowns severely disrupt DCG formation within SCs and disrupt lysosomal processes. SC boundaries marked by dashed circles, Scale bars: 10μm. For graphs, P<0.05:*, P<0.01:**, P<0.001:***, P<0.0001:****, non-significant: n.s. n=28 to 32 cells for all graphs, though the number of datapoints for **H** specifically varied between 9 and 31 for each genotype.

90% in the stronger *Arf1* genotype. Interestingly, the non-acidic compartments that were formed following both *Arf1* knockdowns and the AP-1γ knockdown were often larger than typical secretory compartments, and a significantly greater proportion of them were characterised by diffuse GFP-GPI localisation throughout compartments rather than concentrated GFP signal within DCGs (Fig. 4.1H).

Similarly, following *Arf1* and *AP-1γ* knockdowns, a much greater proportion of acidic compartments also contained unquenched GFP signal (Fig. 4.1B-E and Fig. 4.1I). This residual GFP signal is indicative of incomplete protein degradation and suggests that there is substantially increased trafficking of GFP-GPI to lysosomes and/or an inhibition of lysosome function in SCs following *Arf1* and at least one AP-1 subunit knockdown.

These results provide support for a conserved role for Arf1 and the AP-1 complex in regulating DCG formation in SCs and suggest that cells lacking Arf1 and AP-1 do not form secretory compartments as normal. The secretory compartments that do form possess defects that, firstly, prevent GFP-GPI from concentrating into DCGs effectively, and secondly, increase compartmental trafficking to lysosomes.

4.2.2 Arf1 and AP-1 control Rab identity and DCG biogenesis in Rab11-compartments

Having identified the role of Arf1 and the AP-1 complex in the formation of DCGs and non-acidic compartments, I next sought to understand their effects on different

secretory compartment populations. Accordingly, I induced the same *Arf1* and AP-1 subunit knockdowns used above in a YFP-Rab11 background.

As expected, expressing any *Arf1* or AP-1 RNAis in the YFP-Rab11 background significantly decreased the number of DCGs present in SCs, just as observed in the GFP-GPI background (Fig. 4.2A-E and Fig. 4.2F). Interestingly though, the reduction in DCG numbers was less extreme for knockdowns in the YFP-Rab11 background than in the GFP-GPI background (compare Fig. 4.1F and Fig. 4.2F). This presumably reflects slightly reduced RNAi levels in this background due to less efficient expression by the UAS/GAL4 system. Regardless however, DCG formation was still strongly repressed and the most common phenotype for stronger knockdowns such as *Arf1*-RNAi#1 and *AP-1γ-RNAi* was a total inhibition of DCG formation, consistent with my results in the GFP-GPI background.

Alongside the decline in DCGs, the number of YFP-Rab11-labelled compartments was also significantly reduced in every knockdown line compared to control SCs, with the strongest reductions found once more in SCs expressing *Arf1* RNAis (Fig. 4.2G). Since DCG compartments are normally labelled by Rab11 (see Section 3.2.1), this result is broadly consistent with the decline in DCGs observed.

Interestingly however, although *Arf1* and AP-1 knockdown cells only produced a smaller number of Rab11-positive compartments, I found no significant difference in the proportion of Rab11-compartments that produced DCGs compared to control cells (Fig. 4.2H). This suggests that despite the obvious breakdown in trafficking regulation caused by *Arf1* and AP-1 knockdowns, compartments are capable of initiating DCG formation once they obtain Rab11 identity. The only knockdown for

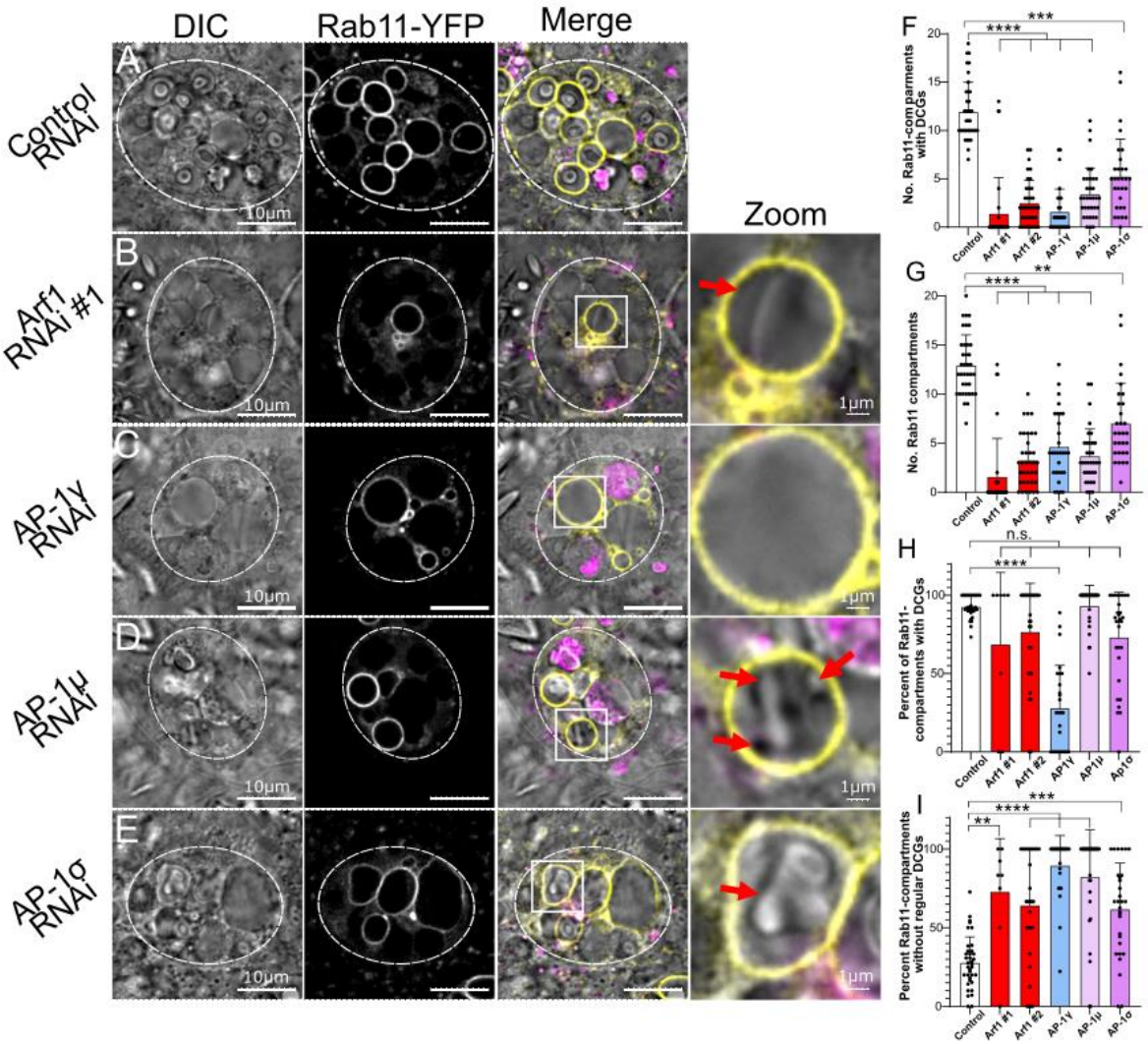

Figure 4.2. Arf1 and the AP-1 complex regulate DCG biogenesis and Rab11-compartment identity. (**A-E**) Wide-field fluorescence images of SCs expressing *YFP-Rab11* together with a control RNAi (**A**), *Arf1*-targeting RNAi (**B**), *AP-1γ*-targeting RNAi (**C**), *AP-1μ*-targeting RNAi (**D**), or *AP-1σ*-targeting RNAi (**E**). In multicoloured images Rab11 is shown in yellow, LysoTracker Red in magenta and DIC images in grayscale. As seen previously, expression of *Arf1* or AP-1 RNAis severely disrupts secretory compartment and DCG organisation, with red arrows indicating atypical DCGs (**A-E**). In particular, *Arf1* and AP-1 knockdowns can result in Rab11-compartments with no DCG (**C**), multiple mini-core aggregates (**D**) or otherwise abnormally shaped DCGs (**B**, **E**). When quantified, knockdown of *Arf1* and AP-1

subunits significantly reduces the number of Rab11-labelled DCG compartments (**F**) and the overall number of Rab11-compartments (**G**) in SCs. Additionally, *Arf1* and AP-1 knockdowns decrease the proportion of Rab11-compartments which form DCGs, though frequently not in a statistically significant manner (**H**). However, all *Arf1* and AP-1 knockdowns do significantly increase the proportion of Rab11-compartments which fail to produce typical DCGs, either because of a lack of any DCG or because of the formation of abnormal DCGs (**I**). Overall, *Arf1* and AP-1 knockdowns severely disrupt Rab11-compartment formation and DCG biogenesis within those compartments. SC boundaries marked by dashed circles. For graphs, P<0.05:*, P<0.01:**, P<0.001:***, P<0.0001:****, non-significant: n.s. n=30 to 37 cells for all graphs, though the number of datapoints for **H** and **I** varied between 8 and 37 for each genotype.

which this was not true was the *AP-1γ* knockdown, where just 28.0 ± 27.3% of Rab11-compartments contained DCGs (e.g. Fig. 4.2C), a significantly smaller proportion than the 92.8 ± 6.8 % that formed DCGs in control cells. The reasoning for this reduced DCG formation in the Rab11-compartments of *AP-1γ* knockdown cells was not immediately clear, particularly since the *AP-1γ* knockdown produced comparable effects to other knockdowns in terms of reductions in DCGs and Rab11-compartments. One potential complicating factor in analysing this particular phenotype was the fact that some "stronger" genotypes such as the *Arf1*-RNAi#1 produced no Rab11-compartments at all in >70% of SCs, meaning the effective sample size was as low as just 8 cells.

Since some DCGs were present in these cells, I proceeded to analyse whether these DCGs develop properly in the absence of normal *Arf1* and AP-1 expression. Interestingly, in all knockdown lines a significantly higher proportion of DCGs were found to exhibit structural abnormalities (Fig. 4.2I). This manifested in secretory compartments containing multiple small "mini-cores" rather than a single DCG and in abnormally shaped, non-spherical granules (Fig. 4.2 B,D,E). From time-lapse imaging of GFP-MFAS during DCG biogenesis (Section 3.2.6), I had noted that DCGs can form from multiple mini-cores which fuse together over time into stable spherical granules. Whilst they are maturing therefore, it was common to see DCGs which had irregular shapes or which were divided between multiple core fragments. This strongly suggests that the abnormal DCGs observed in *Arf1* and AP-1 knockdown cells represent granules that have failed to mature properly, with *t*he average proportion of DCG-compartments displaying these defects ranging from 62.0 ± 29.1% (*AP-1σ-RNAi)* to 89.6 ± 19.0% (*AP-1γ-RNAi)* in knockdowns, compared to 28.2 ± 16.5% in control cells.

Much like our results in the GFP-GPI background, these findings indicate that Arf1 and AP-1 are required for normal DCG biogenesis. They additionally show Arf1 and AP-1 are required for Rab11-compartment formation and for proper DCG maturation after this formation.

4.2.3 Arf1 and AP-1 control Rab identity and DCG biogenesis in Rab6-compartments

To further develop our understanding of Arf1 and AP-1, I carried out the same RNAi knockdowns in the CFP-Rab6 background (Fig. 4.3A-E). As expected, knocking down any of *Arf1*, *AP-1γ, AP-1μ or AP-1σ* induced a severe reduction in the number of DCG compartments (Fig. 4.3F), just as had been observed in other backgrounds. Furthermore, all knockdowns other than the AP-1γ-RNAi also induced a very large decline in the number of Rab6-positive compartments, with the greatest reduction being caused by *Arf1*-RNAi#1 which produced just 1.0 ± 1.2 CFP-Rab6-labelled compartments compared to 9.1 ± 1.8 in control cells (Fig. 4.3G). *Arf1*-RNAi#2, *AP-1μ and AP-1σ* knockdowns also resulted in the number of Rab6-positive compartments in SCs at least halving compared to controls, whilst *AP-1γ* knockdown produced no significant change in the number of Rab6-compartments. Since Rab6 is not the primary marker of DCG compartments, this reduction in Rab6-positive compartments was not necessarily anticipated. One particularly interesting finding related to this reduction in Rab6-compartments was that in both *Arf1* knockdowns, but not in *AP-1* subunit knockdowns, a number of large non-acidic, non-DCG compartments were

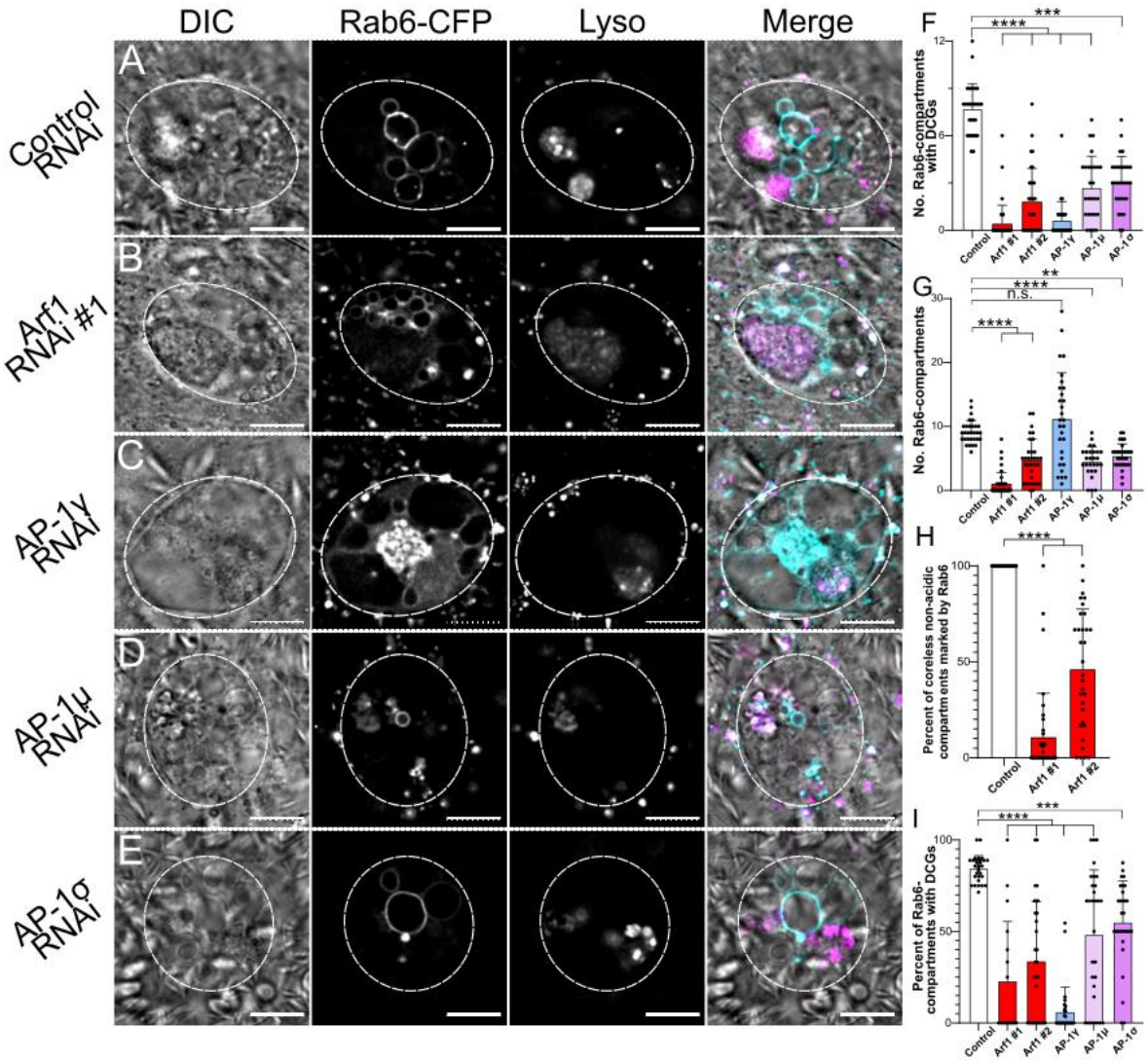

Figure 4.3. Arf1 and the AP-1 complex regulate DCG biogenesis and Rab6-compartment identity. (**A-E**) Wide-field fluorescence images of SCs expressing *CFP-Rab6* together with a control RNAi (**A**), *Arf1*-targeting RNAi (**B**), *AP-1γ*-targeting RNAi (**C**), *AP-1μ*-targeting RNAi (**D**), or *AP-1σ*-targeting RNAi (**E**). In multicoloured images Rab6 is shown in cyan, LysoTracker Red in magenta and DIC images in grayscale. Expression of *Arf1* or AP-1 RNAis severely disrupts Rab6-compartment and DCG organisation (**A-E**). Specifically, knockdown of *Arf1* and AP-1 subunits significantly reduces the number of Rab6-labelled DCG compartments in all cases (**F**) and the overall number of Rab6-compartments in all but one genotype (**G**). Additionally, both *Arf1* knockdowns resulted in the formation of large, non-DCG compartments that were not labelled by Rab6, a

phenomenon not seen in any control cells (**H**). Finally, all *Arf1* and AP-1 subunit knockdowns significantly decreased the proportion of Rab6-compartments found to contain DCGs (**G**). Overall, *Arf1* and AP-1 knockdowns appear to disrupt Rab6-compartment formation and DCG biogenesis within those compartments. SC boundaries marked by dashed circles. Scale bars: 10μm. For graphs, P<0.05:*, P<0.01:**, P<0.001:***, P<0.0001:****, non-significant: n.s. n=27 to 39 cells for all graphs, though the number of datapoints for **I** varied between 17 and 30 for each genotype.

produced that were not labelled with the Golgi-marker CFP-Rab6 as would normally be expected (Fig. 4.3H).

Additionally, every *Arf1* and *AP-1* subunit knockdown resulted in a significant decrease in the proportion of Rab6-compartments forming DCGs (Fig. 4.3I). Given that the rate of DCG biogenesis within Rab11-compartments was mostly unaffected by *Arf1* and *AP-1* knockdowns, the finding that DCG biogenesis within Rab6 compartments is inhibited by *Arf1* and *AP*-1 knockdown provides further support for the idea that DCG biogenesis occurs after Rab11-identity is achieved.

4.2.4 Arf1 and AP-1 are essential regulators of the Rab1 to Rab6 transition

Based on the finding that *Arf1* knockdowns caused SCs to produce large non-DCG compartments that were not labelled by Rab6 (Fig. 4.3H), it was surmised that these non-DCG compartments had failed to mature to Rab6 identity and may therefore retain characteristics of an earlier compartment type. To test this hypothesis, I crossbred *Arf1*-RNAi#2 into the *YFP-Rab1* fusion gene line and then induced expression of the RNAi through breeding with a *w; tub-Gal80^{ts}; dsx-Gal4* driver line followed by incubation at 29°C. In cells expressing *Arf1*-RNAi#2, YFP-Rab1 strongly labelled the large, non-acidic, non-DCG compartments, a phenomenon not observed in any control cells (Fig. 4.4A,B). Given the similar distributions of Rab1 and Rab2 in healthy control cells, I also examined whether YFP-Rab2 was associated with these large coreless compartments. In contrast to Rab1, however, I found no evidence for Rab2's

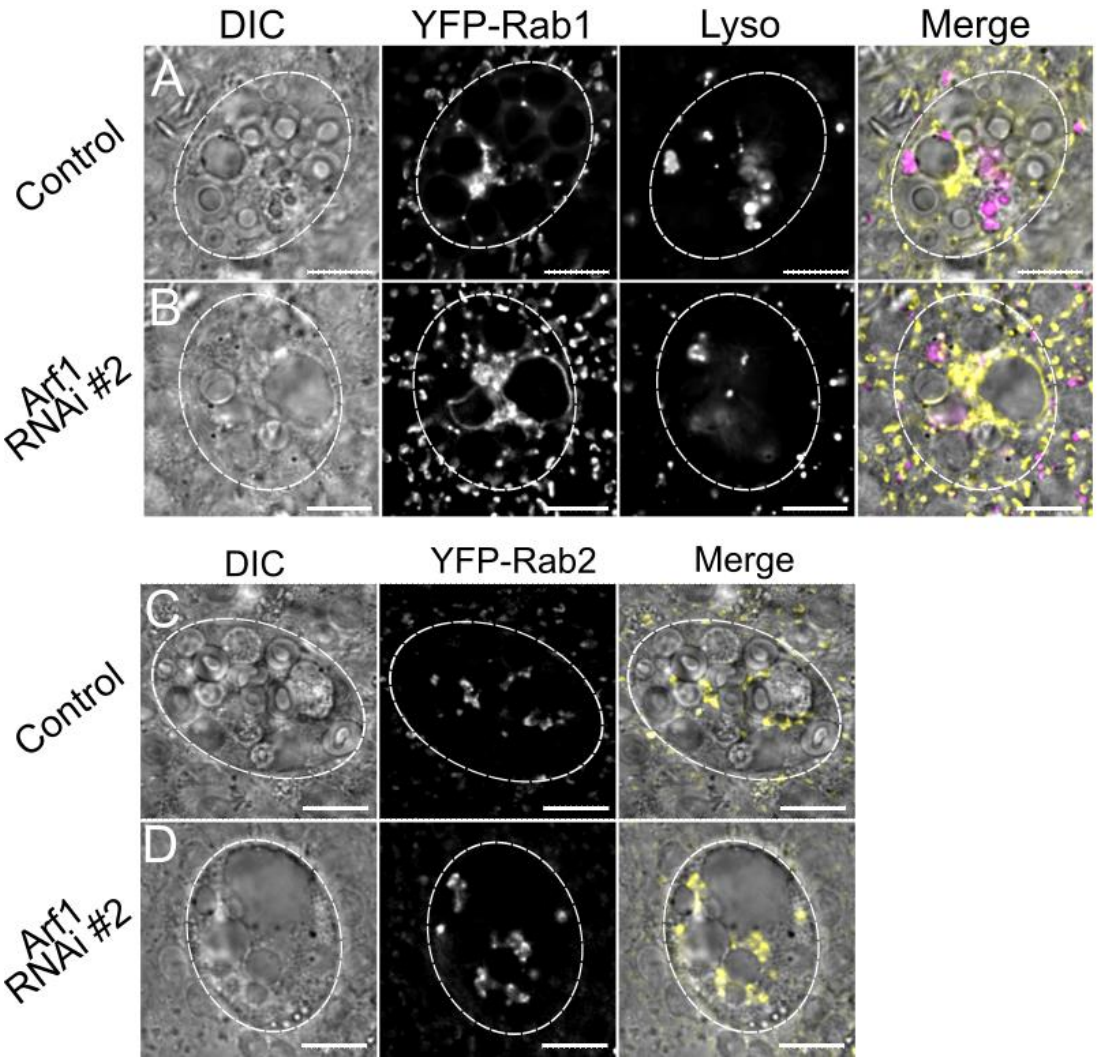

Figure 4.4. Arf1 controls the Rab1 to Rab6 transition on compartment membranes. **(A-D**) Wide-field fluorescence images of SCs expressing *YFP-Rab1* with a control RNAi (**A**) or *Arf1* RNAi (**B**), and SCs expressing *YFP-Rab2* with a control RNAi (**C**) or *Arf1* RNAi (**D**). In multicoloured images Rabs are shown in yellow, LysoTracker Red in magenta and DIC images in grayscale. *Arf1* knockdown induces the formation of large non-DCG compartments labelled by Rab1, a phenomenon not observed in control SCs (**A**,**B**). Since *Arf1* knockdown was earlier found to produce Rab6-negative non-DCG compartments, this suggests that Arf1 facilitates the Rab1 to Rab6 transition. By contrast, *Arf1* knockdown does not induce the formation of any large compartments marked by Rab2 (**C**,**D**). SC boundaries marked by dashed circles, Scale bars: 10µm.

association (Fig. 4.4C,D). Arf1 and the AP-1 complex therefore seem to facilitate the Rab1 to Rab6 transition on SC compartments.

4.2.5 Rab6 and Rab11 control DCG biogenesis in SCs expressing GFP-GPI

Having shown that Arf1 and the AP-1 complex each control DCG biogenesis and regulate the identity of Rab6- and Rab11-compartments, I investigated the role that Rab6 and Rab11 themselves might play in DCG formation. To do this, I used two independent RNAis to knockdown each of *Rab6* and *Rab11* in a cell-type-specific manner in SCs expressing the GFP-GPI marker of DCGs (Fig. 4.5A-C).

Knockdown of either *Rab6* or *Rab11* significantly reduced the number of SC DCGs relative to controls (Fig. 4.5D). Each *Rab* knockdown also reduced the number of large non-acidic compartments formed within SCs (Fig. 4.5E) and, aside from *Rab11*-RNAi#2, every *Rab* knockdown line also resulted in a higher proportion of large non-acidic compartments being marked by diffuse GFP-GPI rather than the concentrated GFP found within DCGs (Fig. 4.5F). Finally, examination of the acidic compartments in *Rab6* and *Rab11* knockdown cells showed that the proportion of acidic compartments containing unquenched GFP was significantly increased compared to controls, suggesting that these knockdowns experience increased trafficking to the lysosomal pathway and/or disruptions to lysosome activity (Fig. 4.5G). These results closely mirrored our findings from *Arf1* and AP-1 knockdowns and demonstrated that both Rab6 and Rab11 are required for DCG biogenesis and large secretory compartment formation.

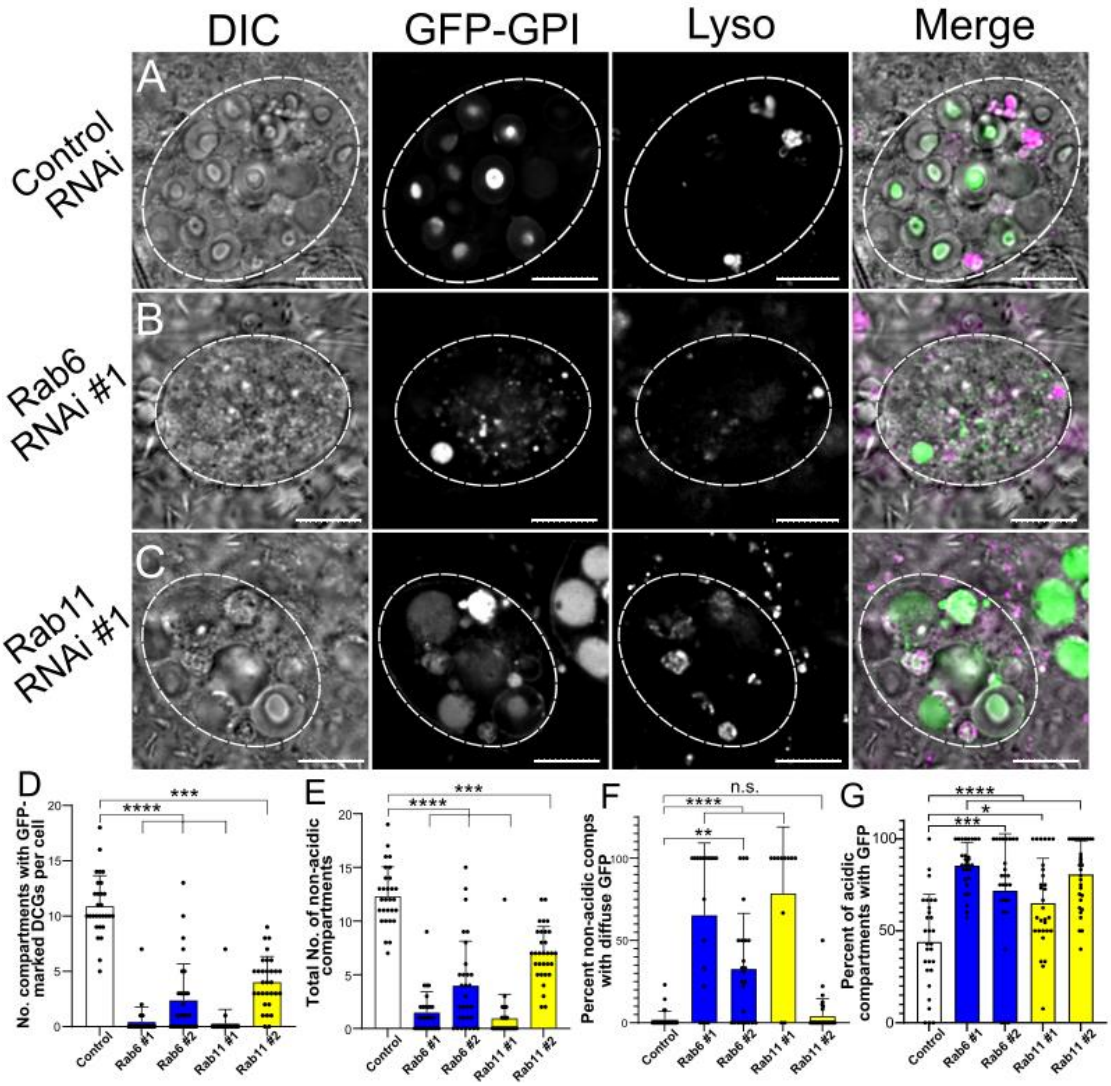

Figure 4.5. Rab6 and Rab11 regulate DCG and secretory compartment biogenesis.

(**A-C**) Wide-field fluorescence images of SCs expressing *GFP-GPI* together with a control RNAi (**A**), *Rab6*-targeting RNAi (**B**) or *Rab11*-targeting RNAi (**C**). In multicoloured images GFP-GPI is shown in green, LysoTracker Red in magenta and DIC images in grayscale. Expression of *Rab6* or *Rab11* RNAis severely disrupts secretory compartment and DCG organisation in a manner similar to *Arf1* and AP-1 knockdowns (**A-C**). For example, knockdown of *Rab6* or *Rab11* significantly reduces the numbers of GFP-GPI-marked DCGs (**D**) and the overall number of non-acidic compartments (**E**) in SCs. Knockdowns also increase the proportion of non-acidic compartments in which GFP-GPI is spread diffusely throughout compartments without concentrating into

DCGs (**F**) and significantly increase the proportion of acidic compartments in which GFP signal remains unquenched (**G**). Overall, *Rab6* and *Rab11* knockdowns disrupt DCG formation and lysosomal processes within SCs. SC boundaries marked by dashed circles, Scale bars: 10μm. For graphs, P<0.05:*, P<0.01:**, P<0.001:***, P<0.0001:****, non-significant: n.s. n=29 to 31 cells for all graphs, though the number of datapoints for **F** specifically varied between 11 and 31 for each genotype.

4.2.6 Rab6 and Rab11 are both required for DCG biogenesis in Rab11-compartments and establishing Rab11-compartment identity

Since DCG-compartments appear to be synonymous with Rab11-compartments in wildtype SCs, I examined the specific effects of *Rab6* and *Rab11* knockdowns in Rab11-compartments using the same inducible *Rab6* and *Rab11* RNAis utilised above. In line with my observations in the GFP-GPI background, knockdown of *Rab6* and *Rab11* resulted in significantly fewer DCG compartments, with fewer *YFP-Rab11* labelled DCG-compartments being present following each Rab knockdown (Fig. 4.6A-C and Fig. 4.6D).

Interestingly, the decline in DCG numbers in the *YFP-Rab11* backgrounds was not as extreme as the decline observed in the GFP-GPI background (Compare Fig. 4.5D and Fig 4.6D). The explanation for this appears to be that knockdown of gene expression in this background is incomplete. I had previously assumed this after knockdown experiments for Arf1 and AP-1 subunits in *CFP-Rab6* and *YFP-Rab11* backgrounds, but it was demonstrated directly in this case by the fact that some fluorescent YFP-Rab11 was still visible in SCs even after *Rab11* knockdown (Fig. 4.6C). Regardless however, both *Rab6* and *Rab11* knockdowns significantly reduced the number of DCGs, with average numbers of DCGs falling from 11.2 ± 2.3 in controls, to between 1.8 ± 2.0 (*Rab11*-RNAi#1) and 5.3 ± 4.7 (*Rab6*-RNAi#1) DCGs per cell (Fig 4.6D).

In addition, following *Rab6* and *Rab11* knockdowns, a significantly greater proportion of Rab11-compartments failed to produce regular, mature DCGs within their lumen, with many compartments found to contain either no DCG (Fig. 4.6B) or else multiple small and abnormal DCG aggregates (Fig. 4.6B,C,E). This further suggests that Rab6

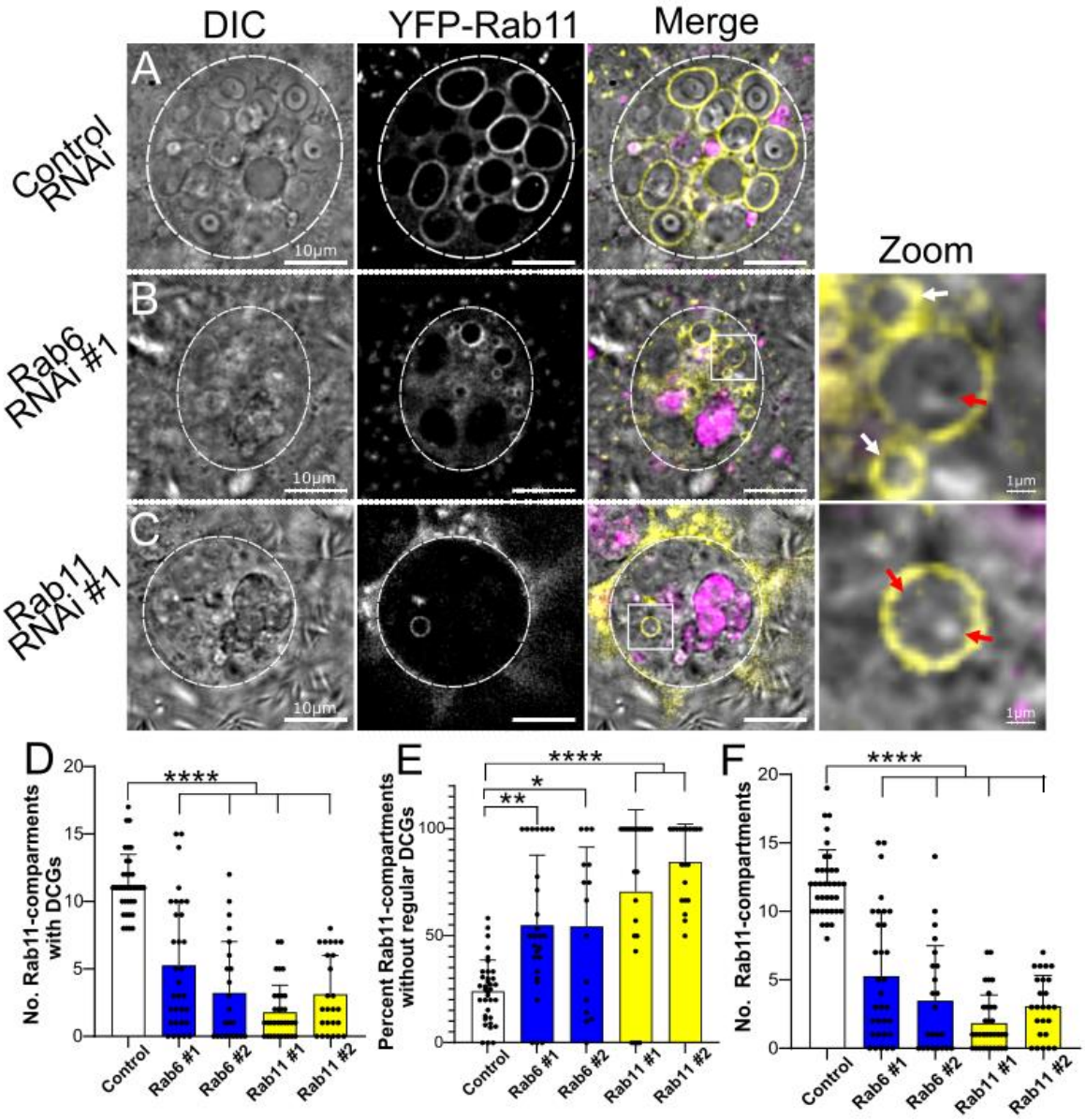

Figure 4.6. Rab6 and Rab11 are both required for Rab11-compartment formation and DCG biogenesis. (**A-E**) Wide-field fluorescence images of SCs expressing *YFP-Rab11* together with a control RNAi (**A**), *Rab6*-targeting RNAi (**B**) or *Rab11*-targeting RNAi (**C**). In multicoloured images Rab11 is shown in yellow, LysoTracker Red in magenta and DIC images in grayscale. Expression of either *Rab6* or *Rab11* RNAis severely disrupts Rab11-compartment formation and DCG organisation (**A-C**). In particular, knockdowns can result in Rab11-compartments with no DCG (examples indicated by white arrows in **B**), or abnormal DCG compartments such as those

containing multiple mini-core aggregates (red arrows in **C**). In addition, knockdown of *Rab6* and *Rab11* significantly reduces the number of Rab11-positive DCG compartments (**D**) and significantly increases the proportion of Rab11-compartments which fail to produce typical DCGs, either because of a lack of any DCG or because of the formation of abnormal DCGs (**E**). Finally, knockdown of both Rab6 and Rab11 decreases overall Rab11-compartment numbers, indicating that Rab6 is necessary for later Rab11-compartment formation (**F**). SC boundaries marked by dashed circles. For graphs, P<0.05:*, P<0.01:**, P<0.001:***, P<0.0001:****, non-significant: n.s. n=23 to 36 cells for all graphs, though the number of datapoints for **E** varied between 15 and 36 for each genotype.

and Rab11 are both required for proper DCG biogenesis and maturation processes to occur.

Beyond DCG biogenesis, the impact of Rab knockdowns on Rab11-identity was also investigated. Unsurprisingly, knockdown of *Rab11* strongly reduced the number of YFP-Rab11-positive compartments compared to controls (Fig. 4.6F). In addition, knocking down *Rab6* greatly reduced the number of large Rab11-positive compartments, with approximately 75% fewer Rab11-compartments being present on average relative to controls. Indeed, in many cases, no Rab11-compartments were present at all. This is consistent with my previous observation of a Rab6 to Rab11 transition and confirms that Rab6 is necessary for the later recruitment of Rab11 to compartment membranes.

4.2.7 The Rab6 to Rab11 transition controls DCG and exosome biogenesis

Finally, I examined the effects of *Rab6* and *Rab11* knockdowns on Rab6-compartments. As expected, knockdown of *Rab6* and *Rab11* resulted in significantly fewer DCGs being present within Rab6-labelled compartments, with a single exception (Fig. 4.7A-C and Fig. 4.7D). In cells expressing *Rab11*-RNAi#2, the average number of Rab6-compartments was significantly increased, which resulted in the total number of Rab6-positive DCG compartments remaining unchanged relative to controls (Fig. 4.7E). By examining the frequency of DCGs in Rab6-compartments, however, it became clear that every *Rab6* and *Rab11* RNAi induced a large decrease in the proportion of Rab6-compartments forming DCGs (Fig. 4.7F). This decrease was statistically significant for each *Rab* knockdown except *Rab6*-RNAi#2 which halved the

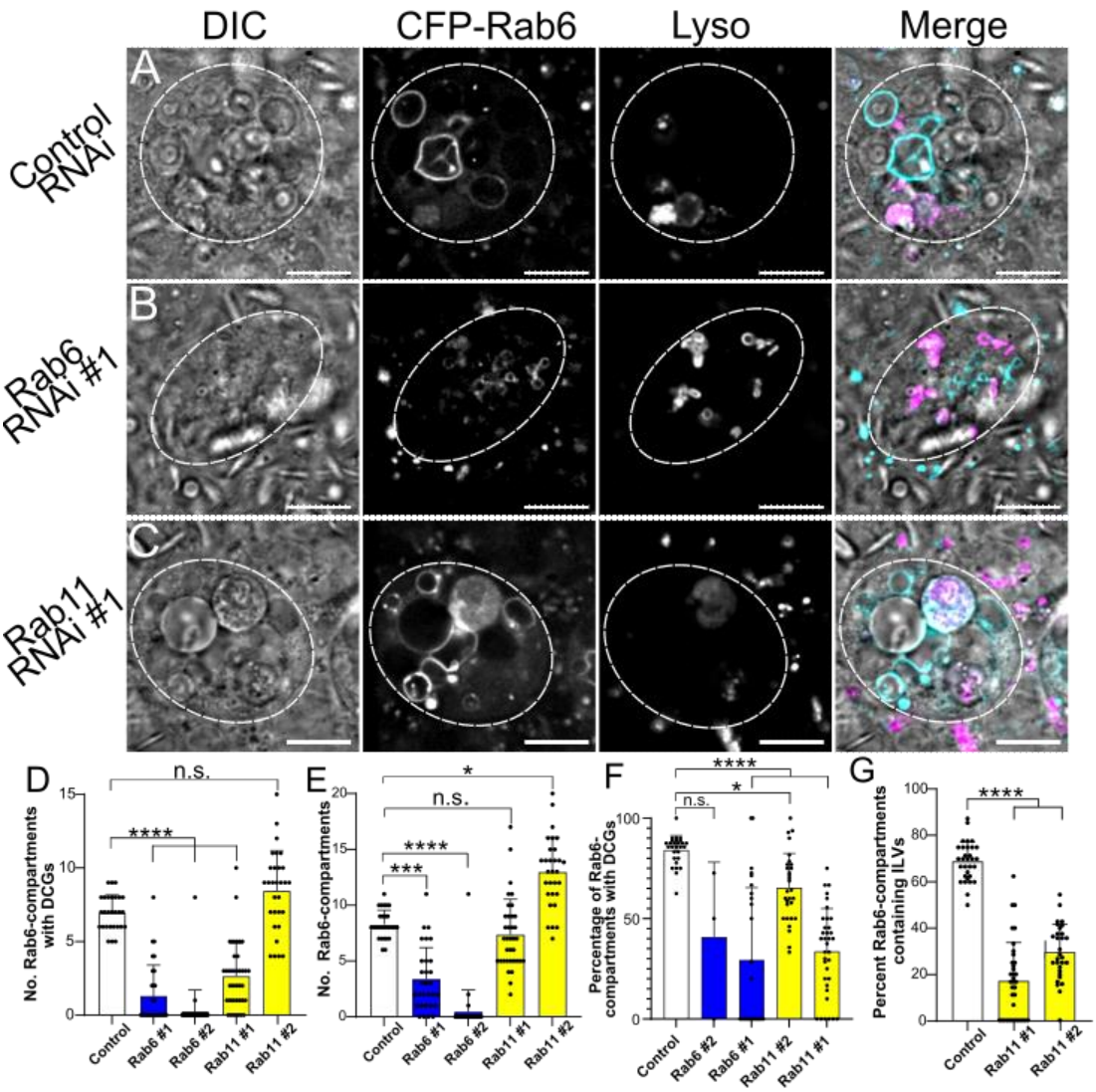

Figure 4.7. The Rab6 to Rab11 transition is specifically required for DCG and exosome biogenesis. (**A-E**) Wide-field fluorescence images of SCs expressing *CFP-Rab6* together with a control RNAi (**A**), *Rab6*-targeting RNAi (**B**) or *Rab11*-targeting RNAi (**C**). In multicoloured images Rab6 is shown in cyan, LysoTracker Red in magenta and DIC images in grayscale. Expression of *Rab6* or *Rab11* RNAis severely disrupts Rab6-compartment and DCG organisation (**A-C**). Knockdown of *Rab6* and *Rab11* significantly reduces the number of Rab6-labelled DCG compartments in all but one case, *Rab11-RNAi#2* (**D**). *Rab6* knockdowns also significantly reduce the number of Rab6-compartments (**E**), though neither *Rab11* knockdown does. Indeed *Rab11-RNAi#1* has no effect on the number of Rab6-compartments whilst *Rab11-RNAi#2*

actually increases the number of Rab6-compartments (**E**). This indicates that Rab11 is not required for Rab6-compartment formation. However, expression of any *Rab6* or *Rab11* RNAi does reduce the proportion of Rab6-compartments which form DCGs (**F**), indicating that Rab11 is necessary for facilitating DCG biogenesis within Rab6-compartments after their formation. Likewise, *Rab11* knockdowns also reduce the proportion of Rab6-compartments able to form ILVs, indicating that Rab11 is also required to trigger ILV biogenesis within Rab6-compartments (**G**). SC boundaries marked by dashed circles. Scale bars: 10μm. For graphs, P<0.05:*, P<0.01:**, P<0.001:***, P<0.0001:****, non-significant: n.s. n=28 to 36 cells for all graphs, though the number of datapoints for **F** varied between 3 and 36 for each genotype.

proportion of Rab6-compartments containing DCGs, but which also only had an effective sample size of 3 cells, since ~90% of SCs contained no Rab6-compartments at all. In combination, the results described above indicate that Rab6 and Rab11 are essential for proper DCG formation in SCs, especially when considered alongside the collapse in DCG numbers seen in GFP-GPI-expressing SCs following *Rab6* and *Rab11* knockdown.

Examining the effect of *Rab* knockdowns on secretory compartment identity, I found that both *Rab6* knockdowns significantly reduced the number of Rab6-positive compartments in SCs, although incomplete knockdown meant that a few Rab6-compartments were retained (Fig. 4.7B,E). Notably however, knocking down *Rab11* did not reduce the number of Rab6-positive compartments (Fig. 4.7C,E). In fact, *Rab11*-RNAi#2 slightly increased the number of large Rab6-positive compartments, whilst *Rab11*-RNAi#1 induced no significant change, suggesting that Rab6 compartments can form normally in the absence of Rab11. This stands in direct contrast to Rab11-compartments, which cannot form properly following *Rab6* knockdown (see Fig. 4.6B,F).

Combining knockdown results from different backgrounds, I find that Rab6 and Rab11 are both essential for the process of DCG biogenesis. What is more, both Rabs are also required for the formation of Rab11-compartments. Importantly however, Rab6 compartments do not require Rab11 to form and are still produced normally following *Rab11* knockdown despite DCG biogenesis being strongly inhibited. This indicates that the materials present in Rab6-compartments are insufficient to trigger DCG biogenesis

and provides good evidence that the recruitment of Rab11 is essential for DCG formation to occur.

Developing this conclusion, I hypothesised that exosome biogenesis is also specifically Rab11-dependent. This was based on my previous finding that ILVs are almost exclusively found in compartments with DCGs (Section 3.2.1) and on time-lapse imaging experiments that show ILV and DCG biogenesis occurring essentially simultaneously (Section 3.2.5). These observations suggested that ILV and DCG biogenesis are closely linked, so I posited that just as observed with DCGs, *Rab11* knockdown would inhibit the formation of ILVs in CFP-Rab6-labelled compartments despite Rab6-compartments being produced at normal or greater than normal levels compared to control cells. Following *Rab11* knockdown, ILV biogenesis was massively reduced in Rab6-compartments (Fig. 4.7G). As with DCG biogenesis, these results indicate that Rab11 must be recruited to compartment membranes for ILV biogenesis to occur, and indicates that Rab6-compartments alone are insufficient for biogenesis to occur.

4.2.8 Dense core granules fail to condense in the absence of the chaperone protein Hsp83

Following an analysis that I conducted of human Rab11a-exosome proteome data acquired by Dr S. Fan (full analysis discussed in Section 6.2.4), I investigated the role of Hsp83, a *Drosophila* Hsp90 protein homologous to Hsp90α in mammals. Hsp90's are an extremely well-conserved chaperone family of proteins found in virtually all organisms that assist protein folding and play an essential role in cell stress adaptation (B. Chen et al., 2006). They are also among the most highly expressed proteins in nature

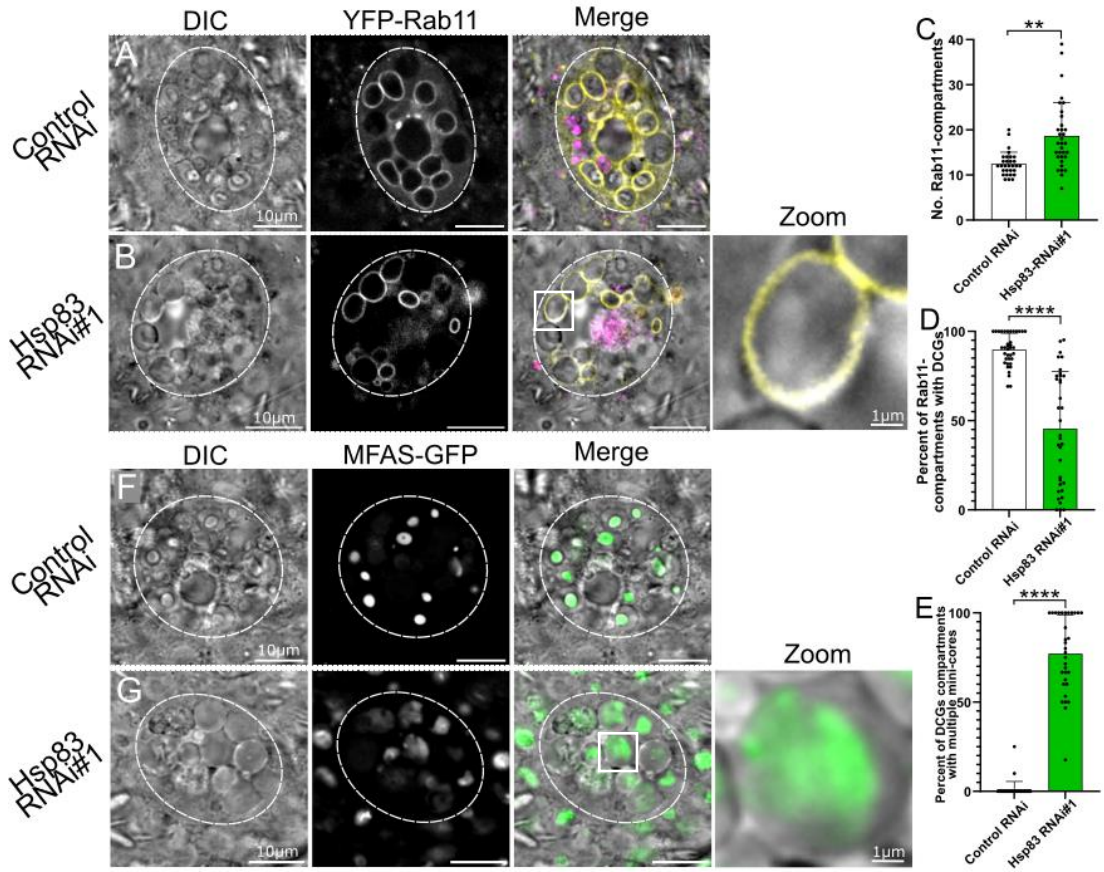

Figure 4.8. The Hsp83 chaperone protein is required for DCG cargo condensation. (**A-B**) Wide-field fluorescence images of SCs expressing *YFP-Rab11* together with a control RNAi (**A**) or *Hsp83*-targeting RNAi (**B**). In multicoloured images Rab11 is shown in yellow, LysoTracker Red in magenta and DIC images in grayscale. Knockdown of *Hsp83* appears to specifically inhibit DCG biogenesis, resulting in Rab11-positive compartments that lack DCGs (e.g. zoom image in **B**). *Hsp83* knockdown slightly increases the number of Rab11-compartments within SCs (**C**) yet significantly reduces the proportion of them which form DCGs (**D**). In addition, in SC compartments where DCGs do form, the majority of these contain multiple mini-cores instead of a single mature DCG (**E**). (**F-G**) Wide-field fluorescence images of SCs expressing *GFP-mfas* together with a control RNAi (**F**) or *Hsp83*-targeting RNAi (**G**). In multicoloured images MFAS is shown in green and DIC images in grayscale. Although Hsp83 knockdown inhibits DCG formation, it does not prevent MFAS accumulation within compartments (e.g. zoom image in **G**). SC boundaries marked by dashed circles. For graphs, P<0.01:**, P<0.0001:****. n=30 to 33 cells for all graphs.

and are estimated to comprise 4%-6% of total proteins in stressed cells (Finka & Goloubinoff, 2013; Zuehlke et al., 2015). Mutations in the human Hsp90α is also associated with the progression of various diseases, including cancer, AD and Parkinson's disease (Birbo et al., 2021; Bohush et al., 2019). Furthermore, Hsp90α is both loaded onto exosomes as an extravesicular secretory cargo and has been shown to induce membrane curvature required for exosome biogenesis (Lauwers et al., 2018; X. Tang et al., 2019).

Because of these associations, I expressed an *Hsp83*-targeting RNAi in SCs with the YFP-Rab11 background (Fig. 4.8A,B). Interestingly, this resulted in an increase in the number of Rab11-positive compartments present in SCs (Fig. 4.8C). However, the most striking effect of *Hsp83* knockdown was the inhibition of DCG biogenesis within Rab11-compartments (Fig. 4.8D, example image in 4.8B). Indeed, the rate of DCG formation within Rab11-compartments effectively halved, from 89.5 ± 8.9% in controls to 45.5 ± 32.0%. This was particularly fascinating as it indicated that *Hsp83* knockdown effectively inhibited DCG biogenesis without disrupting Rab11-compartment formation, two processes I had previously found were very closely related. Of the DCGs that did form, the majority displayed severe defects, with 77.2 ± 21.7% of DCGs split between numerous mini-cores within their compartments (Fig. 4.8E).

Given this fascinating phenotype, I sought to understand the mechanism underlying it by expressing *Hsp83-RNAi#1* in the GFP-MFAS background (Fig. 4.8G,H). In control cells in this experiment, GFP-MFAS was found either at high-density, concentrated into DCGs or at low-density, spread throughout non-DCG compartments (Fig. 4.8G). In *Hsp83* knockdown cells however, MFAS was found in most compartments at relatively

high densities, yet was still spread diffusely throughout compartments and did not concentrate into DCGs (Fig. 4.8H). In addition, a small number of compartments were seen in knockdown cells that had lower concentrations of GFP-MFAS and which resemble immature Rab6-compartments when examined with DIC microscopy, i.e. they were often larger, central and have a darker appearance. These results confirmed that large secretory Rab11-compartments are able to form and mature as normal in the absence of Hsp83, up to and including the accumulation of MFAS within compartments. Crucially however, the accumulated MFAS cannot condense into a DCG. This unique phenotype suggests that Hsp83 promotes DCG condensation in a step that occurs after Rab11-recruitment to compartment membranes.

4.2.9 APPL, GAPDH2 and PI3-Kinase control dense core granule maturation

Given the interesting links between DCG dysregulation and neurodegenerative illnesses, I investigated the role of several neurodegeneration-linked genes in DCG biogenesis. The first, β-Amyloid Precursor Protein-like (APPL), is the *Drosophila* homologue of APP which is cleaved into Amyloid-β (Aβ) peptides which in turn form the neurodegenerative plaques seen in AD (G. Chen et al., 2017; Hampel et al., 2021; O'Brien & Wong, 2011; H. Zheng & Koo, 2011). The second is Glyceraldehyde 3-phosphate dehydrogenase 2 (GAPDH2), homologue of GAPDH, an enzyme conserved from bacteria to humans. GAPDH is named for its role in the glycolytic pathway, but it also moonlights in a surprising range of other processes including as a modulator of protein aggregation (Chaudhary et al., 2021). GAPDH is also a well-known risk factor in

neurodegenerative conditions, with increased nuclear GAPDH activity and GAPDH/amyloid-β coaggregation found to play pathological roles in Alzheimer's disease (Berry, 2004; Butterfield et al., 2010, Itakura et al., 2015). Finally, I investigated Dp110, the catalytic subunit of *Drosophila* class I phosphatidylinositol 3-kinase (PI3-kinase). The best recognised function of class I PI3-kinases is in cell-growth and cell-survival signalling acting downstream of growth factors and insulin amongst other ligands (Fruman et al., 2017; Hemmings & Restuccia, 2012; Hopkins et al., 2020). PI3-kinase also controls important processes in the brain including neuronal maturation and myelination (Sánchez-Alegría et al., 2018), and like APPL and GAPDH2, PI3-kinase activity has been identified as an important factor in the development of neurodegenerative diseases (Fruman et al., 2017; Goyal et al., 2023; Sánchez-Alegría et al., 2018).

Prior to the experiments described here, *APPL*, *GAPDH2* and *Dp110* had each been identified as factors regulating SC DCGs in work led by Dr P. Singh (P. Singh, 2023), Dr C. Mendes (Dar et al., 2021), and myself respectively (Section 5.2.9). More specifically, SC-specific knockdown of each had been found to disrupt DCG formation, resulting in compartments that contained multiple "mini-cores" rather than a single DCG. However, the mechanistic underpinnings of these phenotypes was still unknown. Since I had recently developed new real-time imaging techniques in SCs that could directly image the dynamics of DCG biogenesis, I applied these techniques to understanding how DCG biogenesis changed following *APPL*, *GAPDH2* and *Dp110* knockdown. To do this, I expressed RNAis targeting each of the genes of interest for 5-7 days post-eclosion in males with the GFP-MFAS background and imaged the SCs within dissected accessory glands. To best visualise the movement of multiple mini-

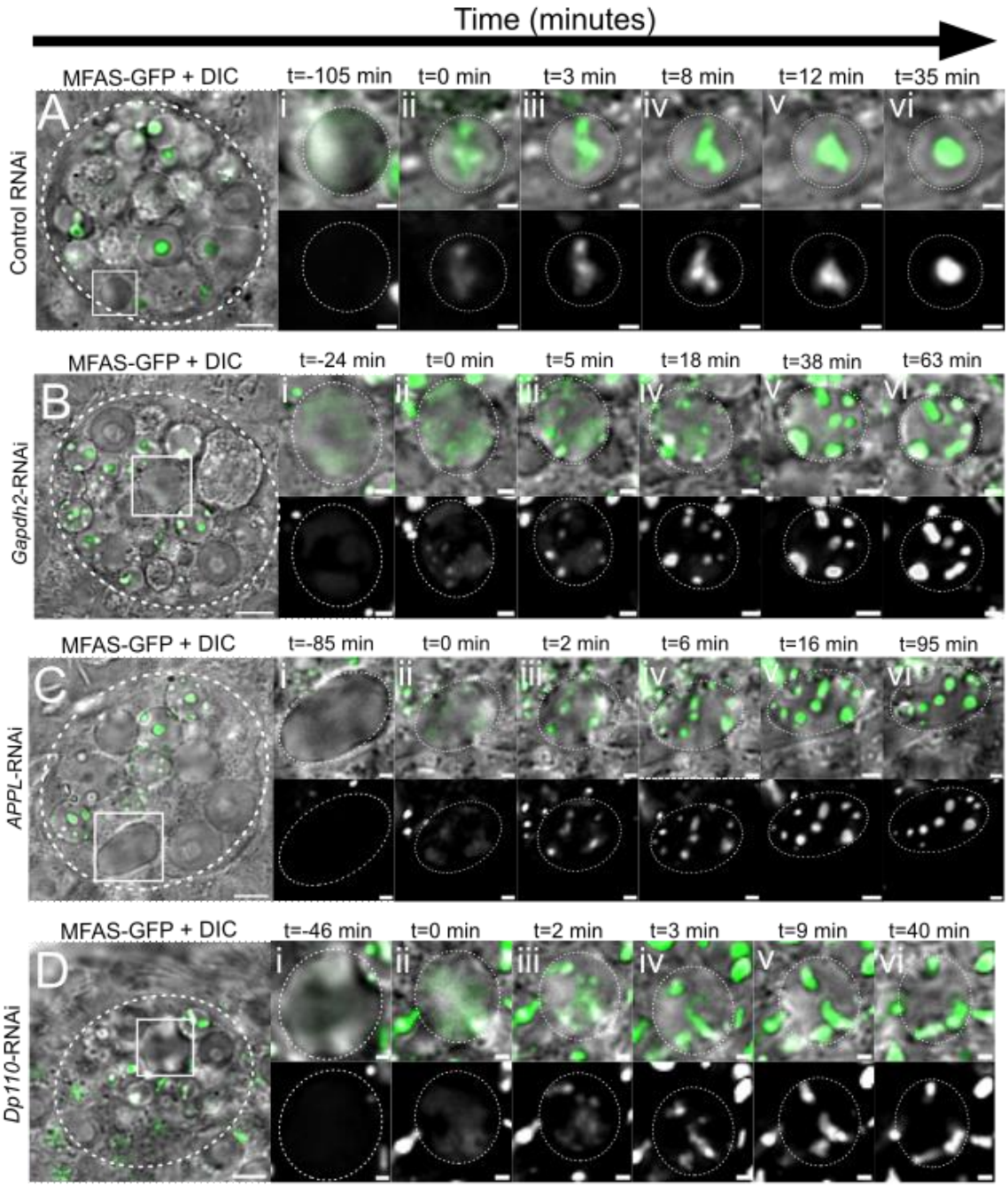

Figure 4.9. APPL, GAPDH2 and Dp110 each regulate DCG maturation post-condensation. Time-lapse imaging of SCs expressing *GFP-mfas* together with a control RNAi (**A**), *Gapdh2*-targeting RNAi (**B**), *APPL*-targeting RNAi (**C**) or *Dp110*-targeting RNAi (**D**). In multicoloured images MFAS is shown in green and DIC images in grayscale. In all cases, including in control SCs, the initial stages of DCG biogenesis remain consistent, with non-DCG compartments gradually accumulating diffuse,

lumenal MFAS in all backgrounds (timepoints **i**-**ii**). Then, within a 2-5 minute timeframe, this diffuse pool of MFAS begins to concentrate into smaller structures such as the central DCG (**A**iii) or mini-cores (**B**iii-**D**iii). From this point onwards, DCG biogenesis/maturation appears to be substantially altered in *Gapdh2*, *APPL* and *Dp110* knockdown cells. Whereas in control cells, MFAS continues to concentrate into a single, regular DCG within 35 minutes (**A**iii-**A**vi), MFAS within *Gapdh2*, *APPL* and *Dp110* knockdown cells remains divided between a large number of mini-cores (timepoints **iii**-**vi**) for indefinite periods. In addition, whereas the mini-cores formed within control cells have been seen to be mobile and capable of homotypic fusion, mini-cores within knockdown backgrounds appear to be less mobile and retain their relative positions to each other for significantly longer periods (timepoints **iv**-**vi**). SC (far left panels) or compartment (other panels) boundaries are marked by dashed circles, Scale bars: (Far left panels) 5μm, (other panels) 1μm.

cores over time, Z-stack projections are used to display GFP-MFAS localisation in panels tracking individual compartments. This means that signal from multiple Z-slices throughout the compartment is compressed into a single 2D plane, with each pixel representing the maximum value of GFP found within that location across Z-stacks.

As discussed in Chapter 3 (Section 3.2.6) and demonstrated again here, immature non-DCG compartments in control SCs undergo several steps during the process of granule biogenesis. Beginning with an immature non-DCG compartment (Fig. 4.9A-i), this compartment is seen to contract in size whilst MFAS concentrates in the lumen over 1-2 hours (Fig. 4.9A-ii). Next, the diffuse pool of GFP-MFAS condenses into several small structures in the compartment lumen termed mini-cores, which are brighter than the surrounding "pool" of GFP-MFAS (Fig. 4.9A-iii). Over the course of 15-20 minutes, these mini-cores merge and consolidate (Fig. 4.9A-iV and V), eventually resulting in a single, spherical DCG located in the centre of the compartment lumen (Fig. 4.9A-vi).

Following *APPL*, *GAPDH2* and *Dp110* knockdown however, this process occurred quite differently. Initially, fairly typical non-DCG compartments were observed in knockdown cells (Fig. 4.9B-D, timepoint i). These compartments appeared to mature as normal at first, contracting in size whilst GFP-MFAS accumulates within their lumens (Fig. 4.9B-D, timepoint ii). Indeed, even the condensation of MFAS into mini-cores appeared to proceed as normal in these compartments (Fig. 4.9B-D, timepoint iii). However, unlike in control cells, the mini-cores in cells lacking APPL, GAPDH2 and PI3-kinase activity appeared to be incapable of fusion, as they remained distinct from each other long

after the typical 15-20 minute consolidation period (Fig. 4.9B-D, timepoints iii-vi). In addition, in at least *APPL* and *Dp110* knockdown cells, the usually mobile mini-cores were notably static and maintained their relative positions to each other over long periods (compare mini-core positions in Fig. 4.9B,D, timepoint V-Vi). This may also be true of mini-cores formed in *Dp110* knockdown cells (e.g. Fig. 4.C, timepoint V-Vi), but the compartments in these cells were exceptionally mobile, meaning that it was hard to assess the motion of individual mini-cores. Finally, in each knockdown background, mini-cores appeared to be associated with the compartment's limiting membrane and therefore localised at the periphery of the compartment.

Overall, time-lapse imaging provided unique insights into the mechanistic function of APPL, GAPDH2 and Dp110 in regulating DCG assembly. These three genes do not appear to regulate events prior to the onset of DCG biogenesis but do contribute to the proper maturation of DCGs from mini-core condensates. Specifically, APPL, GAPDH2 and Dp110 facilitate the homotypic fusion of mini-core condensates, promote the separation of mini-cores from the limiting membrane and – in the cases of at least APPL and Dp110 – promote the mobility of mini-cores within compartments.

4.2.10 Expressing human mutants responsible for familial Alzheimer's disease also disrupts DCG maturation

Following the characterisation of four factors linked to neurodegenerative illness (i.e. Hsp83, APPL, GAPDH2 and Dp110) in DCG biogenesis and maturation, I next investigated the role of two Amyloid-β 42 (Aβ42) mutants, known generally as Iowa and Dutch mutants. The 42 amino acid Aβ42 peptide is one of several peptides that can

arise from the processing of APP (G. Chen et al., 2017). It is also the peptide most closely associated with amyloid formation in AD, and indeed specifically its aggregated form and not its soluble form is associated with worse patient outcomes (Roher et al., 1993; Sturchio et al., 2021). Furthermore, several mutant forms of Aβ42 have been found to cause familial AD in humans, including the $A\beta42_{Iowa}$ and $A\beta42_{Dutch}$ forms (Lin & Pande, 2012). Concurrent work in our group had shown that overexpression of a wildtype form of APPL did not induce large changes in DCG morphology (Singh et al., 2024). However, expressing familial AD mutants $A\beta42_{Iowa}$ and $A\beta42_{Dutch}$ in *Drosophila* SCs disrupted DCG organisation by creating compartments containing numerous rather than individual DCGs (Singh et al., 2024). I therefore I induced the expression of UAS-controlled $A\beta42_{Iowa}$ and $A\beta42_{Dutch}$ for 5-7 days in the GFP-MFAS background to study changes in DCG formation in real-time. GFP-MFAS signal was again displayed as a Z-stack projection for each compartment to better visualise DCG mini-cores.

Overall, the $A\beta42_{Iowa}$ and $A\beta42_{Dutch}$ mutants produced phenotypes very similar to those observed in *APPL* and *Dp110* knockdown experiments (Section 4.2.9). Explaining this, following $A\beta42_{Iowa}$ and $A\beta42_{Dutch}$ expression, immature non-DCG compartments (Fig. 4.10A-C, timepoint i) were seen to mature as they do in control cells, meaning they contracted slightly in size, accumulated GFP-MFAS in their lumens (Fig. 4.10A-C, timepoint ii). This MFAS condensed into numerous mini-cores simultaneously (Fig. 4.10A-C, timepoint iii). After their condensation however, these mini-cores did not undergo fusion with each other and instead remained statically attached to the limiting membrane of compartments (Fig. 4.10B,C, timepoint iv-vi). One notable difference

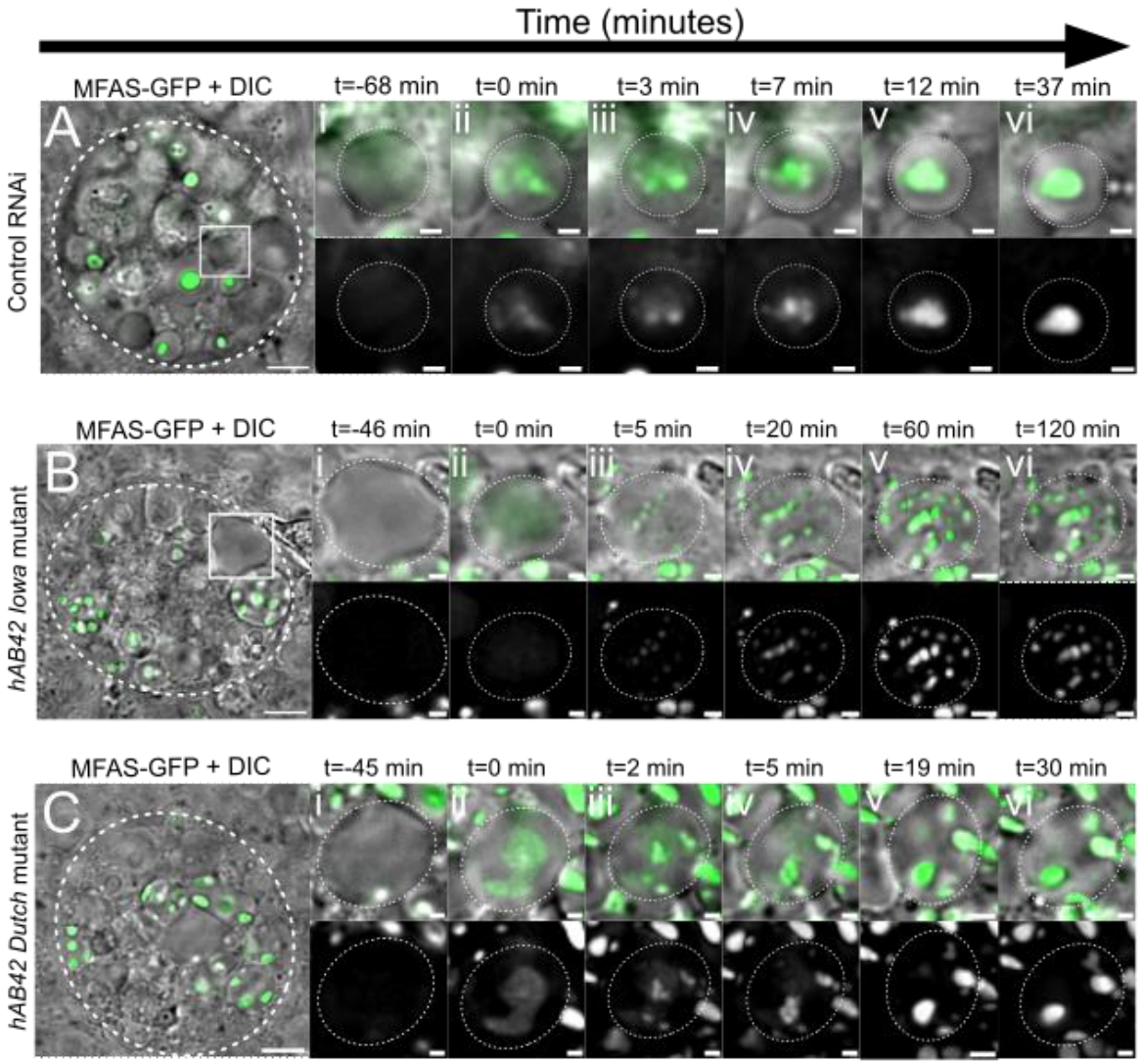

Figure 4.10. Aβ42$_{Iowa}$ and Aβ42$_{Dutch}$ responsible for human familial Alzheimer's disease disrupt DCG maturation in SCs. Time-lapse imaging of SCs expressing *GFP-mfas* together with a control RNAi (**A**), *Aβ42$_{Iowa}$* (**B**) or *Aβ42$_{Dutch}$* (**C**). In multicoloured images MFAS is shown in green and DIC images in grayscale. In all cases, including in control SCs, the initial stages of DCG biogenesis remain consistent, with non-DCG compartments gradually accumulating diffuse, lumenal MFAS in all backgrounds (timepoints **i**-**ii**). Then, within a 2-5 minute timeframe, this diffuse pool of MFAS begins to concentrate into smaller structures such as the central DCG (**A**iii) or mini-cores (**B**iii-**D**iii). From this point onwards, DCG biogenesis/maturation appears to be substantially different in SCs expressing Aβ42 mutants. Whereas in control cells, MFAS continues to

concentrate into a single, regular DCG within 37 minutes (**A**iii-**A**vi), MFAS within compartments of *Aβ42*$_{Iowa}$ and *Aβ42*$_{Dutch}$ expressing cells remains divided between numerous mini-cores (timepoints **iii**-**vi**) for indefinite periods. In addition, whereas mini-cores formed within control cells are generally mobile and capable of homotypic fusion, mini-cores within Aβ42-mutant backgrounds appear to be less mobile and retain their relative positions to each other for significantly longer periods (timepoints **iv**-**vi**). SC (far left panels) or compartment (other panels) boundaries are marked by dashed circles, Scale bars: (Far left panels) 5μm, (other panels) 1μm.

between the Iowa and Dutch mutants was the size of the mini-cores produced and the timing of their formation. Following *Aβ42$_{Iowa}$* Iowa expression, I noted that GFP-MFAS did not appear to accumulate to the same levels as observed in wildtype cells or even other experimental lines (Fig. 4.10A-C, timepoint ii). Instead, mini-core condensation appeared to occur earlier and resulted in notably more and smaller mini-cores being produced.

4.3 Discussion

4.3.1 Core findings

My experiments in SCs offer a range of novel insights into the regulation of DCG biogenesis. What is more, they provide previously unmatched resolution into the role of key regulators at different stages of biogenesis, as the differing effects of regulators on Rab6-, Rab11- and Rab1-compartments as well as DCG cargoes can be viewed individually. Likewise, real-time imaging permits unmatched temporal resolution into several key processes.

As a result, I have been able to produce three particularly significant findings. Firstly, Arf1 and AP-1 do regulate DCGs in SCs in a conserved manner and appear to have novel functions beyond their previously described roles. Secondly, the Rab6 to Rab11 transition I identified in the previous chapter is an essential, novel feature of DCG biogenesis. Thirdly, a range of neurodegeneration-linked genes act as novel regulators of DCG biogenesis and maturation, and their impact on the mechanisms of DCG biogenesis can be analysed in detail through real-time imaging.

4.3.2 SC DCGs are regulated by conserved factors including Arf1 and AP-1

One key finding from my research is that DCGs in SCs are regulated by the conserved factors Arf1 and AP-1. Indeed, Arf1 and AP-1 are important regulators of several different processes during DCG biogenesis. Beginning with their effect on DCG organisation, I found that knocking down either *Arf1* or *AP-1* significantly increases the frequency of DCGs that display abnormal shapes or are divided between multiple "mini-cores". This abnormal organisation resembles the transient organisation of DCG compartments I observed during the normal process of DCG maturation (Section 3.2.6) where multiple mini-cores coexist in compartments prior to fusing together to form a DCG. As such, I suggest that Arf1 and AP-1 are both required for the proper maturation of DCGs following the condensation of DCG cargo proteins into mini-cores.

This finding fits fairly well with previous literature which has shown that Arf1 and AP-1 regulate DCG maturation by facilitating the removal of missorted proteins from DCG compartments via clathrin-coated vesicles (Bonnemaison et al., 2013; Burgess et al., 2011; Klumperman et al., 1998). As such, my findings suggest that *Arf1* and *AP-1* knockdowns retain their conserved function mediating DCG maturation in SCs, likely through this same mechanism. Supporting this, previous work by Dr B. Kroeger showed that clathrin light chain localises to the surface of DCG compartments (Kroeger & Wilson, 2017), although preliminary knockdown experiments of clathrin components did not appear to significantly disrupt DCG organisation. Therefore, it would also be good to investigate the possibility that Arf1 and AP-1 support DCG maturation through other mechanisms. For example, since Arf1 and AP-1 are implicated in a wide array of

trafficking events, they might be required for the formation of small vesicles which deliver important maturation factors to DCG compartments. Alternatively, they may be important for the efficient trafficking of maturation factors to DCG compartments at an earlier stage. To establish the likely mechanism of Arf1 and AP-1 in DCG maturation, I would further investigate the role of clathrin in this process and would examine the effect of Arf1 and AP-1 knockdowns on secretory compartment contraction, since this process is likely to be linked to clathrin-coated vesicle budding. Likewise, it could be informative to express a tagged form of the M6P-R, a receptor known to be extracted by clathrin-coated vesicles, and see how its trafficking changes following *Arf1* or *AP-1* knockdowns.

In addition to disrupting DCG maturation, I found that *Arf1* and *AP-1* knockdowns impair DCG biogenesis, with numerous SCs in each background generating no DCGs at all. A similarly severe phenotype has been reported following *AP-1* and *clathrin* knockdowns induced in the salivary glands of Drosophila larvae (Burgess et al., 2011). The authors of that study suggested this represents evidence of a novel role for Arf1 and AP-1 trafficking, but also acknowledged that suppression of granule biogenesis could result from a failure to recycle important factors back to the TGN from maturing DCG compartments. This explanation may also apply to my findings in SCs, however, I believe my contrasting results in Rab6- and Rab11-compartments support the idea of a novel function for Arf1 and AP-1 in DCG biogenesis. As evidence for this, I found that although the number of Rab11-compartments dropped significantly following Arf1 and AP-1 knockdowns, the proportion of compartments forming DCGs was unaffected. This supports the idea that a transition to Rab11-identity is the determining factor triggering DCG biogenesis. By contrast, the proportion of DCGs formed by Rab6-

compartments is significantly decreased following knockdowns, suggesting that more Rab6-compartments have stalled as non-DCG compartments that lack Rab11-identity. Overall, this suggests that Arf1 and AP-1 have some role in facilitating the Rab6 to Rab11 transition on secretory compartments, possibly by enabling the retrograde trafficking of materials to the Golgi via clathrin-coated vesicles.

Finally, I find evidence that Arf1 facilitates the Rab1 to Rab6 transition that precedes granule formation. My results show that knocking down any of *Arf1*, *AP-1μ* or *AP-1σ* significantly reduces the number of Rab6-compartments formed, and I additionally find that *Arf1* knockdowns result in SCs forming large non-DCG compartments that fail to obtain Rab6 identity and instead retain Rab1 labelling. This highlights another potential function for Arf1 and possibly AP-1 upstream of the regulated secretory pathway.

4.3.3 The novel Rab6 to Rab11 transition controls DCG biogenesis and ILV formation

Another important result from my experiments is the finding that DCG biogenesis and exosome biogenesis are dependent on the novel Rab6 to Rab11 transition that I identified previously. This fits well with my earlier observation that DCGs and ILVs form very shortly after the recruitment of Rab11 to membranes. Across each of the GFP-GPI, CFP-Rab6 and YFP-Rab11 backgrounds, knocking down Rab6 and Rab11 consistently suppressed or abolished DCG formation and caused defects in DCG maturation. Of particular significance is the observation that *Rab11* knockdown inhibits DCG

formation without reducing the formation of Rab6-positive compartments, thereby suggesting that Rab6-compartments cannot initiate DCG biogenesis without the recruitment of Rab11 to membranes.

Similarly, Rab-labelled ILV formation is inhibited following *Rab11* knockdown even in Rab6-compartments, suggesting that the recruitment of Rab11 also regulates exosome biogenesis. This finding provides further evidence of a link between DCG and exosome biogenesis pathways in SCs.

Since the Rab6 to Rab11 transition itself is a novel finding from my work, the identification of its role in DCG biogenesis is equally novel. Importantly however, it is consistent with previous work which has demonstrated that both Rab6 and Rab11 associate with DCG compartments at different stages of maturation. Rab6 has been shown to localise to maturing secretory granule compartments and functions in granule biogenesis (C. Ma & Brill, 2021; Miserey-Lenkei et al., 2010), whilst Rab11 was found to regulate the size of secretory granules following biogenesis (Neuman et al., 2021). Neither these previous studies nor my own findings demonstrate the mechanisms Rab6 and Rab11 harness to carry out these functions, but Rab GTPases generally function through specific effector protein activation. Therefore, the natural next stage of investigation into Rab6 and Rab11 function in DCG and exosome biogenesis would be to investigate the role of particular effector proteins, especially those activated by Rab11. I have begun to investigate a several Rab11-effector proteins (described in Chapter 5), but none of the Rab11-effectors investigated so far have been observed to significantly affect DCG biogenesis, although some do have important impacts on other SC processes.

4.3.4 Neurodegeneration-linked genes regulate the assembly of DCGs

The last major finding from my experiments is the demonstration that numerous genes linked to neurodegenerative illnesses disrupt the dynamic mechanisms involved in DCG biogenesis and maturation. Although previous work has shown links between the dysregulation of DCG cargoes/processing enzymes and neurodegenerative conditions (Quinn et al., 2021, 2023), it has not previously been shown that so many central regulators of neurodegenerative illnesses directly affect DCG biogenesis mechanisms. Using live-cell and real-time imaging, I studied the function of Hsp83, APPL, GAPDH2, Dp110 and human familial AD mutants of the Aβ42 peptide in DCG biogenesis. The role of Hsp83 and Dp110 in DCG biogenesis were first identified by myself, whilst the role GAPDH2 was identified by Dr C. Mendes (Dar et al., 2021) and the functions of APPL/Aβ42 were identified by Dr P. Singh (P. Singh, 2023). For each gene, however, I conducted the first real-time analysis of the changes they induce in DCG biogenesis.

Of these genes, *Hsp83* knockdown produces a unique phenotype, as it completely abolishes DCG formation without disrupting Rab11-compartment organisation and without inhibiting MFAS accumulation inside these compartments. Instead, it seems to specifically disrupt the condensation of MFAS into DCGs or mini-cores. Given my other findings, this suggests that Hsp83 normally acts soon after the recruitment of Rab11 to compartment membranes. Although Hsp83 evidently has a role in promoting DCG protein condensation, it is not immediately clear how this is achieved. One interesting parallel to my observations come from previous studies of mammalian homologue of Hsp83, Hsp90α, which has been shown to bind to amyloid fibrils in vitro

and inhibit their disassembly (Schirmer et al., 2016). Notably however, Hsp90α was also shown to limit initial protein aggregate formation so the relevance of these findings for SC DCG aggregation is uncertain. More broadly, Hsp83 is a member of the Hsp90 family of chaperone proteins that recognise exposed hydrophobic peptide motifs and promote protein refolding (B. Chen et al., 2006; Zuehlke et al., 2015). Therefore, one especially fascinating possibility is that Hsp83 chaperone activity could be required for DCG cargoes to undergo appropriate refolding as maturing compartments become more acidic and acquire higher divalent cation concentrations (Duncan et al., 2003; Shennan et al., 1994). Based on my current findings and wider recognition of Hsp90 interactions with protein aggregates (Rodríguez-Ramos et al., 2023; Schirmer et al., 2016; H. Wang et al., 2021), I suggest this is the current best explanation for Hsp83's role in DCG biogenesis. However, it is also possible that Hsp83 functions through a less direct mechanism that is not understood. To distinguish between these possibilities, fluorescently tagged Hsp83 and MFAS molecules could be used alongside fluorescence resonance energy transfer (FRET) microscopy to determine whether these proteins directly interact and when this interaction may occur in the lifetime of a secretory compartment (Sekar & Periasamy, 2003).

Interestingly, APPL, GAPDH2 and Dp110 each appear to have similar effects on DCG biogenesis. SC-specific knockdown of each gene significantly disrupts the ability of mini-core condensates to fuse yet had no obvious effect on the earlier stages of DCG compartment maturation. Each knockdown also increases association of mini-cores with the limiting membrane of compartments. It is unclear why mini-cores in these backgrounds preferentially associate with membranes. Indeed, this phenotype may actually reflect a failure of DCG cargoes to dissociate from membranes rather than a

novel association with the membrane. Supporting this idea, several transmembrane proteins do participate in DCG biogenesis including receptor proteins that promote cargo sorting into DCGs and cleavable proteins that yield DCG cargoes (Dikeakos & Reudelhuber, 2007; Ji et al., 2017). Perhaps the simplest explanation for the close association of mini-cores with membranes in knockdown backgrounds is that knocking down regulator genes produces defects in DCG cargo folding or condensation that prevent the cleavage of certain membrane-linked factors, or which lead cargo proteins to erroneously aggregate with non-cleavable transmembrane factors or the membrane itself. However, it is also possible that mini-cores fail to detach from the limiting membrane because of defects in ILV biogenesis.

Explaining this, DCGs closely associate with membranous ILVs during and after DCG biogenesis. Indeed, ILVs label large portions of the DCG boundary and form long bridge-like structures that connect the limiting membrane and DCG. Additionally, ILVs and DCGs share surprising regulatory triggers, and form following the Rab6 to Rab11 transition. Finally, previous work in SCs has shown that inhibiting the ESCRT complex, an essential ILV-forming protein complex, disrupts DCG biogenesis and produces mini-core phenotypes (Marie et al., 2023). This close association between DCGs and ILVs raises the possibility that ILVs may have some role in stabilising DCGs at their boundaries, at least during biogenesis. It is therefore interesting to note that GAPDH2 and Dp110 also regulate ILVs in SCs, with *GAPDH2* knockdown disrupting normal ILV clustering (Dar et al., 2021) and *Dp110* knockdown inhibiting ILV formation altogether (see Section 5.2.9). Also interesting is the fact that GAPDH is a cargo protein on the surface of mammalian Rab11a-ILVs and has established roles assisting protein aggregation (Chaudhary et al., 2021; Dar et al., 2021; Marie et al., 2023). I therefore

suggest that DCGs in control SCs may associate with membranes in the form of ILVs, but following knockdown of *GAPDH2* and *Dp110*, mini-cores instead adhere to the limiting membrane and/or fail to properly dissociate from them.

APPL and *Dp110* knockdowns also limit the mobility of mini-cores. Rather than all mini-cores migrating, colliding and fusing within 15 minutes as they do in control cells, mini-cores in these backgrounds can maintain their relative positions for potentially hours. *GAPDH2* knockdown may also limit individual mini-core mobility, but this is harder to confirm because the compartments themselves move and rotate to a much greater degree than in other genotypes. Overall however, I propose that the decreased mobility of mini-cores, their increased association with limiting membranes and their inability to fuse are all linked characteristics. The fusion of mini-cores in control SCs generally takes place in the compartment lumen, away from the limiting membrane. Adhesion of mini-cores to the membrane would therefore limit their ability to migrate, interact and fuse. This model provides a single mechanism to explain three associated characteristics of mini-cores in these knockdowns. Additionally, this model even suggests that mini-cores in knockdown backgrounds may still be capable of fusion, but simply do not come into contact with fusion partners after the early stages of DCG condensation. This helps explain the fact that mini-cores clearly do merge with nearby partners in the first few minutes after cargo condensation, yet cease to fuse later on when no local fusion partners are available. Given the relative simplicity of this model, I suggest that this is the likeliest explanation for the role of APPL and PI3-kinase activity in DCG maturation, as well as potentially GAPDH2.

Remarkably, overexpressing the familial AD mutants *Aβ42$_{Iowa}$* and *Aβ42$_{Dutch}$* produced very similar phenotypes to those seen following *APPL*, *GAPDH2* and *Dp110* knockdowns. Unlike the genes examined through RNAi knockdowns, Aβ42 mutants are directly involved in amyloid aggregation and are not thought to have broad signalling functions like Dp110 (Hampel et al., 2021; Lin & Pande, 2012; C. Wells et al., 2021). Therefore, these results provide quite strong evidence that amyloidogenic factors can disrupt DCG maturation when they come into contact with secretory granules. I suggest that Aβ42$_{Iowa}$ and Aβ42$_{Dutch}$ mutants inhibit proper DCG maturation by causing inappropriate aggregation of DCG cargoes that leads them to adhere to limiting membranes, thereby blocking mini-core motility and preventing further fusion events.

4.4 Conclusions

Overall, based on my findings within the last two chapters, I propose two new models for secretory compartment maturation (Figure 4.11A) and DCG biogenesis (Figure 4.11B). Regarding secretory compartment maturation, I have demonstrated that a series of Rab cascades occur on compartments including a Rab1 to Rab6 transition that appears to be regulated by Arf1 and oversees the formation of large, immature secretory compartments. Similarly, a Rab6 to Rab11 transition mediated by Arf1/AP-1 controls DCG and exosome biogenesis. Although the mechanism remains unclear, previous work has also established that BMP-signalling regulates DCG compartment biogenesis (Redhai et al., 2016).

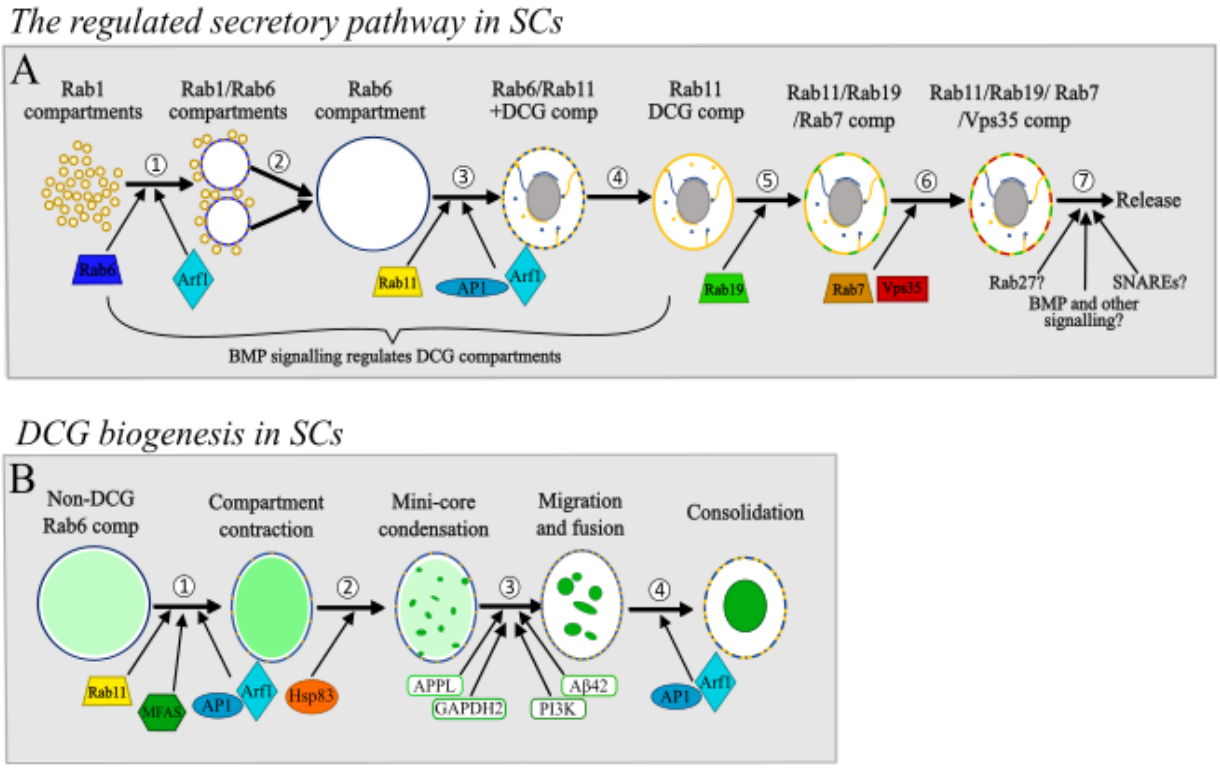

Figure 4.11. A new model of DCG biogenesis and secretory compartment maturation in SCs. (**A**) SC secretory compartments go through a series of Rab cascades that mediate their maturation from small Rab1-positive compartments to mature secretory compartments. The two major events studied here are a Rab1 to Rab6 transition (regulated by Rab6 and Arf1) and a Rab6 to Rab11 transition that triggers ILV and DCG biogenesis (regulated by Rab11, Arf1 and AP-1). DCG compartments also recruit Rab19 transiently and recruit Rab19, Rab7 and Vps35 immediately prior to secretion/lysosomal degradation. BMP-signalling also controls DCG biogenesis through uncertain mechanisms, and may also regulate compartment secretion alongside other factors like Rab27. (**B**) DCG biogenesis involves several previously indistinguishable steps. Non-DCG compartments first begin the Rab6 to Rab11 transition that coincides with compartment contraction and the concentration of DCG cargoes like MFAS. DCG cargoes then condense in an Hsp83-dependent manner, forming mini-cores. Mini-cores then migrate and fuse until consolidating into a single DCG, though these final steps are disrupted following *APPL*, *Gapdh2*, *Dp110*, *Arf1* and *AP-1* knockdowns or mutant *Aβ42* overexpression.

Following DCG formation, Rab19 is also transiently recruited to compartments, potentially multiple times prior to secretion/degradation. Rab19 colocalises with Rab7 and Vps35 on late-stage compartments. It is not clear whether Rab19 or Rab7 is recruited first or whether they functionally interact, but based on previous literature, it seems likely that Rab7 is responsible for recruiting Vps35 and related retromer components (Rojas et al., 2008). Soon after Vps35 recruitment, mature DCG compartments undergo lysosomal degradation or extracellular release in a process that may be overseen by factors including SNAREs, BMP-signalling, and Rab27.

Through the outstanding temporal resolution provided by time-lapse imaging, I have also been able to discern previously unknown mechanisms in DCG biogenesis (Figure 4.11B). Occurring immediately after the onset of the Rab6 to Rab11 transition, non-DCG compartments contract in size whilst DCG cargoes like MFAS concentrate in the lumen. After 1-2 hours, DCG cargoes rapidly condense into mini-cores in an Hsp83-dependent manner. Mini-cores in normal cells are mobile, lumenal and capable of homotypically fusing over 15-20 minutes to form a single granule. However, if any of *APPL*, *Gapdh2*, *Dp110*, *Arf1* and *AP-1* are knocked down, or if amyloidogenic *Aβ42* mutants are expressed, then DCGs form abnormally and remain divided between multiple mini-cores. In the case of *APPL*, *Dp110*, and *Aβ42* manipulations, this may be because the mini-cores formed are membrane-bound, static and incapable of fusion.

Overall, these new models of regulated secretion include a large amount of previously unknown detail, particularly regarding dynamic aspects of DCG biology that have not been appreciated before now. Despite advances however, it will be important to test the relevance of these findings in other organisms/systems and to assess the role of

known DCG cargoes and regulators such as granins within SCs since these are central to our understanding of other DCGs (Bartolomucci et al., 2011; Helle, 2004).

Chapter 5: Rab11-exosome formation in Drosophila SCs

5.1 Introduction and aims

5.1.1 Aims

Alongside DCGs, I was also interested in the regulation of exosome biogenesis within the large secretory compartments of SCs. In particular, I looked to examine the mechanisms controlling exosome subtype-specific biogenesis for a subpopulation of exosomes called Rab11-exosomes which are produced both in *Drosophila* SCs and human cancer cells (Fan et al., 2020). The biology and regulation of exosome subtypes remains very poorly understood, and limitations in current research methods make it difficult to isolate or examine specific subpopulations efficiently (Chuo et al., 2018; Gao et al., 2023). However, due to the large size of the secretory MVEs in SCs, Rab11-ILVs can be viewed in living cells using fluorescence microscopy. Given this fact and the variety of genetic tools available in *Drosophila*, SCs presented an exceptional *ex vivo* model for research into subtype-specific regulation of exosome biogenesis and exosome biology more generally.

In experiments described in the previous two chapters, I found that exosome biogenesis in SCs is dependent upon the Rab6 to Rab11 transition, and that exosome formation does not occur properly when compartment maturation is disrupted. To

develop this research, I looked to identify other factors controlling specifically Rab11-exosome biogenesis. My primary aims were therefore:

1. To outline the mechanism for a Rab11-exosome subtype-specific biogenesis pathway;
2. To identify mechanisms and regulators that are likely to be conserved in human Rab11a-exosome biogenesis;
3. To focus on regulatory factors with links to cancer signalling.

5.1.2 Previous work on Rab11-exosomes

Rab11-exosomes were first identified in the large MVEs of *Drosophila* SCs (Fan et al., 2020). Although only recently discovered, Rab11-exosomes are one of the clearest examples of a *bona fide* exosome subtype as outlined in current models of exosome regulation. Explaining this, Rab11-exosomes possess a unique cargo profile, are regulated by specific signalling stimuli, and induce different signalling effects in recipient cells compared to other exosome subpopulations from the same cells. Furthermore, they are also formed by a discrete biogenesis pathway, with Rab11-exosomes shown to form in Rab11-positive REs instead of Rab7-positive LEs, the previously established site of exosome biogenesis. Perhaps most interestingly though, Rab11a-exosomes have also been identified in human cancer cell lines, providing a strong indication that this exosome subtype is conserved from *Drosophila* to humans.

Beginning with their biogenesis and regulation, Rab11-exosomes were identified for their unique formation within Rab11-marked MVEs in *Drosophila* SCs and were shown to maintain this origin in HCT116 cells, a human colorectal cancer cell line (Fan et al.,

2020). Interestingly, Rab11a-exosomes in human cells were also found to be preferentially released following partial inhibition of Akt signalling, either through rapamycin-induced inhibition or through nutrient stress produced by glutamine starvation. Rab11a-exosomes were also found to house distinct cargoes and, upon their release from HCT116 cells, they could stimulate tumour cell proliferation and other oncogenic effects in a Rab11-dependent, mTORC1-dependent and recipient cell ERK-dependent manner. Given these effects and the role of glutamine as a metabolite in several cancers (J. Zhang et al., 2017), these results indicated that Rab11a-exosomes could be an important feature of understanding exosome signalling in cancer cells and tumour adaptation.

Interestingly, an *in vivo* role for Rab11-exosomes produced by SCs had already been established several years before human cell studies, with it being found that SC-exosomes played a central role in the post-mating response (PMR) of female *Drosophila* (Corrigan et al., 2014). The PMR is a fascinating feature of *Drosophila* reproduction which sees signalling factors transferred in the male seminal fluid induce physiological and behavioural changes in the female following mating. These changes include increased egg-laying (P. S. Chen et al., 1988), increased feeding (Carvalho et al., 2006), decreased immune responses (Fedorka et al., 2007), and decreased receptivity to remating (Manning, 1962). Of these, Rab11-exosomes were found to specifically mediate changes in female remating behaviour but did not affect egg-laying or overall fertility. Although the precise mechanisms of Rab11-exosome signalling have not been established, these effects are thought to result from interactions within the female reproductive tract rather than signalling roles in the male accessory gland. Evidence for this comes from observations that Rab11-exosomes

fuse with sperm cells and interact with epithelial cells in the female reproductive tract (Corrigan et al., 2014). In addition to these findings, Rab11-exosomes were found to be formed via an ESCRT-dependent pathway that required ALIX and the core ESCRT-0/I/II/III complexes. Exosome release was shown to be regulated by BMP signalling.

Although the origin of Rab11-exosomes inside of Rab11-positive MVEs did appear to be conserved in both human and *Drosophila* cells, the divergent signalling functions made it unclear just how similar these two Rab11-exosome systems truly were, particularly in terms of biogenesis mechanisms and regulation (Corrigan et al., 2014; Fan et al., 2020). For example, the role of factors such as Akt/mTORC1, ERK and BMP signalling had only been studied in one or other of fly and human cells. In work conducted immediately before I joined the Wilson laboratory and for a short time after, however, it was shown that Rab11-exosome biogenesis is uniquely dependent upon various accessory ESCRT-III proteins compared to other studied exosome subtypes (Marie et al., 2023). This was shown to be true in both SCs and HCT116 cells and provided strong evidence for conserved mechanisms of biogenesis across *Drosophila* and humans.

Finally, in experiments I conducted looking at secretory compartment maturation, I showed that Rab11-exosome biogenesis occurs essentially simultaneously with DCG biogenesis and depends on the Rab6 to Rab11 transition to occur (see Sections 3.2.5 and 4.2.7). In *Rab11* knockdown SCs, compartments obtain Rab6 identity but fail to produce ILVs as compartment maturation itself is disrupted. Following these discoveries, I was also interested in the factors controlling ILV formation after Rab11-

compartment identity was achieved, i.e. factors specifically regulating Rab11-exosome formation, and not broader compartment maturation.

Therefore, I began my research on the regulation of Rab11-exosome formation and focussed on a few types of molecule that previous findings suggested may be of particular interest. In particular, I examined a number of Rab11-interacting proteins including Sec15 and other exocyst proteins, as well as members of the Rab11-family interacting protein (Rab11-FIP) family. In addition, I examined E-cadherin, a protein known to traffic on Rab11-positive REs and following the identification of novel microdomains on Rab11-compartments, I also tested the function of several microdomain associated factors. Finally, prompted by previous studies which showed that Akt and mTORC1 signalling control human Rab11a-exosome signalling, I assessed the role of the oncogenic PI3K/Akt/mTOR pathway in *Drosophila* Rab11-exosome formation.

5.2 Results

5.2.1 The Rab11-GEF Bet3 helps drive the Rab6 to Rab11 transition and regulates Rab11-ILV biogenesis

Based on my earlier findings that the recruitment of Rab11 acts as a regulatory trigger for exosome biogenesis, I chose to investigate Bet3, a core component of the TRAPP complex which functions as a GEF for Rab11. I therefore expressed a *Bet3*-RNAi in the *CFP-Rab6* (Fig. 5.1A,B) and *YFP-Rab11* (Fig. 5.1C,D) backgrounds to see the effect it would have on compartment and ILV biogenesis. As might have been expected from

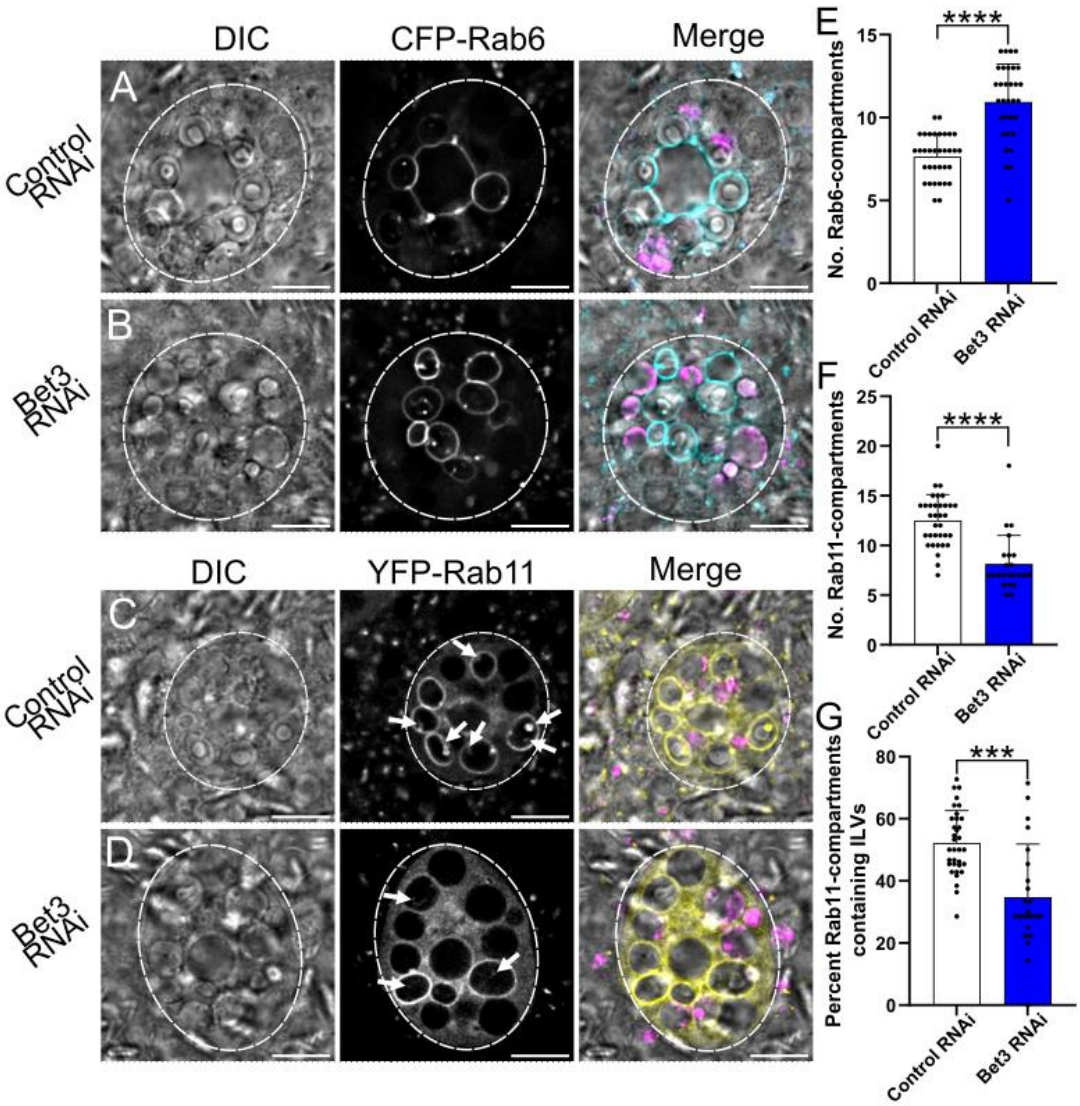

Figure 5.1, The Rab11-GEF *Bet3* controls the Rab6 to Rab11 transition and Rab11-ILV formation. (A-D) Wide-field fluorescence images of SCs expressing *CFP-Rab6* with a control RNAi (**A**) or *Bet3*-targeting RNAi (**B**), and SCs expressing *YFP-Rab11* with a control RNAi (**C**) or *Bet3*-targeting RNAi (**D**). In multicoloured images Rab6 is shown in cyan, Rab11 in yellow, LysoTracker Red in magenta and DIC images in grayscale. All Rab11-ILVs visible in the plane of view in **C** and **D** are indicated by white arrows. *Bet3* knockdown leads to an increase in Rab6-compartments (**E**) and an approximately equal decrease in Rab11-compartment numbers (**F**). *Bet3* knockdown also leads to a decrease in the proportion of Rab11-compartments forming Rab11-ILVs (**G**). Overall, knockdown of *Bet3* appears to shift the balance of the Rab6 to Rab11 transition and affects ILV biogenesis. SC boundaries marked by dashed circles, Scale bars: 10μm. For graphs, P<0.001:***, P<0.0001:****. n=23 to 34 cells for all graphs.

inhibiting the function of a Rab11-GEF, knocking down *Bet3* resulted in a significant increase in the number of Rab6-positive compartments and a decline in the number of Rab11-positive compartments (Fig. 5.1E,F). Additionally, the amount of inactive, cytosolic YFP-Rab11 in knockdown cells was notably greater than in control cells (compare Fig. 5.1C and D). These results were consistent with the idea that Bet3 is required for the Rab6 to Rab11 transition to proceed at normal rates, and in its absence a bottleneck occurs which leads to an accumulation of Rab6-compartments at the expense of Rab11-compartments. Interestingly, knockdown of *Bet3* also significantly reduced the proportion of Rab11-compartments that contained Rab11-ILVs (Fig. 5.1G, also examine arrows in Fig. 5.1C,D). Although it is not clear from these results whether this effect is separate from *Bet3*'s effect on Rab11-compartments more generally, these results may indicate that ILV biogenesis is specifically dependent on Bet3 activity.

5.2.2 ESCRT-0, accessory ESCRT-III proteins and Bet3 regulate female remating behaviour through Rab11-exosome signalling

As part of ongoing investigations into accessory ESCRT-III proteins led by Dr P. Marie, I investigated the role of several factors in regulating Rab11-exosome signalling. The first was CHMP5, an accessory ESCRT-III protein homologous to yeast Vps60, which I investigated by knocking down expression in a YFP-Rab11 background (Fig. 5.2A,B). I found that *CHMP5* knockdown caused no significant change in Rab11-compartment formation but did significantly reduce the proportion of compartments forming Rab11-ILVs (Fig. 5.2C,D). These results confirmed the relevance of *CHMP5* in Rab11-exosome

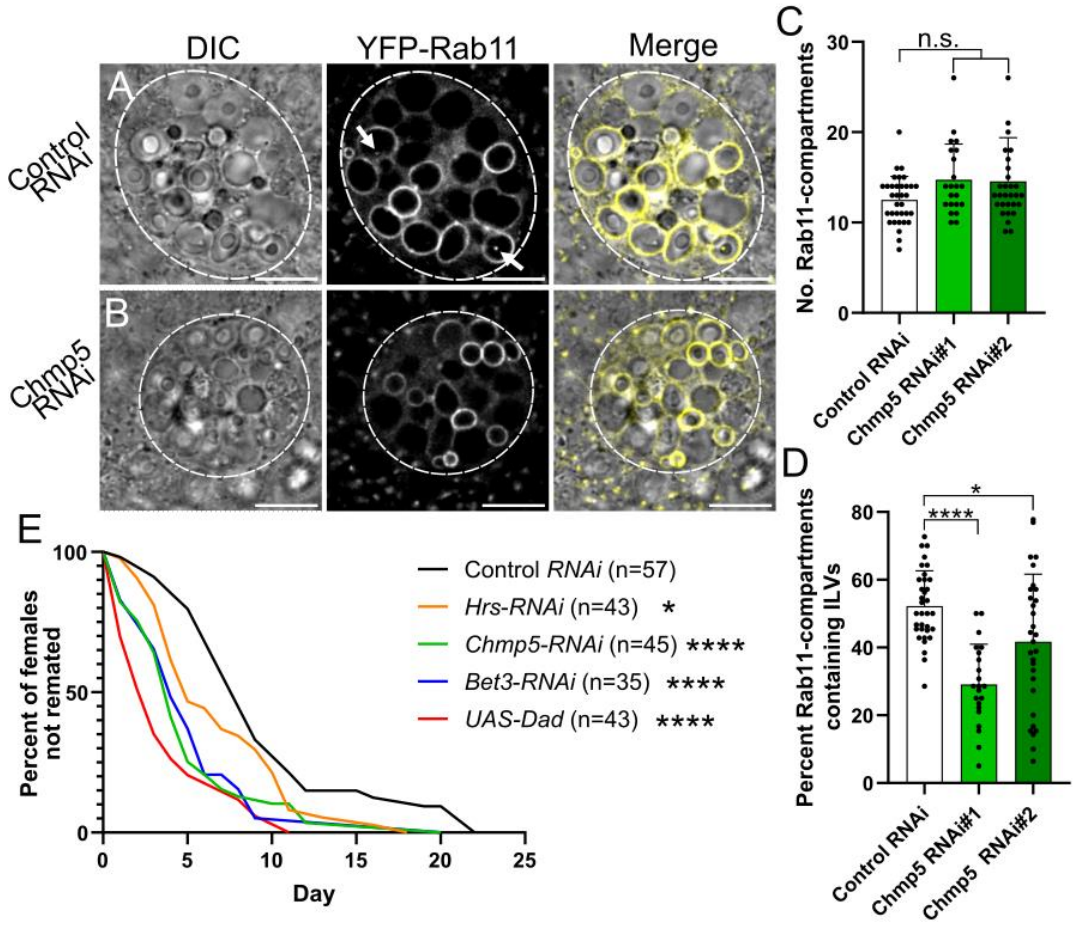

Figure 5.2. ESCRT-0, accessory ESCRT-III proteins and Bet3 regulate Rab11-exosome signalling in the female PMR *in vivo*. (**A-B**) Wide-field fluorescence images of SCs expressing *YFP-Rab11* with a control RNAi (**A**) or *Chmp5*-targeting RNAi (**B**). In multicoloured images Rab11is shown in yellow and DIC images in grayscale. All Rab11-ILVs visible in the plane of view are indicated by white arrows (**A**-**B**). *Chmp5* knockdown has no effect on the number of Rab11-compartments in SCs (**C**) but does significantly reduce the percentage of Rab11-compartments forming Rab11-ILVs (**D**). Additionally, knockdown of *Bet3*, *Chmp5* and *Hrs*, or overexpression of *Dad* in SCs significantly the impedes the SC-mediated effect of mating on female remating behaviour (**E**). SC boundaries marked by dashed circles, Scale bars: 10µm. For graphs, P<0.05: *, P<0.0001: ****, non-significant: n.s.. For bar charts n=22 to 34.

biogenesis and supported concurrent findings that accessory ESCRT-III proteins functioned in Rab11-ILV biogenesis (Marie et al., 2023).

I next looked to examine the effect of several regulators of ILV biogenesis on the actual process of Rab11-exosome signalling. To do this, I knocked down expression of the ESCRT-0 *Hrs*, the accessory ESCRT-IIIs *CHMP1* and *CHMP5*, and the Rab11-GEF *Bet3* in the SCs of virgin males for 6-days post-eclosion and then mated them to virgin w^{1118} females. After this, the females were separated into individual vials and once per day, were introduced to Canton S males for 1 hour to see whether they remated. Since previous genetic manipulations that suppress Rab11-exosome formation and other cellular processes (eg. dominant negative Rab11 and *ALiX* knockdown; Corrigan et al., 2014) increased receptivity to remating seen in females as part of the *Drosophila* PMR (Corrigan et al., 2014), my remating assays allowed me to test more specifically whether Rab11-exosome signalling was involved, by knocking down selective regulators, the *accessory ESCRT-III* genes. As a positive control, I also induced overexpression of *Daughters against dpp* (*Dad*) using a UAS-driven construct which antagonises BMP signalling and inhibits SC secretion in general, including Rab11-exosomes (Corrigan et al., 2014). From this experiment, I found that knocking down each of *Hrs, CHMP1*, *CHMP5* and *Bet3* in male SCs significantly reduced the time required for females to remate compared to controls (Fig. 5.2E). These results tie accessory ESCRT-III function and Rab11 activity to functional Rab11-exosome signalling *in vivo* and confirm that Rab11-exosome signalling depends on the function of these regulators in SCs.

5.2.3 Rab11-positive endosomes carry E-cadherin microdomains on their surfaces which colocalise with Rab11-ILV clusters

Across eukaryotic cells, Rab11-positive REs act as important trafficking centres for a variety of molecules internalised from the cell surface. Given my interest in cancer-related molecules and pathways, I investigated the localisation of E-cadherin (Ecad), an epithelial cadherin molecule whose internalisation away from the plasma membrane plays a vital role in the Epithelial-to-Mesenchymal Transition (EMT) during cancer metastasis (Hazan & Norton, 1998; Reynolds et al., 1994; Santarosa & Maestro, 2021). Following its internalisation, E-cadherin is often trafficked on REs as part of its regulated recycling back to the plasma membrane. Since SCs are an epithelial cell-type, I examined the SC localisation of an Ecad-RFP fusion protein expressed under ubiquitin promoter control in a *YFP-Rab11* background (Fig. 5.3A-C).

Upon visualisation of both fluorescent proteins, it became evident that Ecad-RFP colocalises with YFP-Rab11 on the membrane of Rab11-compartments and labels ~70% of them. Crucially however, Ecad-RFP's distribution was not uniform across the surface of Rab11 compartments and E-cadherin was instead seen to concentrate into small membrane microdomains on the surface of Rab11-positive compartments which have been termed small E-cadherin-positive lipid microdomains (ELMs) (Fig. 5.3A', arrowheads). When viewed in cross-section, these ELMs take on a crescent shaped appearance extending for up to 2µm, with multiple smaller microdomains sometimes seen on individual compartments. Most interestingly of all, ELMs were often seen closely associated with developing Rab11-ILVs adjacent to the limiting

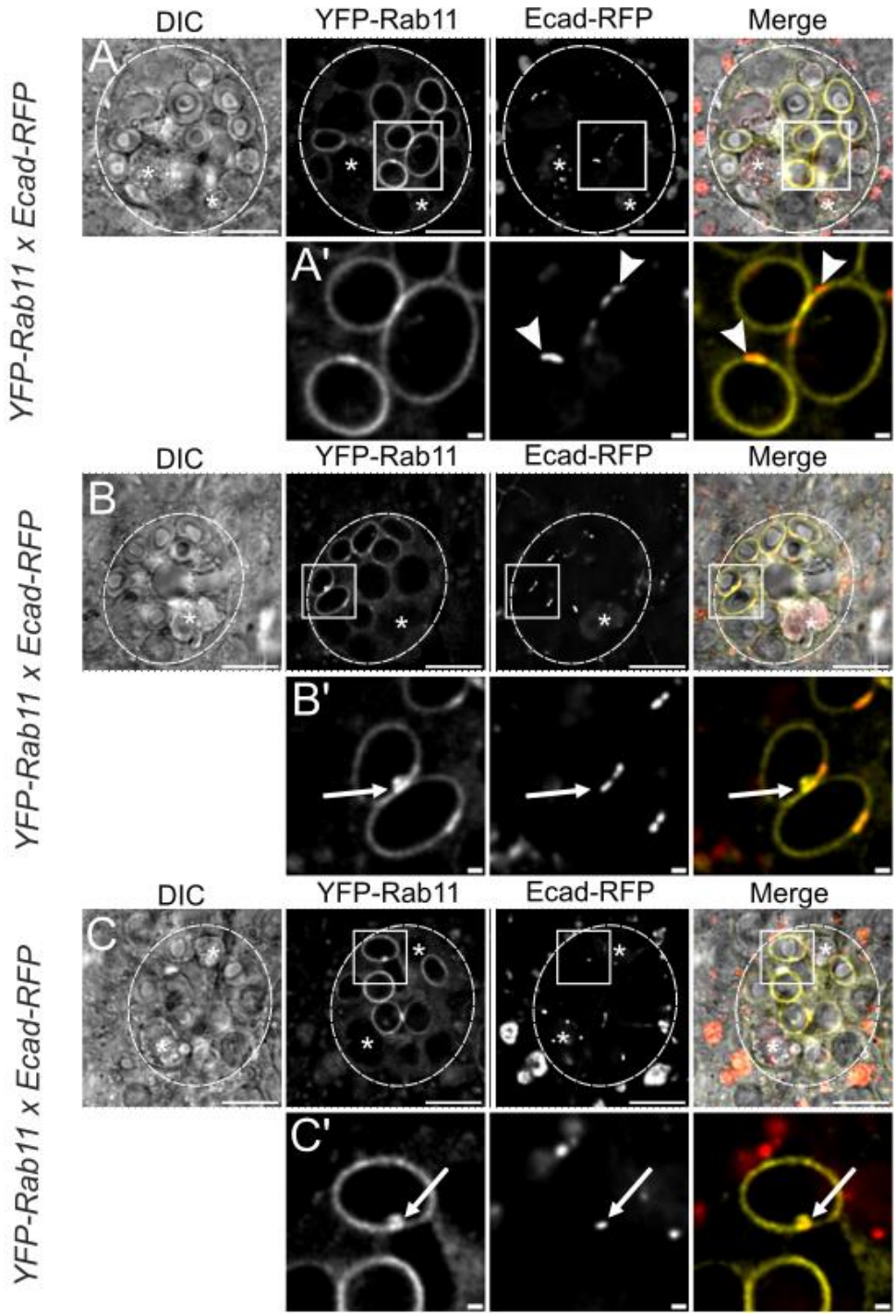

Figure 5.3 E-cadherin labels microdomains on the surface of Rab11-compartments which colocalise with Rab11-ILV clusters. (**A-C**) Wide-field fluorescence images of SCs expressing *YFP-Rab11* and *Ecad-RFP* and (**A'**-**C'**) magnified images of compartments of interest. In multicoloured images Rab11 is shown in yellow, Ecad in red and DIC images in grayscale. Asterixes indicate lysosomal

compartments with intact RFP signal. Expression of *Ecad-RFP* in SCs reveals that Ecad concentrates into small microdomains on the surface of Rab11-compartments (examples highlighted by white arrowheads in **A'**). Further examination also reveals that these microdomains can be associated with developing Rab11-ILVs or ILV clusters (examples highlighted by white arrowheads in **B'** and **C'**). SC boundaries marked by dashed circles, Scale bars: (**A**-**C**) 10µm, (**A'**-**C'**) 1µm.

membrane, a surprisingly direct association that raised the possibility that ELMs function in Rab11-exosome biogenesis (Fig 5.3B',C', arrows).

In addition to these microdomains, Ecad-RFP was also seen to localise to the plasma membrane as expected, and faint RFP signal was also visible inside acidic lysosomal compartments (Fig. 5.3A, compartments labelled by asterisks). Overall, the compartmental distribution of Ecad-RFP was reminiscent of the behaviour of wildtype E-cadherin molecules in epithelial cells, namely localising to the plasma membrane, internalising onto Rab11-compartments and trafficking to degradative pathways.

5.2.4 ELMs function in ILV biogenesis and colocalise with Rab19 and the ESCRT-0 protein

During experiments outlined in Section 3.2.1, I had found that the poorly characterised GTPase Rab19 formed microdomains on the surface of immature Rab6-compartments. To assess whether these Rab19 microdomains were related to the ELMs on Rab11-compartments, I examined the localisation of Rab19 and E-cadherin in cells expressing both the YFP-Rab19 fusion protein and the *Ecad-RFP* transgene (Fig. 5.4A,B). Following their joint expression in SCs, I found a high degree of overlap between these two markers, with very few examples of ELMs that lacked Rab19 colabelling. Furthermore, the interaction between ELMs and Rab-labelled ILVs was also found to hold true for Rab19-labelled ILVs, with some extensive clusters of Rab19-ILVs found associated with microdomain membranes (Fig. 5.4Aii, Bii).

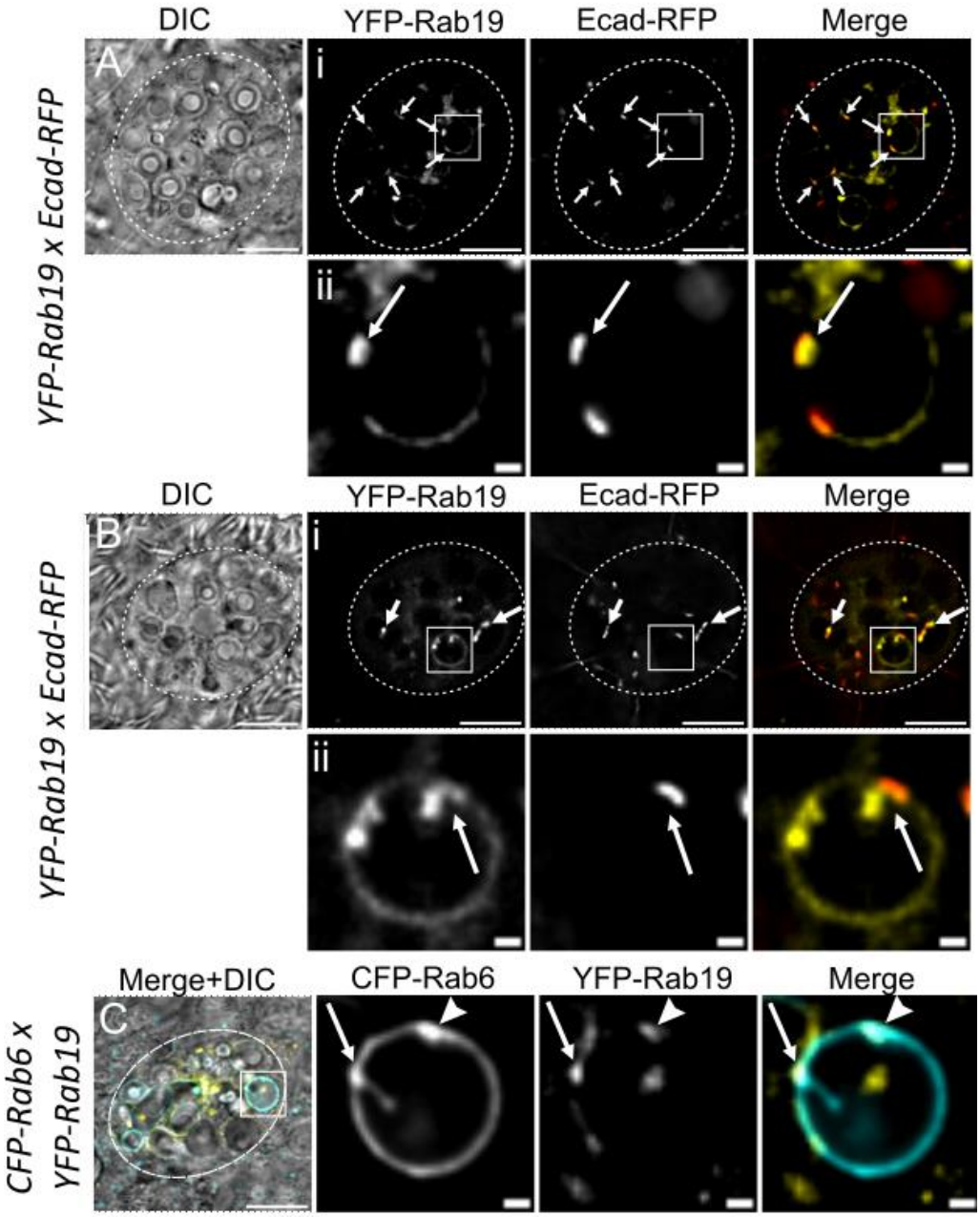

Figure 5.4 ELMs are also labelled by Rab19. (**A-C**) Wide-field fluorescence images of SCs expressing *YFP-Rab19* and *Ecad-RFP* (**A**-**B**) or *YFP-Rab19* and *CFP-Rab6* (**C**). Panels display whole SCs (**A-Bi**) or magnified views of compartments of interest (**Bii-C**). In multicoloured images Rab19 is shown in yellow, Ecad in red, Rab6 in cyan and DIC images in grayscale. Rab19 and Ecad display extensive colocalisation in ELMs throughout SCs, as indicated by white arrows in **A**i and **B**i. Additionally, just as seen with Rab11, ELMs can be seen to associate with ILVs that are labelled by Rab19, with

examples highlighted by white arrows in **A**ii and **B**ii. Finally, when *YFP-Rab19* and *CFP-Rab6* are co-expressed in SCs, Rab19-positive microdomains can be identified on Rab6 compartments (**C**i, arrowhead) and specifically at the base of Rab6-positive ILV-bridges (**C**i, arrow). Rab19 and Ecad therefore seem to colocalise into microdomains that are associated with SC ILVs. SC boundaries marked by dashed circles, Scale bars: (Whole-cell panels) 10μm, (Magnified panels) 1μm.

These findings prompted me to examine the function of ELMs in ILV-biology more closely. The presence of Rab19 microdomains on Rab6-compartments prior to ILV biogenesis suggested that they may have a role in the biogenesis process, an idea supported by limited observations I had made of ILV bridges apparently forming from Rab19-microdomains (Fig. 5.4C). Indeed, this was even observed in compartments that had not yet developed DCGs, strongly suggesting that ILVs were associated with Rab19/E-cadherin microdomains at the first stages of biogenesis. Because of these observations, I investigated ESCRT localisation using a UAS-driven, GFP-tagged form of the core ESCRT-0 protein Hrs. Previous work had established that Rab11-exosome biogenesis is dependent on the core ESCRT complex including Hrs (Marie et al., 2023). Since prolonged overexpression of Hrs-GFP disrupts secretory compartment organisation, male *Drosophila* were maintained at 25°C for 5 days following eclosion and then shifted to 29°C for just 24 hours to induce Hrs-GFP expression in SCs that were also expressing Ecad-RFP.

Under these conditions, Hrs-GFP displayed a punctate distribution across the surfaces of secretory compartments and showed significant, specific colocalisation with the ELMs we had observed previously (Fig 5.5A,B). This suggested that ELMs are able to recruit core ESCRT proteins to the surface of Rab11-compartments and strongly supports the idea that ELMs act as novel sites for Rab11-exosome biogenesis. Providing further support for this idea, I examined the localisation of CFP-Rab6-labelled ILVs in cells following 24 hours of *Hrs-GFP* expression (Fig 5.5C). As observed with cells expressing the YFP-Rab19 and CFP-Rab6 fusion proteins, ILV bridges could be seen forming directly from microdomains labelled by Hrs at the limiting membrane

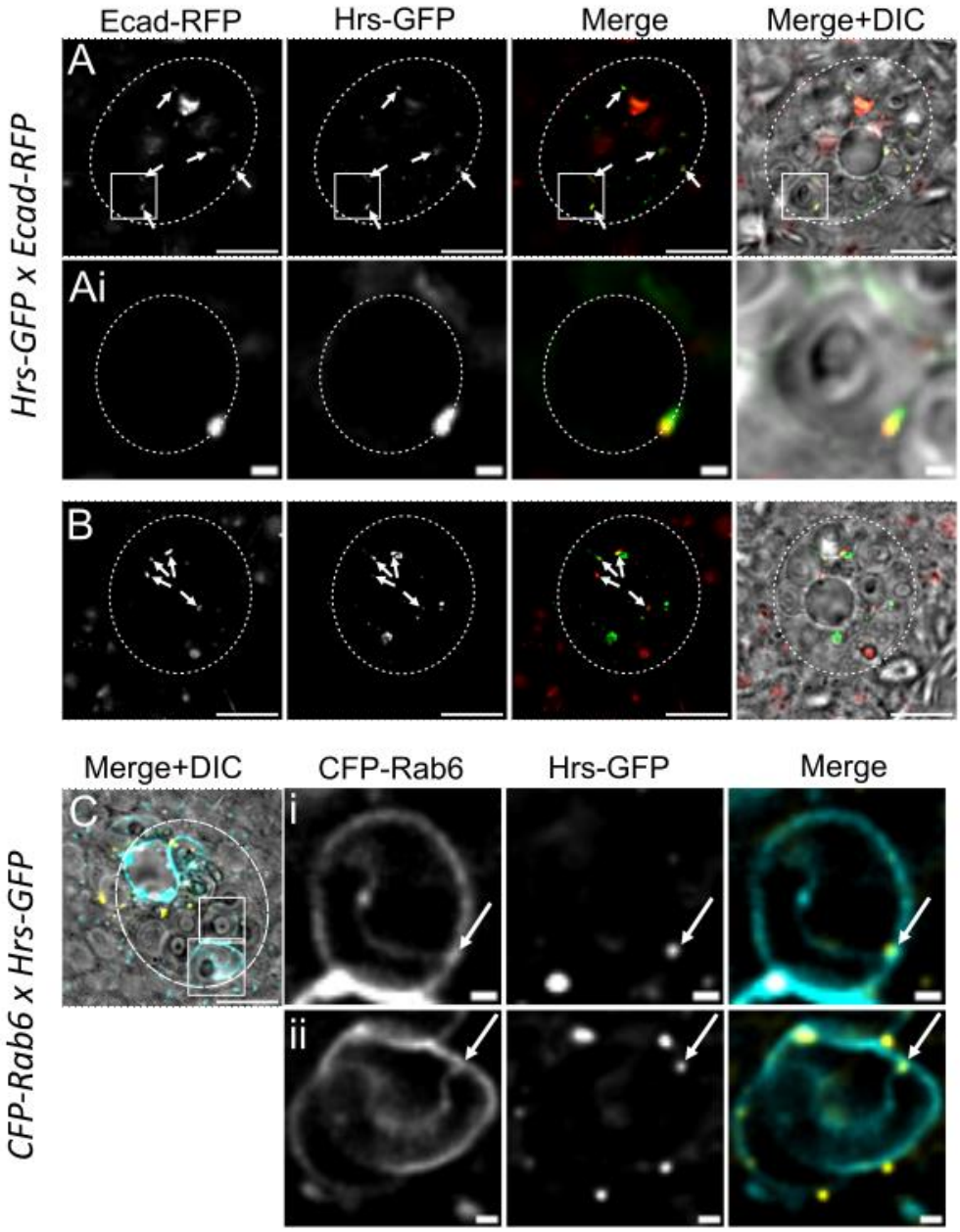

Figure 5.5. ELMs recruit the ESCRT-0 protein Hrs. (**A-C**) Wide-field images of SCs expressing *Hrs-GFP* with *Ecad-RFP* (**A**-**B**) or *CFP-Rab6* (**C**). Panels display whole SCs (**A,B,C**) or magnified views of compartments of interest (**Ai**,**Ci,Cii**). In multicoloured images Hrs is shown in green or yellow, Ecad in red, Rab6 in cyan and DIC images in grayscale. Hrs and Ecad colocalise in ELMs throughout SCs, as indicated by white arrows in **A** and **B**, and by the magnified images in **Ai**. In addition, Hrs-positive microdomains can be identified on Rab6 compartments at the base of Rab6-positive ILV-bridges (**Ci** and **Cii**, white arrows). Hrs therefore seems to localise to the same ILV-associated microdomains as Rab19 and Ecad. SC boundaries marked by dashed circles, Scale bars: (Whole-cell panels) 10μm, (Magnified panels) 1μm.

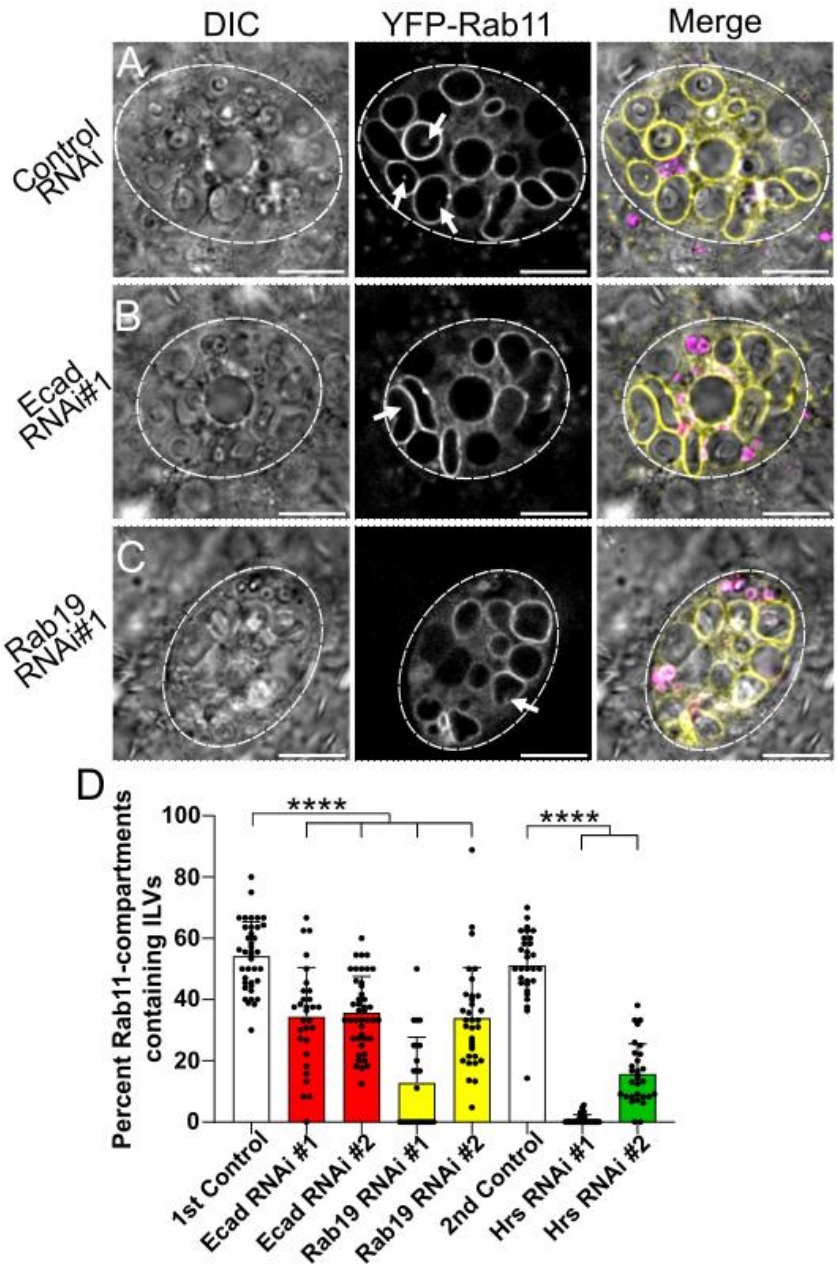

Figure 5.6. ELM-associated proteins promote Rab11-exosome biogenesis. (**A-C**) Wide-field images of SCs expressing *YFP-Rab11* with a control RNAi (**A**), *Ecad* RNAi (**B**), or *Rab19* RNAi (**C**). In multicoloured images Rab11 is shown in yellow, LysoTracker Red in magenta and DIC images in grayscale. All Rab11-ILVs visible in the plane of view are highlighted by white arrows (**A**-**C**). *Ecad, Hrs* and *Rab19* knockdowns each significantly reduce the percentage of Rab11-compartments forming Rab11-ILVs (**D**, 2nd control and Hrs data obtained by Dr Marie (Marie et al., 2023)). SC boundaries marked by dashed circles, Scale bars: 10µm. For graphs, P<0.0001:****. n=24 to 43 cells for all genotypes.

(Fig 5.5Ci-ii). Given the central role of ESCRTs in ILV-biogenesis, I took this to be strong evidence of microdomain function in SC exosome formation.

To test this hypothesis I examined the effects of knocking down each of *E-cadherin*, *Rab19* and *Hrs* on Rab11-ILV biogenesis in SCs using two independent RNAis for each gene (Fig 5.6A-C). For *Hrs*, this knockdown had already been carried out by Dr P. Marie (Marie et al., 2023). If the E-cadherin/Rab19/ESCRT microdomains were involved in exosome biogenesis, I reasoned that knocking down these microdomain components would reduce Rab11-ILV formation, and this is exactly what was found (Fig 5.6D, 2nd Control and *Hrs* data adapted from (Marie et al., 2023)). Indeed, each knockdown reduced ILV formation by at least 40% compared to controls, and in stronger phenotypes such as *Hrs-RNAi#1* or *Rab19-RNAi#1*, Rab11-ILV formation was reduced by as much as 80%-100% of typical rates. Combined with my other observations, I concluded that the E-cadherin/Rab19/Hrs microdomains identified here act as novel sites of Rab11-exosome biogenesis.

5.2.5 Rab11-FIP family proteins regulate Rab11-compartment and microdomain organisation but do not control ILV biogenesis

Given the central role of Rab11 in ILV formation in SCs, I became interested in the highly conserved family of Rab11 effector proteins, Rab11-FIPs (Rab11-family interacting proteins). The *Drosophila* genome encodes two members of the Rab11-FIP family, Nuf and Rip11, which act as motor protein adaptors regulating the trafficking of Rab11-positive REs (Horgan & McCaffrey, 2009; Riggs et al., 2003). Of particular interest to my work was the finding that Rab11 and Rip11 are required for the secretion of insulin granule compartments, which appear analogous to the Rab11-positive DCG

compartments of SCs (Sugawara et al., 2009b). Therefore, I induced knockdown of both *Nuf* and *Rip11* in SCs in the *YFP-Rab11* background (Fig. 5.7 A-C).

Knockdown of both *Nuf* and *Rip11* led to a reduction of 20%-30% in the number of Rab11-compartments compared to control cells (Fig. 5.7D). Intriguingly, both knockdowns also resulted in the formation of large membrane domains with high YFP-Rab11 concentrations on the outside of compartments, referred to as "superdomains" here (example highlighted by red arrows in Fig. 5.7B,C). Superdomains were not observed in control SCs, but *Nuf* and *Rip11* knockdown induced 3.1 ± 1.8 and 2.3 ± 2.0 per cell respectively. Based on these results, I investigated the potential impact of *Rab11-FIP* knockdowns on ELMs. I induced the same *Nuf* and *Rip11* knockdowns in SCs expressing both YFP-Rab11 and Ecad-RFP (Fig. 5.8 A-C). This revealed that the vast majority of superdomain structures were associated with Ecad-RFP, 90.3 ± 13.2% across both genotypes (examples highlighted by white arrows in 5.8B,C).

Given this association, I tested the effect of *Nuf* and *Rip11* knockdowns on E-cadherin microdomains and Rab11-exosome biogenesis. Knockdowns had no apparent effect on the level of Ecad-RFP trafficking on Rab11-compartments, with an almost identical proportion of Rab11-compartments trafficking Ecad-RFP in knockdown cells as in control cells, ~70% in all cases (Fig. 5.8D). Likewise, *Rab11-FIP* knockdowns in the *YFP-Rab11* background produced no significant change in Rab11-ILV formation in Rab11-compartments, despite the disruption it caused in compartment organisation (Fig. 5.8E). Finally, using endogenously expressed, GFP-tagged Nuf, I investigated whether this Rab11-FIP might selectively associate with any microdomains but found that it was distributed evenly across DCG compartments (Fig. 5.8F). Overall, these results

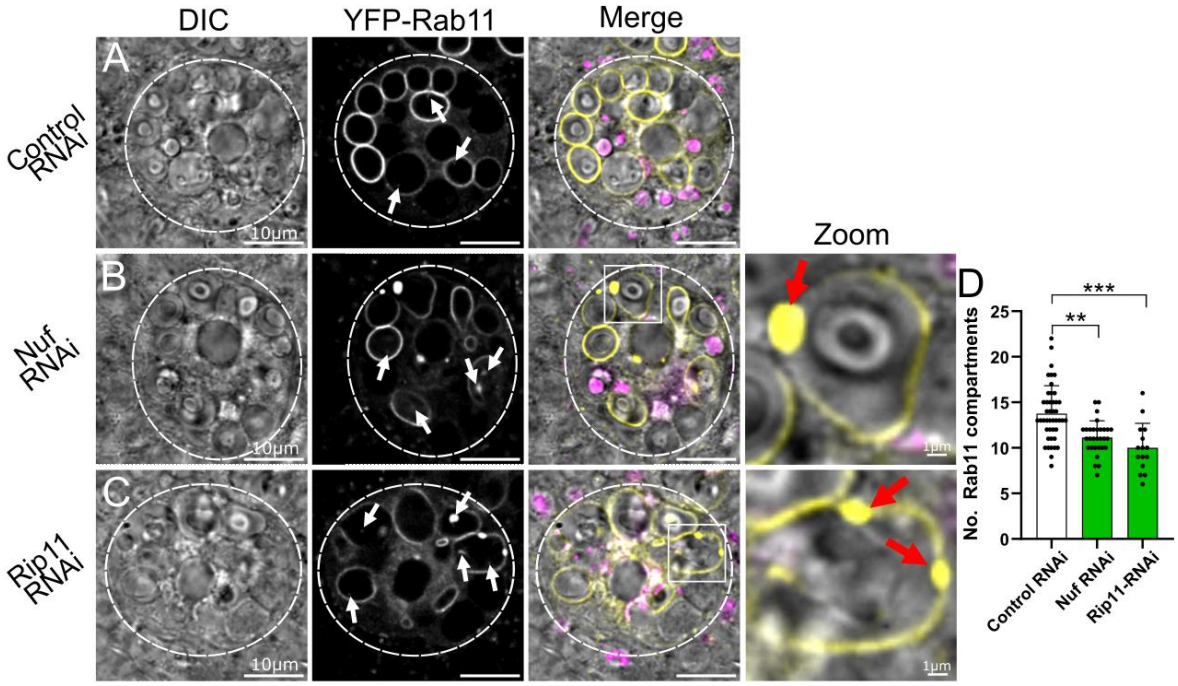

Figure 5.7. Knockdown of *Drosophila* Rab11-FIPs disrupts Rab11-compartment formation and produces large membrane "superdomains". (**A-C**) Wide-field images of SCs expressing *YFP-Rab11* with a control RNAi (**A**), *Nuf*-targeting RNAi (**B**), or *Rip11*-targeting RNAi (**C**). In multicoloured images Rab11 is shown in yellow, LysoTracker Red in magenta and DIC images in grayscale. All Rab11-ILVs visible in the plane of view are highlighted by white arrows (**A**-**C**). Knockdown of *Nuf* and *Rip11* induces the formation of bulging membrane domains on Rab11-compartments termed "superdomains", examples highlighted by red arrows in zoom images (**B**, **C**). Knocking down either *Nuf* or *Rip11* also results in a slight decrease in on Rab11-compartment numbers (**D**) SC boundaries marked by dashed circles. For graph, P<0.01: **, P<0.001: ***. n=15 to 31 cells for all genotypes.

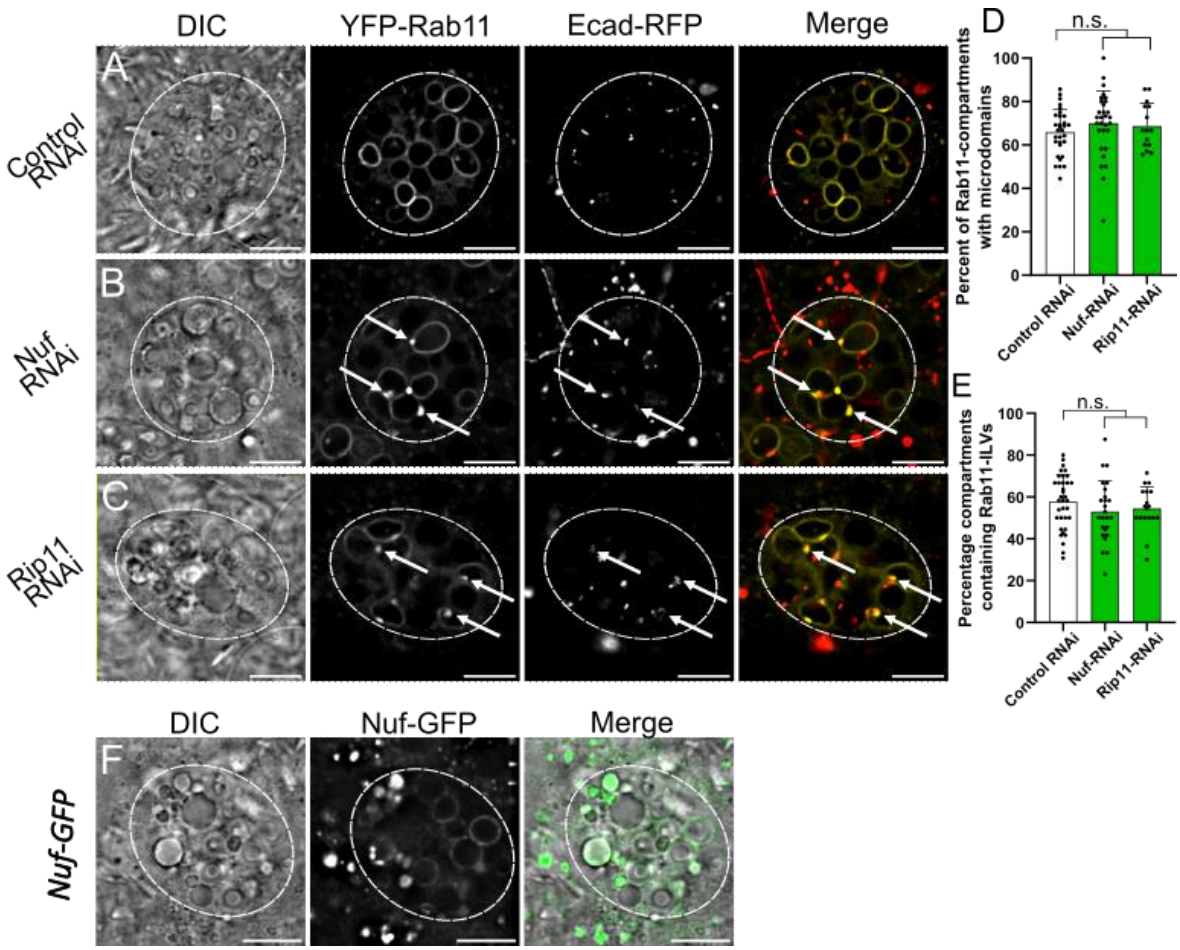

Figure 5.8. Rab11-FIPs do not control Rab11-ILV formation and produces large membrane "superdomains". (**A-C**) Wide-field fluorescence images of SCs expressing *YFP-Rab11* with a control RNAi (**A**), *Nuf*-targeting RNAi (**B**), or *Rip11*-targeting RNAi (**C**). In multicoloured images Rab11 is shown in yellow and Ecad in red. Ecad-RFP colocalised with the large "superdomains" induced following *Nuf* and *Rip11* knockdowns (**B** and **C**, white arrows highlight Ecad-positive superdomains). However, knockdown of *Nuf* and *Rip11* had no effect on the proportion of compartments forming surface-associated ELMs (**D**) or Rab11-ILVs (**E**). Additionally, Nuf-GFP was found to be present across the entire surface of SC compartments and did not concentrate into membrane microdomains. SC boundaries marked by dashed circles, Scale bars: 10µm. For graphs, n.s.: non-significant. n=15 to 31 cells for all genotypes.

show that Nuf and Rip11 are not required for ELM formation or ILV biogenesis but may indirectly influence ELM organisation.

5.2.6 The Rab11-effector Sec15 and the exocyst complex regulate Rab11-compartments and Rab11-exosome biogenesis

I next investigated the role of another Rab11-effector protein, Sec15 (X.-M. Zhang et al., 2004). Sec15 is one of eight protein subunits of the exocyst tethering complex which is essential for tethering secretory vesicles to the plasma membrane prior to SNARE-mediated exocytosis (B. Wu & Guo, 2015). Of the eight exocyst subunits, Sec15 directly interacts with Rab11 in a GTP-dependent manner through its C-terminal domain (S. Wu et al., 2005). This Sec15-Rab11 interaction is conserved from yeast to mammals and is important for mediating processes such as Rab11-dependent, exocyst-dependent lysosome secretion and recycling vesicle exocytosis (Escrevente et al., 2021; Takahashi et al., 2012). Exocyst dysfunction is also implicated in a range of diseases, including numerous forms of cancer as well as neurodegenerative diseases (Halim et al., 2023; Martin-Urdiroz et al., 2016). Because of the important and highly conserved nature of Rab11-exocyst cooperation, I therefore investigated the effect of knocking down a plurality of *Drosophila* exocyst subunits in SCs in the *YFP-Rab11* background, these being *Sec6*, *Sec8*, *Sec15*, *Exo70* and *Exo84* (Fig. 5.9A-D).

One consistent effect of exocyst knockdowns was a change in Rab11-compartment organisation, with a large number of small Rab11-positive DCG compartments being formed. In *Sec6*, *Sec15* and *Exo84* knockdowns, this resulted in significantly more

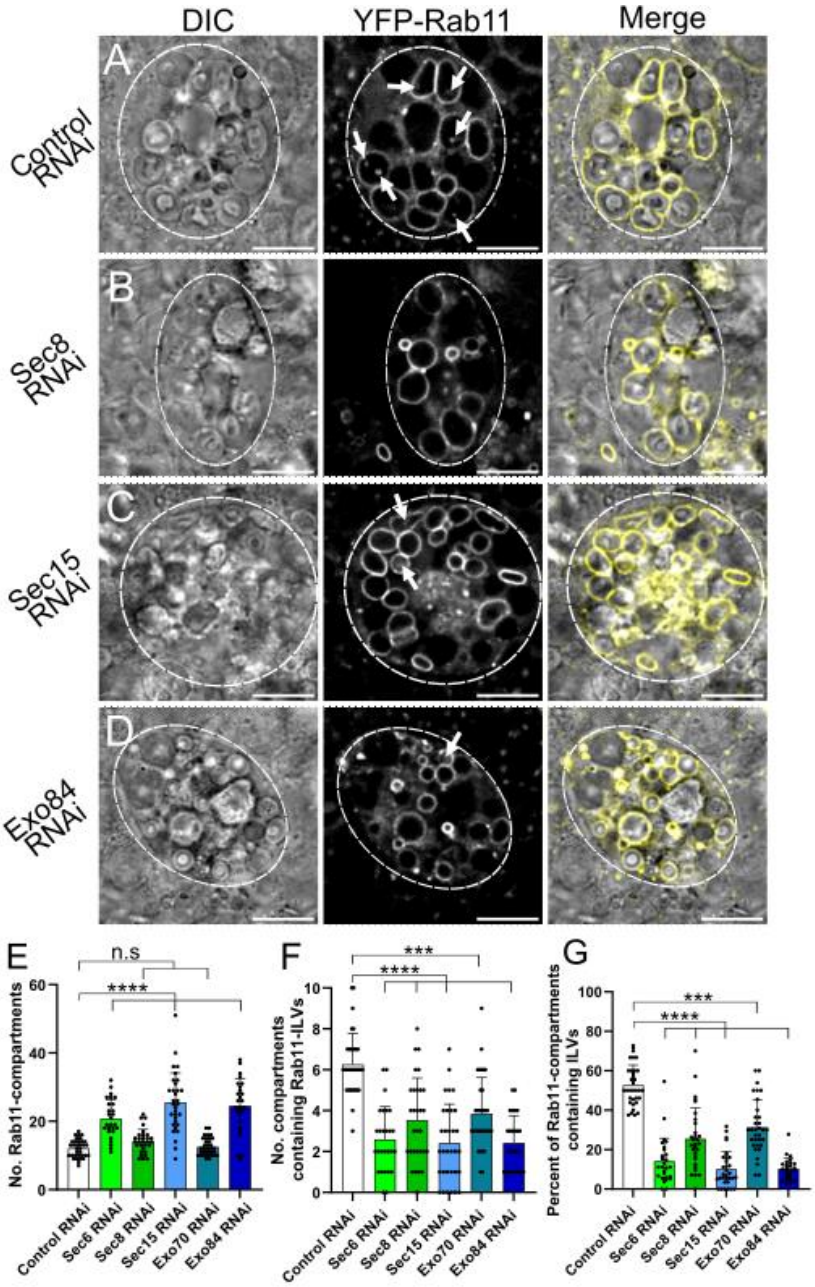

Figure 5.9. The exocyst complex regulates Rab11-compartment dynamics. (**A-D**) Wide-field images of SCs expressing *YFP-Rab11* with a control RNAi (**A**), *Sec8* RNAi (**B**), *Sec15* RNAi (**C**) or *Exo84* RNAi (**D**). In multicoloured images Rab11 is shown in yellow and DIC images in grayscale. All Rab11-ILVs visible in the plane of view are highlighted by white arrows (**A**-**D**). Knocking down three out of five exocyst components significantly increased numbers of Rab11-compartments (E). However, knockdown of all tested exocyst components significantly reduced both the number of Rab11-ILVs present in SCs (**F**) and the proportion of Rab11-compartments forming ILVs (**G**). SC boundaries marked by dashed circles, Scale bars: 10μm. For graphs, P<0.001:***, P<0.0001:****, non-significant: n.s.. n=25 to 34 cells for all graphs.

Rab11-compartments being present within SCs (Fig. 5.9E), but the formation of numerous small DCG compartments was also observed in *Sec8* and *Exo70* knockdown cells (e.g. Fig. 5.9B). The finding that Rab11-compartments accumulate following exocyst subunit knockdowns is consistent with an inhibition of compartment secretion, suggesting that the exocyst complex is required for Rab11-exosome release. Furthermore, regardless of changes in the number of Rab11-compartments, a significantly smaller number and proportion of compartments were found to produce Rab11-ILVs across all knockdowns, indicating that Rab11-exosome biogenesis is disrupted following exocyst inhibition (Fig. 5.9F,G). This implies that the exocyst complex controls exosome formation as well as compartment secretion.

As part of this same analysis of exocyst function in Rab11-exosome biology, I also investigated the proteins Rala and Magi. Rala is a Ras-like small GTPase homologous to mammalian RalA and RalB which interacts with the exocyst proteins Sec5 and Exo84 to regulate protein trafficking and exocytosis (Hazelett & Yeaman, 2012; Yan & Theodorescu, 2018). Interestingly, the trafficking of E-cadherin is regulated by RalA (Shipitsin & Feig, 2004), and Ral GTPases also play important roles in tumourigenesis (Shirakawa & Horiuchi, 2015), cancer cell exosome signalling (Ghoroghi et al., 2021), and even MVE biogenesis (Hyenne et al., 2018). *Drosophila* Rala interacts with Magi (Beller et al., 2002), a scaffolding protein located at adherens junctions which colocalises with and regulates the trafficking of adhesion molecules including E-cadherin (Kotelevets et al., 2005; Nishimura et al., 2000). Like Rala, Magi is also implicated in tumorigenesis and cancer cell proliferation (Wörthmüller & Rüegg, 2021).

By knocking down or inhibiting each of *Rala* and *Magi* in SCs in the *YFP-Rab11* background with two independent RNAis (Fig. 5.10A-C), I found that one RNAi of both genes produced SCs with increased numbers of Rab11-compartments (Fig. 5.10D), perhaps reflecting stronger transgene expression in both cases. Expression of *Rala-RNAi* in particular produced changes in Rab11-compartment organisation that were very similar to those seen following direct exocyst subunit knockdown, with numerous small Rab11-compartments being formed (e.g. Fig. 5.10B). Small compartments were not so prominent in *Magi* knockdown SCs (e.g. Fig. 5.10C). However, in all cases, the formation of Rab11-ILVs was significantly reduced in Rab11-compartments (Fig. 5.10E). These results highlight a role for the conserved Rala and Magi proteins in regulating Rab11-exosome formation. Given the other results described here, these findings suggest that Rala and the exocyst complex may function cooperatively in regulating Rab11-exosome biogenesis and secretion. They also suggest that the function of all these proteins may be linked to microdomain activity through regulation of E-cadherin trafficking, though more work is required to study this possibility.

5.2.7 The microdomain associated protein Prohibitin-2 regulates Rab11-ILV formation and ELM biogenesis

Following the identification of ELMs, I became interested in the role that conserved lipid microdomain-associated proteins may play in Rab11-ILV biogenesis. I therefore examined the function of the highly conserved SPFH (Stomatin, Prohibitin, Flotillin, HflK/C) proteins – a family of lipid microdomain-associated proteins that support the structure of lipid-rafts – in Rab11-ILV formation (Daumke & Lewin, 2022). Members of

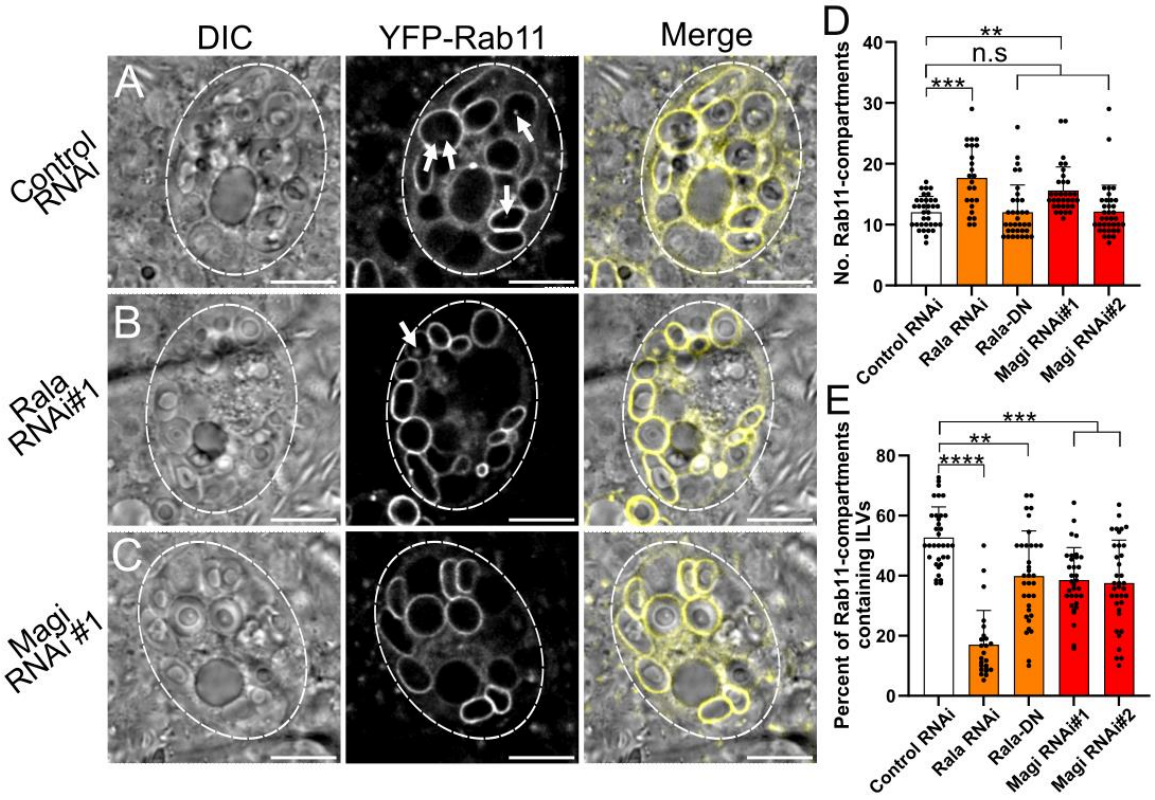

Figure 5.10. *Rala* and *Magi* knockdown suppresses Rab11-exosome biogenesis in SCs. (**A-C**) Wide-field fluorescence images of SCs expressing *YFP-Rab11* with a control RNAi (**A**), *Rala*-targeting RNAi (**B**), or *Magi*-targeting RNAi (**C**). In multicoloured images Rab11 is shown in yellow and DIC images in grayscale. All Rab11-ILVs visible in the plane of view are highlighted by white arrows (**A**-**C**). One RNAi line targeting each of *Rala* and *Magi* significantly increased Rab11-compartment numbers, though expression of dominant-negative Rala and a 2nd *Magi* RNAi had no effect on Rab11-compartment numbers (**D**). By contrast, all RNAi and dominant-negative lines induced a significant reduction in the proportion of Rab11-compartments forming ILVs (**E**). SC boundaries marked by dashed circles, Scale bars: 10μm. For graphs, P<0.01:**, P<0.001:***, P<0.0001:****, non-significant: n.s.. n=33 to 36 cells for all graphs.

this family are defined by SPFH domains which facilitate cholesterol interactions and extensive oligomerisation. Interestingly, SPFH proteins have also been implicated in exosome or extracellular vesicle formation. For example, flotillin 1 and 2 have been identified as exosome cargoes and were found to contribute to a Rab31-dependent, ESCRT-independent ILV-forming pathway (Jeppesen et al., 2023; D. Wei et al., 2021). Likewise, Prohibitin-1 was found to label Hsp70-associated, stress-induced extracellular vesicles produced by the protozoa *Leishmania major* exovesicles (Cruz-Bustos et al., 2018). Given these associations and their central role in microdomain organisation, I therefore induced SC-specific knockdowns of several *Drosophila* SPFH proteins in the *YFP-Rab11* background, namely *Flo1*, *Flo2*, *Mec2*, *Phb1*, *Phb2* and *StomL2* (Fig. 5.11A-G).

Unlike several other genes examined here, SPFH knockdowns did not induce significant changes in the number of Rab11-compartments in SCs (Fig. 5.11H). Likewise, knocking down any of *Flo1*, *Flo2*, *Mec2*, *Phb1* and *StomL2* produced no significant changes in either the number or proportion of Rab11-compartments forming Rab11-ILVs (Fig. 5.11I,J), indicating that these genes have no effect on Rab11-exosome biogenesis. However, knockdown of *Phb2* did impair ILV biogenesis, with a significant decline in both the number and proportion of Rab11-compartments forming Rab11-ILVs (Fig. 5.11I,J). Furthermore, *Phb2* knockdown also disrupted DCG organisation despite having no impact on the number of Rab11-DCG compartments. In fact, an exceptionally high proportion of DCG compartments in *Phb2* knockdown cells were found to house multiple mini-cores in their lumen (Fig. 5.11K, example highlighted by red arrows in Fig. 5.11G), indicating that DCG biogenesis and maturation is disrupted following *Phb2* knockdown.

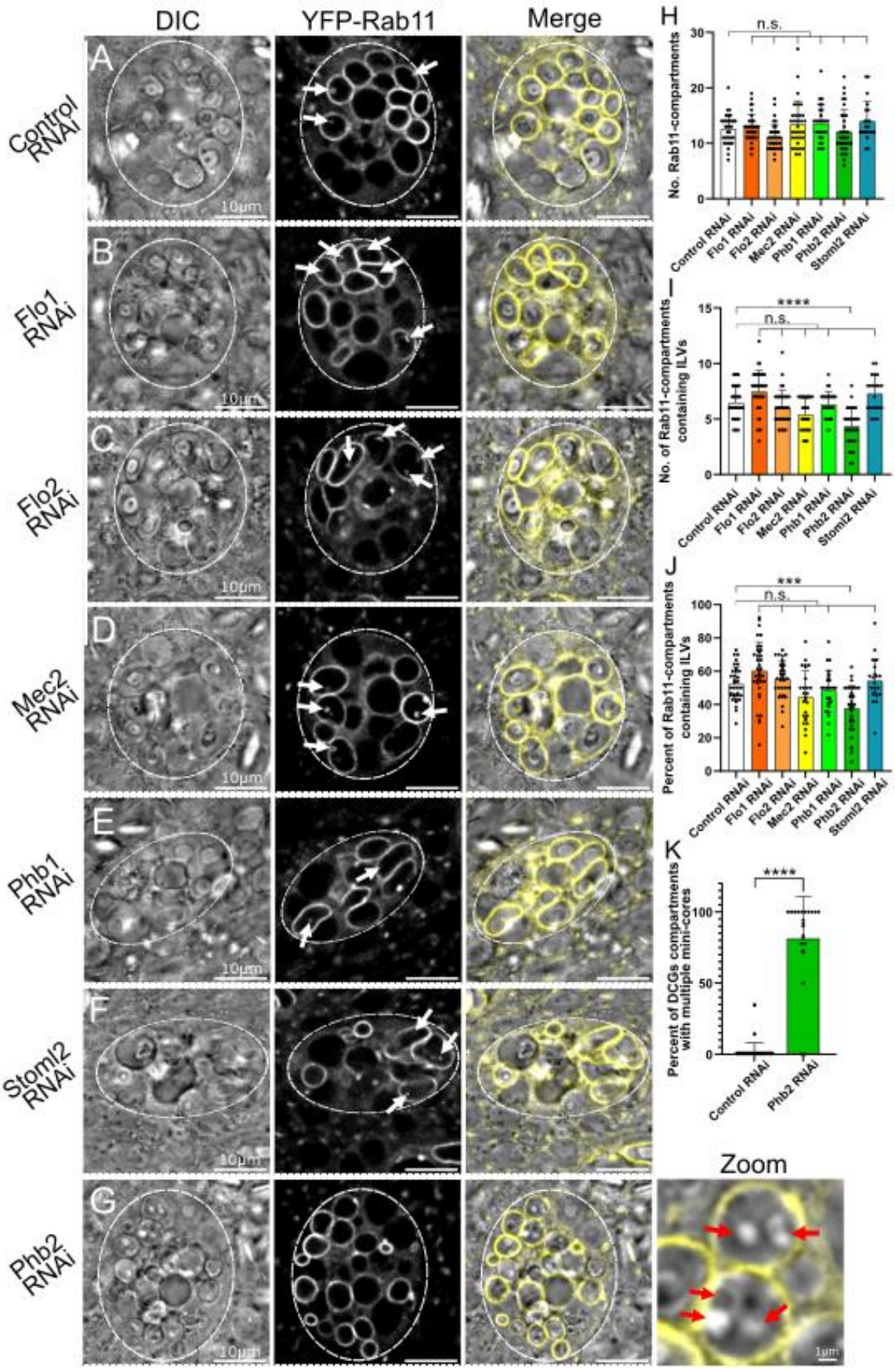
DIC
YFP-Rab11
Merge
A
Control RNAi
B
Flo1 RNAi
C
Flo2 RNAi
D
Mec2 RNAi
E
Phb1 RNAi
F
Stoml2 RNAi
G
Phb2 RNAi
10μm
H
n.s.
No. Rab11-compartments
Control RNAi
Flo1 RNAi
Flo2 RNAi
Mec2 RNAi
Phb1 RNAi
Phb2 RNAi
Stoml2 RNAi
I
****
n.s.
No. of Rab11-compartments containing ILVs
J
***
n.s.
Percent of Rab11-compartments containing ILVs
K
****
Percent of DCGs compartments with multiple mini-cores
Zoom
1μm

Figure 5.11. Phb2 The SPFH protein Phb2 controls Rab11-ILV biogenesis and DCG maturation. (**A-G**) Wide-field fluorescence images of SCs expressing *YFP-Rab11* with a control RNAi (**A**), *Flo1*-targeting RNAi (**B**), *Flo2*-targeting RNAi (**C**), *Mec2*-targeting RNAi (**D**), *Phb1*-targeting RNAi (**E**), *Phb2*-targeting RNAi (**F**), or *StomL2*-targeting RNAi (**G**). In multicoloured images Rab11 is shown in yellow and DIC images in grayscale. All Rab11-ILVs visible in the plane of view are highlighted by white arrows (**A**-**G**). Knockdown of SPFH genes generally had no strong effect on SC organisation. For example, no knockdowns significantly affected the number of Rab11-compartments (**H**) and most had no effect on DCG structure (**A**-**G**). However, knockdown of *Phb2* specifically did have significant effects on both ILV and DCG biogenesis. Following *Phb2* knockdown, Rab11-ILV biogenesis was significantly reduced both in terms of Rab11-ILV numbers (**I**) and the proportion of compartments forming Rab11-ILVs (**J**). In addition, knockdown of *Phb2* strongly disrupted DCG formation, with the vast majority of DCGs forming as multiple mini-cores rather than a single DCG (**K**, example mini-cores highlighted by red arrows in zoom images in **G**). SC boundaries marked by dashed circles. For graphs, P<0.001:***, P<0.0001:****, non-significant: n.s.. n=21 to 37 cells for all graphs.

Of the SPFH proteins tested here, *Phb2* was not expected to play a role in Rab11-compartments since it is primarily localised to mitochondrial membranes (Bavelloni et al., 2015; Y. Wei et al., 2017). Despite also localising to some other areas in the cell such as the nucleolus and having functions in cell proliferation, apoptosis and cancer development (F. Liu et al., 2023; Qi et al., 2023; Z. Zhou et al., 2018), there was no previous report of Phb2 acting at endosomes. Therefore, to test whether Phb2 had any role in supporting ELMs, I knocked down *Phb2* in SCs expressing both YFP-Rab11 and Ecad-RFP (Fig. 5.12A-B). I also knocked down *Mec2*, an SPFH gene whose knockdown induced a slight, non-significant decline in Rab11-ILV formation, for comparison (Fig. 5.12C). As observed in the YFP-Rab11 background, neither *Phb2* or *Mec2* knockdown significantly affected the number of Rab11-compartments in SCs (Fig. 5.12D). However, knocking down specifically *Phb2* did reduce the number of ELMs present in SCs, with both the number and proportion of Rab11-compartments trafficking ELMs being significantly reduced (Fig. 5.12E-F). These results suggest that the SPFH domain protein Phb2 promotes the formation or maintenance of ELMs on Rab11-compartments and, similarly, promotes the biogenesis of Rab11-ILVs and DCGs in SCs.

5.2.8 Vps34 controls Rab11-ILV biogenesis and ELM formation

To further investigate the regulation of Rab11-ILV biogenesis, I examined the function of the class III phosphatidylinositol 3-kinase (PI3-kinase), Vps34, an enzyme that is conserved throughout all eukaryotic life. Following Vps34 recruitment to Golgi/endosomal membranes by Vps15, it is responsible for producing the essential

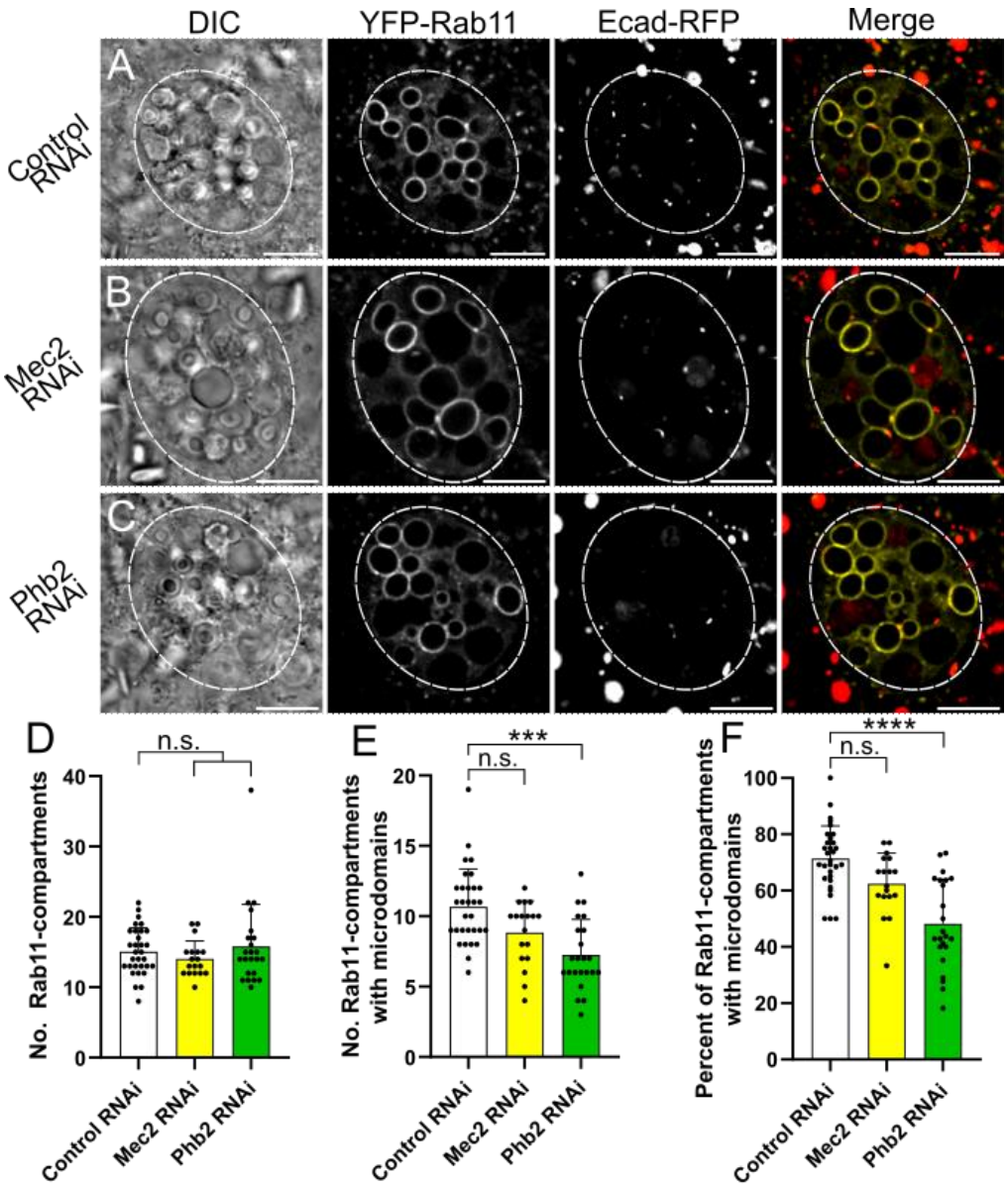

Figure 5.12. *Phb2* knockdown reduces ELM formation on Rab11-compartments.

(**A-C**) Wide-field images of SCs expressing *YFP-Rab11* and *Ecad-RFP* with a control RNAi (**A**), *Mec2* RNAi (**B**), or *Phb2* RNAi (**C**). In multicoloured images Rab11 is shown in yellow and Ecad in red. As before, knockdown of *Mec2* and *Phb2* did not alter the number of Rab11-compartments (**D**). However, *Phb2* knockdown *Mec2* knockdown did significantly reduce the number of Rab11-compartments with surface-associated ELMs (**E**) and the percentage of Rab11-compartments with surface-associated ELMs (**F**). SC boundaries marked by dashed circles, Scale bars: 10µm. For graphs, P<0.001:***, P<0.0001:****, non-significant: n.s.. n=18 to 31 cells for all graphs.

lipid phosphatidylinositol 3-phosphate (PI3P) (Jean & Kiger, 2014; Tremel et al., 2021). In turn, PI3P acts as a recruitment signal for a variety of important effector proteins that oversee processes such as autophagy, endocytosis and RE biogenesis (Jean & Kiger, 2014; Juhász et al., 2008; Marcelić et al., 2022). PI3P residues are also important for recruiting ESCRT-0 complexes to the surface of endosomes, and therefore play an important role in ESCRT-dependent exosome biogenesis (Raiborg et al., 2001). Given that Rab11-exosome biogenesis is an ESCRT-dependent process, I elected to investigate the role of *Drosophila* Vps34 in this process by expressing two independent *Vps34* RNAis in SCs expressing YFP-Rab11 (Fig. 5.13A-B).

Interestingly, despite the essential role of Vps34 in endosomal processes, I found that Vps34 knockdown had only a mild impact on the organisation of SC compartments. No change was observed in the number of Rab11-compartments in SCs following *Vps34-RNAi#1* expression, and only a slight increase was observed following *Vps34-RNAi#2* expression (Fig. 5.13C). However, much larger changes were found in Rab11-ILV formation. Knockdown using *Vps34-RNAi#1* resulted in a strong decline in both the number of Rab11-ILV forming compartments (Fig. 5.13D) and the proportion of compartments which formed ILVs (Fig. 5.13E), with both being reduced by ~40% compared to control SCs. Knockdown using *Vps34-RNAi#2* did not result in significantly fewer Rab11-ILV forming compartments in absolute terms, but it did induce a statistically significant drop in the proportion of compartments forming Rab11-ILVs (Fig. 5.13E). Overall, these findings indicated that Vps34 activity promotes Rab11-exosome biogenesis.

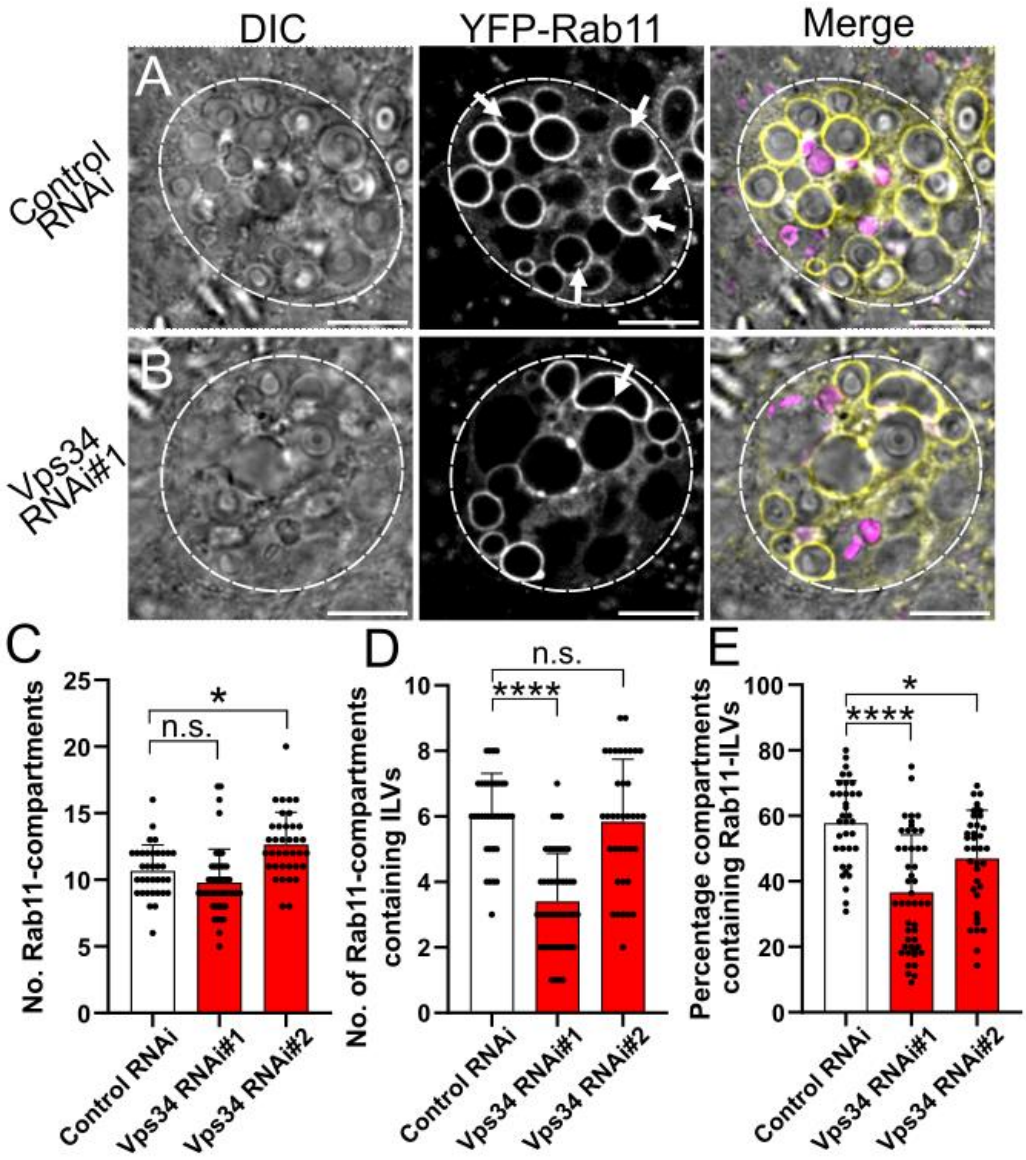

Figure. 5.13. *Vps34* knockdown reduces Rab11-ILV formation in Rab11-compartments. (**A-B**) Wide-field fluorescence images of SCs expressing *YFP-Rab11* with a control RNAi (**A**) or *Vps34*-targeting RNAi (**B**). In multicoloured images Rab11 is shown in yellow and DIC images in grayscale. All Rab11-ILVs visible in the plane of view are highlighted by white arrows (**A**-**B**). Following *Vps34* knockdown, no effect was observed on Rab11-compartment numbers using *Vps34-RNAi#1* although a slight increase in Rab11-compartments was induced by *Vps34-RNAi#1* (**C**). By contrast, only *Vps34-RNAi#1* had a significant effect on the number of Rab11-ILVs present in SCs, causing a significant reduction (**D**). However, both *Vps34* knockdowns induced a significant reduction in the percentage of Rab11-compartments forming Rab11-ILVs (**E**). SC boundaries marked by dashed circles, Scale bars: 10µm. For graphs, P<0.05:*, P<0.0001:****, non-significant: n.s.. n=35 to 47 cells for all graphs.

I next tested the potential role of Vps34 in the biogenesis of ILV-forming ELMs. Vps34 and PI3P residues play an important role in recruiting proteins such as Hrs to endosome membranes (Raiborg et al., 2001). PI3P also facilitates the recycling of internalised E-cadherin through its interaction with SNX16 (J. Xu et al., 2017). Since I had already found that E-cadherin and Hrs localise into SC microdomains, I investigated the effect of *Vps34* knockdown on microdomain trafficking using the Ecad-RFP marker protein (Figure 5.14A-B). Using *Vps34-RNAi#1*, I found that the number and proportion of Rab11-compartments trafficking ELMs fell by ~40% in knockdown cells (Figure 5.14C-D). I next examined the notably elevated lysosome-associated RFP signal in *Vps34* knockdown cells and found that under the same imaging conditions (i.e. 32% laser power, 100ms exposure time), the fluorescent signal from lysosomes in *Vps34* knockdown cells was significantly elevated, being approximately 3 times greater than in control cells (Figure 5.14E). Compared to other fluorescent protein tags, RFP fluorescence is not effectively quenched upon entry into acidic lysosome compartments (Katayama et al., 2008), indicating that far more Ecad-RFP is trafficked to lysosomal compartments following *Vps34* knockdown. This aligns with previous results such as the requirement of PI3P and SNX16 for E-cadherin recycling (Xu et al., 2017), although since PI3P is also required for LE/lysosome function, these results may simply reflect lysosome dysfunction (Futter et al., 2001; Jaber et al., 2016). Overall, these results suggest that Vps34 activity supports both Rab11-exosome biogenesis and ELM formation in SCs.

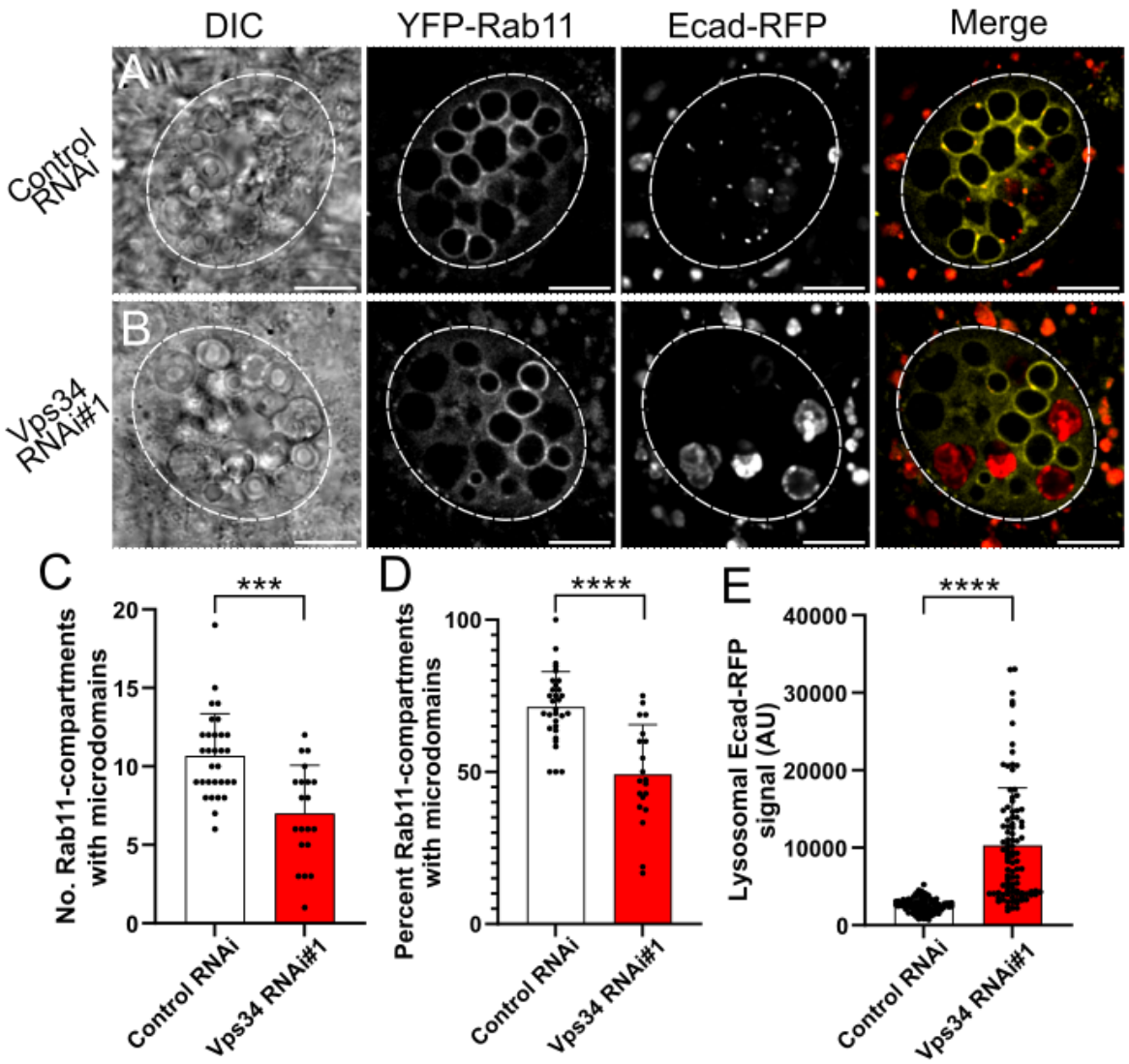

Figure 5.14. *Vps34* knockdown reduces ELM formation on Rab11-compartments.

(**A-C**) Wide-field fluorescence images of SCs expressing *YFP-Rab11* and *Ecad-RFP* with a control RNAi (**A**) or *Vps34*-targeting RNAi (**B**). In multicoloured images Rab11 is shown in yellow and Ecad in red. *Vps34* knockdown induces a significant decrease in the total number of Rab11-compartments with surface-associated ELMs (**C**) and the percentage of Rab11-compartments with surface-associated ELMs (**E**). In addition, *Vps34* knockdown induced a significant increase in lysosomal RFP-signal as judged by the average 16-bit pixel value for fluorescent RFP-signal (**F**). SC boundaries marked by dashed circles, Scale bars: 10μm. For graphs, P<0.001:***, P<0.0001:****. n=20 to 31 cells for all graphs.

5.2.9 PI3K/Akt/mTOR signalling in SCs regulates Rab11-exosome biogenesis

Alongside testing the function of the class III PI3-kinase Vps34 in SCs, I also examined the role of class I PI3-kinase signalling in Rab11-exosome biogenesis. Class I PI3-kinases are highly conserved lipid-modifying kinases that act on the phosphatidylinositol molecule, phosphatidylinositol 4,5-diphosphate (PIP2) to produce phosphatidylinositol 3,4,5-triphosphate (PIP3) (Jean & Kiger, 2014). PIP3 residues recruit and activate a number of downstream proteins and are essential for numerous cell proliferation, cell survival and cancer-promoting pathways. The best known is the oncogenic PI3K/Akt/mTOR pathway (Glaviano et al., 2023). Interestingly, Rab11-exosome signalling was found to be regulated by Akt/mTOR signalling in human cancer cells, with a partial inhibition of mTOR signalling through either rapamycin exposure or nutrient deprivation leading to increased Rab11-exosome secretion (Fan et al., 2020). Because of these associations, I chose to examine the effects of inhibiting the PI3K/Akt/mTOR pathway in SC Rab11-exosome biogenesis. To do this, I used SC-specific RNAi expression to knock down the PI3-kinase *Dp110*, *Akt* and the mTORC1 component *raptor*. I also knocked down the *Insulin-like Receptor* (*InR)*, an upstream receptor tyrosine kinase that activates Dp110, and induced SC-specific expression of *PTEN*, which antagonises Dp110 activity by dephosphorylating PIP3.

By employing each manipulation in a YFP-Rab11 background (Fig. 5.15A-F), I found that SC organisation could change in several ways (Fig. 5.15G). In most cases, the number of Rab11-positive compartments was significantly reduced compared to control cells and some Rab11-compartments were produced which were notably smaller in size.

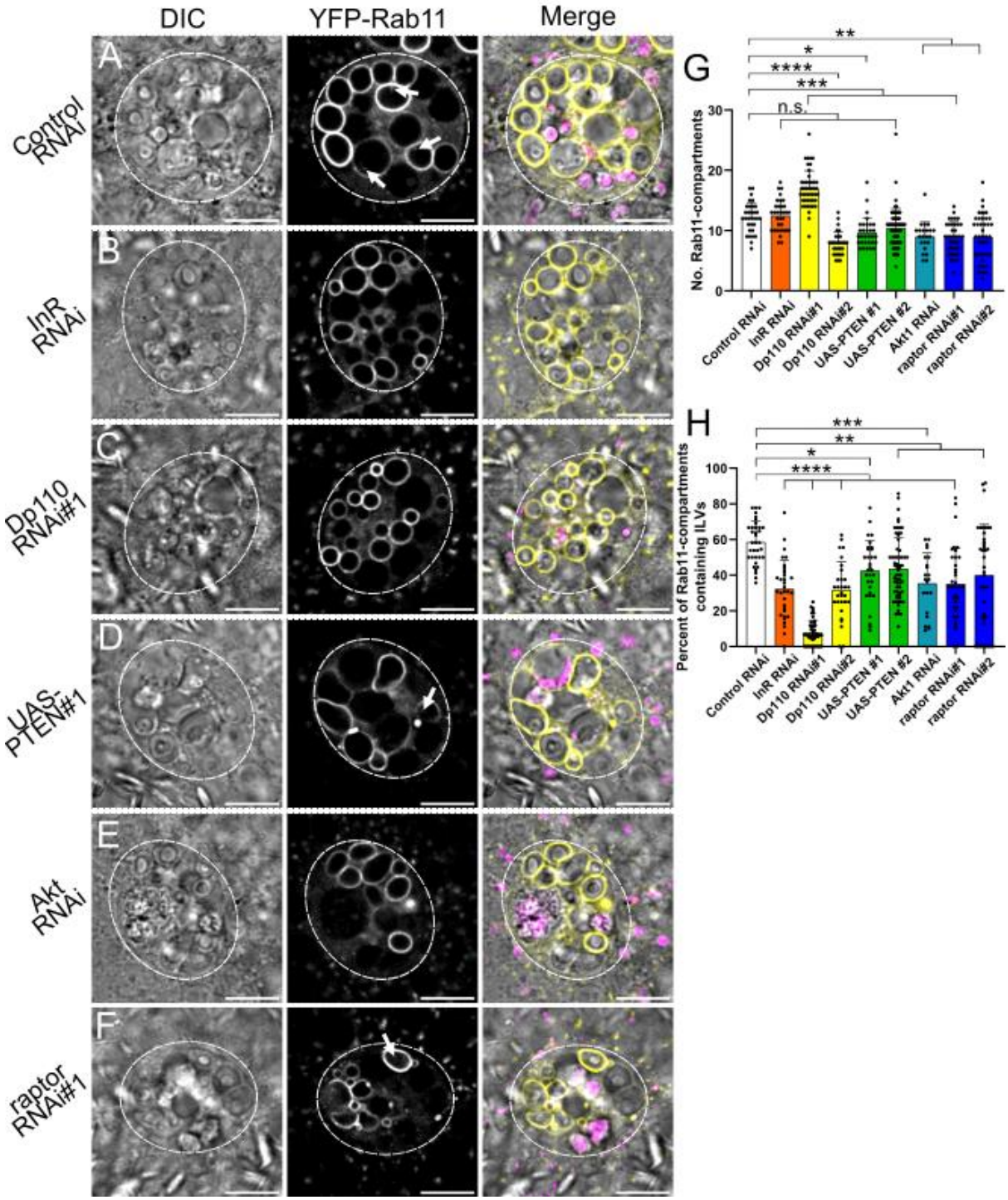

Figure 5.15. Inhibition of the PI3K/Akt/mTOR signalling pathway impairs Rab11-ILV biogenesis. (**A-F**) Wide-field fluorescence images of SCs expressing *YFP-Rab11* with a control RNAi (**A**), *InR* RNAi (**B**), *Dp110* RNAi (**C**), *PTEN* overexpression (**D**), *Akt* RNAi (**E**), or *raptor* RNAi (**F**). In multicoloured images Rab11 is shown in yellow, LysoTracker Red

in magenta and DIC images in grayscale. All Rab11-ILVs visible in the plane of view are highlighted by white arrows (**A**-**F**). Following inhibition of PI3K/Akt/mTOR signalling using *InR*, *Dp110*, *PTEN*, *Akt* and *raptor*, several effects were noted. Firstly, in five of the eight experimental backgrounds, a slight but significant decrease was observed in the number of Rab11-compartments present in SCs whilst one background, *Dp110-RNAi#1* resulted in a significant increase in Rab11-compartments (**G**). Across all experimental backgrounds however, a significant decrease was observed in the percentage of Rab11-compartments forming Rab11-ILVs (**H**). SC boundaries marked by dashed circles, Scale bars: 10μm. For graphs, P<0.05:*, P<0.01:**, P<0.001:***, P<0.0001:****, non-significant: n.s.. n=22 to 63 cells for all graphs.

However, knockdown of *InR* and overexpression of UAS-PTEN#2 had no impact on Rab11-compartment numbers, whilst *Dp110-RNAi#1* actually increased the number of Rab11-compartments compared to controls. Interestingly, expression of *Dp110-RNAi#1* also disrupted the process of DCG biogenesis, an effect explored elsewhere in Section 4.2.9. Regardless of the changes in DCGs and Rab11-compartment numbers however, the effect of PI3K/Akt/mTOR inhibition on Rab11-exosome biogenesis was consistent across all genotypes. Specifically, every genotype examined displayed a significant decrease in the proportion of compartments containing Rab11-ILVs (Fig. 5.15H). Generally, the reduction in Rab11-ILV forming compartments was approximately 50% compared to controls, but the decline in Rab11-ILV formation could be as much as ~90% following *Dp110-RNAi#1* expression. This effect was surprising in some ways, since suppressing Akt/mTORC1 signalling in HCT116 cells had been shown to promote Rab11-exosome activity rather than inhibit it (Fan et al., 2020), although it is worth noting that baseline PI3K/Akt/mTOR signalling is heavily upregulated in this cancer cell population, suggesting that inhibition of Akt/mTORC1 signalling in HCT116 cells may not be equivalent to the blockade induced in SCs.

Given the inhibitory effect of suppressing PI3K/Akt/mTOR signalling on Rab11-ILV biogenesis, I hypothesised that hyperactivating this pathway could result in increased Rab11-ILV formation in SCs. To test this hypothesis, I induced the overexpression of a UAS-controlled *InR* construct and knocked down the *PTEN* antagonist in SCs using two independent RNAis in a YFP-Rab11 background (Fig. 5.16A-C). No manipulations resulted in a disruption of Rab11-compartment morphology or in significant changes

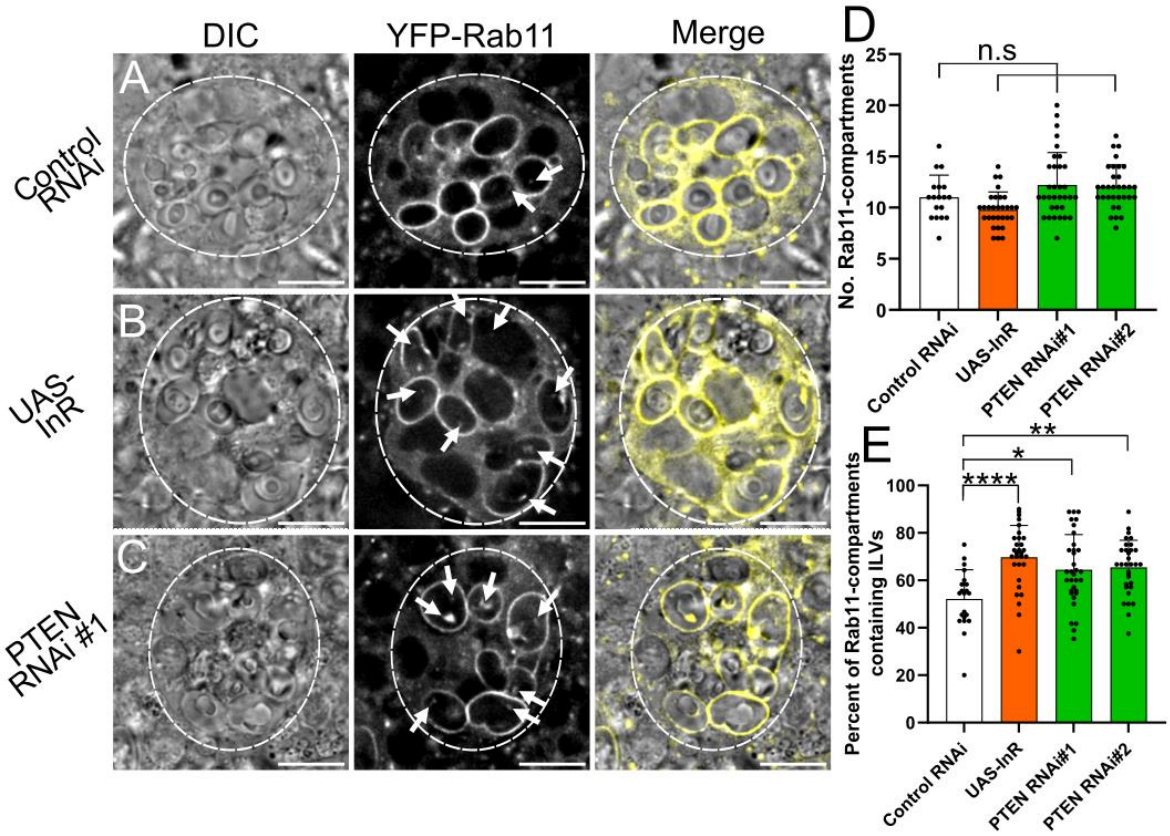

Figure 5.16. Stimulation of the PI3K/Akt/mTOR signalling pathway promotes Rab11-ILV biogenesis. (**A-C**) Wide-field fluorescence images of SCs expressing *YFP-Rab11* with a control RNAi (**A**), *InR* overexpression (**B**) or *PTEN*-targeting RNAi (**C**). In multicoloured images Rab11 is shown in yellow and DIC images in grayscale. All Rab11-ILVs visible in the plane of view are highlighted by white arrows (**A**-**C**). Stimulation of PI3K/Akt/mTOR signalling via *InR* overexpression and *PTEN* knockdown induced no significant change in the number of Rab11-compartments present in SCs (**D**). However, *InR* overexpression and both *PTEN* knockdowns did significantly increase the percentage of Rab11-compartments producing Rab11-ILVs (**E**). SC boundaries marked by dashed circles, Scale bars: 10μm. For graphs, P<0.05:*, P<0.01:**, P<0.001:***, P<0.0001:****, non-significant: n.s.. n=21 to 33 cells for all graphs.

to Rab11-compartment numbers (Fig. 5.16D). However, hyperactivation of PI3K/Akt/mTOR signalling did result in significantly increased Rab11-ILV production in all three cases, with the proportion of Rab11-compartments forming ILVs rising from ~50% in control cells to between ~60-70% in hyperactivated genotypes (Fig. 5.16E). These results provide further evidence of PI3K/Akt/mTOR signalling's specific role in Rab11-exosome biogenesis and support the idea that variable signalling by this pathway could regulate Rab11-exosome signalling *in vivo*.

5.2.10 PI3K/Akt/mTOR signalling also controls E-cadherin microdomain formation

Given my earlier observations that ELM trafficking could be manipulated by various regulators of Rab11-ILV biogenesis, I hypothesised that the PI3K/Akt/mTOR pathway may also control the formation of ILV-forming ELMs. To test this, I suppressed PI3K/Akt/mTOR signalling in SCs expressing YFP-Rab11 and Ecad-RFP through either knockdown of *InR* and *Dp110* or overexpression of *PTEN* (Fig. 5.17A-D). I also examined the effect of hyperactivating PI3K/Akt/mTOR signalling by overexpressing *InR* in the same background (Fig. 5.17E). As hypothesised, inhibition of PI3K/Akt/mTOR signalling resulted in a large decline in the formation of ELMs on Rab11-compartments, mirroring the effects observed for Rab11-ILV biogenesis in these same compartments (Fig. 5.17F-G). Remarkably, hyperactivation of PI3K/Akt/mTOR signalling created the opposite effect, with a significant increase in the number of microdomains present on compartment membranes following *InR* overexpression (Fig. 5.17H).

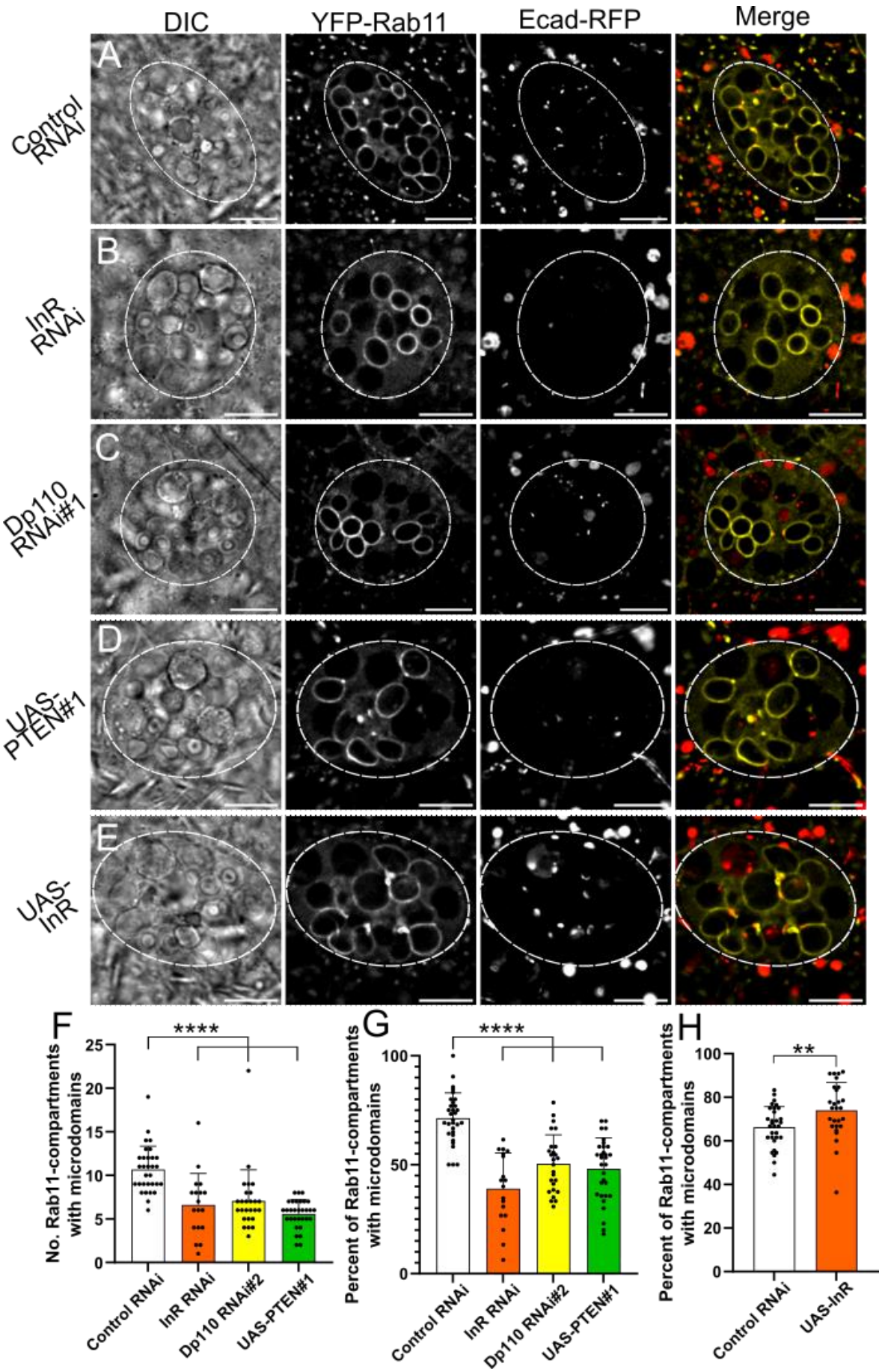
DIC
YFP-Rab11
Ecad-RFP
Merge
A
Control RNAi
B
InR RNAi
C
Dp110 RNAi#1
D
UAS-PTEN#1
E
UAS-InR
F
No. Rab11-compartments with microdomains
****
Control RNAi
InR RNAi
Dp110 RNAi#2
UAS-PTEN#1
G
Percent of Rab11-compartments with microdomains
****
Control RNAi
InR RNAi
Dp110 RNAi#2
UAS-PTEN#1
H
Percent of Rab11-compartments with microdomains
**
Control RNAi
UAS-InR

Figure 5.17. Inhibition of the PI3K/Akt/mTOR signalling pathway blocks ELM formation on Rab11-compartments. (**A-F**) Wide-field fluorescence images of SCs expressing *YFP-Rab11* and *Ecad-RFP* with a control RNAi (**A**), *InR*-targeting RNAi (**B**), *Dp110*-targeting RNAi (**C**), *PTEN* overexpression (**D**) and *InR* overexpression (**E**). In multicoloured images Rab11 is shown in yellow and Ecad in red. Following the inhibition of PI3K/Akt/mTOR signalling through *InR* knockdown, *Dp110* knockdown or *PTEN* overexpression, significantly fewer compartments were found with surface-associated ELMs (**F**, example images **B**-**D**). Likewise, a significantly smaller percentage of Rab11-compartments were identified with surface-associated ELMs (**G**). In contrast to this, overexpressing *InR*, which would be expected to stimulate PI3K/Akt/mTOR signalling, resulted in a significant increase in the proportion of Rab11-compartments forming surface-associated ELMs (**H**). SC boundaries marked by dashed circles, Scale bars: 10μm. For graphs, P<0.01:**, P<0.0001:****. n=18 to 31 cells for all graphs.

5.3 Discussion

5.3.1 Core findings

My results identify a range of novel Rab11-exosome biogenesis regulators, including molecules that have been described in other less well-understood exosome-forming pathways. Most significantly, I identified novel Rab11-compartment microdomains labelled by E-cadherin, Rab19 and the ESCRT-0 protein Hrs, termed E-cadherin-positive lipid microdomains (ELMs). Evidence from a number of experiments suggests that these ELMs act as the site of Rab11-exosome biogenesis *in vivo*. On top of this, I find that Rab11-effector proteins such as the Rab11-FIP proteins control Rab11-compartment organisation whilst Sec15/exocyst complex proteins regulate both compartment organisation and Rab11-ILV biogenesis in SCs. Similarly, the lipid-raft-associated SPFH protein Phb2 was found to have novel roles regulating microdomain and Rab11-ILV biogenesis. Finally, the PI3K/Akt/mTOR pathway was also shown to regulate Rab11-exosome formation and could be manipulated to either increase or decrease ILV production. Crucially, these changes were matched by increases and decreases in the abundance of ELMs on Rab11-compartments, indicating that PI3K/Akt/mTOR signalling may regulate ILV formation through changes in microdomain formation.

5.3.2 Novel E-cadherin microdomains on Rab11-compartments act as sites of Rab11-exosome biogenesis

Whilst cell-surface E-cadherin acts as a tumour suppressor, its internalisation is associated with tumorigenesis and cancer metastasis (Mendonsa et al., 2018). It was therefore of great interest when microdomains labelled by E-cadherin were found to associate with sites of Rab11-ILV invagination. Through colocalisation studies, I established that E-cadherin colocalises with both Rab19 and the ESCRT-0 protein Hrs and found that microdomains labelled by each of E-cadherin, Rab19 and Hrs were associated with ILVs variously labelled by CFP-Rab6, YFP-Rab11 and YFP-Rab19. Crucially, this was even true in compartments where DCGs had not yet formed (e.g. Fig. 5.4C), indicating that ELMs were associated with Rab-labelled ILVs from the time of their biogenesis. Incidentally, these findings also suggest that differently labelled Rab-ILVs possess similar biogenesis mechanisms. Since knockdown of each microdomain-associated protein also reduced Rab11-ILV formation, I concluded that ELMs represented novel sites of ILV formation for Rab11-exosomes.

Further investigation of ELMs revealed a number of other factors that regulated both ELM formation and Rab11-exosome biogenesis. Notably, it was universally found that genetic manipulations that decreased ELM formation also decreased Rab11-ILV biogenesis (e.g. knockdown of *Phb2*, *Vps34* and *Dp110*), whilst factors stimulated ELM formation increased ab11-ILV biogenesis (e.g. *PTEN* RNAis and *InR* knockdown). Additionally, tested factors that had no effect on Rab11-ILV biogenesis also failed to impact ELM formation (e.g. *Nuf, Rip11* and *Mec2*). Based on this consistent association and the finding that ELMs themselves control exosome biogenesis, I propose a new

model for Rab11-exosome regulation in which ELMs act as central platforms coordinating ILV biogenesis (Fig. 5.18).

In this model, ELMs form on non-DCG compartments prior to or during the Rab6 to Rab11-transition, recruit ESCRT-complexes and induce exosome biogenesis (Fig. 5.18A). Rab11-biogenesis can be severely restricted in the absence of ELM components, particularly Rab19 and Hrs. It is also reduced by inhibition of PI3K/Akt/mTOR signalling, Phb2 and Vps34 which control ELM formation (Fig. 5.18B-C). Interestingly, Phb2 and Vps34 are themselves microdomain-associated factors and may be ELM constituents. Also interestingly, knockdown of *Phb2* and *Dp110* each induced abnormal DCG aggregation (Fig. 5.18C), similar to that seen in neurodegeneration-linked genotypes (Sections 4.2.8-4.2.10). Since *Phb2* and *Dp110* homologues are both risk-factors in neurodegeneration (Fernandez-Abascal & Artal-Sanz, 2022; Goyal et al., 2023), this raises the possibility of a link between ELMs and DCG aggregation. Finally, when ELM formation is increased through elevated PI3K/Akt/mTOR signalling, Rab11-exosome biogenesis also increases (Fig. 5.18D). In this model, the formation of ELMs on compartments represents the determining factor in Rab11-ILV formation as it integrates information from a variety of sources such as global signalling pathways, trafficking GTPases and lipid modifying kinases.

Overall, the role of microdomains and lipid-rafts in exosome biogenesis remains poorly understood but is likely to be significant. Ceramide microdomains are proposed to be involved in ESCRT-independent exosome biogenesis (Skryabin et al., 2020; D. Wei et al., 2021), whilst exosomes in mesenchymal stem cells are produced from lipid-rafts internalised from the plasma membrane (Tan et al., 2013). I therefore believe that the

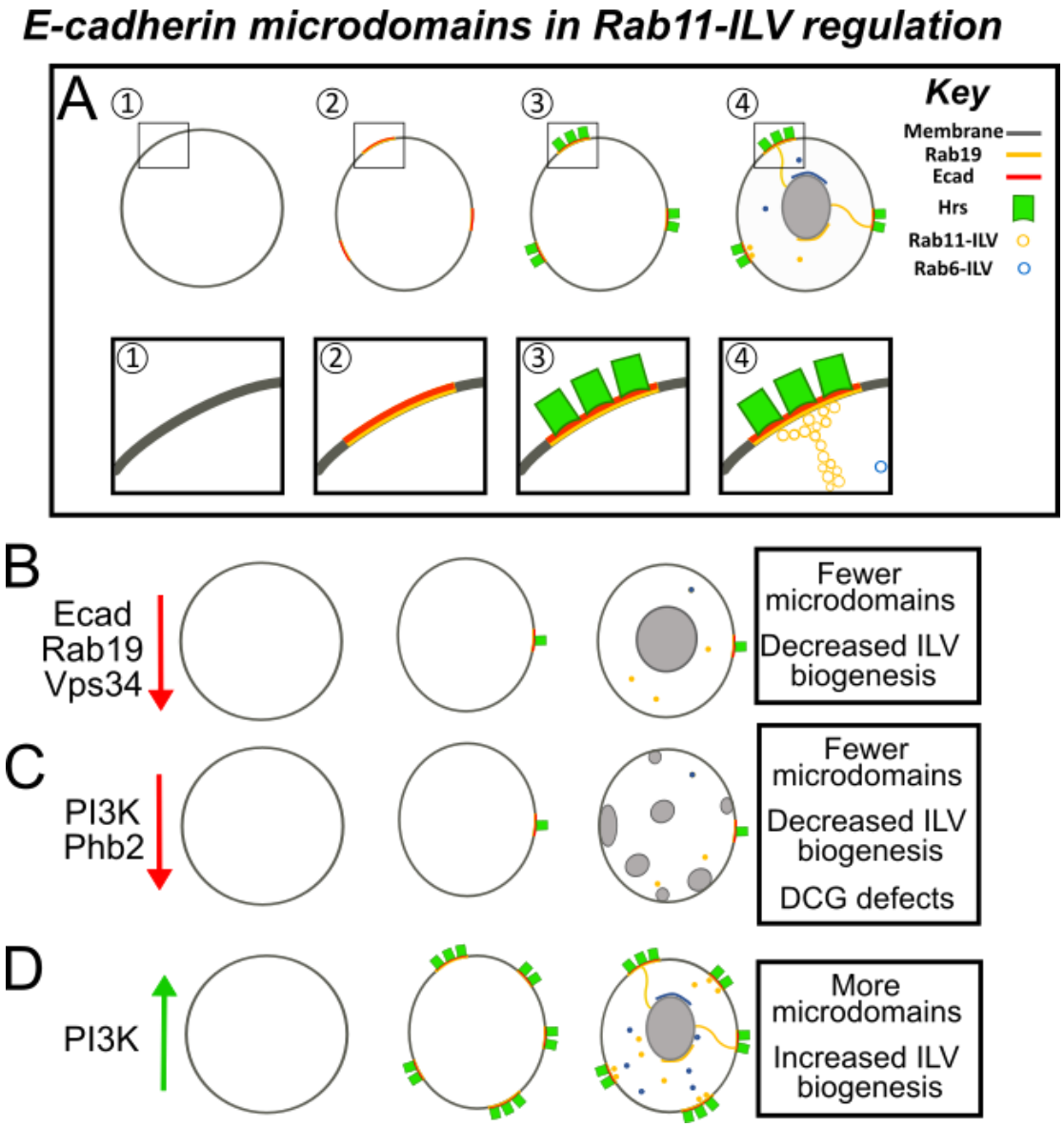

Figure 5.18. Model for ELM control of Rab11-exosome biogenesis. In control cells, ELMs first appear on non-DCG compartments (**A1-2**). E-cadherin and Rab19 are likely recruited first, followed by the ESCRT-0 protein Hrs (**A2-3**) which is known to recruit other ESCRT-complexes. ELMs then drive Rab11-exosome formation approximately simultaneously with DCG biogenesis and the onset of the Rab6 to Rab11 transition (**A4**). Following knockdown of the microdomain components *Ecad* and *Rab19*, or the potential microdomain element *Vps34*, fewer ELMs are formed and fewer Rab11-exosomes are produced (**B**). Similarly, knockdown of the potential microdomain element *Phb2* or the PI3-kinase *Dp110* leads to disrupted ELMs, Rab11-exosome and DCG biogenesis (**C**). Conversely, stimulated PI3K signalling increases microdomain formation and Rab11-exosome biogenesis (**D**).

identification of ELMs within provides an excellent system for further research into exosome-microdomain dynamics. To extend this work, it would initially be useful to confirm the presence of lipid-raft-associated factors like Phb2, PI3P and cholesterol at ELMs. The presence of Vps34-produced PI3P is implied by the presence of Hrs (Raiborg et al., 2001), but Phb2 and cholesterol localisations could be examined using a fluorescent construct and the BODIPY-cholesterol reporter respectively (Hölttä-Vuori et al., 2008).

It would also be beneficial to confirm the role of similar microdomains in human Rab11a-exosome biogenesis, potentially through EM or super-resolution imaging as well as through knockdown of the factors identified here. Additionally, if appropriate lipid-raft proteins can be identified, it should be feasible to incorporate a promiscuous biotin ligase into their structure and then utilise the BioID method to efficiently identify relevant protein-protein interactions occurring within the lipid-raft (Roux et al., 2018). Similarly, expressing other altered forms of lipid-raft proteins could also facilitate subtype-specific exosome engineering efforts that could be used to track exosomes following release, alter their signalling effects or otherwise inform us on different aspects of exosome biology.

5.3.3 Rab11-effectors have variable roles in Rab11-compartments and ILV biogenesis

Having previously found that ILV biogenesis in the large secretory compartments of SCs is dependent on Rab11, I examined a number of known Rab11-interacting

proteins. Overall, no clear mechanism for Rab11's function was found, although interacting proteins did have a range of effects on secretory compartment processes, including some that acted as regulators of Rab11-exosome biogenesis (Fig. 5.18). Perhaps the most straightforward of these was the effect of the Rab11-GEF Bet3, whose knockdown slightly decreased Rab11-compartment numbers and increased Rab6-compartments, suggesting that the Rab6 to Rab11 transition was partially impaired. This was largely expected, but *Bet3* knockdown did produce a slightly surprising decrease in the proportion of Rab11-compartments found producing Rab11-ILVs (Fig. 5.18B). This result potentially highlights a requirement for high levels of Rab11-activity in the process of ILV biogenesis even after Rab11-identity is attained by compartments.

One other unexpected finding came from knockdown of *Nuf* and *Rip11* led to the formation of prominent membrane "superdomains" which were contiguous with the limiting membrane of compartments, but which appeared to physically protrude from the limiting membrane into the cytosol. These superdomains were characterised by high concentrations of Rab11 and E-cadherin, though neither *Nuf n*or *Rip11* knockdown altered of Rab11-ILV biogenesis or ELM formation. Ultimately, the nature of these superdomains is unclear and EM or super-resolution imaging would be useful for determining their structure. Given the primary function of Nuf and Rip11 as adaptor proteins linking Rab11-compartments to cytoskeletal filaments however (Horgan & McCaffrey, 2009; Jing & Prekeris, 2009), I propose that Rab11-FIP knockdowns cause a breakdown in compartment-cytoskeleton tethering. The superdomains observed on the outside of compartments could then reflect abnormal membrane folding due to

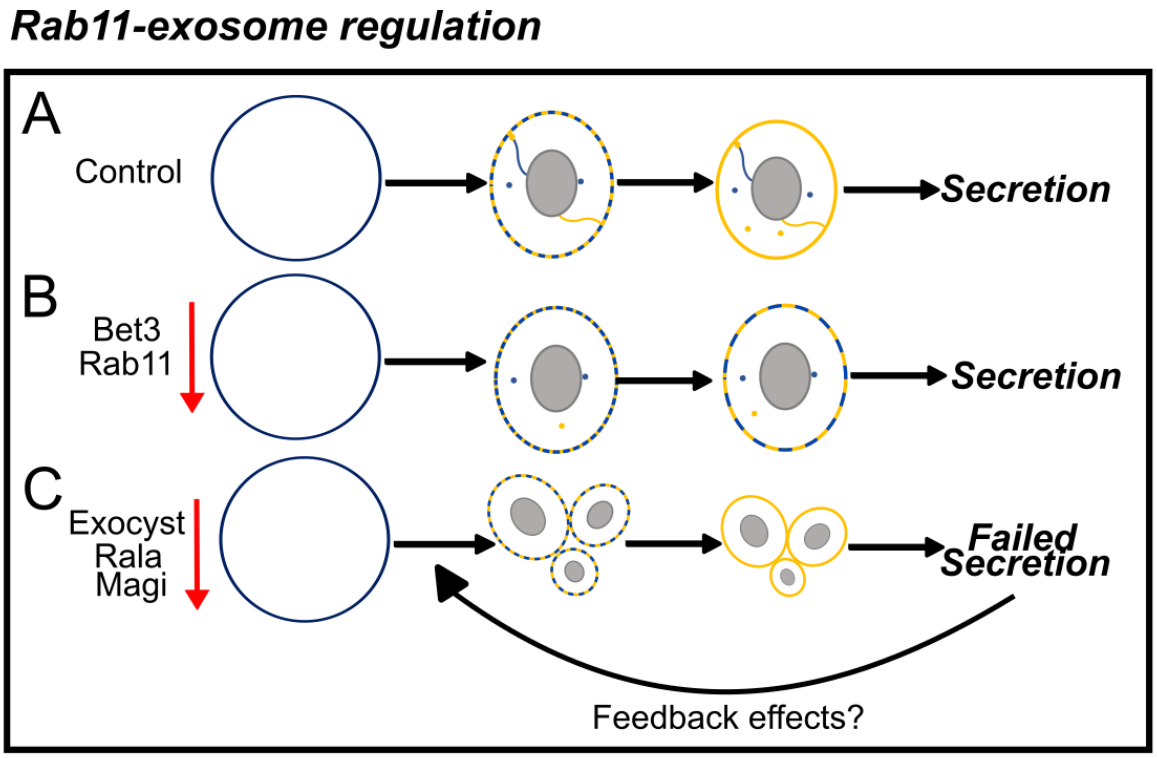

Figure 5.19. Model for Rab11-interacting proteins in Rab11-exosome regulation. In normal cells, non-DCG compartments undergo the Rab6 to Rab11 transition which stimulates DCG and Rab11-exosome biogenesis (**A**). Following knockdown of *Rab11* or its GEF *Bet3*, the Rab6 to Rab11 transition is partially inhibited, leading to extended Rab6-presence on DCG compartments and decreased Rab11-exosome biogenesis (**B**). Following inhibition of the exocyst complex or the associated factors Rala and Magi, the number of Rab11-compartments increases and Rab11-exosome biogenesis is strongly inhibited (**C**). This likely reflects a blockade of Rab11-compartment secretion which may in turn have feedback effects on Rab11-compartment formation and Rab11-ILV biogenesis through impaired recycling of important materials.

unevenly dispersed mechanical tension. If true, this would indicate that cytoskeletal attachments through Nuf and Rip11 play an important role in maintaining secretory compartment structure. Given the presence of E-cadherin on superdomains, it may also suggest that ELMs are somehow involved in attaching compartments to structures like the cytoskeleton. Overall, Rab11-FIPs do not regulate ILV or microdomain biogenesis, but their knockdown does produce a novel phenotype that warrants further study.

Finally, I also investigated the function of the Rab11-effector Sec15 as well as other members of the exocyst complex which facilitates compartment exocytosis in cells (B. Wu & Guo, 2015; X.-M. Zhang et al., 2004). Suppressing expression of exocyst components typically resulted in greater numbers of Rab11-compartments being present in SCs. Interestingly, these compartments were smaller in size and displayed decreased levels of Rab11-ILV formation compared to control cells. Similar effects were also observed following knockdown of *Rala* and *Magi*, two exocyst-associated factors that cooperate with exocyst to modulate intracellular trafficking events (Fig. 5.18C). These effects are broadly consistent with a model in which Rab11-compartments cannot undergo exocytosis following exocyst knockdowns, leading to an accumulation of new Rab11-compartments that are smaller and cannot form Rab11-ILVs due to an inability to recycle resources that would normally join the plasma membrane following secretion.

Notably however, it was also true that decreased Rab11-exosome biogenesis was also observed even in knockdowns where no significant change in Rab11-compartment numbers was observed, implying that these effects are independent of inhibited

secretion. This therefore raises the possibility that the exocyst complex plays a more direct role in Rab11-exosome formation and does not simply act through feedback effects from the recycling of Rab11-cargo materials. One interesting alternative explanation is that the exocyst complex controls Rab11-exosome biogenesis through the intracellular trafficking of ELM components. Indeed, the exocyst complex, Rala and Magi are all known to regulate the trafficking, internalisation and recycling of E-cadherin (Kotelevets et al., 2005; Langevin et al., 2005; Shipitsin & Feig, 2004; Wörthmüller & Rüegg, 2021). To assess the contributions of inhibited secretion and ELM formation on Rab11-exosomes biogenesis in these knockdowns, it will be useful to analyse the concentration of exosomes in the accessory gland lumen using previously established methods (Marie et al., 2023) and to examine the formation of Ecad-RFP labelled microdomains in each exocyst, *Rala* and *Magi* knockdown background.

Overall, no clear mechanism for regulating ILV biogenesis, DCG biogenesis or exosome secretion emerged from my studies of Rab11-effector proteins, although these effectors do seem to be involved in several steps in the pathway. The exocyst complex remains a highly interesting candidate for further research into the regulation of Rab11-exosomes, but other Rab11-effector proteins should also be studied in future research.

5.3.4 PI3K/Akt/mTOR signalling is a conserved regulatory mechanism controlling Rab11-exosome biogenesis

The final major finding described in this chapter is the discovery that the PI3K/Akt/mTOR pathway is an important regulator of both Rab11-exosome biogenesis and ELM formation in SCs. Inhibiting virtually any activating component of this pathway from its initial activation by the tyrosine receptor kinase InR, to the formation of PIP3 lipid residues, to mTOR complex activity significantly reduced ILV formation. Indeed, direct knockdown of the PI3-kinase *Dp110* with one RNAi almost entirely eliminated Rab11-ILV formation, indicating that this pathway may be an essential regulator of ILV biogenesis. Furthermore, inhibition of PI3K/Akt/mTOR signalling through *InR* knockdown, *Dp110* knockdown or *PTEN* overexpression also reduced microdomain formation.

Interestingly, the stronger *Dp110* knockdown (*Dp110-RNAi#1*) also produced two other noteworthy changes in Rab11-compartments. Firstly, it led to significant defects in DCG biogenesis (explored in Section 4.2.9), and secondly it resulted in a significant accumulation of Rab11-compartments in SCs. The fact that these changes were observed specifically in the genotype with the strongest inhibition of Rab11-ILV biogenesis is interesting, as it suggests that ILV formation may have an impact on these other processes. The effect on DCG biogenesis provides further evidence of a link between Rab11-ILV and DCG regulation, whilst the increase in Rab11-compartments may suggest that Rab11-compartments are unable to be secreted when ILV biogenesis does not occur properly, perhaps due to a failure to pass quality control checks at the point of secretion.

Regardless, the consistent inhibition of Rab11-ILV biogenesis following PI3K/Akt/mTOR inhibition suggests that this pathway does functionally regulate Rab11-exosome formation. This idea is further supported by the fact that Rab11-exosome biogenesis was actively increased following manipulations that stimulate PI3K/Akt/mTOR signalling in three separate genotypes. These findings are particularly interesting as the Akt/mTOR pathway was also found to regulate Rab11-exosome biogenesis in human HCT116 cells (Fan et al., 2020), indicating that PI3K/Akt/mTOR signalling is a conserved regulator of this exosome subtype that could modulate Rab11-exosome signalling in response to oncogenic signalling stimuli. However, it is important to note that PI3K/Akt/mTOR signalling in HCT116 cells had an inhibitory effect on Rab11-exosome biogenesis rather than a stimulatory effect as I found in SCs (Fan et al., 2020). This contradiction appears to be best explained by the fact that HCT116 cells are a population of immortalised cancer cells where PI3K/Akt/mTOR signalling is already heavily dysregulated by an activating mutation in PI3K, to the extent that strong inhibition of PI3K signalling in these cells is sufficient to inhibit cell viability and promote apoptosis (Stefani et al., 2021). Therefore, whilst it is clear that PI3K/Akt/mTOR signalling can regulate Rab11-exosome signalling in both human and *Drosophila* systems, I suggest that findings from the *in vivo* SC-model, as opposed to the human cancer model, are more likely to represent the general function of this pathway in Rab11-exosome biogenesis.

As discussed above, I also found that manipulating the PI3K/Akt/mTOR pathway is sufficient to either increase or decrease the trafficking of ELMs on Rab11-compartments, approximately in line with the increases and decreases induced for Rab11-ILV formation. This finding provides some of the strongest evidence that cell

signalling stimuli can be integrated into Rab11-exosome biogenesis pathways through the activity of exosome-forming ELMs. Whilst this is discussed in more detail above, further exploration of the PI3K/Akt/mTOR pathway's role in Rab11-exosome biogenesis will require additional study of ELMs as well so that the mechanisms of regulation can be understood. In addition to the experiments described in this chapter, I also attempted to utilise GFP-tagged, phosphatidylinositol-binding pleckstrin homology (PH) domains from proteins such as Akt to examine the localisation of PI3K signalling complexes and certain downstream proteins, but these were unsuccessful. Therefore, further examination of PI3K/Akt/mTOR signalling's roles may include examining downstream elements of this pathway such as the kinase S6K and its targets so that specific effector proteins can be identified. Additionally, if suitable models can be developed in plated cells where PI3K/Akt/mTOR signalling is not as dysregulated as in HCT116 cells, then it would also be informative to study whether Rab11a-exosomes secretion changes in response to PI3K/Akt/mTOR signalling and whether changes in Rab11-exosome proteomes and transcriptomes can be detected following altered signalling. Finally, it would be interesting to assess the effects of other oncogenic, stress-related pathways on Rab11-exosome formation. In preliminary experiments not presented here for example, I found that Licorne, an upstream activator of p38 MAPK stress signalling, also promoted Rab11-exosome formation. Once the core mechanisms involved in PI3K/Akt/mTOR's regulation of Rab11-exosome biogenesis are understood, it would be very interesting to examine whether stimuli from other pathways such as p38 signalling can be integrated using the same regulatory pathways.

Chapter 6: SUMOylation controls Rab11-exosome biogenesis and cargo loading in Drosophila SCs

6.1 Introduction and aims

6.1.1 Aims

As part of my investigations into the regulation of Rab11-exosomes, I investigated the possibility that the ubiquitin-like molecule SUMO controls Rab11-exosome biogenesis. In particular, I examined the hypothesis that SUMO is a novel exosome regulator that may function similarly to ubiquitin in the classical ESCRT-dependent pathway. In that pathway, monoubiquitin tags on exosome cargoes recruit ESCRT-0 proteins to the surface of MVE compartments, leading to the formation of ILVs which incorporate the ubiquitinated proteins. Since previous findings in the lab had suggested that inhibition of Rab11-exosome biogenesis did not affect ubiquitinated cargo trafficking, I sought to test whether the ubiquitin-like SUMO played any role in Rab11-exosome biogenesis and cargo selection.

6.1.2 Previous work

The evidence that ubiquitinated proteins are not specifically targeted to Rab11-exosomea comes primarily from investigations by Dr P. Marie, which showed that whilst knocking down core ESCRT complex proteins inhibited ILV formation and

induced an accumulation of ubiquitinated proteins on SC-compartments, knocking down the accessory ESCRT-III proteins inhibited Rab11-ILV formation without any associated build-up in ubiquitinated proteins on endosomal compartments (Marie et al., 2023). Given the novel requirement for accessory ESCRT-III proteins in Rab11-exosome biogenesis, this finding indicated that Rab11-ILV formation did not require ubiquitin, since specifically inhibiting this pathway did not lead to ubiquitin accumulation even when blocking the broader ESCRT-dependent pathway did.

This reasoning led our lab to consider alternative possibilities for the pathways controlling Rab11-exosome biogenesis besides the well-established ESCRT-dependent, ubiquitin-dependent biogenesis pathway. Since core ESCRT0/I/II-complexes are still required for Rab11-exosome formation (Corrigan et al., 2014; Fan et al., 2020; Marie et al., 2023), I examined the wider literature and found limited reports supporting the idea of ESCRT-dependent, ubiquitin-independent mechanisms of cargo sorting and ILV biogenesis. For example, it was shown that fusing proteins to artificial ESCRT-like constructs leads to the sorting of proteins as ILV cargoes independently of ubquitination (Mageswaran et al., 2014). This indicates that particular cargo proteins can be sorted into ILVs by binding to ESCRTs directly, although it does not demonstrate the existence of a ubiquitin-independent pathway for forming ILVs themselves. In another interesting study, stress-induced p38 MAPK signalling resulted in EGFR internalisation and packaging into ILVs through a mechanism that was independent of ubiquitin but dependent on Hrs and the accessory ESCRT ALIX (Tomas et al., 2015). Both Hrs and ALIX have been shown to be required for Rab11-exosome biogenesis in SCs (Corrigan et al., 2014), which potentially suggests that the pathway outlined in the p38 MAPK study may have parallels to the Rab11-exosome

biogenesis pathway in SCs. Beyond these details however, only minimal mechanistic details were understood of the primarily hypothetical ESCRT-dependent, ubiquitin-independent exosome pathway.

Given the central role of ubiquitin in cargo selection and ESCRT recruitment, we hypothesised that another post-translational modification may act as an exosome-targeting signal in the absence of ubiquitin. More specifically, we hypothesised that another ubiquitin-like protein (UBL) family member may be attached to Rab11-exosome cargoes to drive ESCRT recruitment. UBLs are a family of small, evolutionarily related proteins that can be covalently added to target peptides as post-translational modifications (Cappadocia & Lima, 2018; Hochstrasser, 2009; Pirone et al., 2017). This family includes ubiquitin itself as well as a plethora of similar proteins which function in much the same way as ubiquitin, utilising E1, E2 and E3 enzymes to activate, conjugate and ligate UBL monomers to targeted proteins. Indeed, just like ubiquitin itself, many UBLs are joined to target proteins at exposed lysine residues, a fact which can lead to competition between different UBLs for the shared ligation sites. Partly because of this, UBLs have diversified and acquired distinct functions within cells, although the precise role of many UBLs is often not well understood.

The human genome contains at least 9 families of UBLs including ubiquitin, whilst the *Drosophila* genome maintains 5 UBL families, possessing a single homolog for each. Of the four non-ubiquitin UBLs present in *Drosophila*, our attention was drawn to Small Ubiquitin-like Modifier (SUMO), a ubiquitin-like molecule which functions in cell-stress responses and whose dysregulation is an important driver of cancer progression (Enserink, 2015; Gu et al., 2023; Ryu et al., 2020; Seeler & Dejean, 2017). Not only is

SUMO the most abundant and well conserved UBL besides ubiquitin, but it also possesses several intriguing links to aspects of exosome biology. For example, SUMOylation of the RNA binding protein hnRNPA2B1 is known to control its loading into exosome vesicles through an ALIX-dependent pathway, a novel example of a non-ubiquitin UBL modification acting as a targeting signal for exosome cargo loading (Diao et al., 2023; Villarroya-Beltri et al., 2013). Likewise, fusion of SUMO2 to GFP and alpha synuclein proteins in mouse neuroblastoma cells was found to dramatically increase their loading into ESCRT-dependent, exosome-like EVs (Kunadt et al., 2015).

Furthermore, several notable links also exist between SUMO and the accessory ESCRT-III proteins which are specifically required for Rab11-exosome biogenesis. For example, the SUMO E2 conjugating enzyme Ubc9 is known to interact directly with CHMP1A and CHMP5 in humans (Tsang et al., 2006), the *Drosophila* homologues of which (Chmp1 and Chmp5) I have shown are required for Rab11-exosome signalling in the female PMR *in vivo* (Section 5.2.2). Additionally, ESCRT proteins such as Tsg101 possess SUMO-interacting motifs, perhaps offering an alternative mechanism by which target proteins could be recognised by the ESCRT machinery (Kunadt et al., 2015).

Overall then, my primary research were to:

1) Test SUMO's role in Rab11-exosome biogenesis;
2) Attempt to establish its mechanism of action;
3) Identify potential Rab11-exosome cargo proteins targeted by SUMOylation.

6.2 Results

6.2.1 SUMO is required for Rab11-exosome biogenesis

The first step in these investigations was to examine whether SUMO was in fact involved in Rab11-exosome biogenesis. To do this, I expressed three independent RNAi lines targeting SUMO expression in SCs (Fig. 6.1A-C). These knockdown experiments were conducted in cooperation with Dr P. Marie, and in each case, *SUMO* knockdown resulted in a decrease in the number of Rab11-compartments forming Rab11-ILVs, although this decrease was not statistically significant for *SUMO-RNAi#1* (Fig. 6.1D). Crucially though, the proportion of Rab11-compartments which formed Rab11-ILVs was significantly reduced in every knockdown (Fig. 6.1E). In the stronger phenotypes, the proportion of compartments forming ILVs dropped from 49.7 ± 15.3% in controls to as little as 3.1 ± 6.9% following *SUMO-RNAi#2* expression, strongly indicating that SUMO is required for Rab11-exosome biogenesis to occur. However, these conclusions were complicated by the fact that *SUMO* knockdowns severely altered SC organisation (e.g. DIC views Fig. 6.1A-C). This disruption manifested in large increases in Rab11-compartment numbers (Figure. 6.1F) and reduced size for individual compartments. Because of the strength of these effects, it was unclear whether SUMO was specifically required for Rab11-ILV biogenesis or whether the inhibition of ILV formation was due to wider endosome dysfunction following *SUMO* knockdown.

To address this uncertainty, I inhibited the action of two other essential components in the SUMOylation pathway, namely Lesswright (Lwr), the sole Drosophila E2-conjugating enzyme and Ulp1, a SUMO-cleaving protease that is required for proper

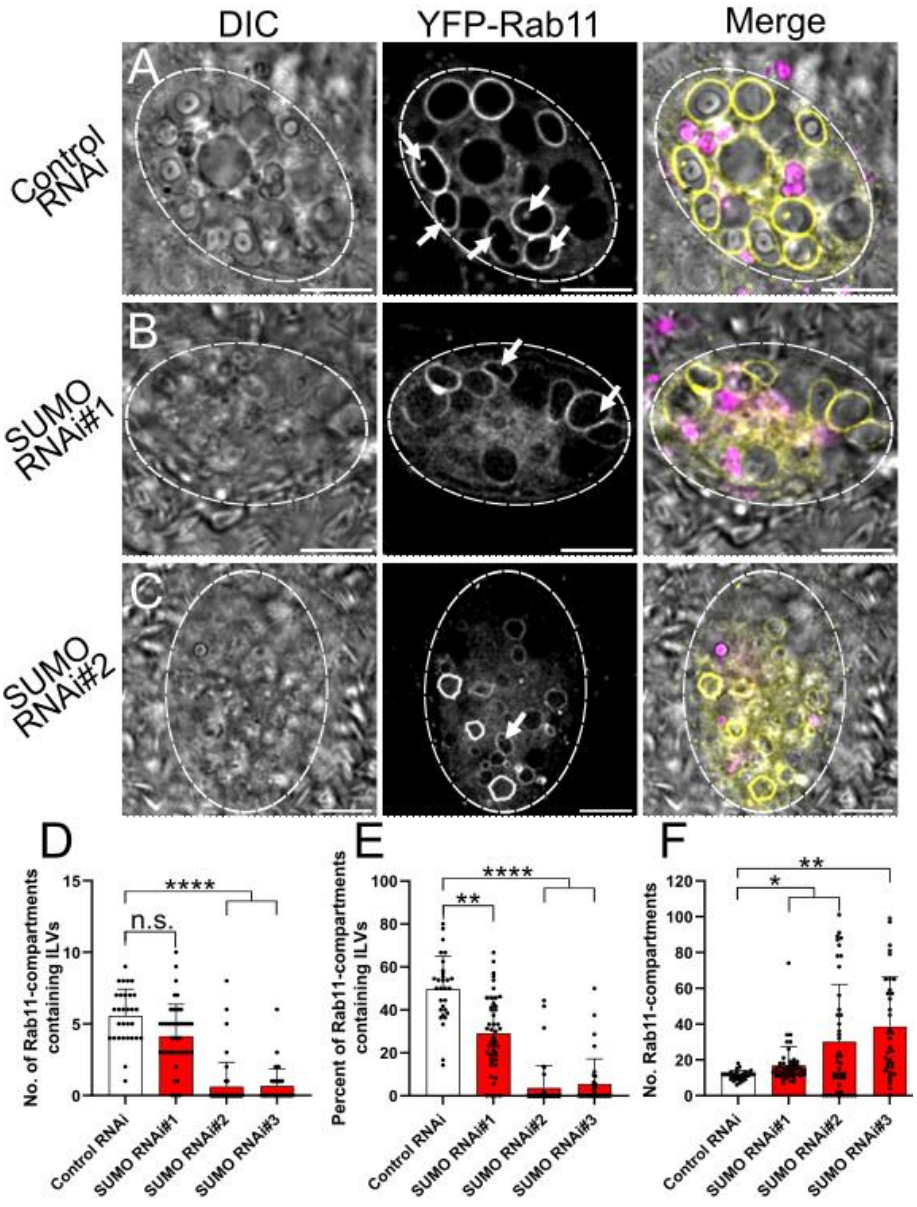

Figure 6.1. *SUMO* knockdown inhibits Rab11-ILV biogenesis and SC compartment organisation. (**A-C**) Wide-field fluorescence images of SCs expressing *YFP-Rab11* together with a control RNAi (**A**) or *SUMO*-targeting RNAis (**B**, **C**). In multicoloured images Rab11 is shown in yellow, LysoTracker Red in magenta and DIC images in grayscale. All Rab11-ILVs visible in the plane of view are highlighted by white arrows (**A-C**). Knockdown of *SUMO* using three different RNAis significantly reduced the number of Rab11-compartments forming Rab11-ILVs (**D**), significantly reduced the proportion of Rab11-compartments forming Rab11-ILVs (**E**), and significantly increased the total number of Rab11-compartments (**F**). SC boundaries marked by dashed circles, Scale bars: 10µm. For graphs, P<0.05:*, P<0.01:**, P<0.001:***, P<0.0001:****, non-significant: n.s.. n=30 to 47 cells for all graphs.

SUMO peptide maturation (Cao & Courey, 2017). To inhibit *lwr* activity, I either knocked down its expression with an RNAi or overexpressed a dominant-negative form of the enzyme under UAS control, whilst to inhibit Ulp1 activity I utilised an RNAi (Figure. 6.2A-C). As seen following direct *SUMO* knockdowns, knockdown of *Ulp1* led to a significantly increased number of Rab11-positive compartments being formed in SCs (Fig. 6.2D). In contrast, knockdown of *lwr* or expression of a dominant negative Lwr protein had no significant impact on the number of Rab11-compartments formed by SCs, indicating that Lwr inhibition was not disrupting general SC trafficking processes (Fig. 6.2D). In spite of this, examination of Rab11-ILVs showed that both *Ulp1* and *lwr* inhibition significantly reduced the total number of ILV-forming compartments (Fig. 6.2E) and resulted in a sharp decline in the proportion of Rab11-compartments that formed Rab11-ILVs (Fig. 6.2F). These results reinforce the role of SUMO in facilitating Rab11-ILV formation. In particular, the inhibition of Lwr activity through two different mechanisms indicates that SUMO does specifically regulate Rab11-ILV biogenesis, since no broader effects were observed in terms of Rab11-compartment numbers or organisation.

6.2.2 Both *Drosophila* E3 ligases take part in Rab11-exosome biogenesis

As part of the same analysis into SUMO's function in Rab11-exosome biogenesis, I investigated the role of the two *Drosophila* E3 ligases involved in SUMOylation, Suppressor of variegation 2-10 (Su(var)2-10) and Tonalli (Tna). Unlike in the better-known ubiquitination pathway, the process of SUMO ligation to target proteins does

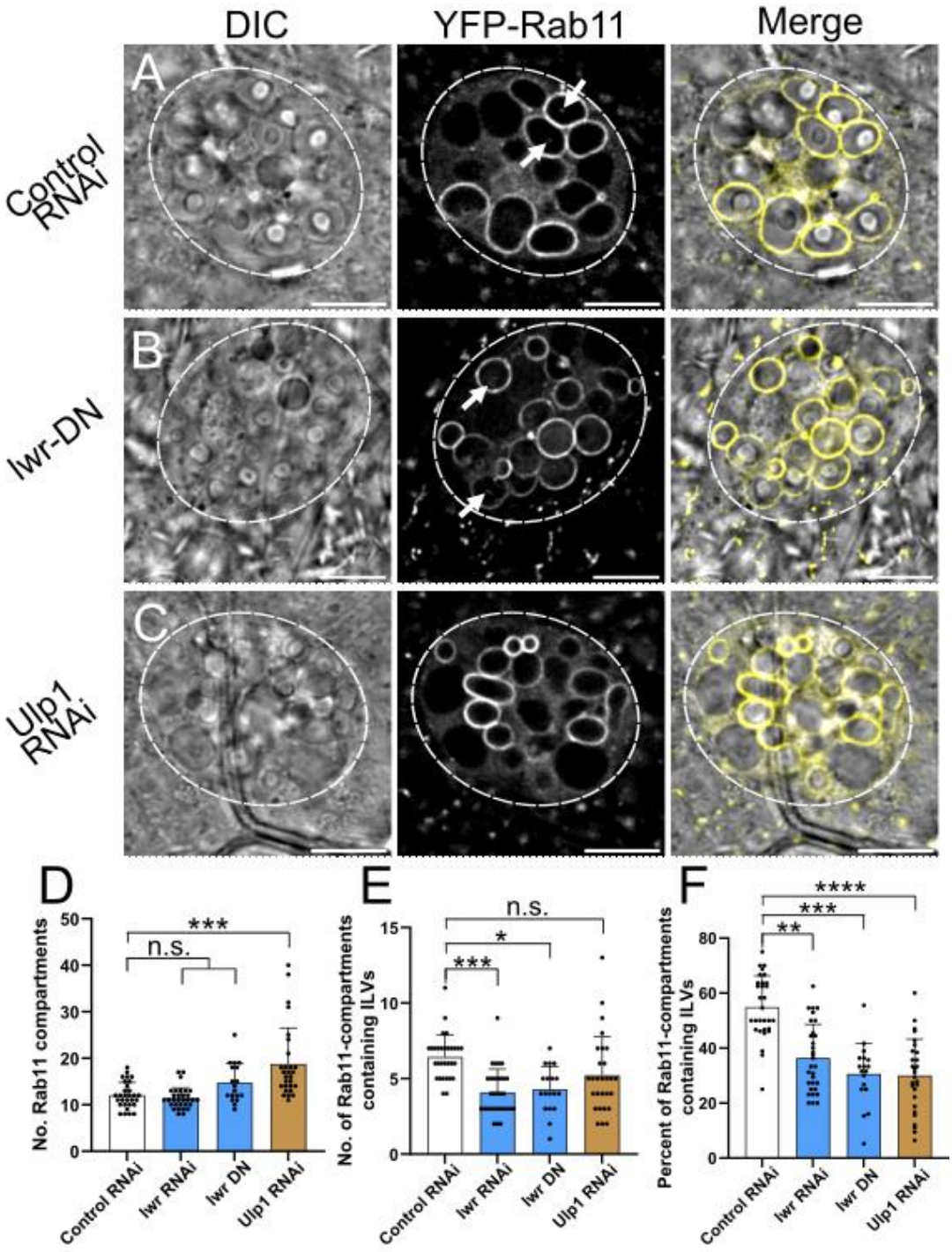

Figure 6.2. Inhibiting essential SUMOylation enzymes specifically blocks Rab11-ILV biogenesis. (**A-C**) Wide-field fluorescence images of SCs expressing *YFP-Rab11* together with a control RNAi (**A**), dominant-negative *lwr* (**B**), or *Ulp1*-targeting RNAi (**C**). In multicoloured images Rab11 is shown in yellow and DIC images in grayscale. All Rab11-ILVs visible in the plane of view are highlighted by white arrows (**A**-**C**).

Knockdown of SUMO's E2 enzyme *Lwr* had no effect on the number of Rab11-compartments in SCs, though knockdown of the processing enzyme *Ulp1* did increase Rab11-compartment numbers (**D**). In contrast, whilst *Ulp1* knockdown had no effect on the number of Rab11-ILV forming compartments, *lwr* knockdown significantly reduced Rab11-ILV forming compartments (**E**). However, knockdown of both *Ulp1* and *lwr* significantly decreased the proportion of Rab11-compartments forming Rab11-ILVs (**F**). SC boundaries marked by dashed circles, Scale bars: 10μm. For graphs, P<0.05:*, P<0.01:**, P<0.001:***, P<0.0001:****, non-significant: n.s.. n=18 to 31 cells for all graphs.

not strictly require E3 ligases (Tozluoğlu et al., 2010). This is because the E2 enzyme lwr is capable of attaching SUMO to targets by itself. Having said that, the two E3 ligases do increase the efficiency of ligation and provide specificity to SUMO targeting, since each of Su(var)2-10 and Tna targets distinct populations of proteins. Because of this dynamic, there were several possible outcomes that could arise from knocking down each of *Su(var)2-10* and *tna*. The two most likely outcomes were that only one E3 ligase would have an effect on Rab11-exosome biogenesis or that both would. If only one E3 ligase functioned in Rab11-exosome formation, this could suggest that only a narrow set of targets require SUMOylation for Rab11-biogenesis to occur. If both E3s were required, this would imply that a broader set of proteins are SUMOylated. To distinguish between these possibilities, I induced two independent RNAi knockdowns for each of *Su(var)2-10* and *tna* in the YFP-Rab11 background (Fig. 6.3A-C).

As observed from the knockdown of some other SUMOylation-related genes, one RNAi targeting each of *Su(var)2-10* and *tna* induced an increase in the number of Rab11-compartments present in SCs (Fig. 6.3D), although these increases were not as large as those observed following direct *SUMO* knockdowns (compare to Fig. 6.1F). However, the second knockdown for *tna* induced no significant changes in Rab11-compartment numbers, whilst the second knockdown for *Su(var)2-10* actually resulted in a modest decrease in Rab11-compartments (Fig. 6.3D). Irrespective however, every E3 ligase knockdown resulted in a significant decline in the number of Rab11-compartments forming Rab11-ILVs (Fig. 6.3E), and in the proportion of compartments forming Rab11-ILVs (Fig. 6.3F). These results provided further evidence of SUMO's role in Rab11-exosome biogenesis and indicated that Rab11-exosome biogenesis

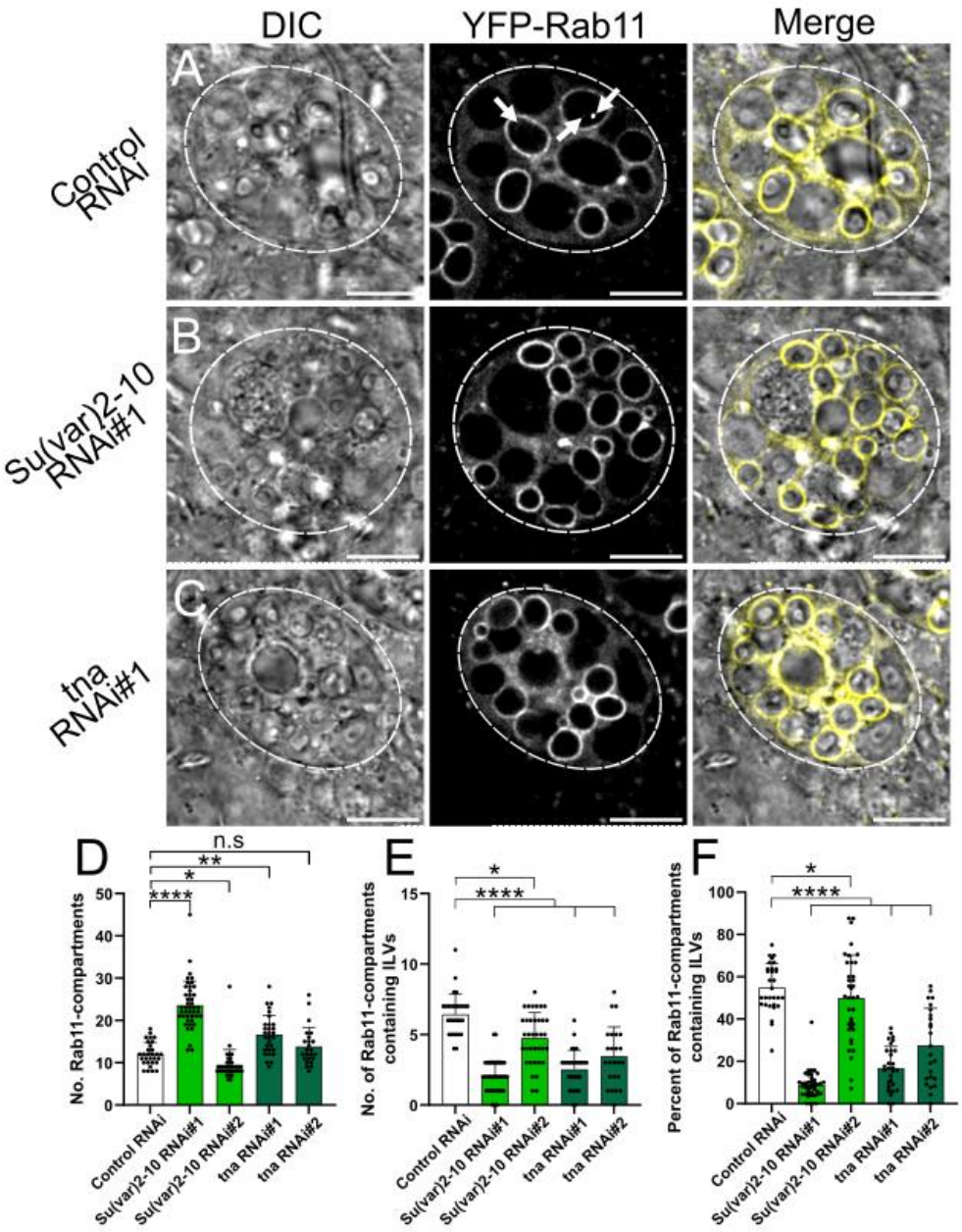

Figure 6.3. Knockdown of both SUMO E3 ligases inhibits Rab11-ILV formation (**A**-**C**). Wide-field fluorescence images of SCs expressing *YFP-Rab11* together with a control RNAi (**A**), *Su(Var)2-10*-targeting RNAi (**B**), or *tna*-targeting RNAi (**C**). In multicoloured images Rab11 is shown in yellow and DIC images in grayscale. All Rab11-ILVs visible in the plane of view are highlighted by white arrows (**A**-**C**). Knockdown of both E3 enzymes, *tna* and *Su(Var)2-10*, resulted in varied effects on Rab11-compartment numbers. Expression of *Su(Var)2-10-RNAi#1* and *tna-RNAi#1* both increased Rab11-compartment numbers whilst their 2nd RNAis decreased or did not affect Rab11-compartment numbers respectively (**D**). However, expression of any

tna or *Su(Var)2-10* RNAi did lead to significant decreases in the number of Rab11-ILV forming compartments (**E**) and the proportion of Rab11-compartments forming ILVs (**F**). SC boundaries marked by dashed circles, Scale bars: 10µm. For graphs, P<0.05:*, P<0.01:**, P<0.001:***, P<0.0001:****, non-significant: n.s.. n=24 to 44 cells for all graphs.

potentially involved a broad population of proteins being SUMOylated since both E3 ligases contribute to Rab11-ILV formation.

6.2.3 SUMOylation controls the trafficking of ELMs in SCs

Through my broader examination of factors controlling Rab11-exosome biogenesis, I identified microdomains labelled by E-cadherin, Rab19 and Hrs that appear to act as novel sites of ILV biogenesis (Section 5.2.3 and 5.2.4). Equally interesting, I identified several factors that regulate both Rab11-ILV formation and ELM assembly (Section 5.2.7, 5.2.8 and 5.2.10), which suggests that different regulators may control Rab11-ILV formation through the assembly of ELMs. I therefore tested the effect that SUMOylation had on ELM trafficking and assembly. To do this, I inhibited SUMOylation by expressing dominant-negative *lwr* with *SUMO-RNAi#1*, and by inducing knockdowns of the two *Drosophila* E3 ligases, *Su(var)2-10* and *tna* in cells expressing YFP-Rab11 and Ecad-RFP (Fig. 6.4A-D).

As observed in the YFP-Rab11 background, *Su(var)2-10-RNAi#1* and *tna-RNAi#1* induced significant increases in the number of Rab11-compartments in SCs (Fig. 6.4E). Interestingly, in cells expressing *SUMO-RNAi#1* and dominant-negative *lwr* together, no significant change was observed in Rab11-compartments (Fig. 6.4E). In all backgrounds however, both the number and proportion of Rab11-compartments found with surface-associated ELMs was significantly reduced (Fig. 6.4F, G), suggesting that SUMOylation promotes ELM assembly as well as Rab11-ILV formation. This provides yet another example of Rab11-exosome regulators also controlling ELM formation on Rab11-compartments. Furthermore, the fact that both

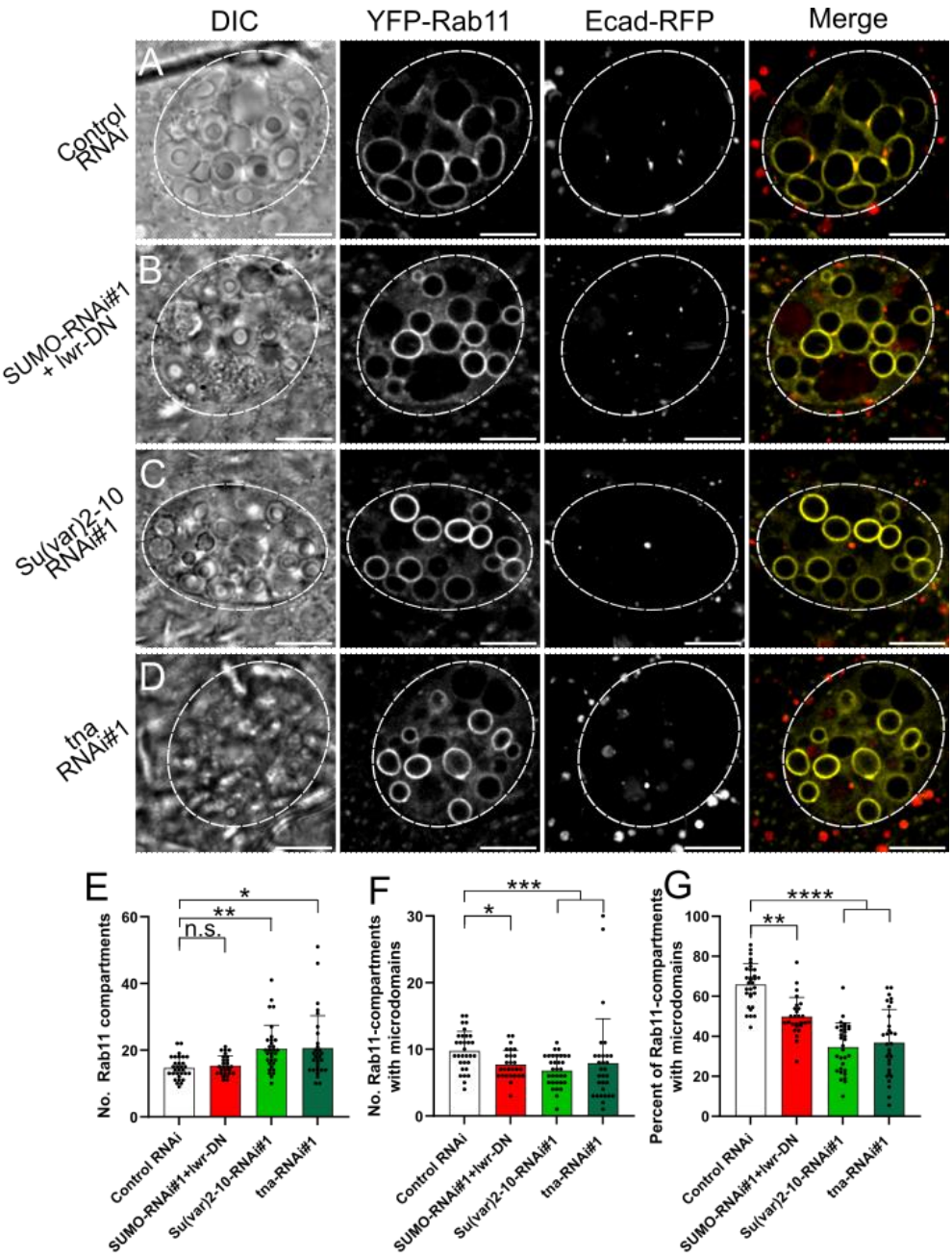

Figure 6.4. Inhibiting SUMOylation reduces ELM formation (**A-C**) Wide-field images of SCs expressing *YFP-Rab11* and *Ecad-RFP* together with a control RNAi (**A**), *SUMO* RNAi and dominant-negative *lwr* (**B**), *Su(Var)2-10* RNAi (**C**), or *tna* RNAi (**D**). In multicoloured images Rab11 is shown in yellow and Ecad in red. Knockdown of *SUMO* and *lwr* caused no change in Rab11-compartment numbers though knockdown of both E3 enzymes did increase Rab11-compartments (**D**). Knocking down any of these targets also resulted in significant decreases in the number of (**E**) and proportion of (**F**) Rab11-compartments with surface-associated ELMs. SC boundaries marked by dashed circles, Scale bars: 10µm. For graphs, P<0.05:*, P<0.01:**, P<0.001:***, P<0.0001:****, non-significant: n.s.. n=27 to 32 cells for all graphs.

SUMO E3 ligases influenced ELM assembly indicates that a variety of microdomain-associated or microdomain-regulatory proteins are likely to be SUMOylated.

6.2.4 Homologues of human Rab11a-exosome cargoes include conserved targets of SUMOylation

One key limitation of the *Drosophila* SC model is that biochemical analysis of secreted vesicles is impractical. SCs make up only about 4% of all secretory cells in the accessory gland and the luminal content of the gland appears viscous and highly lipid-rich, making EV separation challenging (Chapman & Davies, 2004; Kalb et al., 1993; C. Wilson et al., 2017).. As such, it is generally not possible to directly assess the molecular composition of Rab11-exosomes or compare their composition to conserved human equivalents, i.e. Rab11a-exosomes. However, having established a role for SUMOylation in Rab11-exosome biogenesis and ELM formation, I was eager to identify the targets of SUMOylation that were involved in these processes. Since my working hypothesis was that SUMO was attached to Rab11-exosome cargo proteins as a cargo-sorting tag, I began seeking a way to identify likely SUMOylated Rab11-exosome cargoes without use of proteomic approaches in *Drosophila*.

To do this, I relied on the assumption that the process of Rab11-exosome biogenesis was conserved to a large degree between *Drosophila* SCs and human cancer cells, including in terms of at least some protein cargoes. Therefore, I examined a proteomic analysis of vesicles enriched in Rab11a-exosome preparations from human HCT116 cells, published in Fan et al., 2020. This provided a list of 48 proteins that were

significantly enriched in human Rab11a-exosomes. I next used the homologue search tool available on flybase.org to identify the best homologue for each protein in flies (Gramates et al., 2022). For a given human protein, only *Drosophila* genes with a score of 8 out of 14 or above using the homologue search tool were classed as homologues and generally, only the top-scored homologue was included for further analysis, unless two genes had equivalent scores.

I next proceeded to evaluate the potential SUMOylation status of human and *Drosophila* proteins as assessed in Drabikowski et al., 2018, where SUMOylated proteins across seven model organisms including humans and flies were either identified through mass-spectroscopy or else predicted based on conserved SUMOylation sites. Protein homologues that were indicated to be SUMOylated in both humans and flies were then prioritised for further study. In addition, I also included the *Drosophila* proteins Prominin-like (PromL) and Dally-like protein (Dlp) as candidates for further investigation despite not showing evidence of SUMOylation. This decision was primarily due to these proteins' roles as membrane-associated proteins, which I reasoned could make them of interest as markers of Rab11-ILVs and Rab11-compartments, if they were in fact involved in exosome biogenesis. One interesting observation from the SUMOylation analysis was that 71% of enriched proteins (34 out of 48) in Rab11a-exosomes were either confirmed to be or predicted to be SUMOylated, compared to just 15-20% of proteins estimated to be SUMOylated in the general proteome of humans (Drabikowski et al., 2018).

Finally, *Drosophila* genes in my list were ranked based on their expression within SCs as assessed by transcriptomic analyses published in Immarigeon et al., 2021.

At this stage, I also elected to investigate two candidates that were exceptionally highly expressed in SCs and indicated to be SUMOylated in humans and flies. These were Hsp83 and Arc1, the 9th and 10th most expressed genes in SCs respectively. Of these, Hsp83 is homologous to Hsp90α, a protein that was found to be enriched in Rab11a-exosome preparations during subsequent unpublished proteomic analyses and which is known to promote exosome biogenesis (Lauwers et al., 2018). In comparison, Arc1's homologue, Arc, was not detected in Rab11a-exosome preparations but was of interest for several other reasons. Firstly, Arc is a key neuronal regulator whose SUMOylation controls long term potentiation and excitatory neuron homeostasis (Craig & Henley, 2012; Nair et al., 2017). Secondly, Arc is an important risk factor in AD which has been shown to control activity-dependent β-amyloid formation through its interactions with presenilin1 on APP-positive, Arc-positive REs (Bi et al., 2018; Dorostkar & Herms, 2012; J. Wu et al., 2011). Since Rab11-compartments in SCs are thought to be APP-positive REs (P. J. Singh et al., 2024), this raised intriguing parallels with processes occurring in SCs. And finally, Arc1's structure allows it to participate in a novel EV biogenesis pathway that may be relevant for understanding Rab11-exosome formation. Explaining this, Arc proteins are retrovirus-derived GAG-like proteins, structurally similar to retroviral capsid proteins (Campillos et al., 2006; Cottee et al., 2024). As a result, Arc1 expressed in *Drosophila* neuromuscular junctions is able to drive exosome-like vesicle assembly in synaptic MVEs through the formation of a capsid like shell that recruits *Arc1* and other mRNA molecules (Ashley et al., 2018). Given the exceptionally high expression of Arc1 in SCs, this novel pathway raised the possibility that Arc1 acts in a similar manner to promote Rab11-exosome formation in SCs.

Overall, my analysis resulted in a selection of 17 candidate genes which were prioritised for further study in SCs (Table 6.1), as well as a list of 35 enriched human proteins which were not immediately investigated (Table 6.2). With the exception of *Drosophila* genes specifically mentioned above, the prioritised candidates were:

1) homologous to proteins enriched in Rab11a-exosomes;
2) targets/predicted targets of SUMOylation in *Drosophila*;
3) homologous to targets/predicted targets of SUMOylation in humans;
4) expressed in *Drosophila* SCs.

Human gene	SUMO status	Fly homologue	SUMO status	Expression in SCs (Rank percentile)
KPNB1	Identified	Fs(2)Ket	Identified	92
RAP1B	Identified	Rap1	Identified	50
SRSF3	Identified	Rbp1	Identified	77
ALDOA	Identified	Ald1	Identified	97
HNRNPA2B1	Identified	Hrb98DE	Identified	89
		Hrb87F	Identified	89
NPM1	Identified	Nlp	Identified	96
SETSIP	Identified	Set	Identified	82
PKM	Identified	PyK	Identified	98
RAC1	Identified	Rac1	Identified	87
		Rac2	Predicted	85
SCARB1	Predicted	emp	Predicted	61
HSPA1B	Predicted	Hsc70-4	Predicted	99
PROM1	N/A	PromL	N/A	65
GPC1	N/A	dlp	N/A	41
HSP90AA1	Identified	Hsp83	Predicted	99
Arc	Identified	Arc1	Identified	99

Table 6.1. Table of candidate Rab11-exosome cargoes investigated in my genetic screen and their human homologues. SUMOylation data are extracted from Drabikowski et al., 2018. SC expression data are from Immarigeon et al., 2021. Note 99% SC expression rank means that the gene expression level is in the top 1% of all genes expressed in SCs.

Human gene	SUMO status	Fly homologue	SUMO status	Reason for not examining
CHMP5	Predicted	Chmp5	Identified	Already examined
ACTN4	Identified	Actn	Identified	Stocks not yet acquired, available for future research
ILF2	Identified	CG5641	Identified	
ZC3H15	Identified	CG8635	Predicted	
TSPAN4	Predicted	Tsp5D	Predicted	
TSPAN9	Predicted	Tsp5D	Predicted	
TSPAN14	Predicted	Tsp26A	Predicted	
EEF1A2	Identified	eEF1a1	Predicted	Knockdown likely to disrupt fundamental cell processes
EEF2	Identified	eEF2	Predicted	
EEF1B2	Predicted	eEF1B	Identified	
RPL29	Identified	RpL29	N/A	No evidence of SUMOylation in *Drosophila*
HNRNPC	Identified	CG42458	N/A	
SRSF1	Identified	SF2	N/A	
SARS1	Identified	SerRS	N/A	
PAICS	Identified	Paics	N/A	
CSE1L	Identified	Cse1	N/A	
SCN7A	Predicted	para	N/A	
TINAGL1	Predicted	Swim	N/A	
PTPRK	N/A	Ptp36E	N/A	
IST1	N/A	Ist1	N/A	
DIP2B	N/A	DIP2	N/A	
CHMP1B	N/A	Chmp1	N/A	
CHMP1A	N/A	Chmp1	N/A	
MAGEB2	N/A	MAGE	N/A	
PCSK9	Identified	No homologue		No close homologues
HMGA1	Identified	No homologue		
FN1	Identified	No homologue		
HLA-C	Predicted	No homologue		
CPNE8	Predicted	No homologue		
SDCBP	N/A	No homologue		
PTGFRN	N/A	No homologue		
MFGE8	N/A	No homologue		
ST14	N/A	No homologue		
TOLLIP	N/A	No homologue		
MDK	N/A	No homologue		

Table 6.2. Table of proteins identified as enriched in Rab11a-exosomes, which were not investigated in genetic screen.

6.2.5 Homologues of SUMOylated human Rab11a-exosome cargoes contribute to Rab11-exosome biogenesis in SCs

I screened 17 selected candidate genes using publicly available RNAi lines to assess their function in Rab11-exosome biogenesis in SCs. Where possible, two independent RNAi knockdowns were employed for each gene so that overall 30 RNAi knockdowns were analysed in the *YFP-Rab11* genetic background (Fig. 6.5A-F)

Overall, only 6 knockdown lines had a significant impact on the number of SC Rab11-compartments (Fig. 6.5G). Of these, three lines (*Ald1-RNAi#2*, *Arc1-RNAi#2* and *Rbp-RNAi#2*) produced mild changes that only achieved a significance of $P<0.05$. In a group of this size, the false discovery rate would imply that between one and two "significant" changes is likely to be due to chance variations. However, three other knockdowns produced more sizeable changes, with each inducing significant increases in Rab11-compartment numbers. These were *Hsp83-RNAi#1*, *Hsc70-4-RNAi#2* ($P<0.01$ in both cases) and *Hrb98DE-RNAi* ($P<0.0001$). Notably, for five of these six genes, the other RNAi knockdown employed did not cause significant changes in Rab11-compartment numbers, with the only exception to this being *Hrb98DE* where only one knockdown was utilised. Overall then, whilst knocking down some candidate genes could affect wider Rab11-compartment biogenesis processes, in general candidate knockdown did not result in major disruption of SC secretory compartments.

By contrast, candidate genes displayed a range of effects on Rab11-exosome biogenesis. Knockdown of 6 candidates (*Ald1*, *dlp*, *Emp*, *Hrb87F*, *Rbp1* and *Set*) produced no effects on Rab11-exosome biogenesis (Fig. 6.5H) or Rab11-compartment organisation (e.g. Fig. 6.5B,C). More interestingly, knockdown of 7 genes (*Arc1*,

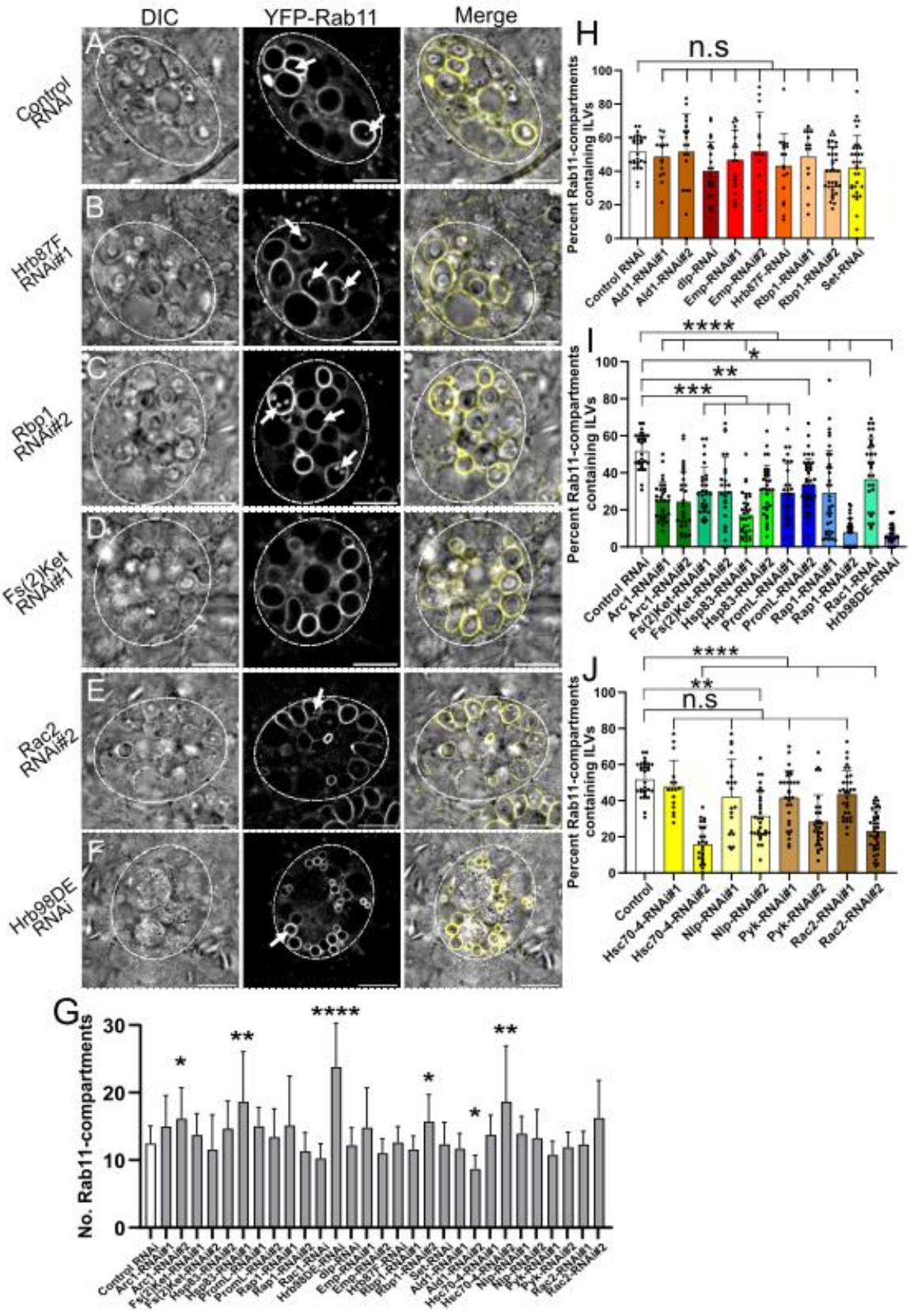
DIC
YFP-Rab11
Merge
A
Control RNAi
B
Hrb87F RNAi#1
C
Rbp1 RNAi#2
D
Fs(2)Ket RNAi#1
E
Rac2 RNAi#2
F
Hrb98DE RNAi
H
n.s
Percent Rab11-compartments containing ILVs
Control RNAi
Ald1-RNAi#1
Ald1-RNAi#2
dip-RNAi
Emp-RNAi#1
Emp-RNAi#2
Hrb87F-RNAi
Rbp1-RNAi#1
Rbp1-RNAi#2
Set-RNAi
I
****
*
**
***
Percent Rab11-compartments containing ILVs
Control RNAi
Arc1-RNAi#1
Arc1-RNAi#2
Fs(2)Ket-RNAi#1
Fs(2)Ket-RNAi#2
Hsp83-RNAi#1
Hsp83-RNAi#2
PromL-RNAi#1
PromL-RNAi#2
Rap1-RNAi#1
Rap1-RNAi#2
Rac1-RNAi
Hrb98DE-RNAi
J
****
**
n.s
Percent Rab11-compartments containing ILVs
Control
Hsc70-4-RNAi#1
Hsc70-4-RNAi#2
Nip-RNAi#1
Nip-RNAi#2
Pyk-RNAi#1
Pyk-RNAi#2
Rac2-RNAi#1
Rac2-RNAi#2
G
No. Rab11-compartments

Figure 6.5. Homologues of human Rab11a-exosome proteins function in *Drosophila* Rab11-exosome biogenesis. (**A-F**) Wide-field fluorescence images of SCs expressing *YFP-Rab11* together with a control RNAi (**A**), *Hrb87F*-targeting RNAi (**B**), *Rbp1*-targeting RNAi (**C**) *Fs(2)Ket*-targeting RNAi (**D**), *Rac2*-targeting RNAi (**E**) or *Hrb98DE*-targeting RNAi (**F**). In multicoloured images Rab11 is shown in yellow and DIC images in grayscale. All Rab11-ILVs visible in the plane of view are highlighted by white arrows (**A**-**F**). Knockdown of the 17 candidate genes produced varied results. Across 29 knockdown lines, just 6 significantly altered Rab11-compartment numbers, *Arc1-RNAi#2*, *Hsp83-RNAi#1*, *Hrb98DE-RNAi*, *Rbp1-RNAi#2*, *Ald1-RNAi#2* and *Hsc70-4-RNAi#2* (**G**). In addition, 6 genes were found to have no effect on Rab11-ILV formation when knocked down, *Ald1*, *dlp*, *Emp*, *Hrb87F*, *Rbp1* and *Set* (**H**, with example images in **B** and **C**). However, knockdown of 7 genes was determined to affect ILV formation, these being *Fs(2)Ket*, *Hsp83*, *PromL*, *Rap1*, *Rac1* and *Hrb98DE*. Each knockdown of these genes significantly reduced the proportion of Rab11-compartments able to form ILVs (**I**, with example images in **D** and **F**). Finally, a set of 4 genes was found to have inconsistent effects on Rab11-ILV biogenesis when knocked down, with only one of two knockdown lines of *Hsc70-4*, *Nlp*, *Pyk* and *Rac2* significantly altering the proportion of Rab11-ILV forming compartments (**J**, with an example image in **E**). SC boundaries marked by dashed circles, Scale bars: 10μm. For graphs, P<0.05:*, P<0.01:**, P<0.001:***, P<0.0001:****, non-significant: n.s.. n=15 to 42 cells for all graphs.

Fs(2)Ket, *Hsp83*, *PromL*, *Rap1*, *Rac1* and *Hrb98DE*) significantly reduced Rab11-ILV biogenesis (Fig. 6.5I), whilst another 4 genes (*Hsc70-4*, *Nlp*, *Pyk* and *Rac2*) produced mixed effects where only one of the two knockdown lines significantly reduced Rab11-exosome biogenesis (Fig. 6.5J). Of the knockdowns that did significantly reduce Rab11-ILV biogenesis, around half had no wider effects on Rab11-compartments, with SCs still producing typical secretory compartments and DCGs (e.g. Fig. 6.5D). This was true for *Fs(2)Ket*, *PromL*, *Rac1, Nlp, Pyk* and *Hsc70-4* knockdowns, with the exception of *Hsc70-4-RNAi#2* which increased Rab11-compartment numbers as noted before. However, knocking down any of *Arc1*, *Hsp83*, *Rap1*, *Hrb98DE* and *Rac2-RNAi#2* both significantly reduced Rab11-ILV formation and disrupted the formation of DCGs (examples in Fig. 6.7 and Fig. 6.8).

Overall, approximately 40% of tested genes reduced Rab11-exosome formation. Since these proteins are hypothesised to represent Rab11-exosome cargoes, this suggests that Rab11-ILV biogenesis occurs at diminished rates when certain cargoes are not present, possibly because these proteins act as both cargoes and regulators/structural components. Although I am unable to review every candidate in detail, it is interesting to note that *Hrb98DE* knockdown induced the strongest suppression of Rab11-ILV formation (Fig. 6.5F, I). This is noteworthy because Hrb98DE is the homologue of hnRNPA2B1, an RNA-binding protein that is one of very few proteins shown to be sorted to exosomes in a SUMO-dependent manner (Villarroya-Beltri et al., 2013).

Another important result was observed with *dlp* knockdown, which produced no significant changes in Rab11-ILV, Rab11-compartment or DCG formation. The reason this is interesting is that expressing a UAS-driven, GFP-tagged form of Dlp results in

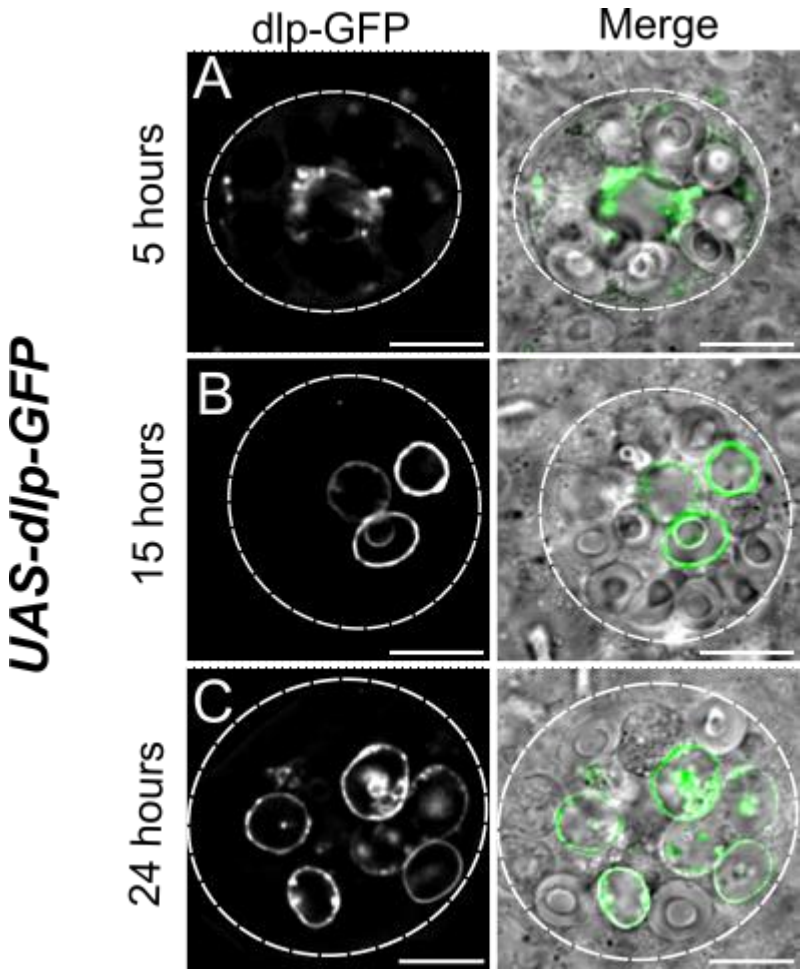

Figure 6.6. The glypican-like protein Dlp is trafficked into SC ILVs when overexpressed in SCs. (**A-C**) Wide-field fluorescence images of SCs expressing *dlp-GFP* for variable expression times up to 24 hours. In multicoloured images dlp is shown in green and DIC images in grayscale. (**A**) After 5 hours, Dlp-GFP marked small, centrally located compartments similar in distribution to Rab1-compartments. (**B**) After 15 hours, Dlp-GFP marked secretory compartment membranes and ILVs associated with the boundaries of DCG. (**C**) After 24 hours, *dlp-GFP* marked a greater number of compartments and ILVs but severely disrupts SC architecture and DCG structure. SC boundaries marked by dashed circles, Scale bars: 10μm

GFP sorting into ILV-like structures that associate with DCG boundaries (Fig. 6.6A-C). Although expression of this construct eventually disrupts DCG structure, its localisation indicates that Dlp is sorted into ILVs and suggests that not all ILV cargo knockdowns impair exosome biogenesis.

6.2.6 *Hsp83* and *Rap1* knockdown blocks Rab11-exosome biogenesis and DCG condensation

Of 30 RNAi lines tested during this screen, RNAis targeting *Hsp83* and *Rap1* produced the second and third strongest inhibition of Rab11-ILV formation respectively (Fig. 6.5I). Equally fascinating, however, knocking down *Hsp83* or *Rap1* also disrupted DCG biogenesis (Fig. 6.7A-E). For example, *Hsp83* knockdown resulted in numerous Rab11-compartments that completely lacked DCGs, or resulted in DCGs that were divided between multiple mini-cores within a compartment (Fig. 6.7B-C). The complete absence of a DCG in some compartments was a novel phenotype; since I had previously shown that Rab11 regulates the onset of DCG biogenesis in wild type genetic backgrounds (Section 4.2.7), I conducted a detailed analysis of the *Hsp83-RNAi#1* genotype and found that Hsp83 is specifically required for DCG protein condensation (Section 4.2.8).

Interestingly, knockdown of *Rap1* using *Rap1-RNAi#2* also induced the formation of numerous Rab11-compartments that lack DCGs, whilst expression of *Rap1-RNAi#1* promoted the formation of Rab11-compartments with severely abnormal, mini-core DCGs (Fig. 6.7D-E). This suggests that Rap1 inhibition produces similar effects to

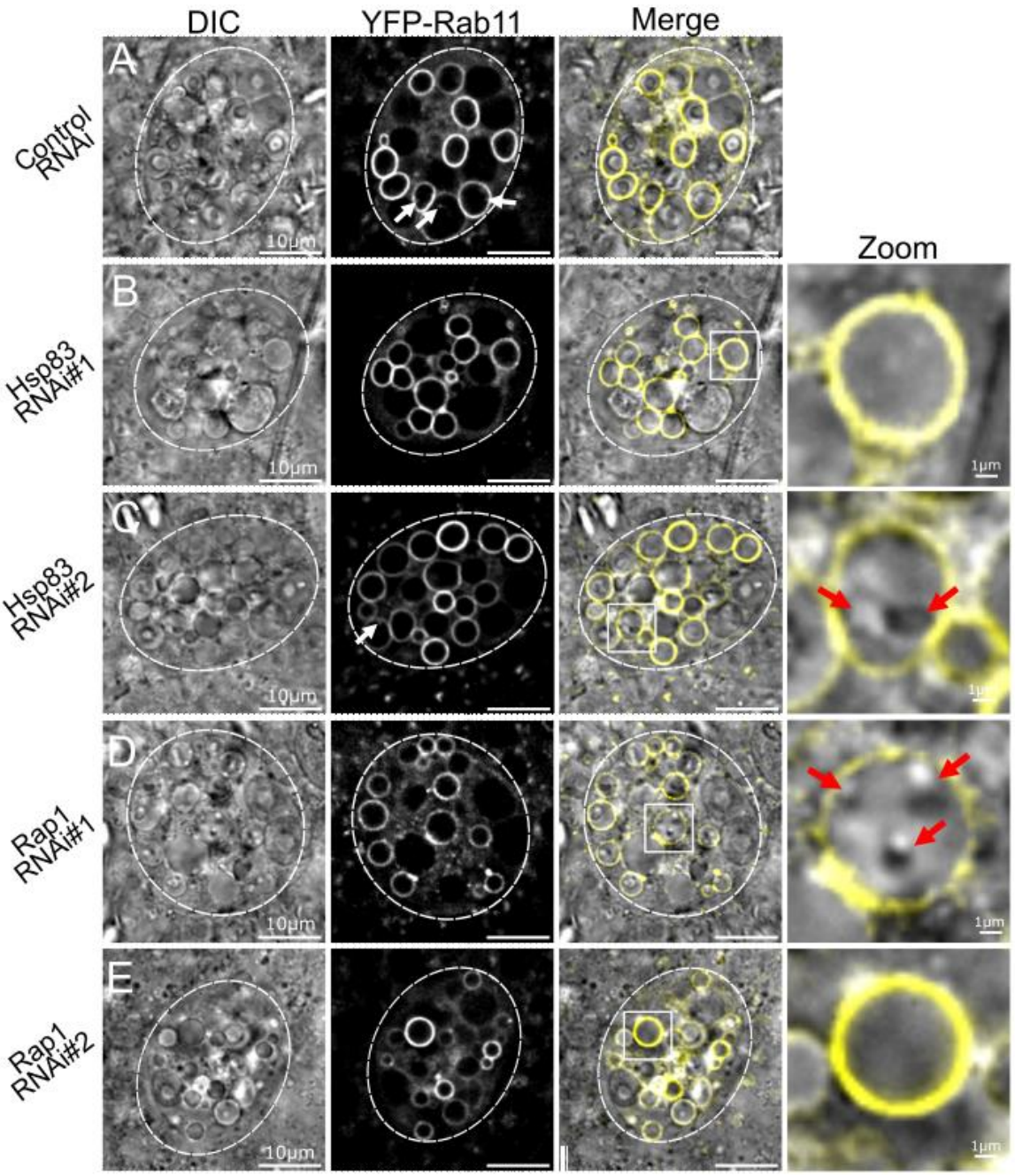

Figure 6.7. *Hsp83* and *Rap1* knockdowns inhibit normal DCG biogenesis in Rab11-compartments. (**A-F**) Wide-field fluorescence images of SCs expressing *YFP-Rab11* with a control RNAi (**A**), *Hsp83* RNAis (**B-C**) or *Rap1* RNAis (**D-E**). In multicoloured images Rab11 is shown in yellow and DIC images in grayscale. All Rab11-ILVs visible in the plane of view are highlighted by white arrows (**A**-**E**). Following knockdown of either *Hsp83* or *Rap1*, the formation of DCGs is acutely disrupted. Both knockdowns can result in Rab11-positive compartments that either totally lack DCGs (examples in **B** and **E**) or which form multiple mini-cores in place of a single DCG (examples in **C** and **D**, mini-cores highlighted by red arrows). SC boundaries marked by dashed circles.

Hsp83 knockdown, with strong knockdown of either factor preventing DCG condensation. This is an interesting idea given the very different nature of these proteins, with Hsp83 being an Hsp90-family chaperone protein that can be trafficked to the lumen of endosomal compartments and Rap1 being a cancer-associated GTPase with diverse functions in intracellular trafficking and signalling pathways (Knox & Brown, 2002; Lauwers et al., 2018; Y.-L. Zhang et al., 2017; Zuehlke et al., 2015). Ultimately, much more work is required to understand the role of Hsp83 and Rap1 in Rab11-exosome and DCG biogenesis, as well as the relationship between ILVs and DCGs observed in SCs.

6.2.7 Retrovirus-related Arc1 controls Rab11-exosome biogenesis

Following two knockdowns of the retrovirus-related, GAG-like gene *Arc1*, Rab11-ILV biogenesis was effectively halved compared to control SCs (Fig.6.5I). In addition, many DCG-compartments were found to house multiple mini-cores instead of typical secretory granules (example highlighted by red arrows in Fig. 6.8B). Given these effects, I became interested in the role of Arc1 in driving exosome-like vesicle biogenesis in presynaptic MVEs (Ashley et al., 2018). In this pathway, GAG-like Arc1 is proposed to form a capsid-like structure that recruits its own mRNA and promotes EV-biogenesis in MVEs. Given the striking role of Arc1 in Rab11-exosome and DCG formation, I hypothesised that Arc1 may drive Rab11-exosome biogenesis through a similar mechanism.

Therefore, I aimed to test two aspects of Arc1 biology within SC ILVs using fluorescently tagged Arc1 constructs (Ashley et al., 2018; Montana & Littleton, 2006). Firstly, I examined whether Arc1 could be observed concentrating within SC ILVs and secondly,

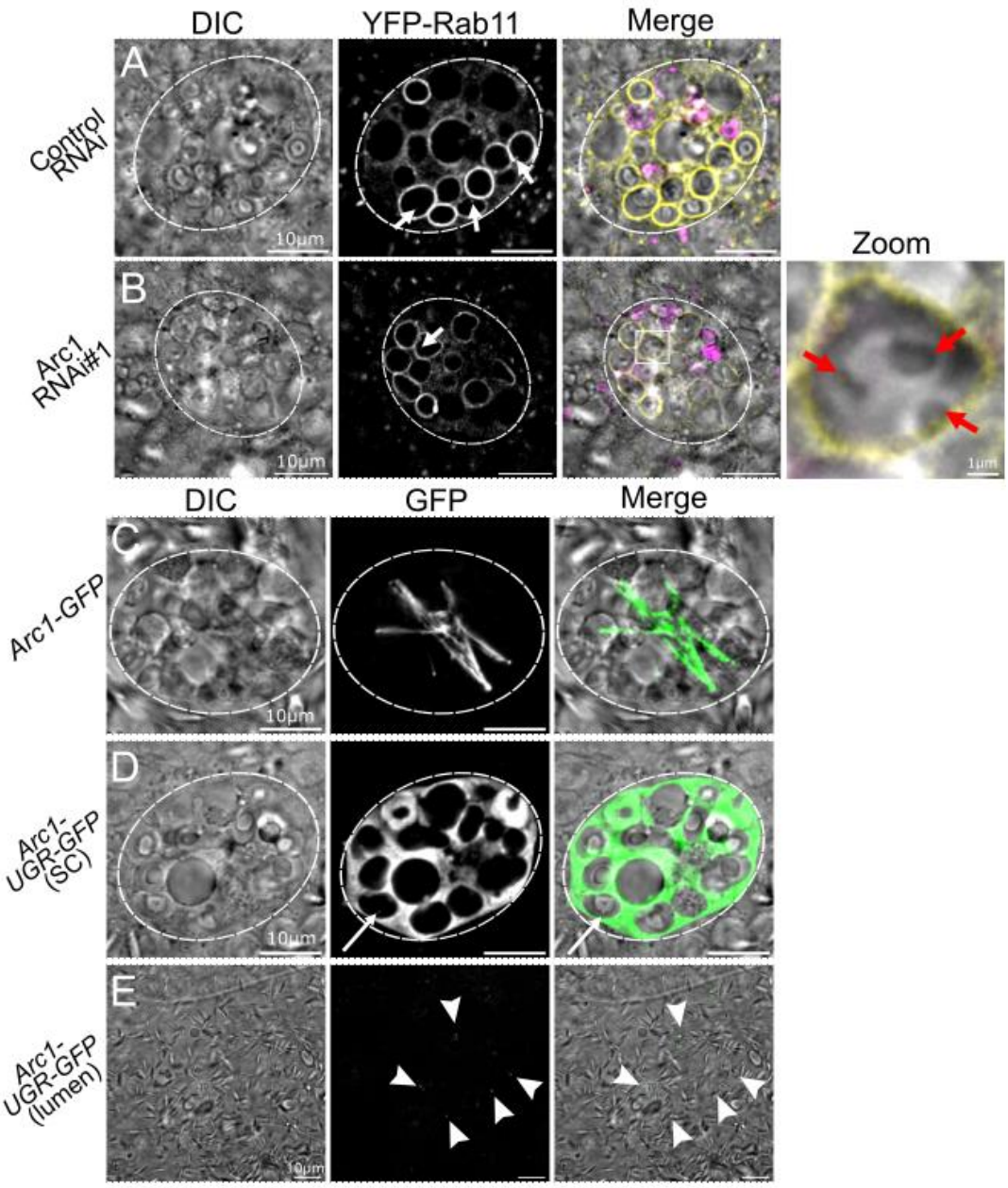

Figure 6.8. The GAG-like protein Arc1 controls Rab11-exosome biogenesis and a partial Arc1 protein can be sorted into SC exosomes. (**A-B**) Wide-field fluorescence images of SCs expressing *YFP-Rab11* together with a control RNAi (**A**), or *Arc1*-targeting RNAi (**B**). In multicoloured images Rab11 is shown in yellow, LysoTracker Red in magenta and DIC images in grayscale. All Rab11-ILVs visible in the plane of view are highlighted by white arrows (**A**-**B**). As well as reducing Rab11-ILV formation, knockdown of *Arc1* disrupted DCG biogenesis, resulting in the formation of numerous

mini-core aggregates instead of a single DCG (**B**, red arrows indicate mini-cores). (**C-E**) Wide-field fluorescence images of SCs expressing full-length *Arc1-GFP* (**C**) or *Arc1-UGR-GFP* (**D**), and of Z-stack projections of Arc1-UGR-GFP fluorescence in the extracellular space of the accessory gland lumen (**E**). In multicoloured images GFP is shown in green and DIC images in grayscale. Full length Arc1-GFP appeared to primarily label filamentous structures that are likely to represent microtubules (**C**). Arc1-UGR-GFP meanwhile accumulated non-specifically within the cytoplasm of SCs, though it could also be seen within ILVs of SC compartments (**D**, white arrow indicates GFP-positive ILV). When the extracellular space of the accessory gland lumen is also examined, GFP-positive vesicles could also be seen (**E**), indicating that SC ILVs had been secreted as exosomes containing this construct, though the specificity of packaging remains unclear. SC boundaries marked by dashed circles.

I tested whether Arc1 could be transferred between cells in the accessory gland. To do this, I used two constructs, a full-length Arc1-GFP fusion protein (Montana & Littleton, 2006), and a GFP-tagged form of the UGR-element, which is a partial genetic duplication of the Arc1 gene which includes a portion of the Arc1-3'UTR and ORF (Ashley et al., 2018). Significantly, the Arc1-UGR-GFP construct was shown to be capable of being transferred between cells within Arc1-EVs. Both *Arc1-GFP* and *Arc1-UGR-GFP* were UAS-controlled constructs expressed specifically in SCs (Fig. 6.8C-E).

Interestingly, expression of the full length Arc1-GFP resulted in the labelling of filaments that are most likely microtubule filaments with which Arc1 associates (Fig. 6.8C) (Fujimoto et al., 2004). This labelling was exceptionally strong, and no signal was detected from other regions of the cell including ILVs. In addition, no GFP was observed outside of SCs, indicating that Arc1-GFP had not been transferred to other cell types. Similarly, GFP was observed in cells besides SCs following expression of Arc1-UGR-GFP. However, expression of Arc1-UGR-GFP did lead to GFP labelling throughout the cytoplasm of SCs (Fig. 6.8D). Importantly, Arc1-UGR-GFP was present in puncta within the lumen of secretory compartments, often associated with the boundary of DCGs (Fig. 6.8D, arrow). Furthermore, GFP-labelled vesicles were present in the lumen of accessory glands following Arc1-UGR-GFP expression (Fig. 6.8E). These results indicate that, although Arc1 transfer was not detected in other cells of the accessory gland, GFP-tagged Arc1-UGR is able to be incorporated into SC-ILVs which are then secreted extracellularly as exosomes. This provides support for the idea that Arc1 is incorporated into Rab11-exosomes in SCs, although the abundance of cytosolic GFP-signal does raise the possibility that this packaging into exosomes is not specific.

Ultimately, more time and study is required to understand the role of Arc1 in Rab11-exosome formation, but it remains an extremely interesting putative regulator.

6.3 Discussion

6.3.1 Core findings

Building on evidence from previous research into Rab11-exosomes, I investigated the role of SUMOylation in Rab11-ILV biogenesis. I found that the core SUMOylation machinery regulates Rab11-exosome biogenesis, with every tested knockdown/inhibition of the SUMOylation machinery leading to significant reductions in ILV formation. In addition, inhibiting SUMOylation also disrupted the formation of E-cadherin-positive microdomains on Rab11-compartments. Finally, by examining the proteome of human Rab11a-exosome preparations, I identified a number of novel *Drosophila* Rab11-exosome regulators. In all but one example, these regulators were homologous to human proteins identified in Rab11a-exosome samples. Additionally, in the vast majority of cases these proteins are SUMOylated in both humans and *Drosophila*. Overall, these finding indicate that SUMOylation is required for Rab11-exosome biogenesis and are consistent with a model where SUMOylated cargo proteins control Rab11-exosome formation. Furthermore, they provide strong additional evidence for a link between Rab11-ILV and DCG biogenesis, which may have central relevance to our understanding of protein aggregation, amyloidogenesis and exosome signalling.

6.3.2 SUMO's effects on Rab11-exosome and ELM biogenesis

To understand the role of SUMO in Rab11-ILV formation, I inhibited the activity of several essential proteins in the SUMOylation pathway, these being SUMO itself, the maturation factor Ulp1 and the E2 enzyme Lwr (Cao & Courey, 2017). Knockdown/inhibition of any of these factors resulted in significant declines in Rab11-ILV formation, with ILV biogenesis being totally abolished in most SCs expressing either *SUMO-RNAi#1* or *SUMO-RNAi#2*. Although these stronger RNAi knockdowns also disrupted Rab11-compartment formation, inhibiting the action of Lwr had no effect on wider SC organisation, yet did still reduce Rab11-ILV biogenesis, indicating that SUMOylation specifically regulates this process. Of course, even this genetic manipulation could be having other major effects on cell biological processes in SCs, which indirectly affect Rab11-ILV biogenesis. But the fact that I have also shown that several putative SUMOylation targets, which are proposed Rab11a-exosome cargos in humans, also control Rab11-ILV biogenesis, argues against this idea.

Interestingly, knocking down both of the E3 ligases, Su(var)2-10 and Tna, also significantly reduced Rab11-ILV biogenesis. This is notable because both E3 enzymes are non-essential in the SUMOylation pathway and are instead used to increase ligation efficiency for specific sets of proteins (Tozluoğlu et al., 2010). Since Rab11-exosome biogenesis is affected by both E3 enzymes, this suggests that a variety of proteins are SUMOylated, and not just one or a few proteins that are targeted by one of the E3 ligases.

In addition to their direct impact on Rab11-ILV formation, I found that inhibition of both the core SUMOylation pathway through joint SUMO knockdown and Lwr inhibition

reduced ELM formation. Likewise, knockdown of either E3 ligase also reduced microdomain formation. These results provide yet another example of Rab11-exosome regulators also controlling ELM formation as seen with Phb2, Vps34 and PI3K/Akt/mTOR signalling (Sections 5.2.7, 5.2.8, 5.2.10) and indicates that SUMO may control Rab11-exosome formation through the assembly of ILV-regulatory microdomains. Overall, these results strongly support a role for SUMOylation in regulating Rab11-ILV biogenesis.

To better understand the association between SUMO and ELMs, I attempted to conduct immunofluorescent labelling of SUMOylated proteins so that I could directly assess the localisation of SUMOylated proteins and determine whether any are present at ELMs. Initially, I attempted to directly label SUMO with an anti-SUMO antibody, however this failed to label any structures, even ones known to be enriched in SUMO such as nuclei. I then expressed an HA-tagged form of SUMO under heat shock-promoter control and used anti-HA antibodies to try to detect HA-SUMO distribution. Although this approach did lead to the labelling of SUMO-rich structures such as nuclei, the anti-HA antibody also labelled structures even in control cells where HA-SUMO was not expressed. Ultimately, despite repeated attempts to optimise this protocol, I was unable to acquire reliable data from these experiments. Although these experiments could be informative in the future, if different markers, antibodies, fixatives, etc are used, it is also important to note that SUMOylated proteins are likely to be expressed throughout the cell and specific loci of SUMOylated protein accumulation may therefore be difficult to detect.

6.3.3 Conserved Rab11-exosome cargoes

6.3.3.1 Overview

To identify potential SUMOylated Rab11-exosome cargo proteins, I searched for candidates that were:

1) Homologous to cargoes enriched in Rab11a-exosomes (Fan et al., 2020);
2) SUMOylated in humans and *Drosophila* (Drabikowski et al., 2018);
3) Expressed at relatively high levels in SCs (Immarigeon, Frei, Delbare, Gligorov, Machado Almeida, Grey, Fabbro, Nagoshi, Billeter, Wolfner, et al., 2021).

In 14 of the 17 candidates investigated, all three qualities were present and two were present for the remaining four candidates investigates, those being Dlp, PromL and Arc1. By expressing RNAis targeting each candidate, I identified seven genes whose knockdown consistently and significantly suppressed Rab11-ILV formation, those being *Arc1*, *Fs(2)Ket*, *Hsp83*, *PromL*, *Rap1*, *Rac1* and *Hrb98DE*. I also identified a further four genes whose knockdown using one RNAi, but not the other, reduced Rab11-exosome formation, these being *Hsc70-4*, *Nlp*, *Pyk* and *Rac2*.

Of the knockdowns that did reduce Rab11-ILV formation, it was notable that the majority had minimal or no effect on Rab11-compartment formation, whilst around half also had no effect on other aspects of SC organisation such as DCG formation. This suggests that at least these knockdowns may affect Rab11-exosome biogenesis specifically and not wider endosomal processes. Interestingly though, *Arc1*, *Hsp83*, *Rap1*, *Hrb98DE* and *Rac2-RNAi#2* knockdowns each also altered DCG structure. Of

particular interest were the effects observed for *Hsp83* and *Rap1* knockdowns as these resulted in Rab11-compartments forming that completely lacked DCGs.

This led me to investigate the strongest example of this phenotype (*Hsp83-RNAi#1*) in greater detail (see Section 4.2.8). Ultimately, I found that Hsp83 was not necessary for the accumulation of the DCG cargo MFAS but was required for its condensation. A similar analysis of *Rap1-RNAi#2* which produced a related phenotype has not yet been conducted, but these findings do raise intriguing questions regarding the nature of this phenotype.

One striking aspect of these results is the exceptionally different nature of Hsp83 and Rap1 as proteins. Hsp83 is a member of the universally conserved Hsp90 family of chaperone proteins that oversee protein refolding (B. Chen et al., 2006; Zuehlke et al., 2015), whilst Rap1 is a signalling GTPase which regulates pathways controlling metastasis, cancer signalling (Y.-L. Zhang et al., 2017), and endosomal trafficking of factors such as E-cadherin (Knox & Brown, 2002; L. Li et al., 2010). Given the extreme difference in the biology of Hsp83 and Rap1, it is uncertain how knockdown of these two genes create such similar phenotypes. In Section 4.3.4, I proposed that Hsp83 may control DCG biogenesis through a direct interaction with DCG cargoes that facilitates aggregate formation through cargo refolding. Since Hsp83 is localised within the lumen of compartments, I suggest that Hsp83 is not involved in ELM formation and instead takes part in downstream events required for Rab11-exosome formation. This may involve Hsp83-mediated membrane deformation, similar to that described for Hsp90α in other exosome signalling pathways (Lauwers et al., 2018). Additionally, since Hsp83 is a lumenal protein, it would be expected to be present as a cargo on the outside of

exosomes, something that has been observed in tumour-derived exosomes (X. Tang et al., 2019).

By contrast, no direct mechanism for Rap1's role in Rab11-exosome biogenesis is immediately obvious at this stage. However, alongside its potential role as a Rab11-exosome cargo, it is also notable that Rap1 activity can directly stimulate PI3K/Akt/mTOR signalling which appears to be an important regulator of Rab11-exosome formation (Mutvei et al., 2020). Also notable are recent findings which indicate that human Rap1 interacts with and stimulates γ-secretase (Swanson et al., 2023), a proteolytic complex that cleaves important type-I transmembrane proteins including APP (Hur, 2022; X. Zhang et al., 2014). This processing by γ-secretase then renders soluble peptides including Aβ40 and Aβ42 which go on to form aggregates and amyloid. Overall then, I suggest that Rap1 may play a role in γ-secretase-dependent processing of transmembrane factors which regulate DCG condensation. This fits well with observations that, in the absence of Rap1, DCGs either fail to condense or remain attached to the membrane, possibly due to being anchored to uncleaved transmembrane factors.

Overall, *Hsp83* and *Rap1* knockdowns are just two cases out of many I have identified where the inhibition of Rab11-ILV biogenesis is associated with DCG defects, though they are among the strongest. Other examples include knockdowns for genes as seemingly disconnected as the PI3-kinase *Dp110*, the GTPase *Rab11* (Section 4.2.6), the lipid-raft protein *Phb2* (section 5.2.7), and several genes identified in this screen. This implies a deeper link between Rab11-ILV and DCG regulation that may be relevant

for understanding the roles of Hsp83, Rap1 and many other regulators identified through my research.

6.3.3.2 Cargoes and SUMOylation

One question that arises from this screen is whether the proteins tested here represent Rab11-exosome cargoes. Based on the fairly high success rate of identifying new Rab11-exosome biogenesis regulators in the screen and the fact that all but one gene tested here was homologous to proteins identified in Rab11a-exosome-enriched small EV preparations in humans, I suggest that there is sufficient evidence to treat this cohort as if it contains Rab11-exosome cargoes. However, for most individual candidates, their status as cargo proteins is yet to be shown and the role of SUMOylation in regulating these candidates has also not been demonstrated. Despite this, certain evidence does support these ideas.

The most direct evidence of these proteins being cargoes comes from the GPI-anchored protein Dlp, which is a divergent Glypican-1-like protein (Khare & Baumgartner, 2000; Svensson et al., 2012). Although its knockdown was not shown to disrupt Rab11-ILV biogenesis, expressing a GFP-tagged form of Dlp resulted in it labelling the limiting membrane of DCG compartments as well as ILVs associated with the boundary of DCGs. This not only supports the idea that Dlp is a genuine Rab11-exosome cargo, it also indicates that some cargoes can be knocked down without significantly reducing Rab11-ILV formation. Furthermore, this result also provides interesting context for our understanding of the GFP-GPI construct which acts as a DCG marker in SCs (Chapter 4). Initially it was not clear why GPI-anchored GFP would

concentrate into DCGs, but Dlp's distribution suggests that there may be a more general association between GPI-anchored proteins and DCGs. Ideally, fluorescently-tagged forms of other screened proteins could also be used to confirm their inclusion into Rab11-exosomes. In this vein, I have already attempted to express GFP-tagged forms of the Rab11-ILV regulators Rap1, Rac1 and Hrb98DE in SCs. Unfortunately, however, these GFP-tagged constructs were found to simply accumulate at high levels in the cytoplasm of SCs making it impossible to determine whether these proteins were also associated with the membranes of DCG compartments or other structures. It is frequently the case that membrane-associated proteins act as better markers of ILVs and exosomes than cytosolic ones, primarily because of this general distribution within the cell.

Perhaps the best evidence for cargo SUMOylation comes from Hrb98DE, a strong regulator of Rab11-ILV biogenesis and the homologue of mammalian hnRNPA2B1. Of significance here, hnRNPA2B1 is known to be sorted into exosomes based on its SUMOylation (Villarroya-Beltri et al., 2013). Furthermore, in Rab11a-exosome preparations, the percentage of enriched proteins that are known or expected to be SUMOylated was a remarkably high 71%, compared to just 15-20% of proteins that are thought to be SUMOylated generally in humans. It is of interest that a second RNA binding protein, Arc1, is also involved in Rab11-exosome biogenesis.

Overall, this screen offers indirect support for the idea of a SUMO-dependent cargo loading mechanism during Rab11-exosome biogenesis and potentially provides numerous avenues for future research that could confirm this mechanistic pathway. One general scheme for future research would be to use fluorescence imaging to

identify exosome cargoes from the candidates screened here and then assess how cargo loading changes following site-directed mutagenesis of the lysine residues at conserved SUMOylation sites. Based on the hypothesis that SUMO acts as a cargo-sorting tag, it would be expected that mutating SUMOylation sites would selectively prevent that cargo's loading.

6.3.3.3 Arc1 as a regulator of Rab11-exosome biogenesis

Among the most fascinating Rab11-exosome regulators identified in my screen of Rab11-exosome cargo candidates was Arc1. *Arc1* knockdown induced significant reductions in Rab11-ILV formation and resulted in the abnormal aggregation of DCG mini-cores. Following this finding, I hypothesised that Arc1 may facilitate Rab11-exosome biogenesis through a similar mechanism to that observed at *Drosophila* neuromuscular junctions in which Arc1 proteins form a capsid-like shell that recruits its own mRNA and inserts into the membrane of neuronal MVEs to form an exosome-like vesicle (Ashley et al., 2018).

With this mechanism in mind, I investigated whether fluorescently tagged Arc1 constructs could be observed in SC ILVs and whether they could be transferred from SCs to other cell types in accessory glands, as has been shown at neuromuscular junctions (Ashley et al., 2018). For this I used two constructs, a full-length Arc1-GFP fusion protein (Montana & Littleton, 2006), and a GFP-tagged form of the UGR-element which includes portions of the Arc1 3'UTR and ORF (Ashley et al., 2018). Overall expressing these constructs produced mixed results, with full length Arc1-GFP labelling what appeared to be microtubules and Arc1-UGR-GFP essentially saturating

the cytoplasm, but also being incorporated into ILVs that were then secreted as exosomes into the accessory gland lumen. Neither construct was visible in cells beyond SCs. These initial results did not clearly demonstrate whether Arc1 is specifically incorporated into Rab11-exosomes and as such, the role of Arc1 in Rab11-exosome biogenesis requires further attention.

Arc1 nevertheless remains an extremely interesting candidate for future research, especially considering its effect on DCG biogenesis as well as Rab11-ILV formation. This joint effect on Rab11-exosome and DCG biogenesis has been observed across numerous SC regulators and may reflect an inherent link between Rab11-ILV formation and DCG condensation/DCG separation from membranes. Specifically in the case of Arc1 however, it is interesting to note that both Arc1 and its mammalian homologue, Arc, are implicated as causal factors in neurodegenerative disease (Bi et al., 2018; Dorostkar & Herms, 2012; Schulz et al., 2023). In particular, Arc1 overexpression has been found to increase phosphorylated-tau levels and drive neurodegeneration in *Drosophila* brains. Furthermore, Arc has also been shown to directly contribute to amyloid formation within APP-positive endosomes through an interaction with the γ-secretase component presenilin-1 (J. Wu et al., 2011). This is interesting because current research in the Wilson laboratory indicates that SC Rab11-compartments also represent APP-positive compartments (P. J. Singh et al., 2024). Overall, Arc1's role in DCG biogenesis requires further study to understand, but current evidence indicates that it may be tied to highly interesting mechanisms involving neurodegeneration linked factors such as tau, APPL and presenilin1.

Finally, one interesting feature of Arc1 in EV biology is that the loading of *Arc1* mRNA appears to specifically require Gypsy-like GAG repeats present in the 3'UTR (Ashley et al., 2018). As such, if Arc1 is involved in Rab11-exosome biogenesis and takes part in mRNA loading, then fusing the 3'UTR sequence of Arc1 to other genes of interest could enable the loading of numerous engineered RNA molecules that could be used to dissect Rab11-exosome signalling mechanisms. As an example I am already pursuing experimentally, I hypothesise that attaching *Arc1-3'UTR* to the coding sequence of Cre and FLP recombinases should facilitate their transfer to the recipient cells of Rab11-exosomes, whose specific identity within the female reproductive tract is presently unknown. Upon transfer to recipient cells, these recombinase transcripts should then be translated into functional enzymes that can recombine specific DNA sequences (Nern et al., 2011), leading to the expression of a marker gene such as GFP. If successful, this would provide strong support for the role of Arc1 in Rab11-exosome formation and RNA loading. It would also confirm the identify of Rab11-exosome recipient cells, thereby opening up new research possibilities for understanding the mechanisms of exosome signalling within an *in vivo* model and across two genetically-independent individuals.

Chapter 7: Conclusions and future directions

7.1 Overview

Within my thesis I have explored several fundamental yet understudied aspects of exosome, endosome and DCG biology. To do this, I built on previous work carried out within the *Drosophila* SC system as well as other experimental models used in collaborating laboratories. My work was especially informed by previous findings which examined the identity of certain compartments in fixed SCs (Prince et al., 2019), detailed the presence/regulation of DCGs in SCs (Redhai et al., 2016), and identified/described the conserved Rab11-exosome subtype in human cancer cells and SCs (Corrigan et al., 2014; Dar et al., 2021; Fan et al., 2020; Marie et al., 2023). Through my own research in SCs, including the development of new time-lapse imaging protocols, I have made significant advances in studying secretory compartment identity, DCG regulation and Rab11-exosome biogenesis, as reflected by the findings included in this thesis and in other publications.

For example, my characterisation of SC compartments, identification of a Rab6 to Rab11 transition and examination of Arf1, AP-1, Rab6 and Rab11 in DCG biogenesis were each included in (A. Wells et al., 2023). Likewise, real-time imaging of DCG biogenesis in control and neurodegeneration-linked genotypes is posted in preprint form in (P. J. Singh et al., 2024), whilst my contributions to the study of accessory ESCRT-III protein function in Rab11-exosome signalling were included in (Marie et al.,

2023). Additionally, although not included in any currently published work, I also expect my examination of Rab19, Rab7 and Vps35 on late-stage DCG compartments, identification of ILV-forming microdomains, and investigation of SUMOylation and SUMOylated proteins as putative Rab11-exosome cargoes to form the core of other manuscripts in the short to medium term. Therefore, although more work is required to fully understand the processes regulating DCG and exosome formation in SCs, I believe my work represents a novel contribution to the field of secretory biology.

7.2 Summary of findings

My results are perhaps best viewed in two parts. The first includes results presented in Chapters 3 and 4, through which I constructed new models of secretory compartment maturation and DCG biogenesis (Fig. 7.1A,B). The second includes results from Chapters 5 and 6, which provided new models for Rab11-exosome regulation (Fig. 7.2 and Fig. 7.3).

7.2.1 Compartment maturation and DCG biogenesis

Through a mixture of quantitative live-cell imaging and real-time imaging, both using endogenously expressed fluorescent Rab fusion-proteins, I found that secretory compartment maturation was defined by at least five stages (Fig. 7.1A):

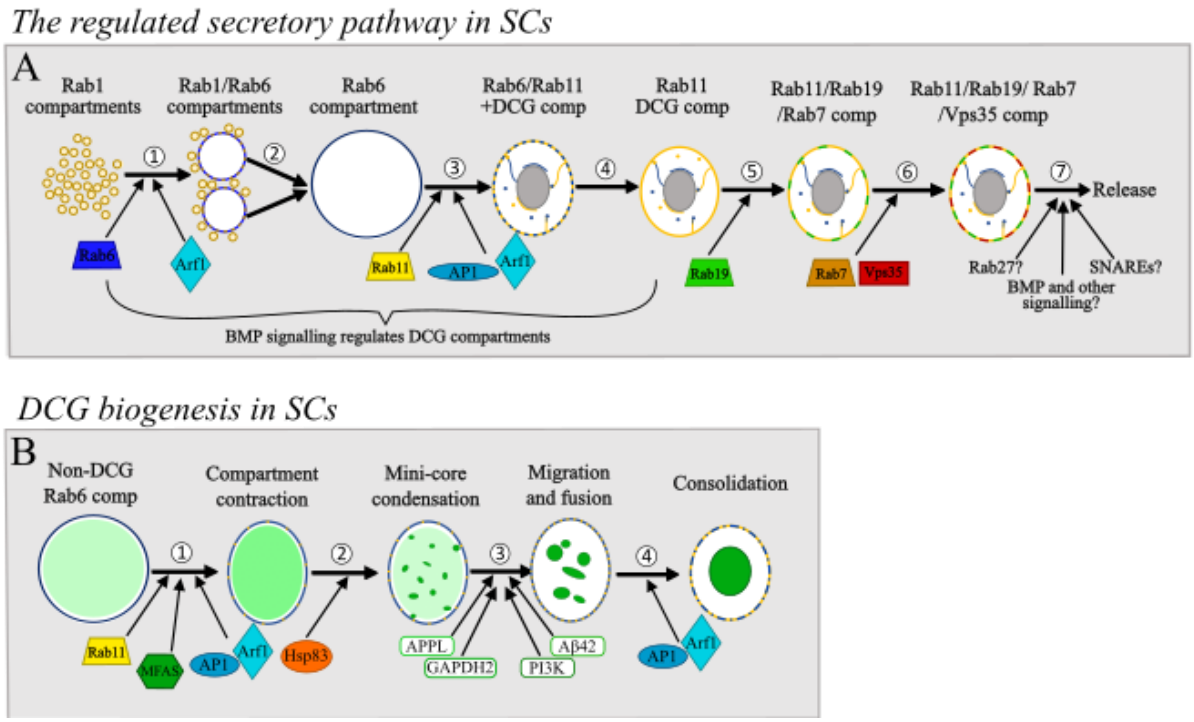

Figure 7.1, (adapted from Fig. 4.11). DCG biogenesis and secretory compartment maturation in SCs. (**A**) SC secretory compartments go through a series of Rab cascades that mediate their maturation from small Rab1-positive compartments to mature secretory compartments. The two major events studied here are a Rab1 to Rab6 transition (regulated by Rab6 and Arf1) and a Rab6 to Rab11 transition that triggers ILV and DCG biogenesis (regulated by Rab11, Arf1 and AP-1). DCG compartments also recruit Rab19 transiently and recruit Rab19, Rab7 and Vps35 immediately prior to secretion/lysosomal degradation. BMP-signalling also controls DCG biogenesis through uncertain mechanisms, and may also regulate compartment secretion alongside other factors like Rab27. (**B**) DCG biogenesis involves several previously indistinguishable steps. Non-DCG compartments first begin the Rab6 to Rab11 transition that coincides with compartment contraction and the concentration of DCG cargoes like MFAS. DCG cargoes then condense in an Hsp83-dependent manner, forming mini-cores. Mini-cores then migrate and fuse until consolidating into a single DCG, though these final steps are disrupted following *APPL*, *Gapdh2*, *Dp110*, *Arf1* and *AP-1* knockdowns or mutant *Aβ42* overexpression.

1) Non-DCG Rab6-compartments form from smaller Rab1-compartments;
2) Non-DCG Rab6-compartments transition to Rab11-compartments;
3) During the Rab6 to Rab11 transition, DCG and exosome biogenesis occurs;
4) Immature DCG compartments transiently associate with Rab19;
5) Mature DCG compartments can associate with factors including Rab19, Rab7 and Vps35 and then undergo secretion and degradation.

Among these findings, the identification of a Rab6 to Rab11 transition that accompanied DCG and exosome biogenesis was a novel discovery, though one that did fit with the established roles of Rab6 and Rab11 as DCG regulators (C. Ma & Brill, 2021; Neuman et al., 2021). Likewise, time-lapse imaging experiments demonstrated a previously unknown role for homotypic fusion during the Rab1 to Rab6 transition and showed that DCGs can form via a process involving the rapid condensation and subsequent fusion of numerous mini-cores. Finally, SC characterisation also highlighted interesting dynamics of Rab19 on DCG compartments, suggesting a potential role for this poorly characterised protein in processes such as compartment secretion.

Building on these observations, I examined regulators of DCG biogenesis and found evidence that DCG biogenesis in SCs is controlled by the conserved DCG regulators Arf1 and AP-1. I also found evidence that the novel Rab6 to Rab11 transition was specifically required for DCG and exosome formation to occur. Interestingly, I found that Arf1 and AP-1 appeared to mediate this Rab6 to Rab11 transition as well as the Rab1 to Rab6 transition that preceded it. Knocking down *Arf1* or *AP-1* impaired DCG

formation within maturing Rab6-compartments, whilst *Arf1* knockdown resulted in large non-DCG compartments retaining Rab1-positive identity. Overall, these results highlighted a novel effect of the conserved DCG regulator Arf1 in controlling SC compartment maturation.

Comparing time-lapse imaging of DCG biogenesis in control SCs to experimental SCs also provided outstanding temporal resolution for understanding novel DCG regulators, including several neurodegeneration-linked genes (Fig. 7.1B). For example, I identified Hsp83 as a specific regulator of DCG cargo condensation. I also found evidence that APPL, GAPDH2, Dp110, $A\beta42_{Iowa}$ and $A\beta42_{Dutch}$ each mediate subsequent DCG maturation, a process that is normally separated from DCG cargo condensation by only a matter of minutes.

Overall, these results highlighted a set of new regulatory processes controlling secretory compartment/DCG maturation and provided insights into the temporal regulation of these processes. They also highlighted the relevance of several evolutionarily conserved regulatory mechanisms to SC secretory processes, suggesting that other pathways involved in these events may also be conserved in other organisms and cell-types.

7.2.2 Rab11-exosome regulation

Having identified the Rab6 to Rab11 transition as a central factor controlling exosome biogenesis in SCs, I proceeded to investigate Rab11-associated proteins (Fig. 7.2). In collaboration with Dr P. Marie, I showed that accessory ESCRT-III proteins and the

Rab11-GEF Bet3 regulated Rab11-exosome signalling *in vivo* in the female post-mating response (PMR). I then investigated the role of Rab11-FIPs, which act as cytoskeletal adaptors for Rab11-compartments (Horgan & McCaffrey, 2009; Jing & Prekeris, 2009), and the exocyst complex which is linked to Rab11 through Sec15 activity (S. Wu et al., 2005; X.-M. Zhang et al., 2004). Overall, I found that Rab11-FIPs controlled Rab11-compartment organisation but had no impact on Rab11-exosome biogenesis, whilst Sec15 and the exocyst complex regulated both Rab11-compartment secretion and Rab11-ILV biogenesis. This was also true for two factors associated with exocyst-mediated trafficking, Rala and Magi (Hazelett & Yeaman, 2012; Kotelevets et al., 2005; Wörthmüller & Rüegg, 2021) suggesting an interesting link between the biogenesis and secretory machineries of Rab11-exosomes.

However, likely my most significant finding from investigating Rab11-exosome biogenesis was the discovery of novel Ecadherin-positive lipid microdomains (ELMs) associated with the membrane of SC Rab11-compartments. ELMs were marked by concentrations of Rab11, Rab19, E-cadherin and Hrs and were found to physically associate with ILVs essentially from the time of their biogenesis. Knockdown of microdomain-associated proteins inhibited Rab11-exosome formation, thereby indicating that ELMs represented sites of active ILV-biogenesis (Fig. 7.3).

I next examined microdomain-associated factors including the SPFH family of lipid-raft scaffolding proteins and Vps34, a lipid modifying kinase that produces essential PI3P

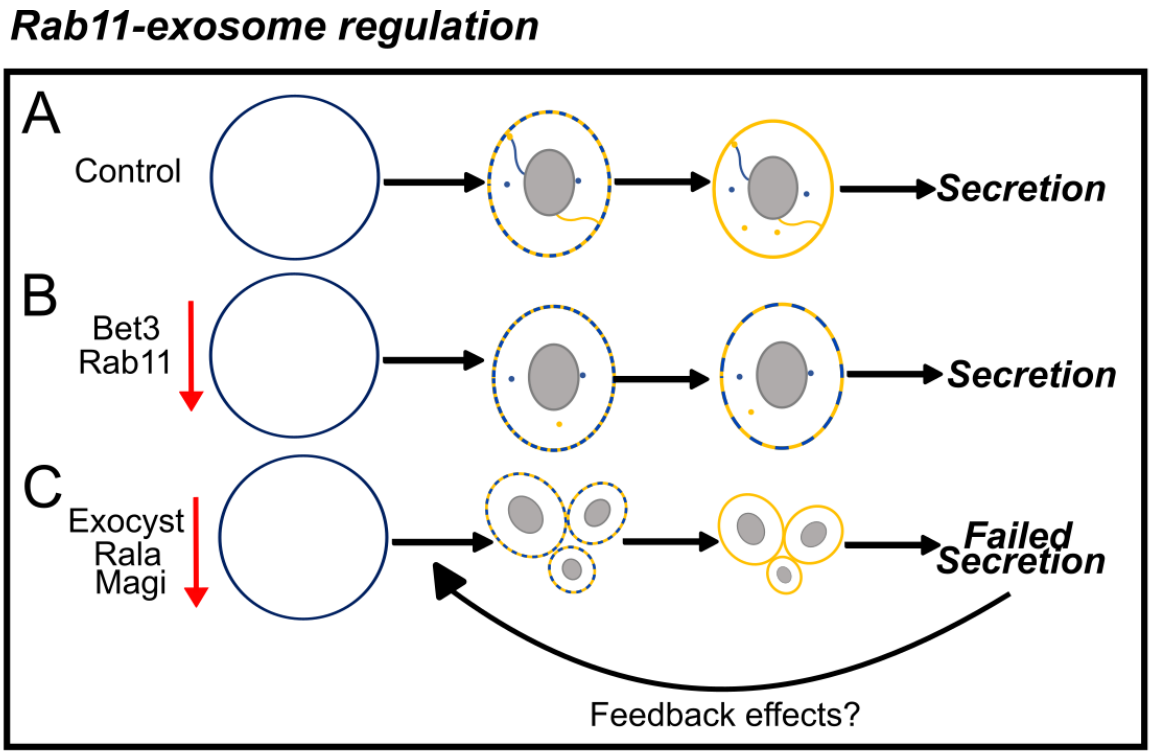

Figure 7.2, (adapted from Fig. 5.19). Model for Rab11-interacting proteins in Rab11-exosome regulation. In normal cells, non-DCG compartments undergo the Rab6 to Rab11 transition which stimulates DCG and Rab11-exosome biogenesis (**A**). Following knockdown of *Rab11* or its GEF *Bet3*, the Rab6 to Rab11 transition is partially inhibited, leading to extended Rab6-presence on DCG compartments and decreased Rab11-exosome biogenesis (**B**). Following inhibition of the exocyst complex or the associated factors Rala and Magi, the number of Rab11-compartments increases and Rab11-exosome biogenesis is strongly inhibited (**C**). This likely reflects a blockade of Rab11-compartment secretion which may in turn have feedback effects on Rab11-compartment formation and Rab11-ILV biogenesis through impaired recycling of important materials.

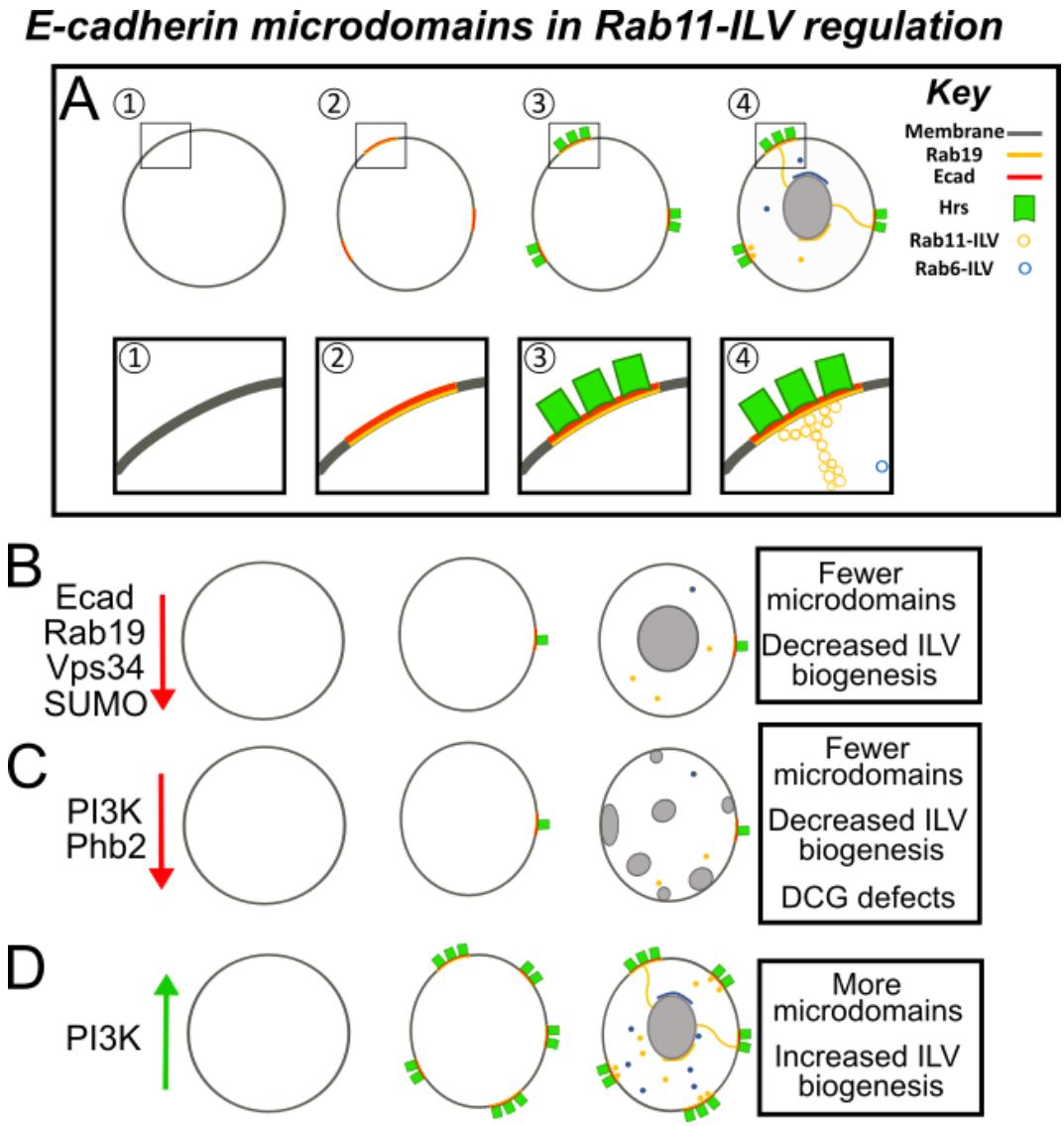

Figure 7.3, (adapted from Fig. 5.19). Model for ELM control of Rab11-exosome biogenesis. ELMs first appear on non-DCG compartments (**A1-2**). E-cadherin and Rab19 are likely recruited first, followed by ESCRT-0 proteins (**A2-3**) which recruit other ESCRT-complexes. ELMs then drive Rab11-exosome formation approximately simultaneously with DCG biogenesis and the onset of the Rab6 to Rab11 transition (**A4**). Following knockdown of the microdomain components *Ecad* and *Rab19*, or the potential microdomain element *Vps34* and the putative exosome cargo tag *SUMO*, fewer ELMs are formed and fewer Rab11-exosomes are produced (**B**). Similarly, knockdown of the potential microdomain element *Phb2* or the PI3-kinase *Dp110* leads to disrupted ELMs, Rab11-exosome and DCG biogenesis (**C**). Conversely, stimulated PI3K signalling increases microdomain formation and Rab11-exosome biogenesis (**D**).

residues in other ESCRT-microdomains. I found that both the SPFH protein Phb2 and Vps34 supported normal Rab11-exosome biogenesis and ELM assembly. Interestingly, I found that PI3K/Akt/mTOR signalling also controls both Rab11-exosomes and ELMs, with suppression of the PI3K/Akt/mTOR pathway inhibiting Rab11-ILV and ELM formation, and stimulation of PI3K/Akt/mTOR signalling increasing Rab11-ILV and ELM biogenesis. These results highlighted a strong correlation between the rates of ELM assembly and Rab11-exosome biogenesis and suggested that global signalling pathways can control the formation of ELMs to modulate Rab11-exosome signalling.

Finally, I examined the role of SUMOylation in Rab11-exosome biogenesis and cargo loading (Chapter 6). Building on previous indications that Rab11-exosome biogenesis occurs in a ubiquitin-independent manner (Marie et al., 2023), I showed that inhibiting any aspect of the SUMOylation pathway significantly reduced Rab11-exosome and ELM biogenesis. I therefore investigated whether SUMO acted as a tag for Rab11-exosome cargoes by identifying SUMO-targeted human Rab11a-exosome cargoes with conserved SUMOylatable homologues in *Drosophila*. By knocking down the *Drosophila* homologues of these cargoes in SCs, I successfully identified a range of new Rab11-exosome regulators as well as several DCG regulators, e.g. *Hsp83, Rap1, Hrb98DE* and *Arc1*.

Overall, my findings identify a range of novel Rab11-exosome regulators and putative Rab11-exosome cargoes. They also highlight ELMs as novel sites of exosome biogenesis and provide evidence that ELMs can integrate various stimuli to regulate Rab11-exosome signalling. This is significant for wider exosome research because, although exosome signalling is known to adapt to global signalling events, no central

mechanism has previously been established that could account for the changes observed in response to different signals in SCs. Based on my findings, I propose that the assembly of ELMs could represent a central mechanism for generation of at least the Rab11-exosome subtype. Evidencing this, I have shown that ELM formation integrates stimuli from numerous sources including global signalling cascades such as the PI3K/Akt/mTOR pathway, the recycling of cell-surface molecules like E-cadherin and the activity of trafficking GTPases like Rab11 and Rab19. Microdomain activity is similarly regulated by SUMOylation, a process that may reflect exosome cargo loading, and requires Vps34, an enzyme that is specifically, transiently activated at discrete stages of endosome maturation. Because of this, I suggest that ELMs may provide a versatile platform through which we can understand Rab11-exosome regulation, determine Rab11a-exosome function and manipulate Rab11a-biogenesis, both in disease and biotechnological scenarios.

7.3 Implications for disease

Although my research was focussed primarily on the fundamental biology of DCG and exosome biogenesis, I found that DCG regulation frequently interacted with important neurodegeneration-linked pathways, whilst the regulators of Rab11-exosome biogenesis were frequently implicated in cancer-promoting pathways. The significance of these pathological associations is currently uncertain, but I propose that these pathological associations may reflect genuine roles for DCGs and Rab11-exosomes in neurodegenerative disease and cancer signalling.

7.3.1 DCGs and neurodegeneration

Examining these associations, I found that a diverse set of proteins implicated in neurodegenerative disease regulated DCG formation. This was particularly interesting because neurodegeneration is generally thought to result from aberrant extracellular protein aggregation and β-amyloid accumulation, whilst DCGs represent one of very few sites of protein aggregation/ β-amyloid formation under normal physiological conditions (Colomer et al., 1996; Jacob et al., 2016). It was therefore striking that knocking down the homologues of important neurodegenerative risk factors such as the PI3-kinase *Dp110*, the glycolytic enzyme *GAPDH2* or amyloid-β forming *APPL* resulted in aberrant DCG aggregation. Even more remarkably, expression of the human familial-AD mutants $A\beta42_{Iowa}$ and $A\beta42_{Dutch}$ in SCs also produced abnormal DCG aggregates, whilst knockdown of *Hsp83*, the homologue of Hsp90α which directly interacts with amyloid-β (Rodríguez-Ramos et al., 2023; Schirmer et al., 2016), resulted in a total inhibition of DCG condensation altogether. It should be noted that the first observations of APPL and Aβ42 phenotypes were made by Dr P. Singh (P. J. Singh et al., 2024), whilst the observations of GAPDH2 were made by Dr C. Mendes (Dar et al., 2021) and that my contributions were in identifying the roles of Dp110 and Hsp83, and in developing time-lapse imaging techniques that allowed examination of the mechanisms of DCG biogenesis in each background.

Ultimately, it is surprising that such a variety of neurodegeneration-linked genes should control DCG biogenesis in non-neuronal SCs, particularly potentially neuron-specific factors, such APPL, $A\beta42_{Iowa}$ or $A\beta42_{Dutch}$. However, Preman Singh and Bhavna Verma

have found that despite low levels of gene expression, both *Appl* knockdown and a null mutation interfere with DCG biogenesis (Singh et al., 2024). In addition, aside from the effects of Hsp83, which controls DCG condensation, it is also remarkable how consistent the effects of most genotypes were. Time-lapse imaging demonstrated that, with the possible exception of GAPDH2, each knockdown or overexpression genotype listed above results in the formation of numerous, membrane-bound mini-cores that are immobile and incapable of fusion. It will now be interesting to text how other neurodegeneration-linked risk factors, such as Arc1 and Phb2, affect the motility of DCG compartments and the mini-cores they produce when knocked down, and how these genes modulate $A\beta42_{Iowa}$ and $A\beta42_{Dutch}$ phenotypes. By themselves, my findings already indicate that a range of AD-associated factors are acting via consistent mechanisms to disrupt normal DCG aggregation, compartment motility and aggregate separation from membranes, strongly suggesting that these processes may be linked to the fundamental pathology of this disease. They also indicate that protein aggregates in large SC DCGs are a good system for studying the effects of other neurodegeneration-linked genes on protein aggregation, secretion and endolysosomal trafficking *in vivo*.

Indeed, given the known functions of proteins such as Arc1 and APP in endosome-dependent β-amyloid formation (J. Wu et al., 2011), and given the emerging overlap between endosome and secretory granule regulation (C. Ma et al., 2020; C. Ma & Brill, 2021), I suggest that the pathways identified in SCs may reflect authentic, *in vivo* mechanisms contributing to neuronal amyloid formation in neurodegenerative disease and beyond. It is already well recognised that endosomal dysregulation plays a key role in neurodegenerative conditions, with factors like retromer dysfunction and *Vps35*

mutations being heavily implicated in neurodegenerative progression (Sassone et al., 2021; Sullivan et al., 2011). It is also recognised that DCG-related factors such as the granins CHGA and VGF are differentially expressed in AD patients (Quinn et al., 2023), whilst abnormal DCG cargo processing is implicated in neurodegenerative disease (Quinn et al., 2021; Wen G et al., 2021). Alongside recent findings from the Brill laboratory in particular, which identify cross-talk between endosomal and regulated secretory compartments (C. Ma et al., 2020; C. Ma & Brill, 2021), my results suggest that dysregulation of trafficking processes in neurons could allow amyloidogenic factors from endosomes to enter DCG compartments and seed amyloid formation, or vice versa, and trigger disease in these cells. Since neurons have abundant regulated secretory compartments, this could also then provide a mechanism for extracellular amyloid secretion as a secondary consequence of these initiating events.

7.3.2 Rab11-exosomes and cancer

It is widely accepted that exosome signalling plays an important role in cancers, with many studies having demonstrated oncogenic effects for cancer-derived exosome secretions (Paskeh et al., 2022; Tai et al., 2018; Xie et al., 2022). What is less clear, however is the role that specific exosome subtypes play in cancer signalling and the mechanisms that are involved in altering exosome biogenesis/cargo-loading in cancer cells. Based my results, I propose that Rab11-exosomes are a promising model for understanding cancer exosome regulation. The most direct connection between Rab11-exosomes and cancer comes from initial studies which identified Rab11a-exosomes from human cancer cell secretions and demonstrated their role in cancer

signalling (Fan et al., 2020). Since then, in work I have contributed to or led, Rab11-exosomes in *Drosophila* SCs and human cancer cells have been shown to be regulated by conserved mechanisms (e.g. requiring accessory ESCRT-III's, (Marie et al., 2023)) and seem likely to share some conserved cargo proteins.

It is therefore very interesting to note the numerous and consistent roles of oncogenic factors in regulating SC Rab11-exosomes despite the fact that SCs represent an *in vivo*, non-cancerous model. As examples, each of Phb2 (Qi et al., 2023), Hsp90α (Birbo et al., 2021), and Rab43 (Z. Huang et al., 2020; Y. Jiang et al., 2019), a homologue of Rab19, are implicated in cancer-promoting pathways. Of particular interest in my opinion, however, are the roles of E-cadherin, PI3K/Akt/mTOR signalling and SUMOylation since each appear to be central regulators of cancer signalling and Rab11-exosome formation.

Loss of E-cadherin from the cell-surface is an important step in cancer metastasis that also promotes oncogenic-signalling pathways (Mendonsa et al., 2018; A. Wells et al., 2008). Interestingly though, the removal of E-cadherin from the cell-surface often occurs through E-cadherin internalisation (Lock & Stow, 2005; J. Xu et al., 2017), an event which we would expect to lead to increased E-cadherin on Rab11-positive compartments and therefore increased Rab11-exosome formation. Notably, this is a correlation we do see in SCs, with greater E-cadherin trafficking on Rab11-compartments being associated with greater Rab11-exosome formation.

In comparison, PI3K/Akt/mTOR signalling is an upstream regulator of innumerable pro-survival and pro-growth pathways that is frequently overactivated in cancers (Fruman et al., 2017; Glaviano et al., 2023). Akt/mTOR signalling is also known to contribute to

the appropriation of exosome signalling following stress-related/cancer-related signalling, including in human Rab11a-exosomes where Akt and mTOR signalling has been implicated (Fan et al., 2020; Jeong & Kim, 2023). It was therefore of great interest when, in the *in vivo* SC model, I found that inhibition of PI3K/Akt/mTOR signalling restricted Rab11-exosome and ELM formation, whilst hyper-activation of PI3K/Akt/mTOR signalling increased their biogenesis. Translating these findings into a typical cancer context, we would therefore expect elevated levels of PI3K/Akt/mTOR signalling to facilitate increased Rab11-exosome biogenesis, which may then promote proliferative cancer signalling.

Finally, SUMOylation is associated with cell stress responses and is frequently mobilised in cancer-promoting pathways (Gu et al., 2023; Ryu et al., 2020). SUMOylation has also been found to directly control the loading of specific exosome cargoes such as hnRNPA2B1 (Villarroya-Beltri et al., 2013). My own experiments in SCs suggest that SUMOylation promotes Rab11-exosome biogenesis and ELM formation and indicate that a high number of SUMOylated proteins may act as conserved Rab11-exosome cargoes including Hrb98DE, the homologue of hnRNPA2B1. Therefore, extrapolating these findings to a hypothetical cancer environment, increased SUMO mobilisation could be expected to promote the formation of ELMs and Rab11-exosomes. If SUMO does in fact act as a tag for Rab11-exosome cargoes, then increased SUMOylation could also designate greater numbers of cargo proteins to match elevated Rab11-exosome formation.

Overall then, major Rab11-exosome-regulating pathways also act as pivotal regulators of cancer progression and, under typical cancer conditions, may be expected to

upregulate Rab11-exosome formation and ELM assembly. Combined with the established role of Rab11a-exosomes in cancer cells, I believe this provides an excellent basis to study Rab11-exosomes as a potentially widespread contributor to exosomal cancer signalling events.

7.4 Future work

Overall, I have outlined what I believe to be important advances in our understanding of the fundamental biology of DCGs and Rab11-exosomes. I have also outlined reasons why my observations of novel DCG- and exosome-regulating pathways may be relevant for understanding mechanisms of neurodegeneration and cancer signalling. For these reasons, I believe that my findings provide a variety of promising routes for continued research into DCG, exosome and intracellular trafficking regulation. Indeed, throughout Chapters 3 to 6, I have suggested a number of specific experiments that could provide insights into the functions of various regulators and the mechanisms they act through. As a final contribution to this thesis, I will therefore highlight general approaches and avenues for research that I believe could be especially promising.

Given its exceptionally recent characterisation, I believe that investigation of the Rab6 to Rab11 transition is likely to offer many opportunities to explore novel biological processes. Furthermore, considering the relatively short period between its onset and the onset of DCG and Rab11-exosome biogenesis which it controls, I suggest that the Rab6 to Rab11 transition provides a compact, well-defined window in which numerous

physiologically significant processes are concentrated. To best utilise this opportunity, I would recommend characterising this transition in as fine detail as possible. For example, it seems possible that this relatively brief window may see changes in compartment pH, divalent cation import and DCG cargo cleavage (eg. see Singh et al., 2024) that could be relevant for understanding DCG condensation. It also seems likely that factors required for Rab11-exosome biogenesis are recruited in this window, perhaps driven by changes in the lipid composition of compartment microdomains. Improved time-lapse imaging techniques may be an especially helpful tool in these efforts, yet so would more novel approaches that could report on the activity or interactions of particular regulators, for example through two-part fluorescent reporters (Gomes et al., 2016; Tebo & Gautier, 2019) or FRET-based approaches or FRET-based approaches (Sekar & Periasamy, 2003).

Likewise, I believe that the identification of ELMs provides an exceptionally valuable means to study the regulation of Rab11-exosome biogenesis since it allows for easy assessment of which regulators directly associate with the exosome-forming machinery. This may be especially important for understanding the role of SUMOylated proteins and cargo loading during Rab11-exosome biogenesis. As with the Rab6 to Rab11 transition then, I would recommend characterising the components and interactions present within these microdomains as far as possible. Where particularly interesting interactions are identified, mutations that disrupt the interaction could then be induced to discern the mechanism of interaction. For example, following identification of cargo-ESCRT interaction, mutations of lysines believed to be targeted by SUMOylation could be used to assess the involvement of SUMOylation.

Additionally, I believe that diversity of genetic tools available in *Drosophila* paired with the unique biology of the SC-system can and should be utilised to produce a toolset for creating engineered EVs within the Rab11-exosome signalling pathway (Esmaeili et al., 2022; L. Huang et al., 2023). This project would first require the identification/confirmation of appropriate Rab11-exosome cargoes but would provide an outstanding model for exosome research in which the regulators, cargoes and signalling effects of Rab11-exosomes could each be altered in an inducible manner within an *in vivo* exosome pathway. I have already outlined plans to use Arc1-related mRNA reporters to identify the recipient cells of Rab11-exosomes (Section 6.3.3.3), though other molecules such as Hrb98DE may also provide good avenues for engineered RNA transfer. Since Rab11-exosomes are produced in males and then transferred to females, the donor and recipient cells would be genetically independent and could provide a valuable model for understanding the mechanisms involved in exosome-targeting. This system may also offer insights into functional effects of DCG aggregation defects on processes such as exosome-targeting and signalling outcomes, shedding light on the currently enigmatic association between DCGs and exosomes.

Finally, to confirm the relevance of any findings within SCs for other systems, it will be necessary to conduct parallel experiments in other organisms. The best models for these experiments are likely to be mammalian cell lines used for the study of neurodegeneration and cancer exosome signalling since these can confirm the conservation of particular pathways across evolution and assess the role of different mechanisms in relevant pathologies. Plated cell lines also have the advantage of being

well suited for proteomic/transcriptomic analyses and for allowing detailed biochemical analysis of important molecular interactions.

Overall, I believe the *Drosophila* SC model has the capacity to develop into a defining system for the study of exosomes, DCGs and intracellular trafficking. Future developments in genetic toolsets and single-cell analyses are likely to enhance the explanatory power of this system and facilitate even greater insights into the fundamental biology of important secretory processes.

Chapter 8: Appendix

8.1 Different temperature regimes and expression of fluorescent *Rab6*, *Rab11* and *Rab19* gene-traps do not affect SC organisation

Wide-field imaging of SCs expressing any of *CFP-Rab6*, *YFP-Rab11* or *YFP-Rab19* showed that the expression of these fusion proteins had no observable effect on SC organisation and no impact on the number of DCG-containing compartments as assessed by DIC microscopy (Fig. 8.1A). To maintain consistency with later experiments where the temperature-controlled *UAS-GAL4-GAL80^{ts}* gene expression system was used, SC morphology was analysed in males aged at 29°C for 6 days following eclosion. Previous studies have indicated that adult exposure to 29°C does not affect SC morphology (e.g. Corrigan et al., 2014; Fan et al., 2020; Marie et al., 2023). This observation was confirmed by examining the numbers of large non-acidic compartments labelled by the CFP-Rab6 and YFP-Rab11 fusion constructs, which did not significantly vary between males raised at 19°C and 29°C. Likewise the number of DCG compartments was not affected by temperature either (Fig. 8.1 B,C). Overall, no significant changes in gross SC organisation were observed between individuals raised at 19°C and 29°C (Fig. 8.1 D-G).

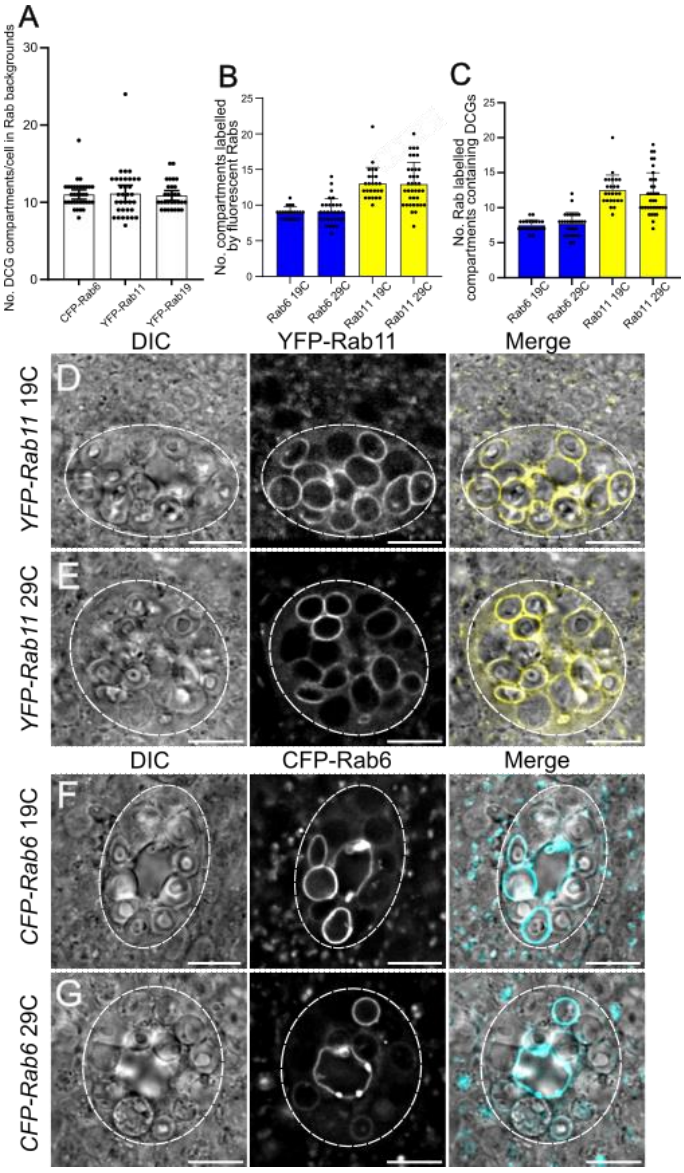

Figure 8.1. Different temperature regimes and expression of fluorescent *Rab6*, *Rab11* and *Rab19* proteins does not affect SC organisation. Bar chart showing number of DCG compartments in different Rab-fusion-protein backgrounds (**A**). Bar charts showing number of non-acidic compartments (**B**) and DCG compartments (**C**) labelled by Rab6 and Rab11 at different temperatures. (**D-G**) Wide-field fluorescence images of SCs expressing *YFP-Rab11* at 19°C (**D**) and 29°C (**E**) or *CFP-Rab6* at 19°C (**F**) and 29°C (**G**). Panels display representative images from DIC microscopy, Rab fluorescence, and merge images. SCs boundaries marked by dashed circles, Scale bars: 10µm.

8.2 Manual image analysis protocols

8.2.1 Compartment identity and ILV presence

In SCs expressing any fluorescent marker of large secretory compartment membranes (e.g. CFP-Rab6, YFP-Rab7, YFP-Rab11, YFP-Rab19), it was typical to count the number of labelled compartments. To take these measurements reliably and reproducibly, images were always visualised at 200% magnification. Compartments were only counted as having a given identity if they met the following criteria:

1) Compartments possessed fluorescent signal around the entirety of their limiting membrane;
2) That fluorescent signal was notably above the background, cytosolic signal. Whenever this was not obvious, the transect tool was used to assess whether fluorescent signal increased at the limiting membrane;
3) Compartments had a diameter >1 μm at their widest point. For compartments smaller than this, internal structures like ILVs and DCGs could not be reliably assessed.

To assess Rab-labelled exosome formation within compartments, fluorescent puncta and other structures were used as proxies for ILVs. To ensure exosome formation was assessed consistently across genotypes, fluorescent structures were only counted as ILVs if they met the following criteria:

1) Fluorescent puncta were visibly separated from the limiting membrane or were part of a larger fluorescent structure such as “ILV-bridges” that protruded from limiting membranes for >0.3 μm;

2) Signal from the puncta persisted for at least three Z-planes (i.e. did not appear to be a random artefact).
3) The puncta were spatially separated from the membrane at the top or bottom by least 2 Z-slices OR appeared in Z-planes that comprised the centre of the compartment.

8.2.2 DCG presence and abnormality

In all live-cell imaging genotypes, the number of DCGs within SCs was assessed using DIC microscopy. In SCs expressing the DCG markers *GFP-GPI* or *GFP-mfas*, the fluorescent signal from these markers could also be used to assess DCG numbers. However, when it became necessary to assess whether DCGs had matured correctly and possessed normal morphologies, only the DIC channel of images was used and cells expressing *GFP-GPI* were not used for analyses. This is because cells expressing GFP-GPI possessed an elevated number of abnormal DCGs compared to control SCs. In the vast majority of control SC compartments, DCGs possessed uniform, spherical morphologies. DCG compartments were assessed to be abnormal if they fulfilled at least one of the following criteria in any Z-plane besides the first (apical) or last (basal) two which were in focus:

1) A single compartment possessed multiple minicores;
2) Single DCGs possessed acute internal angles >180° rather than being spherical;
3) Single DCGs possessed two or more acute external angles.

8.2.3 Ecad microdomain count

In quantitative experiments, E-cadherin (Ecad) was visualised in SCs using an *Ecad-RFP* fluorescent transgene under *ubi* regulatory sequences. For these analyses, Ecad-RFP signal was determined to represent E-cadherin microdomains when the following criteria were met in any Z-planes besides the first (apical) or last (basal) two slices of the limiting membrane which were in focus:

1) Ecad-RFP signal co-localised with the limiting membrane of large secretory compartments;
2) Ecad-RFP signal extended for >0.3 µm and persisted across at least 3 Z-slices;

9.0 Bibliography

Abdullah, M., Nakamura, T., Ferdous, T., Gao, Y., Chen, Y., Zou, K., & Michikawa, M. (2021). Cholesterol Regulates Exosome Release in Cultured Astrocytes. *Frontiers in Immunology*, *12*. https://doi.org/10.3389/fimmu.2021.722581

Abrami, L., Brandi, L., Moayeri, M., Brown, M. J., Krantz, B. A., Leppla, S. H., & van der Goot, F. G. (2013). Hijacking Multivesicular Bodies Enables Long-Term and Exosome-Mediated Long-Distance Action of Anthrax Toxin. *Cell Reports*, *5*(4), 986–996. https://doi.org/10.1016/j.celrep.2013.10.019

Abusamra, A. J., Zhong, Z., Zheng, X., Li, M., Ichim, T. E., Chin, J. L., & Min, W.-P. (2005). Tumor exosomes expressing Fas ligand mediate CD8+ T-cell apoptosis. *Blood Cells, Molecules, and Diseases*, *35*(2), 169–173. https://doi.org/https://doi.org/10.1016/j.bcmd.2005.07.001

Ailion, M., Hannemann, M., Dalton, S., Pappas, A., Watanabe, S., Hegermann, J., Liu, Q., Han, H. F., Gu, M., Goulding, M. Q., Sasidharan, N., Schuske, K., Hullett, P., Eimer, S., & Jorgensen, E. M. (2014). Two Rab2 interactors regulate dense-core vesicle maturation. *Neuron*, *82*(1), 167–180. https://doi.org/10.1016/j.neuron.2014.02.017

Allison, R., Lumb, J. H., Fassier, C., Connell, J. W., Ten Martin, D., Seaman, M. N. J., Hazan, J., & Reid, E. (2013). An ESCRT–spastin interaction promotes fission of recycling tubules from the endosome. *Journal of Cell Biology*, *202*(3), 527–543. https://doi.org/10.1083/jcb.201211045

Alvarez, C., Garcia-Mata, R., Brandon, E., & Sztul, E. (2003). COPI Recruitment Is Modulated by a Rab1b-dependent Mechanism. *Molecular Biology of the Cell*, *14*, 2116–2127. https://doi.org/10.1091/mbc.E02-09

Aqil, F., & Gupta, R. C. (2022). Exosomes in Cancer Therapy. *Cancers*, *14*(3). https://doi.org/10.3390/cancers14030500

Arvan, P., & Castle, D. (1998). Sorting and storage during secretory granule biogenesis: Looking backward and looking forward. *Biochemical Journal*, *332*(3), 593–610. https://doi.org/10.1042/bj3320593

Arya, S. B., Collie, S. P., & Parent, C. A. (2024). The ins-and-outs of exosome biogenesis, secretion, and internalization. *Trends in Cell Biology*, *34*(2), 90–108. https://doi.org/https://doi.org/10.1016/j.tcb.2023.06.006

Ashley, J., Cordy, B., Lucia, D., Fradkin, L. G., Budnik, V., & Thomson, T. (2018). Retrovirus-like Gag Protein Arc1 Binds RNA and Traffics across Synaptic Boutons. *Cell*, *172*(1), 262-274.e11. https://doi.org/10.1016/j.cell.2017.12.022

Austin, C., Hinners, I., & Tooze, S. A. (2000). Direct and GTP-dependent interaction of ADP-ribosylation factor 1 with clathrin adaptor protein AP-1 on immature secretory granules. *Journal of Biological Chemistry*, *275*(29), 21862–21869. https://doi.org/10.1074/jbc.M908875199

Babaei, M., & Rezaie, J. (2021). Application of stem cell-derived exosomes in ischemic diseases: opportunity and limitations. *Journal of Translational Medicine*, *19*(1), 196. https://doi.org/10.1186/s12967-021-02863-w

Bai, S., Hou, W., Yao, Y., Meng, J., Wei, Y., Hu, F., Hu, X., Wu, J., Zhang, N., Xu, R., Tian, F., Wang, B., Liao, H., Du, Y., Fang, H., He, W., Liu, Y., Shen, B., & Du, J. (2022). Exocyst controls exosome biogenesis via Rab11a. *Molecular Therapy - Nucleic Acids*, *27*, 535–546. https://doi.org/10.1016/j.omtn.2021.12.023

Baietti, M. F., Zhang, Z., Mortier, E., Melchior, A., Degeest, G., Geeraerts, A., Ivarsson, Y., Depoortere, F., Coomans, C., Vermeiren, E., Zimmermann, P., & David, G. (2012).

Syndecan–syntenin–ALIX regulates the biogenesis of exosomes. *Nature Cell Biology*, *14*(7), 677–685. https://doi.org/10.1038/ncb2502

Bartolomucci, A., Possenti, R., Mahata, S. K., Fischer-Colbrie, R., Loh, Y. P., & Salton, S. R. J. (2011). The Extended Granin Family: Structure, Function, and Biomedical Implications. *Endocrine Reviews*, *32*(6), 755–797. https://doi.org/10.1210/er.2010-0027

Bauerfeind, R., & Huttner, W. B. (1993). Biogenesis of constitutive secretory vesicles, secretory granules and synaptic vesicles. *Current Opinion in Cell Biology*, *5*(4), 628–635. https://doi.org/https://doi.org/10.1016/0955-0674(93)90132-A

Bavelloni, A., Piazzi, M., Raffini, M., Faenza, I., & Blalock, W. L. (2015). Prohibitin 2: At a communications crossroads. *IUBMB Life*, *67*(4), 239–254. https://doi.org/https://doi.org/10.1002/iub.1366

Bearrows, S. C., Bauchle, C. J., Becker, M., Haldeman, J. M., Swaminathan, S., & Stephens, S. B. (2019). Chromogranin B regulates early-stage insulin granule trafficking from the Golgi in pancreatic islet β-cells. *Journal of Cell Science*, *132*(13), jcs231373. https://doi.org/10.1242/jcs.231373

Beller, M., Blanke, S., Brentrup, D., & Jäckle, H. (2002). Identification and expression of Ima, a novel Ral-interacting Drosophila protein. *Mechanisms of Development*, *119*, S253–S260. https://doi.org/https://doi.org/10.1016/S0925-4773(03)00125-4

Berry, M. D. (2004). Glyceraldehyde-3-phosphate dehydrogenase as a target for small-molecule disease-modifying therapies in human neurodegenerative disorders. *Journal of Psychiatry and Neuroscience*, *29*(5), 337. http://jpn.ca/content/29/5/337.abstract

Bi, R., Kong, L.-L., Xu, M., Li, G.-D., Zhang, D.-F., Li, T., Fang, Y., Zhang, C., Zhang, B., Yao, Y.-G., & Initiative, A. D. N. (2018). The Arc Gene Confers Genetic Susceptibility to

Alzheimer's Disease in Han Chinese. *Molecular Neurobiology*, *55*(2), 1217–1226. https://doi.org/10.1007/s12035-017-0397-6

Birbo, B., Madu, E. E., Madu, C. O., Jain, A., & Lu, Y. (2021). Role of HSP90 in Cancer. *International Journal of Molecular Sciences*, *22*(19). https://doi.org/10.3390/ijms221910317

Bobrie, A., Krumeich, S., Reyal, F., Recchi, C., Moita, L. F., Seabra, M. C., Ostrowski, M., & Théry, C. (2012). Rab27a Supports Exosome-Dependent and -Independent Mechanisms That Modify the Tumor Microenvironment and Can Promote Tumor Progression. *Cancer Research*, *72*(19), 4920–4930. https://doi.org/10.1158/0008-5472.CAN-12-0925

Bogan, J. S., Xu, Y., & Hao, M. (2012). Cholesterol Accumulation Increases Insulin Granule Size and Impairs Membrane Trafficking. *Traffic*, *13*(11), 1466–1480. https://doi.org/https://doi.org/10.1111/j.1600-0854.2012.01407.x

Bohush, A., Bieganowski, P., & Filipek, A. (2019). Hsp90 and its co-chaperones in neurodegenerative diseases. In *International Journal of Molecular Sciences* (Vol. 20, Issue 20). MDPI AG. https://doi.org/10.3390/ijms20204976

Bonnemaison, M. L., Eipper, B. A., & Mains, R. E. (2013). Role of adaptor proteins in secretory granule biogenesis and maturation. In *Frontiers in Endocrinology* (Vol. 4, Issue AUG). https://doi.org/10.3389/fendo.2013.00101

Borchers, A.-C., Janz, M., Schäfer, J.-H., Moeller, A., Kümmel, D., Paululat, A., Ungermann, C., & Langemeyer, L. (2023). Regulatory sites in the Mon1–Ccz1 complex control Rab5 to Rab7 transition and endosome maturation. *Proceedings of the National Academy of Sciences*, *120*(30), e2303750120. https://doi.org/10.1073/pnas.2303750120

Bowman, G. R., Cowan, A. T., & Turkewitz, A. P. (2009). *Chapter 10: Biogenesis of Dense-Core Secretory Granules*.

Braulke, T., & Bonifacino, J. S. (2009). Sorting of lysosomal proteins. *Biochimica et Biophysica Acta (BBA) - Molecular Cell Research*, *1793*(4), 605–614. https://doi.org/https://doi.org/10.1016/j.bbamcr.2008.10.016

Bröcker, C., Kuhlee, A., Gatsogiannis, C., Kleine Balderhaar, H. J., Hönscher, C., Engelbrecht-Vandré, S., Ungermann, C., & Raunser, S. (2012). Molecular architecture of the multisubunit homotypic fusion and vacuole protein sorting (HOPS) tethering complex. *Proceedings of the National Academy of Sciences of the United States of America*, *109*(6), 1991–1996. https://doi.org/10.1073/pnas.1117797109

Brunner, Y., Couté, Y., Iezzi, M., Foti, M., Fukuda, M., Hochstrasser, D. F., Wollheim, C. B., & Sanchez, J.-C. (2007). Proteomics Analysis of Insulin Secretory Granules*S. *Molecular & Cellular Proteomics*, *6*(6), 1007–1017. https://doi.org/https://doi.org/10.1074/mcp.M600443-MCP200

Bucci, C., Thomsen, P., Nicoziani, P., McCarthy, J., & van Deurs, B. (2000). Rab7: A Key to Lysosome Biogenesis □ V. In *Molecular Biology of the Cell* (Vol. 11). www.molbiolcell.org.

Buckles, T. C., Ohashi, Y., Tremel, S., McLaughlin, S. H., Pardon, E., Steyaert, J., Gordon, M. T., Williams, R. L., & Falke, J. J. (2020). The G-Protein Rab5A Activates VPS34 Complex II, a Class III PI3K, by a Dual Regulatory Mechanism. *Biophysical Journal*, *119*(11), 2205–2218. https://doi.org/10.1016/j.bpj.2020.10.028

Burgess, J., Jauregui, M., Tan, J., Rollins, J., Lallet, S., Leventis, P. A., Boulianne, G. L., Chang, H. C., Borgne, R. Le, Krämer, H., & Brill, J. A. (2011). AP-1 and clathrin are essential for secretory granule biogenesis in Drosophila. *Molecular Biology of the Cell*, *22*(12), 2094–2105. https://doi.org/10.1091/mbc.E11-01-0054

Buser, D. P., & Spang, A. (2023). Protein sorting from endosomes to the TGN. In *Frontiers in Cell and Developmental Biology* (Vol. 11). Frontiers Media S.A. https://doi.org/10.3389/fcell.2023.1140605

Butterfield, D. A., Hardas, S. S., & Lange, M. L. B. (2010). Oxidatively Modified Glyceraldehyde-3-Phosphate Dehydrogenase (GAPDH) and Alzheimer's Disease: Many Pathways to Neurodegeneration. *Journal of Alzheimer's Disease*, *20*, 369–393. https://doi.org/10.3233/JAD-2010-1375

Buzas, E. I. (2023). The roles of extracellular vesicles in the immune system. *Nature Reviews Immunology*, *23*(4), 236–250. https://doi.org/10.1038/s41577-022-00763-8

Campelo, F., Tian, M., & von Blume, J. (2023). Rediscovering the intricacies of secretory granule biogenesis. *Current Opinion in Cell Biology*, *85*, 102231. https://doi.org/https://doi.org/10.1016/j.ceb.2023.102231

Campillos, M., Doerks, T., Shah, P. K., & Bork, P. (2006). Computational characterization of multiple Gag-like human proteins. *Trends in Genetics*, *22*(11), 585–589. https://doi.org/10.1016/j.tig.2006.09.006

Cao, J., & Courey, A. J. (2017). SUMO in Drosophila Development. In V. G. Wilson (Ed.), *SUMO Regulation of Cellular Processes* (pp. 249–257). Springer International Publishing. https://doi.org/10.1007/978-3-319-50044-7_15

Cappadocia, L., & Lima, C. D. (2018). Ubiquitin-like Protein Conjugation: Structures, Chemistry, and Mechanism. *Chemical Reviews*, *118*(3), 889–918. https://doi.org/10.1021/acs.chemrev.6b00737

Carmon, O., Laguerre, F., Riachy, L., Delestre-Delacour, C., Wang, Q., Tanguy, E., Jeandel, L., Cartier, D., Thahouly, T., & Haeberlé, A.-M. (2020). Chromogranin A preferential interaction with Golgi phosphatidic acid induces membrane deformation and

contributes to secretory granule biogenesis. *FASEB Journal*, *34*(5), 6769–6790. https://doi.org/10.1096/fj.202000074Rï

Carvalho, G. B., Kapahi, P., Anderson, D. J., & Benzer, S. (2006). Allocrine Modulation of Feeding Behavior by the Sex Peptide of Drosophila. *Current Biology*, *16*(7), 692–696. https://doi.org/10.1016/j.cub.2006.02.064

Cendron, L., Rothenberger, S., Cassari, L., Dettin, M., & Pasquato, A. (2023). Chapter One - Proprotein convertases regulate trafficking and maturation of key proteins within the secretory pathway. In R. Donev (Ed.), *Advances in Protein Chemistry and Structural Biology* (Vol. 133, pp. 1–54). Academic Press. https://doi.org/https://doi.org/10.1016/bs.apcsb.2022.10.001

Chairoungdua, A., Smith, D. L., Pochard, P., Hull, M., & Caplan, M. J. (2010). Exosome release of β-catenin: a novel mechanism that antagonizes Wnt signaling. *Journal of Cell Biology*, *190*(6), 1079–1091. https://doi.org/10.1083/jcb.201002049

Chalmers, A. D., & Whitley, P. (2012). Continuous endocytic recycling of tight junction proteins: how and why? *Essays in Biochemistry*, *53*, 41–54. https://doi.org/10.1042/bse0530041

Chanat, E., & Huttner, W. B. (1991). Milieu-induced, selective aggregation of regulated secretory proteins in the trans-Golgi network. *Journal of Cell Biology*, *115*(6), 1505–1519. https://doi.org/10.1083/jcb.115.6.1505

Chandra, M., Chin, Y. K.-Y., Mas, C., Feathers, J. R., Paul, B., Datta, S., Chen, K.-E., Jia, X., Yang, Z., Norwood, S. J., Mohanty, B., Bugarcic, A., Teasdale, R. D., Henne, W. M., Mobli, M., & Collins, B. M. (2019). Classification of the human phox homology (PX) domains based on their phosphoinositide binding specificities. *Nature Communications*, *10*(1), 1528. https://doi.org/10.1038/s41467-019-09355-y

Chapman, T., & Davies, S. J. (2004). Functions and analysis of the seminal fluid proteins of male Drosophila melanogaster fruit flies. *Peptides*, *25*(9), 1477–1490. https://doi.org/https://doi.org/10.1016/j.peptides.2003.10.023

Chaudhary, S., Dhiman, A., Patidar, A., Malhotra, H., Talukdar, S., Dilawari, R., Chaubey, G. K., Modanwal, R., Raje, C. I., & Raje, M. (2021). Moonlighting glyceraldehyde-3-phosphate dehydrogenase (GAPDH) modulates protein aggregation. *Biochimica et Biophysica Acta (BBA) - Molecular Basis of Disease*, *1867*(10), 166202. https://doi.org/https://doi.org/10.1016/j.bbadis.2021.166202

Chaumet, A., Wright, G. D., Seet, S. H., Tham, K. M., Gounko, N. V, & Bard, F. (2015). Nuclear envelope-associated endosomes deliver surface proteins to the nucleus. *Nature Communications*, *6*(1), 8218. https://doi.org/10.1038/ncomms9218

Chen, B., Zhong, D., & Monteiro, A. (2006). Comparative genomics and evolution of the HSP90 family of genes across all kingdoms of organisms. *BMC Genomics*, *7*(1), 156. https://doi.org/10.1186/1471-2164-7-156

Chen, C., Zong, S., Wang, Z., Lu, J., Zhu, D., Zhang, Y., Zhang, R., & Cui, Y. (2018). Visualization and intracellular dynamic tracking of exosomes and exosomal miRNAs using single molecule localization microscopy. *Nanoscale*, *10*(11), 5154–5162. https://doi.org/10.1039/C7NR08800K

Chen, G., Xu, T., Yan, Y., Zhou, Y., Jiang, Y., Melcher, K., & Xu, H. E. (2017). Amyloid beta: structure, biology and structure-based therapeutic development. *Acta Pharmacologica Sinica*, *38*(9), 1205–1235. https://doi.org/10.1038/aps.2017.28

Chen, J., Li, P., Zhang, T., Xu, Z., Huang, X., Wang, R., & Du, L. (2022). Review on Strategies and Technologies for Exosome Isolation and Purification. In *Frontiers in Bioengineering*

and Biotechnology (Vol. 9). Frontiers Media S.A. https://doi.org/10.3389/fbioe.2021.811971

Chen, K.-E., Healy, M. D., & Collins, B. M. (2019). Towards a molecular understanding of endosomal trafficking by Retromer and Retriever. *Traffic*, *20*(7), 465–478. https://doi.org/https://doi.org/10.1111/tra.12649

Chen, P. S., Stumm-Zollinger, E., Aigaki, T., Balmer, J., Bienz, M., & Böhlen, P. (1988). A male accessory gland peptide that regulates reproductive behavior of female D. melanogaster. *Cell*, *54*(3), 291–298. https://doi.org/10.1016/0092-8674(88)90192-4

Chen, P.-C., Hsieh, M.-H., Kuo, W.-S., Wu, L. S.-H., Kao, H.-F., Liu, L.-F., Liu, Z.-G., Jeng, W.-Y., & Wang, J.-Y. (2022). Moonlighting glyceraldehyde-3-phosphate dehydrogenase (GAPDH) protein of Lactobacillus gasseri attenuates allergic asthma via immunometabolic change in macrophages. *Journal of Biomedical Science*, *29*(1), 75. https://doi.org/10.1186/s12929-022-00861-8

Chen, Y.-G., & Shields, D. (1996). ADP-ribosylation Factor-1 Stimulates Formation of Nascent Secretory Vesicles from the trans-Golgi Network of Endocrine Cells (∗). *Journal of Biological Chemistry*, *271*(10), 5297–5300. https://doi.org/10.1074/jbc.271.10.5297

Chen, Y.-G., Siddhanta, A., Austin, C. D., Hammond, S. M., Sung, T.-C., Frohman, M. A., Morris, A. J., & Shields, D. (1997). Phospholipase D Stimulates Release of Nascent Secretory Vesicles from the trans-Golgi Network. *Journal of Cell Biology*, *138*(3), 495–504. https://doi.org/10.1083/jcb.138.3.495

Chhatar, S., & Lal, G. (2021). Role of adrenergic receptor signalling in neuroimmune communication. *Current Research in Immunology*, *2*, 202–217. https://doi.org/https://doi.org/10.1016/j.crimmu.2021.11.001

Christ, L., Wenzel, E. M., Liestøl, K., Raiborg, C., Campsteijn, C., & Stenmark, H. (2016). ALIX and ESCRT-I/II function as parallel ESCRT-III recruiters in cytokinetic abscission. *Journal of Cell Biology*, *212*(5), 499–513. https://doi.org/10.1083/jcb.201507009

Christianson, H. C., Svensson, K. J., van Kuppevelt, T. H., Li, J.-P., & Belting, M. (2013). Cancer cell exosomes depend on cell-surface heparan sulfate proteoglycans for their internalization and functional activity. *Proceedings of the National Academy of Sciences*, *110*(43), 17380–17385. https://doi.org/10.1073/pnas.1304266110

Chung, K.-N., Walter, P., Aponte, G. W., & Moore, H.-P. H. (1989). Molecular Sorting in the Secretory Pathway. *Science*, *243*(4888), 192–197. https://doi.org/10.1126/science.2911732

Chuo, S. T.-Y., Chien, J. C.-Y., & Lai, C. P.-K. (2018). Imaging extracellular vesicles: current and emerging methods. *Journal of Biomedical Science*, *25*(1), 91. https://doi.org/10.1186/s12929-018-0494-5

Clermont, Y., Xia, L., Rambourg, A., Turner, J. D., & Hermo, L. (1993). Transport of casein submicelles and formation of secretion granules in the golgi apparatus of epithelial cells of the lactating mammary gland of the rat. *The Anatomical Record*, *235*(3), 363–373. https://doi.org/https://doi.org/10.1002/ar.1092350305

Cockcroft, S., Thomas, G. M. H., Fensome, A., Geny, B., Cunningham, E., Gout, I., Hiles, I., Totty, N. F., Truong, O., & Hsuan, J. J. (1994). Phospholipase D: a Downstream Effector of ARF in Granulocytes. *Science*, *263*(5146), 523–526. https://doi.org/10.1126/science.8290961

Colomer, V., Kicska, G. A., & Rindler, M. J. (1996). Secretory Granule Content Proteins and the Luminal Domains of Granule Membrane Proteins Aggregate in Vitro at Mildly

Acidic pH (∗). *Journal of Biological Chemistry*, *271*(1), 48–55. https://doi.org/10.1074/jbc.271.1.48

Corrigan, L., Redhai, S., Leiblich, A., Fan, S. J., Perera, S. M. W., Patel, R., Gandy, C., Mark Wainwright, S., Morris, J. F., Hamdy, F., Goberdhan, D. C. I., & Wilson, C. (2014). BMP-regulated exosomes from Drosophila male reproductive glands reprogram female behavior. *Journal of Cell Biology*, *206*(5), 671–688. https://doi.org/10.1083/jcb.201401072

Cottee, M. A., Letham, S. C., Young, G. R., Stoye, J. P., & Taylor, I. A. (2024). Structure of Drosophila melanogaster ARC1 reveals a repurposed molecule with characteristics of retroviral Gag. *Science Advances*, *6*(1), eaay6354. https://doi.org/10.1126/sciadv.aay6354

Cox, J. V., Kansal, R., & Whitt, M. A. (2016). Rab43 regulates the sorting of a subset of membrane protein cargo through the medial Golgi. *Molecular Biology of the Cell*, *27*(11), 1834–1844. https://doi.org/10.1091/mbc.E15-03-0123

Cozza, A., Melissari, E., Iacopetti, P., Mariotti, V., Tedde, A., Nacmias, B., Conte, A., Sorbi, S., & Pellegrini, S. (2008). SNPs in Neurotrophin System Genes and Alzheimer's Disease in an Italian Population. *Journal of Alzheimer's Disease*, *15*, 61–70. https://doi.org/10.3233/JAD-2008-15105

Craig, T. J., & Henley, J. M. (2012). SUMOylation, Arc and the regulation homeostatic synaptic scaling. *Communicative & Integrative Biology*, *5*(6), 634–636. https://doi.org/10.4161/cib.21712

Cruz-Bustos, T., Ibarrola-Vannucci, A. K., Díaz-Lozano, I., Ramírez, J. L., & Osuna, A. (2018). Characterization and functionality of two members of the SPFH protein superfamily,

prohibitin 1 and 2 in Leishmania major. *Parasites & Vectors*, *11*(1), 622. https://doi.org/10.1186/s13071-018-3195-8

Csizmadia, T., & Juhász, G. (2020). Chapter Eleven - Crinophagy mechanisms and its potential role in human health and disease. In A. B. Martinez & L. Galluzzi (Eds.), *Progress in Molecular Biology and Translational Science* (Vol. 172, pp. 239–255). Academic Press. https://doi.org/https://doi.org/10.1016/bs.pmbts.2020.02.002

Csizmadia, T., Lőrincz, P., Hegedűs, K., Széplaki, S., Lőw, P., & Juhász, G. (2017). Molecular mechanisms of developmentally programmed crinophagy in Drosophila. *Journal of Cell Biology*, *217*(1), 361–374. https://doi.org/10.1083/jcb.201702145

Cui, Y., Carosi, J. M., Yang, Z., Ariotti, N., Kerr, M. C., Parton, R. G., Sargeant, T. J., & Teasdale, R. D. (2018). Retromer has a selective function in cargo sorting via endosome transport carriers. *Journal of Cell Biology*, *218*(2), 615–631. https://doi.org/10.1083/jcb.201806153

D'Agostino, L., Nie, Y., Goswami, S., Tong, K., Yu, S., Bandyopadhyay, S., Flores, J., Zhang, X., Balasubramanian, I., Joseph, I., Sakamori, R., Farrell, V., Li, Q., Yang, C. S., Gao, B., Ferraris, R. P., Yehia, G., Bonder, E. M., Goldenring, J. R., … Gao, N. (2019). Recycling Endosomes in Mature Epithelia Restrain Tumorigenic Signaling. *Cancer Research*, *79*(16), 4099–4112. https://doi.org/10.1158/0008-5472.CAN-18-4075

Dar, G. H., Mendes, C. C., Kuan, W.-L., Speciale, A. A., Conceição, M., Görgens, A., Uliyakina, I., Lobo, M. J., Lim, W. F., EL Andaloussi, S., Mäger, I., Roberts, T. C., Barker, R. A., Goberdhan, D. C. I., Wilson, C., & Wood, M. J. A. (2021). GAPDH controls extracellular vesicle biogenesis and enhances the therapeutic potential of EV mediated siRNA delivery to the brain. *Nature Communications*, *12*(1), 6666. https://doi.org/10.1038/s41467-021-27056-3

Daumke, O., & Lewin, G. R. (2022). SPFH protein cage — one ring to rule them all. *Cell Research*, *32*(2), 117–118. https://doi.org/10.1038/s41422-021-00605-7

David, G., & Zimmermann, P. (2016). Heparanase tailors syndecan for exosome production. *Molecular & Cellular Oncology*, *3*(3), e1047556. https://doi.org/10.1080/23723556.2015.1047556

de Godoy, M. A., Saraiva, L. M., de Carvalho, L. R. P., Vasconcelos-dos-Santos, A., Beiral, H. J. V, Ramos, A. B., Silva, L. R. de P., Leal, R. B., Monteiro, V. H. S., Braga, C. V, de Araujo-Silva, C. A., Sinis, L. C., Bodart-Santos, V., Kasai-Brunswick, T. H., Alcantara, C. de L., Lima, A. P. C. A., da Cunha-e Silva, N. L., Galina, A., Vieyra, A., … Ferreira, S. T. (2018). Mesenchymal stem cells and cell-derived extracellular vesicles protect hippocampal neurons from oxidative stress and synapse damage induced by amyloid-β oligomers. *Journal of Biological Chemistry*, *293*(6), 1957–1975. https://doi.org/10.1074/jbc.M117.807180

Deepa Maheshvare, M., Raha, S., König, M., & Pal, D. (2023). A pathway model of glucose-stimulated insulin secretion in the pancreatic β-cell. *Frontiers in Endocrinology*, *14*. https://doi.org/10.3389/fendo.2023.1185656

Delevoye, C., Heiligenstein, X., Ripoll, L., Gilles-Marsens, F., Dennis, M. K., Linares, R. A., Derman, L., Gokhale, A., Morel, E., Faundez, V., Marks, M. S., & Raposo, G. (2016). BLOC-1 Brings Together the Actin and Microtubule Cytoskeletons to Generate Recycling Endosomes. *Current Biology*, *26*(1), 1–13. https://doi.org/https://doi.org/10.1016/j.cub.2015.11.020

Delevoye, C., Miserey-Lenkei, S., Montagnac, G., Gilles-Marsens, F., Paul-Gilloteaux, P., Giordano, F., Waharte, F., Marks, M. S., Goud, B., & Raposo, G. (2014). Recycling endosome tubule morphogenesis from sorting endosomes requires the kinesin motor KIF13A. *Cell Reports*, *6*(3), 445–454. https://doi.org/10.1016/j.celrep.2014.01.002

Dey, A., Norrbom, C., Zhu, X., Stein, J., Zhang, C., Ueda, K., & Steiner, D. F. (2004). Furin and Prohormone Convertase 1/3 Are Major Convertases in the Processing of Mouse Pro-Growth Hormone-Releasing Hormone. *Endocrinology*, *145*(4), 1961–1971. https://doi.org/10.1210/en.2003-1472

Diao, X., Guo, C., Zheng, H., Zhao, K., Luo, Y., An, M., Lin, Y., Chen, J., Li, Y., Li, Y., Gao, X., Zhang, J., Zhou, M., Bai, W., Liu, L., Wang, G., Zhang, L., He, X., Zhang, R., … Li, S. (2023). SUMOylation-triggered ALIX activation modulates extracellular vesicles circTLCD4-RWDD3 to promote lymphatic metastasis of non-small cell lung cancer. *Signal Transduction and Targeted Therapy*, *8*(1), 426. https://doi.org/10.1038/s41392-023-01685-0

Diaz-Rohrer, B., Castello-Serrano, I., Chan, S. H., Wang, H.-Y., Shurer, C. R., Levental, K. R., & Levental, I. (2023). Rab3 mediates a pathway for endocytic sorting and plasma membrane recycling of ordered microdomains. *Proceedings of the National Academy of Sciences*, *120*(10), e2207461120. https://doi.org/10.1073/pnas.2207461120

Dickson, L. J., Liu, S., & Storrie, B. (2020). Rab6 is required for rapid, cisternal-specific, intra-Golgi cargo transport. *Scientific Reports*, *10*(1). https://doi.org/10.1038/s41598-020-73276-w

Dietzl, G., Chen, D., Schnorrer, F., Su, K.-C., Barinova, Y., Fellner, M., Gasser, B., Kinsey, K., Oppel, S., Scheiblauer, S., Couto, A., Marra, V., Keleman, K., & Dickson, B. J. (2007). A genome-wide transgenic RNAi library for conditional gene inactivation in Drosophila. *Nature*, *448*(7150), 151–156. https://doi.org/10.1038/nature05954

Dikeakos, J. D., & Reudelhuber, T. L. (2007). Sending proteins to dense core secretory granules: still a lot to sort out. *Journal of Cell Biology*, *177*(2), 191–196. https://doi.org/10.1083/jcb.200701024

Dixson, A. C., Dawson, T. R., Di Vizio, D., & Weaver, A. M. (2023). Context-specific regulation of extracellular vesicle biogenesis and cargo selection. *Nature Reviews Molecular Cell Biology*, *24*(7), 454–476. https://doi.org/10.1038/s41580-023-00576-0

Donaldson, J. G., Cassel, D., Kahn, R. A., & Klausner, R. D. (1992). ADP-ribosylation factor, a small GTP-binding protein, is required for binding of the coatomer protein beta-COP to Golgi membranes. *Proceedings of the National Academy of Sciences*, *89*(14), 6408–6412. https://doi.org/10.1073/pnas.89.14.6408

Dorostkar, M. M., & Herms, J. (2012). Arc illuminates Alzheimer's pathophysiology. *Nature Neuroscience*, *15*(10), 1323–1325. https://doi.org/10.1038/nn.3226

Drabikowski, K., Ferralli, J., Kistowski, M., Oledzki, J., Dadlez, M., & Chiquet-Ehrismann, R. (2018). Comprehensive list of SUMO targets in Caenorhabditis elegans and its implication for evolutionary conservation of SUMO signaling. *Scientific Reports*, *8*(1), 1139. https://doi.org/10.1038/s41598-018-19424-9

Duncan, R. R., Greaves, J., Wiegand, U. K., Matskevich, I., Bodammer, G., Apps, D. K., Shipston, M. J., & Chow, R. H. (2003). Functional and spatial segregation of secretory vesicle pools according to vesicle age. *Nature*, *422*(6928), 176–180. https://doi.org/10.1038/nature01389

Dunst, S., Kazimiers, T., von Zadow, F., Jambor, H., Sagner, A., Brankatschk, B., Mahmoud, A., Spannl, S., Tomancak, P., Eaton, S., & Brankatschk, M. (2015). Endogenously Tagged Rab Proteins: A Resource to Study Membrane Trafficking in Drosophila. *Developmental Cell*, *33*(3), 351–365. https://doi.org/10.1016/j.devcel.2015.03.022

Elias, S., Delestre, C., Ory, S., Marais, S., Courel, M., Vazquez-Martinez, R., Bernard, S., Coquet, L., Malagon, M. M., Driouich, A., Chan, P., Gasman, S., Anouar, Y., & Montero-Hadjadje, M. (2012). Chromogranin A Induces the Biogenesis of Granules with Calcium-

and Actin-Dependent Dynamics and Exocytosis in Constitutively Secreting Cells. *Endocrinology*, *153*(9), 4444–4456. https://doi.org/10.1210/en.2012-1436

Emdin, S. O., Dodson, G. G., Cutfield, J. M., & Cutfield, S. M. (1980). Hypothesis Role of Zinc in Insulin Biosynthesis Some Possible Zinc-lnsulin Interactions in the Pancreatic B-cell. In *Diabetologia* (Vol. 19).

Emmanouilidou, E., Melachroinou, K., Roumeliotis, T., Garbis, S. D., Ntzouni, M., Margaritis, L. H., Stefanis, L., & Vekrellis, K. (2010). Cell-Produced α-Synuclein Is Secreted in a Calcium-Dependent Manner by Exosomes and Impacts Neuronal Survival. *The Journal of Neuroscience*, *30*(20), 6838. https://doi.org/10.1523/JNEUROSCI.5699-09.2010

Enserink, J. M. (2015). Sumo and the cellular stress response. *Cell Division*, *10*(1), 4. https://doi.org/10.1186/s13008-015-0010-1

Escrevente, C., Bento-Lopes, L., Ramalho, J. S., & Barral, D. C. (2021). Rab11 is required for lysosome exocytosis through the interaction with Rab3a, Sec15 and GRAB. *Journal of Cell Science*, *134*(11), jcs246694. https://doi.org/10.1242/jcs.246694

Esmaeili, A., Alini, M., Baghaban Eslaminejad, M., & Hosseini, S. (2022). Engineering strategies for customizing extracellular vesicle uptake in a therapeutic context. *Stem Cell Research & Therapy*, *13*(1), 129. https://doi.org/10.1186/s13287-022-02806-2

Falcón-Pérez, J. M., Nazarian, R., Sabatti, C., & Dell'Angelica, E. C. (2005). Distribution and dynamics of Lamp1-containing endocytic organelles in fibroblasts deficient in BLOC-3. *Journal of Cell Science*, *118*(22), 5243–5255. https://doi.org/10.1242/jcs.02633

Fan, S., Kroeger, B., Marie, P. P., Bridges, E. M., Mason, J. D., McCormick, K., Zois, C. E., Sheldon, H., Khalid Alham, N., Johnson, E., Ellis, M., Stefana, M. I., Mendes, C. C., Wainwright, S. M., Cunningham, C., Hamdy, F. C., Morris, J. F., Harris, A. L., Wilson, C., &

Goberdhan, D. C. (2020). Glutamine deprivation alters the origin and function of cancer cell exosomes. *The EMBO Journal*, *39*(16). https://doi.org/10.15252/embj.2019103009

Fares, J., Kashyap, R., & Zimmermann, P. (2017). Syntenin: Key player in cancer exosome biogenesis and uptake? *Cell Adhesion & Migration*, *11*(2), 124–126. https://doi.org/10.1080/19336918.2016.1225632

Faúndez, V., Horng, J.-T., & Kelly, R. B. (1997). ADP Ribosylation Factor 1 Is Required for Synaptic Vesicle Budding in PC12 Cells. In *The Journal of Cell Biology* (Vol. 138, Issue 3). http://www.jcb.org

Fedorka, K. M., Linder, J. E., Winterhalter, W., & Promislow, D. (2007). Post-mating disparity between potential and realized immune response in Drosophila melanogaster. *Proceedings of the Royal Society B: Biological Sciences*, *274*(1614), 1211–1217. https://doi.org/10.1098/rspb.2006.0394

Feng, D., Zhao, W.-L., Ye, Y.-Y., Bai, X.-C., Liu, R.-Q., Chang, L.-F., Zhou, Q., & Sui, S.-F. (2010). Cellular Internalization of Exosomes Occurs Through Phagocytosis. *Traffic*, *11*(5), 675–687. https://doi.org/https://doi.org/10.1111/j.1600-0854.2010.01041.x

Fernandez-Abascal, J., & Artal-Sanz, M. (2022). Prohibitins in neurodegeneration and mitochondrial homeostasis. In *Frontiers in Aging* (Vol. 3). Frontiers Media S.A. https://doi.org/10.3389/fragi.2022.1043300

Ferro, E., Bosia, C., & Campa, C. C. (2021). RAB11-Mediated Trafficking and Human Cancers: An Updated Review. *Biology*, *10*(1). https://doi.org/10.3390/biology10010026

Finka, A., & Goloubinoff, P. (2013). Proteomic data from human cell cultures refine mechanisms of chaperone-mediated protein homeostasis. *Cell Stress and Chaperones*, *18*(5), 591–605. https://doi.org/https://doi.org/10.1007/s12192-013-0413-3

Fruman, D. A., Chiu, H., Hopkins, B. D., Bagrodia, S., Cantley, L. C., & Abraham, R. T. (2017). The PI3K Pathway in Human Disease. *Cell*, *170*(4), 605–635. https://doi.org/10.1016/j.cell.2017.07.029

Fujimoto, T., Tanaka, H., Kumamaru, E., Okamura, K., & Miki, N. (2004). Arc interacts with microtubules/microtubule-associated protein 2 and attenuates microtubule-associated protein 2 immunoreactivity in the dendrites. *Journal of Neuroscience Research*, *76*(1), 51–63. https://doi.org/https://doi.org/10.1002/jnr.20056

Futter, C. E., Collinson, L. M., Backer, J. M., & Hopkins, C. R. (2001). Human VPS34 is required for internal vesicle formation within multivesicular endosomes. *Journal of Cell Biology*, *155*(7), 1251–1264. https://doi.org/10.1083/jcb.200108152

Gabel, C. A., & Foster, S. A. (1986). Lysosomal enzyme trafficking in mannose 6-phosphate receptor-positive mouse L-cells: demonstration of a steady state accumulation of phosphorylated acid hydrolases. *Journal of Cell Biology*, *102*(3), 943–950. https://doi.org/10.1083/jcb.102.3.943

Galea, G., & Simpson, J. C. (2015). High-content analysis of Rab protein function at the ER-Golgi interface. *Bioarchitecture*, *5*(3–4), 44–53. https://doi.org/10.1080/19490992.2015.1102826

Gao, J., Li, A., Hu, J., Feng, L., Liu, L., & Shen, Z. (2023). Recent developments in isolating methods for exosomes. In *Frontiers in Bioengineering and Biotechnology* (Vol. 10). Frontiers Media S.A. https://doi.org/10.3389/fbioe.2022.1100892

Garcin, E. D. (2019). GAPDH as a model non-canonical AU-rich RNA binding protein. *Seminars in Cell & Developmental Biology*, *86*, 162–173. https://doi.org/https://doi.org/10.1016/j.semcdb.2018.03.013

Germanos, M., Gao, A., Taper, M., Yau, B., & Kebede, M. A. (2021). Inside the insulin secretory granule. In *Metabolites* (Vol. 11, Issue 8). MDPI. https://doi.org/10.3390/metabo11080515

Gershlick, D. C., & Lucas, M. (2017). Endosomal Trafficking: Retromer and Retriever Are Relatives in Recycling. *Current Biology*, *27*(22), R1233–R1236. https://doi.org/https://doi.org/10.1016/j.cub.2017.10.004

Ghoroghi, S., Mary, B., Larnicol, A., Asokan, N., Klein, A., Osmani, N., Busnelli, I., Delalande, F., Paul, N., Halary, S., Gros, F., Fouillen, L., Haeberle, A.-M., Royer, C., Spiegelhalter, C., André-Grégoire, G., Mittelheisser, V., Detappe, A., Murphy, K., … Hyenne, V. (2021). Ral GTPases promote breast cancer metastasis by controlling biogenesis and organ targeting of exosomes. *ELife*, *10*, e61539. https://doi.org/10.7554/eLife.61539

Ghossoub, R., Lembo, F., Rubio, A., Gaillard, C. B., Bouchet, J., Vitale, N., Slavík, J., Machala, M., & Zimmermann, P. (2014). Syntenin-ALIX exosome biogenesis and budding into multivesicular bodies are controlled by ARF6 and PLD2. *Nature Communications*, *5*(1), 3477. https://doi.org/10.1038/ncomms4477

Gilchrist, A., Au, C. E., Hiding, J., Bell, A. W., Fernandez-Rodriguez, J., Lesimple, S., Nagaya, H., Roy, L., Gosline, S. J. C., Hallett, M., Paiement, J., Kearney, R. E. E., Nilsson, T., & Bergeron, J. J. M. (2006). Quantitative Proteomics Analysis of the Secretory Pathway. *Cell*, *127*(6), 1265–1281. https://doi.org/10.1016/j.cell.2006.10.036

Gilleron, J., Gerdes, J. M., & Zeigerer, A. (2019). Metabolic regulation through the endosomal system. *Traffic*, *20*(8), 552–570. https://doi.org/https://doi.org/10.1111/tra.12670

Gillingham, A. K., Sinka, R., Torres, I. L., Lilley, K. S., & Munro, S. (2014). Toward a Comprehensive Map of the Effectors of Rab GTPases. *Developmental Cell*, *31*(3), 358. https://doi.org/10.1016/j.devcel.2014.10.007

Gillooly, D. J., Morrow, I. C., Lindsay, M., Gould, R., Bryant, N. J., Gaullier, J., Parton, R. G., & Stenmark, H. (2000). Localization of phosphatidylinositol 3-phosphate in yeast and mammalian cells. *The EMBO Journal*, *19*(17), 4577-4588–4588. https://doi.org/https://doi.org/10.1093/emboj/19.17.4577

Glaviano, A., Foo, A. S. C., Lam, H. Y., Yap, K. C. H., Jacot, W., Jones, R. H., Eng, H., Nair, M. G., Makvandi, P., Geoerger, B., Kulke, M. H., Baird, R. D., Prabhu, J. S., Carbone, D., Pecoraro, C., Teh, D. B. L., Sethi, G., Cavalieri, V., Lin, K. H., … Kumar, A. P. (2023). PI3K/AKT/mTOR signaling transduction pathway and targeted therapies in cancer. *Molecular Cancer*, *22*(1), 138. https://doi.org/10.1186/s12943-023-01827-6

Glombik, M. M., Krömer, A., Salm, T., Huttner, W. B., & Gerdes, H. (1999). The disulfide‐bonded loop of chromogranin B mediates membrane binding and directs sorting from the *trans*‐Golgi network to secretory granules. *The EMBO Journal*, *18*(4), 1059-1070–1070. https://doi.org/https://doi.org/10.1093/emboj/18.4.1059

Goldenring, J. R. (2015). Recycling endosomes. *Current Opinion in Cell Biology*, *35*, 117–122. https://doi.org/https://doi.org/10.1016/j.ceb.2015.04.018

Gomes, A. C., Kordala, A. J., Strack, R., Wang, X., Geslain, R., Delaney, K., Clark, W. C., Keenan, R., & Pan, T. (2016). A dual fluorescent reporter for the investigation of methionine mistranslation in live cells. *RNA*, *22*(3), 467–476. https://doi.org/10.1261/rna.054163.115

Gonda, A., Kabagwira, J., Senthil, G. N., & Wall, N. R. (2019). Internalization of Exosomes through Receptor-Mediated Endocytosis. *Molecular Cancer Research*, *17*(2), 337–347. https://doi.org/10.1158/1541-7786.MCR-18-0891

Goud, B., Liu, S., & Storrie, B. (2018). Rab proteins as major determinants of the Golgi complex structure. *Small GTPases*, *9*(1–2), 66–75. https://doi.org/10.1080/21541248.2017.1384087

Goyal, A., Agrawal, A., Verma, A., & Dubey, N. (2023). The PI3K-AKT pathway: A plausible therapeutic target in Parkinson's disease. *Experimental and Molecular Pathology*, *129*, 104846. https://doi.org/https://doi.org/10.1016/j.yexmp.2022.104846

Gramates, L. S., Agapite, J., Attrill, H., Calvi, B. R., Crosby, M. A., dos Santos, G., Goodman, J. L., Goutte-Gattat, D., Jenkins, V. K., Kaufman, T., Larkin, A., Matthews, B. B., Millburn, G., Strelets, V. B., & Consortium, the F. (2022). FlyBase: a guided tour of highlighted features. *Genetics*, *220*(4), iyac035. https://doi.org/10.1093/genetics/iyac035

Grant, B. D., & Donaldson, J. G. (2009). Pathways and mechanisms of endocytic recycling. *Nature Reviews Molecular Cell Biology*, *10*(9), 597–608. https://doi.org/10.1038/nrm2755

Grey, M., Dunning, C. J., Gaspar, R., Grey, C., Brundin, P., Sparr, E., & Linse, S. (2015). Acceleration of α-Synuclein Aggregation by Exosomes * . *Journal of Biological Chemistry*, *290*(5), 2969–2982. https://doi.org/10.1074/jbc.M114.585703

Gu, Y., Fang, Y., Wu, X., Xu, T., Hu, T., Xu, Y., Ma, P., Wang, Q., & Shu, Y. (2023). The emerging roles of SUMOylation in the tumor microenvironment and therapeutic implications. *Experimental Hematology & Oncology*, *12*(1), 58. https://doi.org/10.1186/s40164-023-00420-3

Guan, S., Li, Q., Liu, P., Xuan, X., & Du, Y. (2014). Experimental immunologyUmbilical cord blood-derived dendritic cells loaded with BGC823 tumor antigens and DC-derived exosomes stimulate efficient cytotoxic T-lymphocyte responses and antitumor

immunity in vitro and in vivo. *Central European Journal Of Immunology*, *39*(2), 142–151. https://doi.org/10.5114/ceji.2014.43713

Guichard, A., McGillivray, S. M., Cruz-Moreno, B., van Sorge, N. M., Nizet, V., & Bier, E. (2010). Anthrax toxins cooperatively inhibit endocytic recycling by the Rab11/Sec15 exocyst. *Nature*, *467*(7317), 854–858. https://doi.org/10.1038/nature09446

Guo, Y., Ji, X., Liu, J., Fan, D., Zhou, Q., Chen, C., Wang, W., Wang, G., Wang, H., Yuan, W., Ji, Z., & Sun, Z. (2019). Effects of exosomes on pre-metastatic niche formation in tumors. *Molecular Cancer*, *18*(1), 39. https://doi.org/10.1186/s12943-019-0995-1

Gurung, S., Perocheau, D., Touramanidou, L., & Baruteau, J. (2021). The exosome journey: from biogenesis to uptake and intracellular signalling. *Cell Communication and Signaling*, *19*(1), 47. https://doi.org/10.1186/s12964-021-00730-1

Halim, D. O., Munson, M., & Gao, F.-B. (2023). The exocyst complex in neurological disorders. *Human Genetics*, *142*(8), 1263–1270. https://doi.org/10.1007/s00439-023-02558-w

Ham, S., Lima, L. G., Chai, E. P. Z., Muller, A., Lobb, R. J., Krumeich, S., Wen, S. W., Wiegmans, A. P., & Möller, A. (2018). Breast cancer-derived exosomes alter macrophage polarization via gp130/STAT3 signaling. *Frontiers in Immunology*, *9*(MAY). https://doi.org/10.3389/fimmu.2018.00871

Hammel, I., Lagunoff, D., & Galli, S. J. (2010). Regulation of secretory granule size by the precise generation and fusion of unit granules. *Journal of Cellular and Molecular Medicine*, *14*(7), 1904–1916. https://doi.org/https://doi.org/10.1111/j.1582-4934.2010.01071.x

Hampel, H., Hardy, J., Blennow, K., Chen, C., Perry, G., Kim, S. H., Villemagne, V. L., Aisen, P., Vendruscolo, M., Iwatsubo, T., Masters, C. L., Cho, M., Lannfelt, L., Cummings, J. L., & Vergallo, A. (2021). The Amyloid-β Pathway in Alzheimer's Disease. In *Molecular*

Psychiatry (Vol. 26, Issue 10, pp. 5481–5503). Springer Nature. https://doi.org/10.1038/s41380-021-01249-0

Harding, C., Heuser, J., & Stahl, P. (1983). Receptor-mediated endocytosis of transferrin and recycling of the transferrin receptor in rat reticulocytes. *Journal of Cell Biology*, *97*(2), 329–339. https://doi.org/10.1083/jcb.97.2.329

Harris, D. A., Patel, S. H., Gucek, M., Hendrix, A., Westbroek, W., & Taraska, J. W. (2015). Exosomes Released from Breast Cancer Carcinomas Stimulate Cell Movement. *PLOS ONE*, *10*(3), e0117495-. https://doi.org/10.1371/journal.pone.0117495

Hazan, R. B., & Norton, L. (1998). The Epidermal Growth Factor Receptor Modulates the Interaction of E-cadherin with the Actin Cytoskeleton *. *Journal of Biological Chemistry*, *273*(15), 9078–9084. https://doi.org/10.1074/jbc.273.15.9078

Hazelett, C. C., & Yeaman, C. (2012). Sec5 and Exo84 Mediate Distinct Aspects of RalA-Dependent Cell Polarization. *PLOS ONE*, *7*(6), e39602-. https://doi.org/10.1371/journal.pone.0039602

He, J., Ren, W., Wang, W., Han, W., Jiang, L., Zhang, D., & Guo, M. (2022). Exosomal targeting and its potential clinical application. *Drug Delivery and Translational Research*, *12*(10), 2385–2402. https://doi.org/10.1007/s13346-021-01087-1

Heidarzadeh, M., Zarebkohan, A., Rahbarghazi, R., & Sokullu, E. (2023). Protein corona and exosomes: new challenges and prospects. *Cell Communication and Signaling*, *21*(1), 64. https://doi.org/10.1186/s12964-023-01089-1

Helle, K. B. (2004). The granin family of uniquely acidic proteins of the diffuse neuroendocrine system: comparative and functional aspects. *Biological Reviews*, *79*(4), 769–794. https://doi.org/DOI: 10.1017/S146479310400644X

Hemmings, B. A., & Restuccia, D. F. (2012). PI3K-PKB/Akt pathway. *Cold Spring Harbor Perspectives in Biology*, *4*(9). https://doi.org/10.1101/cshperspect.a011189

Henne, W. M., Buchkovich, N. J., & Emr, S. D. (2011). The ESCRT Pathway. *Developmental Cell*, *21*(1), 77–91. https://doi.org/https://doi.org/10.1016/j.devcel.2011.05.015

Herndon, L. A., Chapman, T., Kalb, J. M., Lewin, S., Partridge, L., & Wolfner, M. F. (1997). Mating and hormonal triggers regulate accessory gland gene expression in male Drosophila. *Journal of Insect Physiology*, *43*(12), 1117–1123. https://doi.org/https://doi.org/10.1016/S0022-1910(97)00062-0

Herold, Z., Doleschall, M., & Somogyi, A. (2021). Role and function of granin proteins in diabetes mellitus. *World Journal of Diabetes*, *12*(7), 1081–1092. https://doi.org/10.4239/wjd.v12.i7.1081

Hirano, S., Kawasaki, M., Ura, H., Kato, R., Raiborg, C., Stenmark, H., & Wakatsuki, S. (2006). Double-sided ubiquitin binding of Hrs-UIM in endosomal protein sorting. *Nature Structural & Molecular Biology*, *13*(3), 272–277. https://doi.org/10.1038/nsmb1051

Hochstrasser, M. (2009). Origin and function of ubiquitin-like proteins. *Nature*, *458*(7237), 422–429. https://doi.org/10.1038/nature07958

Hölttä-Vuori, M., Uronen, R.-L., Repakova, J., Salonen, E., Vattulainen, I., Panula, P., Li, Z., Bittman, R., & Ikonen, E. (2008). BODIPY-Cholesterol: A New Tool to Visualize Sterol Trafficking in Living Cells and Organisms. *Traffic*, *9*(11), 1839–1849. https://doi.org/https://doi.org/10.1111/j.1600-0854.2008.00801.x

Homma, Y., Hiragi, S., & Fukuda, M. (2021). Rab family of small GTPases: an updated view on their regulation and functions. In *FEBS Journal* (Vol. 288, Issue 1, pp. 36–55). Blackwell Publishing Ltd. https://doi.org/10.1111/febs.15453

Hopkins, B. D., Goncalves, M. D., & Cantley, L. C. (2020). Insulin–PI3K signalling: an evolutionarily insulated metabolic driver of cancer. In *Nature Reviews Endocrinology* (Vol. 16, Issue 5, pp. 276–283). Nature Research. https://doi.org/10.1038/s41574-020-0329-9

Horgan, C. P., & McCaffrey, M. W. (2009). The dynamic Rab11-FIPs. *Biochemical Society Transactions*, *37*(5), 1032–1036. https://doi.org/10.1042/BST0371032

Hosaka, M., Suda, M., Sakai, Y., Izumi, T., Watanabe, T., & Takeuchi, T. (2004). Secretogranin III Binds to Cholesterol in the Secretory Granule Membrane as an Adapter for Chromogranin A *. *Journal of Biological Chemistry*, *279*(5), 3627–3634. https://doi.org/10.1074/jbc.M310104200

Hosseini-Beheshti, E., Choi, W., Weiswald, L.-B., Kharmate, G., Ghaffari, M., Roshan-Moniri, M., Hassona, M. D., Chan, L., Chin, M. Y., Tai, I. T., Rennie, P. S., Fazli, L., & Tomlinson Guns, E. S. (2016). Exosomes confer pro-survival signals to alter the phenotype of prostate cells in their surrounding environment. *Oncotarget*, *7*(12), 14639–14658. www.impactjournals.com/oncotarget/

Hsu, C., Morohashi, Y., Yoshimura, S., Manrique-Hoyos, N., Jung, S., Lauterbach, M. A., Bakhti, M., Grønborg, M., Möbius, W., Rhee, J., Barr, F. A., & Simons, M. (2010). Regulation of exosome secretion by Rab35 and its GTPase-activating proteins TBC1D10A–C. *Journal of Cell Biology*, *189*(2), 223–232. https://doi.org/10.1083/jcb.200911018

Hu, Y.-B., Dammer, E. B., Ren, R.-J., & Wang, G. (2015). The endosomal-lysosomal system: from acidification and cargo sorting to neurodegeneration. *Translational Neurodegeneration*, *4*(1), 18. https://doi.org/10.1186/s40035-015-0041-1

Huang, J., Ding, Z., Luo, Q., & Xu, W. (2019). Cancer cell-derived exosomes promote cell proliferation and inhibit cell apoptosis of both normal lung fibroblasts and non-small cell lung cancer cell through delivering alpha-smooth muscle actin. *American Journal of Translational Research*, *11*, 1711–1723.

Huang, J. H., Chen, Y. N., He, H., Fu, C. H., Xu, Z. Y., & Lin, F. Y. (2023). Schwann cells-derived exosomes promote functional recovery after spinal cord injury by promoting angiogenesis. *Frontiers in Cellular Neuroscience*, *16*. https://doi.org/10.3389/fncel.2022.1077071

Huang, L., Wu, E., Liao, J., Wei, Z., Wang, J., & Chen, Z. (2023). Research Advances of Engineered Exosomes as Drug Delivery Carrier. *ACS Omega*, *8*(46), 43374–43387. https://doi.org/10.1021/acsomega.3c04479

Huang, Z., Liang, H., & Chen, L. (2020). Rab43 promotes gastric cancer cell proliferation and metastasis via regulating the pi3k/akt signaling pathway. *OncoTargets and Therapy*, *13*, 2193–2202. https://doi.org/10.2147/OTT.S237356

Huh, Y. H., Jeon, S. H., & Yoo, S. H. (2003). Chromogranin B-induced Secretory Granule Biogenesis: COMPARISON WITH THE SIMILAR ROLE OF CHROMOGRANIN A *. *Journal of Biological Chemistry*, *278*(42), 40581–40589. https://doi.org/10.1074/jbc.M304942200

Huo, D., Su, F., Yang, H., & Sun, L. (2023). Exosomal microRNAs regulate the heat stress response in sea cucumber Apostichopus japonicus. *Ecotoxicology and Environmental Safety*, *249*, 114419. https://doi.org/https://doi.org/10.1016/j.ecoenv.2022.114419

Hur, J.-Y. (2022). γ-Secretase in Alzheimer's disease. *Experimental & Molecular Medicine*, *54*(4), 433–446. https://doi.org/10.1038/s12276-022-00754-8

Huttner, W. B., Gerdes, H. H., & Rosa, P. (1991). The granin (chromogranin/secretogranin) family. *Trends in Biochemical Sciences*, *16*(1), 27–30. https://doi.org/10.1016/0968-0004(91)90012-k

Hyenne, V., Labouesse, M., & Goetz, J. G. (2018). The Small GTPase Ral orchestrates MVB biogenesis and exosome secretion. *Small GTPases*, *9*(6), 445–451. https://doi.org/10.1080/21541248.2016.1251378

Imjeti, N. S., Menck, K., Egea-Jimenez, A. L., Lecointre, C., Lembo, F., Bouguenina, H., Badache, A., Ghossoub, R., David, G., Roche, S., & Zimmermann, P. (2017). Syntenin mediates SRC function in exosomal cell-to-cell communication. *Proceedings of the National Academy of Sciences*, *114*(47), 12495–12500. https://doi.org/10.1073/pnas.1713433114

Immarigeon, C., Frei, Y., Delbare, S. Y. N., Gligorov, D., Machado Almeida, P., Grey, J., Fabbro, L., Nagoshi, E., Billeter, J.-C., Wolfner B, M. F., Karch, F., & Maeda, R. K. (2021). Identification of a micropeptide and multiple secondary cell genes that modulate Drosophila male reproductive success. *Proc Natl Acad Sci U S A*, *118*(15). https://doi.org/10.1073/pnas.2001897118/-/DCSupplemental

Immarigeon, C., Frei, Y., Delbare, S. Y. N., Gligorov, D., Machado Almeida, P., Grey, J., Fabbro, L., Nagoshi, E., Billeter, J.-C., Wolfner, M. F., Karch, F., & Maeda, R. K. (2021). Identification of a micropeptide and multiple secondary cell genes that modulate Drosophila male reproductive success. *Proceedings of the National Academy of Sciences*, *118*(15), e2001897118. https://doi.org/10.1073/pnas.2001897118

Iwanami, N., Nakamura, Y., Satoh, T., Liu, Z., & Satoh, A. K. (2016). Rab6 Is Required for Multiple Apical Transport Pathways but Not the Basolateral Transport Pathway in Drosophila Photoreceptors. *PLoS Genetics*, *12*(2). https://doi.org/10.1371/journal.pgen.1005828

Izco, M., Carlos, E., & Alvarez-Erviti, L. (2022). Impact of endolysosomal dysfunction upon exosomes in neurodegenerative diseases. *Neurobiology of Disease*, *166*, 105651. https://doi.org/https://doi.org/10.1016/j.nbd.2022.105651

Izquierdo-Useros, N., Naranjo-Gómez, M., Archer, J., Hatch, S. C., Erkizia, I., Blanco, J., Borràs, F. E., Puertas, M. C., Connor, J. H., Fernández-Figueras, M. T., Moore, L., Clotet, B., Gummuluru, S., & Martinez-Picado, J. (2009). Capture and transfer of HIV-1 particles by mature dendritic cells converges with the exosome-dissemination pathway. *Blood*, *113*(12), 2732–2741. https://doi.org/10.1182/blood-2008-05-158642

Jaber, N., Mohd-Naim, N., Wang, Z., DeLeon, J. L., Kim, S., Zhong, H., Sheshadri, N., Dou, Z., Edinger, A. L., Du, G., Braga, V. M. M., & Zong, W.-X. (2016). Vps34 regulates Rab7 and late endocytic trafficking through recruitment of the GTPase-activating protein Armus. *Journal of Cell Science*, *129*(23), 4424–4435. https://doi.org/10.1242/jcs.192260

Jacob, R. S., Das, S., Ghosh, S., Anoop, A., Jha, N. N., Khan, T., Singru, P., Kumar, A., & Maji, S. K. (2016). Amyloid formation of growth hormone in presence of zinc: Relevance to its storage in secretory granules. *Scientific Reports*, *6*. https://doi.org/10.1038/srep23370

Jadli, A. S., Parasor, A., Gomes, K. P., Shandilya, R., & Patel, V. B. (2021). Exosomes in Cardiovascular Diseases: Pathological Potential of Nano-Messenger. *Frontiers in Cardiovascular Medicine*, *8*. https://doi.org/10.3389/fcvm.2021.767488

Jean, S., & Kiger, A. A. (2014). Classes of phosphoinositide 3-kinases at a glance. *Journal of Cell Science*, *127*(5), 923–928. https://doi.org/10.1242/jcs.093773

Jeong, Y.-M., & Kim, W. (2023). FIR-preconditioning promotes Akt-mTOR-exosome manufacture in cooperation with MITF to boost resilience of rat bone marrow-derived stem cells. *Heliyon*, *9*(4). https://doi.org/10.1016/j.heliyon.2023.e15003

Jeppesen, D. K., Zhang, Q., Franklin, J. L., & Coffey, R. J. (2023). Extracellular vesicles and nanoparticles: emerging complexities. *Trends in Cell Biology*, *33*(8), 667–681. https://doi.org/10.1016/j.tcb.2023.01.002

Jewett, C. E., Soh, A. W. J., Lin, C. H., Lu, Q., Lencer, E., Westlake, C. J., Pearson, C. G., & Prekeris, R. (2021). RAB19 Directs Cortical Remodeling and Membrane Growth for Primary Ciliogenesis. *Developmental Cell*, *56*(3), 325-340.e8. https://doi.org/10.1016/j.devcel.2020.12.003

Ji, L., Wu, H.-T., Qin, X.-Y., & Lan, R. (2017). Dissecting carboxypeptidase E: properties, functions and pathophysiological roles in disease. *Endocrine Connections*, *6*(4), R18–R38. https://doi.org/10.1530/EC-17-0020

Jiang, H., Patel, P. H., Kohlmaier, A., Grenley, M. O., McEwen, D. G., & Edgar, B. A. (2009). Cytokine/Jak/Stat Signaling Mediates Regeneration and Homeostasis in the Drosophila Midgut. *Cell*, *137*(7), 1343–1355. https://doi.org/10.1016/j.cell.2009.05.014

Jiang, Y., He, R., Shi, Y., Liang, J., & Zhao, L. (2020). Plasma exosomes protect against cerebral ischemia/reperfusion injury via exosomal HSP70 mediated suppression of ROS. *Life Sciences*, *256*, 117987. https://doi.org/https://doi.org/10.1016/j.lfs.2020.117987

Jiang, Y., Sun, Y., Hu, J., Yu, N., Liu, H., Fan, J., Ning, X., Li, Y., Liu, B., Sun, Y., Zhang, J., Qiu, X., Fu, S., Zhou, C., & Xu, H. (2019). A germline mutation in Rab43 gene identified from a cancer family predisposes to a hereditary liver-colon cancer syndrome. *BMC Cancer*, *19*(1), 613. https://doi.org/10.1186/s12885-019-5845-4

Jin, H., Tang, Y., Yang, L., Peng, X., Li, B., Fan, Q., Wei, S., Yang, S., Li, X., Wu, B., Huang, M., Tang, S., Liu, J., & Li, H. (2021). Rab GTPases: Central Coordinators of Membrane

Trafficking in Cancer. In *Frontiers in Cell and Developmental Biology* (Vol. 9). Frontiers Media S.A. https://doi.org/10.3389/fcell.2021.648384

Jing, J., & Prekeris, R. (2009). *Polarized endocytic transport: The roles of Rab11 and Rab11-FIPs in regulating cell polarity*.

Joshi, B. S., de Beer, M. A., Giepmans, B. N. G., & Zuhorn, I. S. (2020). Endocytosis of Extracellular Vesicles and Release of Their Cargo from Endosomes. *ACS Nano*, *14*(4), 4444–4455. https://doi.org/10.1021/acsnano.9b10033

Juan, T., & Fürthauer, M. (2018). Biogenesis and function of ESCRT-dependent extracellular vesicles. *Seminars in Cell & Developmental Biology*, *74*, 66–77. https://doi.org/https://doi.org/10.1016/j.semcdb.2017.08.022

Juhász, G., Hill, J. H., Yan, Y., Sass, M., Baehrecke, E. H., Backer, J. M., & Neufeld, T. P. (2008). The class III PI(3)K Vps34 promotes autophagy and endocytosis but not TOR signaling in Drosophila. *Journal of Cell Biology*, *181*(4), 655–666. https://doi.org/10.1083/jcb.200712051

Kalb, J. M., DiBenedetto, A. J., & Wolfner, M. F. (1993). Probing the function of Drosophila melanogaster accessory glands by directed cell ablation. *Proceedings of the National Academy of Sciences*, *90*(17), 8093–8097. https://doi.org/10.1073/pnas.90.17.8093

Kang, X., Zuo, Z., Hong, W., Tang, H., & Geng, W. (2019). Progress of Research on Exosomes in the Protection Against Ischemic Brain Injury. In *Frontiers in Neuroscience* (Vol. 13). Frontiers Media S.A. https://doi.org/10.3389/fnins.2019.01149

Katayama, H., Yamamoto, A., Mizushima, N., Yoshimori, T., & Miyawaki, A. (2008). GFP-like Proteins Stably Accumulate in Lysosomes. *Cell Structure and Function*, *33*, 1–12. https://doi.org/10.1247/csf.07011

Katoh, K., Shibata, H., Suzuki, H., Nara, A., Ishidoh, K., Kominami, E., Yoshimori, T., & Maki, M. (2003). The ALG-2-interacting Protein Alix Associates with CHMP4b, a Human Homologue of Yeast Snf7 That Is Involved in Multivesicular Body Sorting *. *Journal of Biological Chemistry*, *278*(40), 39104–39113. https://doi.org/10.1074/jbc.M301604200

Kawamura, S., Nagano, M., Toshima, J. Y., & Toshima, J. (2014). Analysis of subcellular localization and function of the yeast Rab6 homologue, Ypt6p, using a novel amino-terminal tagging strategy. *Biochemical and Biophysical Research Communications*, *450*(1), 519–525. https://doi.org/10.1016/j.bbrc.2014.06.002

Kelly, E. E., Horgan, C. P., & McCaffrey, M. W. (2012). Rab11 proteins in health and disease. *Biochemical Society Transactions*, *40*(6), 1360–1367. https://doi.org/10.1042/BST20120157

Khan, I., & Steeg, P. S. (2021). Endocytosis: a pivotal pathway for regulating metastasis. *British Journal of Cancer*, *124*(1), 66–75. https://doi.org/10.1038/s41416-020-01179-8

Khare, N., & Baumgartner, S. (2000). Dally-like protein, a new Drosophila glypican with expression overlapping with wingless. *Mechanisms of Development*, *99*(1), 199–202. https://doi.org/https://doi.org/10.1016/S0925-4773(00)00502-5

Kim, T., Gondré-Lewis, M. C., Arnaoutova, I., & Loh, Y. P. (2006). Dense-Core Secretory Granule Biogenesis. *Physiology*, *21*(2), 124–133. https://doi.org/10.1152/physiol.00043.2005

Klumperman, J., Kuliawat, R., Griffith, J. M., Geuze, H. J., & Arvan, P. (1998). Mannose 6-Phosphate Receptors Are Sorted from Immature Secretory Granules via Adaptor Protein AP-1, Clathrin, and Syntaxin 6-positive Vesicles. In *The Journal of Cell Biology* (Vol. 141, Issue 2). http://www.jcb.org

Klumperman, J., & Raposo, G. (2014). The Complex Ultrastructure of the Endolysosomal System. *Cold Spring Harbor Perspectives in Biology*, *6*(10), a016857. https://doi.org/10.1101/cshperspect.a016857

Knox, A. L., & Brown, N. H. (2002). Rap1 GTPase Regulation of Adherens Junction Positioning and Cell Adhesion. *Science*, *295*(5558), 1285–1288. https://doi.org/10.1126/science.1067549

Kong, L., Huang, S., Bao, Y., Chen, Y., Hua, C., & Gao, S. (2023). Crucial roles of Rab22a in endosomal cargo recycling. *Traffic*, *24*(9), 397–412. https://doi.org/https://doi.org/10.1111/tra.12907

Kotelevets, L., van Hengel, J., Bruyneel, E., Mareel, M., van Roy, F., & Chastre, E. (2005). Implication of the MAGI-1b/PTEN signalosome in stabilization of adherens junctions and suppression of invasiveness. *The FASEB Journal*, *19*(1), 115–117. https://doi.org/https://doi.org/10.1096/fj.04-1942fje

Kovtun, O., Leneva, N., Bykov, Y. S., Ariotti, N., Teasdale, R. D., Schaffer, M., Engel, B. D., Owen, David. J., Briggs, J. A. G., & Collins, B. M. (2018). Structure of the membrane-assembled retromer coat determined by cryo-electron tomography. *Nature*, *561*(7724), 561–564. https://doi.org/10.1038/s41586-018-0526-z

Kowal, J., Tkach, M., & Théry, C. (2014). Biogenesis and secretion of exosomes. *Current Opinion in Cell Biology*, *29*, 116–125. https://doi.org/https://doi.org/10.1016/j.ceb.2014.05.004

Kroeger, B. R. (2017). *The genetic regulation and subcellular dynamics of secretory and endolysosomal organelles of Drosophila secondary cells*.

Kroeger, B. R., & Wilson, C. (2017). *The genetic regulation and subcellular dynamics of secretory and endolysosomal organelles of Drosophila secondary cells*.

Krylova, S. V, & Feng, D. (2023). The Machinery of Exosomes: Biogenesis, Release, and Uptake. *International Journal of Molecular Sciences*, *24*(2). https://doi.org/10.3390/ijms24021337

Kuliawat, R., & Arvan, P. (1992). Protein targeting via the “constitutive-like” secretory pathway in isolated pancreatic islets: passive sorting in the immature granule compartment. *Journal of Cell Biology*, *118*(3), 521–529. https://doi.org/10.1083/jcb.118.3.521

Kunadt, M., Eckermann, K., Stuendl, A., Gong, J., Russo, B., Strauss, K., Rai, S., Kügler, S., Falomir Lockhart, L., Schwalbe, M., Krumova, P., Oliveira, L. M. A., Bähr, M., Möbius, W., Levin, J., Giese, A., Kruse, N., Mollenhauer, B., Geiss-Friedlander, R., … Schneider, A. (2015). Extracellular vesicle sorting of α-Synuclein is regulated by sumoylation. *Acta Neuropathologica*, *129*(5), 695–713. https://doi.org/10.1007/s00401-015-1408-1

Kutateladze, T. G. (2006). Phosphatidylinositol 3-phosphate recognition and membrane docking by the FYVE domain. *Biochimica et Biophysica Acta (BBA) - Molecular and Cell Biology of Lipids*, *1761*(8), 868–877. https://doi.org/https://doi.org/10.1016/j.bbalip.2006.03.011

Kvainickas, A., Jimenez-Orgaz, A., Nägele, H., Hu, Z., Dengjel, J., & Steinberg, F. (2017). Cargo-selective SNX-BAR proteins mediate retromer trimer independent retrograde transport. *Journal of Cell Biology*, *216*(11), 3677–3693. https://doi.org/10.1083/jcb.201702137

Lafourcade, C., Sobo, K., Kieffer-Jaquinod, S., Garin, J., & van der Goot, F. G. (2008). Regulation of the V-ATPase along the Endocytic Pathway Occurs through Reversible Subunit Association and Membrane Localization. *PLOS ONE*, *3*(7), e2758-. https://doi.org/10.1371/journal.pone.0002758

Langevin, J., Morgan, M. J., Rossé, C., Racine, V., Sibarita, J.-B., Aresta, S., Murthy, M., Schwarz, T., Camonis, J., & Bellaïche, Y. (2005). Drosophila Exocyst Components Sec5, Sec6, and Sec15 Regulate DE-Cadherin Trafficking from Recycling Endosomes to the Plasma Membrane. *Developmental Cell*, *9*(3), 365–376. https://doi.org/https://doi.org/10.1016/j.devcel.2005.07.013

Larios, J., Mercier, V., Roux, A., & Gruenberg, J. (2020). ALIX- and ESCRT-III–dependent sorting of tetraspanins to exosomes. *Journal of Cell Biology*, *219*(3). https://doi.org/10.1083/jcb.201904113

Laulagnier, K., Javalet, C., Hemming, F. J., Chivet, M., Lachenal, G., Blot, B., Chatellard, C., & Sadoul, R. (2018). Amyloid precursor protein products concentrate in a subset of exosomes specifically endocytosed by neurons. *Cellular and Molecular Life Sciences*, *75*(4), 757–773. https://doi.org/10.1007/s00018-017-2664-0

Lauwers, E., Wang, Y. C., Gallardo, R., Van der Kant, R., Michiels, E., Swerts, J., Baatsen, P., Zaiter, S. S., McAlpine, S. R., Gounko, N. V., Rousseau, F., Schymkowitz, J., & Verstreken, P. (2018). Hsp90 Mediates Membrane Deformation and Exosome Release. *Molecular Cell*, *71*(5), 689-702.e9. https://doi.org/10.1016/j.molcel.2018.07.016

Le, T. K. C., Dao, X. D., Nguyen, D. V., Luu, D. H., Bui, T. M. H., Le, T. H., Nguyen, H. T., Le, T. N., Hosaka, T., & Nguyen, T. T. T. (2023). Insulin signaling and its application. In *Frontiers in Endocrinology* (Vol. 14). Frontiers Media SA. https://doi.org/10.3389/fendo.2023.1226655

Lee, P. H., Anaya, M., Ladinsky, M. S., Reitsma, J. M., & Zinn, K. (2023). An extracellular vesicle targeting ligand that binds to Arc proteins and facilitates Arc transport in vivo. *ELife*, *12*, e82874. https://doi.org/10.7554/eLife.82874

Lehane, M. J. (1988). Size of secretory granules from midgut cells of the stablefly, Stomoxys calcitrans. *Tissue and Cell*, *20*(5), 763–770. https://doi.org/https://doi.org/10.1016/0040-8166(88)90021-3

Li, B. X., Satoh, A. K., & Ready, D. F. (2007). Myosin V, Rab11, and dRip11 direct apical secretion and cellular morphogenesis in developing Drosophila photoreceptors. *Journal of Cell Biology*, *177*(4), 659–669. https://doi.org/10.1083/jcb.200610157

Li, J., Zhang, Y., Dong, P.-Y., Yang, G.-M., & Gurunathan, S. (2023). A comprehensive review on the composition, biogenesis, purification, and multifunctional role of exosome as delivery vehicles for cancer therapy. *Biomedicine & Pharmacotherapy*, *165*, 115087. https://doi.org/https://doi.org/10.1016/j.biopha.2023.115087

Li, L., Wang, S., Jezierski, A., Moalim-Nour, L., Mohib, K., Parks, R. J., Retta, S. F., & Wang, L. (2010). A unique interplay between Rap1 and E-cadherin in the endocytic pathway regulates self-renewal of human embryonic stem cells. *Stem Cells*, *28*(2), 247–257. https://doi.org/10.1002/stem.289

Li, M., Du, W., Zhou, M., Zheng, L., Song, E., & Hou, J. (2018). Proteomic analysis of insulin secretory granules in INS-1 cells by protein correlation profiling. *Biophysics Reports*, *4*(6), 329–338. https://doi.org/10.1007/s41048-018-0061-3

Liese, S., Wenzel, E. M., Kjos, I., Rojas Molina, R., Schultz, S. W., Brech, A., Stenmark, H., Raiborg, C., & Carlson, A. (2020). Protein crowding mediates membrane remodeling in upstream ESCRT-induced formation of intraluminal vesicles. *Proceedings of the National Academy of Sciences*, *117*(46), 28614–28624. https://doi.org/10.1073/pnas.2014228117

Lin, Y.-S., & Pande, V. S. (2012). Effects of Familial Mutations on the Monomer Structure of Aβ$_{42}$. *Biophysical Journal*, *103*(12), L47–L49. https://doi.org/10.1016/j.bpj.2012.11.009

Liu, C., Liu, D., Wang, S., Gan, L., Yang, X., & Ma, C. (2023). Identification of the SNARE complex that mediates the fusion of multivesicular bodies with the plasma membrane in exosome secretion. *Journal of Extracellular Vesicles*, *12*(9), 12356. https://doi.org/https://doi.org/10.1002/jev2.12356

Liu, F., Zhang, Y., Guo, Z., & Ren, A. J. (2023). The Role of Prohibitin-2 in Diseases. In *Frontiers in Bioscience - Landmark* (Vol. 28, Issue 9). IMR Press Limited. https://doi.org/10.31083/j.fbl2809211

Liu, Z., Xu, Y., Wan, Y., Gao, J., Chu, Y., & Li, J. (2019). Exosomes from adipose-derived mesenchymal stem cells prevent cardiomyocyte apoptosis induced by oxidative stress. *Cell Death Discovery*, *5*(1), 79. https://doi.org/10.1038/s41420-019-0159-5

Lock, J. G., & Stow, J. L. (2005). Rab11 in Recycling Endosomes Regulates the Sorting and Basolateral Transport of E-Cadherin □ V. *Molecular Biology of the Cell*, *16*, 1744–1755. https://doi.org/10.1091/mbc.E04

Lorenson, M. Y., Robson, D. L., & Jacobs, L. S. (1983). Divalent cation inhibition of hormone release from isolated adenohypophysial secretory granules. *Journal of Biological Chemistry*, *258*(14), 8618–8622. https://doi.org/10.1016/s0021-9258(18)32101-x

Luhtala, N., & Odorizzi, G. (2004). Bro1 coordinates deubiquitination in the multivesicular body pathway by recruiting Doa4 to endosomes. *Journal of Cell Biology*, *166*(5), 717–729. https://doi.org/10.1083/jcb.200403139

Lund, V. K., Madsen, K. L., & Kjaerulff, O. (2018). Drosophila Rab2 controls endosome-lysosome fusion and LAMP delivery to late endosomes. *Autophagy*, *14*(9), 1520–1542. https://doi.org/10.1080/15548627.2018.1458170

Ma, C., & Brill, J. A. (2021). Endosomal Rab GTPases regulate secretory granule maturation in Drosophila larval salivary glands. *Communicative and Integrative Biology*, *14*(1), 15–20. https://doi.org/10.1080/19420889.2021.1874663

Ma, C., Yang, Y., Kim, T., Chen, C. H., Polevoy, G., Vissa, M., Burgess, J., & Brill, J. A. (2020). An early endosome–derived retrograde trafficking pathway promotes secretory granule maturation. *Journal of Cell Biology*, *219*(3), e201808017. https://doi.org/10.1083/jcb.201808017

Ma, L., Ouyang, Q., Werthmann, G. C., Thompson, H. M., & Morrow, E. M. (2017). Live-cell microscopy and fluorescence-based measurement of luminal pH in intracellular organelles. *Frontiers in Cell and Developmental Biology*, *5*(AUG). https://doi.org/10.3389/fcell.2017.00071

MacDonald, C., Payne, J. A., Aboian, M., Smith, W., Katzmann, D. J., & Piper, R. C. (2015). A Family of Tetraspans Organizes Cargo for Sorting into Multivesicular Bodies. *Developmental Cell*, *33*(3), 328–342. https://doi.org/10.1016/j.devcel.2015.03.007

Machesky, L. M. (2019). Rab11FIP proteins link endocytic recycling vesicles for cytoskeletal transport and tethering. *Bioscience Reports*, *39*(1), BSR20182219. https://doi.org/10.1042/BSR20182219

Mageswaran, S. K., Dixon, M. G., Curtiss, M., Keener, J. P., & Babst, M. (2014). Binding to Any ESCRT Can Mediate Ubiquitin-Independent Cargo Sorting. *Traffic*, *15*(2), 212–229. https://doi.org/https://doi.org/10.1111/tra.12135

Makin, O. S., Atkins, E., Sikorski, P., Johansson, J., & Serpell, L. C. (2005). Molecular basis for amyloid fibril formation and stability. *Proceedings of the National Academy of Sciences*, *102*(2), 315–320. https://doi.org/10.1073/pnas.0406847102

Malik, B. R., Maddison, D. C., Smith, G. A., & Peters, O. M. (2019). Autophagic and endo-lysosomal dysfunction in neurodegenerative disease. *Molecular Brain*, *12*(1), 100. https://doi.org/10.1186/s13041-019-0504-x

Manning, A. (1962). A Sperm Factor Affecting the Receptivity of Drosophila Melanogaster Females. *Nature*, *194*(4825), 252–253. https://doi.org/10.1038/194252a0

Mao, Y., Wang, Y., Dong, L., Zhang, Y., Zhang, Y., Wang, C., Zhang, Q., Yang, S., Cao, L., Zhang, X., Li, X., & Fu, Z. (2019). Hypoxic exosomes facilitate angiogenesis and metastasis in esophageal squamous cell carcinoma through altering the phenotype and transcriptome of endothelial cells. *Journal of Experimental & Clinical Cancer Research*, *38*(1), 389. https://doi.org/10.1186/s13046-019-1384-8

Marcelić, M., Mahmutefendić Lučin, H., Jurak Begonja, A., Blagojević Zagorac, G., & Lučin, P. (2022). Early Endosomal Vps34-Derived Phosphatidylinositol-3-Phosphate Is Indispensable for the Biogenesis of the Endosomal Recycling Compartment. *Cells*, *11*(6). https://doi.org/10.3390/cells11060962

Marchese, A., Paing, M. M., Temple, B. R. S., & Trejo, J. (2008). G Protein–Coupled Receptor Sorting to Endosomes and Lysosomes. *Annual Review of Pharmacology and Toxicology*, *48*(Volume 48, 2008), 601–629. https://doi.org/https://doi.org/10.1146/annurev.pharmtox.48.113006.094646

Marco, S., Neilson, M., Moore, M., Perez-Garcia, A., Hall, H., Mitchell, L., Lilla, S., Blanco, G. R., Hedley, A., Zanivan, S., & Norman, J. C. (2021). Nuclear-capture of endosomes

depletes nuclear G-actin to promote SRF/MRTF activation and cancer cell invasion. *Nature Communications*, *12*(1), 6829. https://doi.org/10.1038/s41467-021-26839-y

Marie, P. P., Fan, S. J., Mason, J., Wells, A., Mendes, C. C., Wainwright, S. M., Scott, S., Fischer, R., Harris, A. L., Wilson, C., & Goberdhan, D. C. I. (2023). Accessory ESCRT-III proteins are conserved and selective regulators of Rab11a-exosome formation. *Journal of Extracellular Vesicles*, *12*(3). https://doi.org/10.1002/jev2.12311

Martin-Urdiroz, M., Deeks, M. J., Horton, C. G., Dawe, H. R., & Jourdain, I. (2016). The exocyst complex in health and disease. In *Frontiers in Cell and Developmental Biology* (Vol. 4, Issue APR). Frontiers Media S.A. https://doi.org/10.3389/fcell.2016.00024

Matsumoto, Y., Kano, M., Murakami, K., Toyozumi, T., Suito, H., Takahashi, M., Sekino, N., Shiraishi, T., Kamata, T., Ryuzaki, T., Hirasawa, S., Kinoshita, K., & Matsubara, H. (2020). Tumor-derived exosomes influence the cell cycle and cell migration of human esophageal cancer cell lines. *Cancer Science*, *111*(12), 4348–4358. https://doi.org/https://doi.org/10.1111/cas.14660

Matsuo, H., Chevallier, J., Mayran, N., Le Blanc, I., Ferguson, C., Fauré, J., Blanc, N. S., Matile, S., Dubochet, J., Sadoul, R., Parton, R. G., Vilbois, F., & Gruenberg, J. (2004). Role of LBPA and Alix in Multivesicular Liposome Formation and Endosome Organization. *Science*, *303*(5657), 531–534. https://doi.org/10.1126/science.1092425

McCullough, J., Frost, A., & Sundquist, W. I. (2018). Structures, Functions, and Dynamics of ESCRT-III/Vps4 Membrane Remodeling and Fission Complexes. *Annual Review of Cell and Developmental Biology*, *34*(1), 85–109. https://doi.org/10.1146/annurev-cellbio-100616-060600

McGuire, S. E., Le, P. T., Osborn, A. J., Matsumoto, K., & Davis, R. L. (2003). Spatiotemporal Rescue of Memory Dysfunction in Drosophila. *Science*, *302*(5651), 1765–1768. https://doi.org/10.1126/science.1089035

Mendonsa, A. M., Na, T.-Y., & Gumbiner, B. M. (2018). E-cadherin in contact inhibition and cancer. *Oncogene*, *37*(35), 4769–4780. https://doi.org/10.1038/s41388-018-0304-2

Miao, C., Wang, X., Zhou, W., & Huang, J. (2021). The emerging roles of exosomes in autoimmune diseases, with special emphasis on microRNAs in exosomes. *Pharmacological Research*, *169*, 105680. https://doi.org/https://doi.org/10.1016/j.phrs.2021.105680

Miaomiao, S., Xiaoqian, W., Yuwei, S., Chao, C., Chenbo, Y., Yinghao, L., Yichen, H., Jiao, S., & Kuisheng, C. (2023). Cancer-associated fibroblast-derived exosome microRNA-21 promotes angiogenesis in multiple myeloma. *Scientific Reports*, *13*(1), 9671. https://doi.org/10.1038/s41598-023-36092-6

Miranda, A. M., Lasiecka, Z. M., Xu, Y., Neufeld, J., Shahriar, S., Simoes, S., Chan, R. B., Oliveira, T. G., Small, S. A., & Di Paolo, G. (2018). Neuronal lysosomal dysfunction releases exosomes harboring APP C-terminal fragments and unique lipid signatures. *Nature Communications*, *9*(1), 291. https://doi.org/10.1038/s41467-017-02533-w

Mironov, A. A., & Arvan, P. (2008). Origins of the regulated secretory pathway. In A. A. Mironov & M. Pavelka (Eds.), *The Golgi Apparatus: State of the art 110 years after Camillo Golgi's discovery* (pp. 485–519). Springer Vienna. https://doi.org/10.1007/978-3-211-76310-0_30

Miserey-Lenkei, S., Chalancon, G., Bardin, S., Formstecher, E., Goud, B., & Echard, A. (2010). Rab and actomyosin-dependent fission of transport vesicles at the golgi complex. *Nature Cell Biology*, *12*(7), 645–654. https://doi.org/10.1038/ncb2067

Mitchell, K. J., Lai, F. A., & Rutter, G. A. (2003). Ryanodine Receptor Type I and Nicotinic Acid Adenine Dinucleotide Phosphate Receptors Mediate Ca^{2+} Release from Insulin-containing Vesicles in Living Pancreatic β-Cells (MIN6) *. *Journal of Biological Chemistry*, *278*(13), 11057–11064. https://doi.org/10.1074/jbc.M210257200

Mizuno, E., Kawahata, K., Kato, M., Kitamura, N., & Komada, M. (2003). STAM Proteins Bind Ubiquitinated Proteins on the Early Endosome via the VHS Domain and Ubiquitin-interacting Motif. *Molecular Biology of the Cell*, *14*(9), 3675–3689. https://doi.org/10.1091/mbc.e02-12-0823

Möbius, W., Van Donselaar, E., Ohno-Iwashita, Y., Shimada, Y., Heijnen, H. F. G., Slot, J. W., & Geuze, H. J. (2003). Recycling Compartments and the Internal Vesicles of Multivesicular Bodies Harbor Most of the Cholesterol Found in the Endocytic Pathway. *Traffic*, *4*(4), 222–231. https://doi.org/https://doi.org/10.1034/j.1600-0854.2003.00072.x

Moeinabadi-Bidgoli, K., Rezaee, M., Hossein-Khannazer, N., Babajani, A., Aghdaei, H. A., Arki, M. K., Afaghi, S., Niknejad, H., & Vosough, M. (2023). Exosomes for angiogenesis induction in ischemic disorders. *Journal of Cellular and Molecular Medicine*, *27*(6), 763–787. https://doi.org/https://doi.org/10.1111/jcmm.17689

Montana, E. S., & Littleton, J. T. (2006). Expression Profiling of a Hypercontraction-induced Myopathy in Drosophila Suggests a Compensatory Cytoskeletal Remodeling Response * . *Journal of Biological Chemistry*, *281*(12), 8100–8109. https://doi.org/10.1074/jbc.M512468200

Montecalvo, A., Larregina, A. T., Shufesky, W. J., Beer Stolz, D., Sullivan, M. L. G., Karlsson, J. M., Baty, C. J., Gibson, G. A., Erdos, G., Wang, Z., Milosevic, J., Tkacheva, O. A., Divito, S. J., Jordan, R., Lyons-Weiler, J., Watkins, S. C., & Morelli, A. E. (2012). Mechanism of transfer of functional microRNAs between mouse dendritic cells via exosomes. *Blood*, *119*(3), 756–766. https://doi.org/10.1182/blood-2011-02-338004

Montero-Hadjadje, M., Elias, S., Chevalier, L., Benard, M., Tanguy, Y., Turquier, V., Galas, L., Yon, L., Malagon, M. M., Driouich, A., Gasman, S., & Anouar, Y. (2009). Chromogranin A Promotes Peptide Hormone Sorting to Mobile Granules in Constitutively and Regulated Secreting Cells: ROLE OF CONSERVED N- AND C-TERMINAL PEPTIDES*. *Journal of Biological Chemistry*, *284*(18), 12420–12431. https://doi.org/10.1074/jbc.M805607200

Mutvei, A. P., Nagiec, M. J., Hamann, J. C., Kim, S. G., Vincent, C. T., & Blenis, J. (2020). Rap1-GTPases control mTORC1 activity by coordinating lysosome organization with amino acid availability. *Nature Communications*, *11*(1), 1416. https://doi.org/10.1038/s41467-020-15156-5

Nair, R. R., Patil, S., Tiron, A., Kanhema, T., Panja, D., Schiro, L., Parobczak, K., Wilczynski, G., & Bramham, C. R. (2017). Dynamic Arc SUMOylation and selective interaction with F-actin-binding protein drebrin a in LTP Consolidation in vivo. *Frontiers in Synaptic Neuroscience*, *9*(MAY). https://doi.org/10.3389/fnsyn.2017.00008

Nakano, T., Goto, S., Takaoka, Y., Tseng, H.-P., Fujimura, T., Kawamoto, S., Ono, K., & Chen, C.-L. (2018). A novel moonlight function of glyceraldehyde-3-phosphate dehydrogenase (GAPDH) for immunomodulation. *BioFactors*, *44*(6), 597–608. https://doi.org/https://doi.org/10.1002/biof.1379

Naslavsky, N., & Caplan, S. (2018). The enigmatic endosome – sorting the ins and outs of endocytic trafficking. *Journal of Cell Science*, *131*(13), jcs216499. https://doi.org/10.1242/jcs.216499

Natori, S., & Huttner, W. B. (1996). Chromogranin B (secretogranin I) promotes sorting to the regulated secretory pathway of processing intermediates derived from a peptide hormone precursor. *Proceedings of the National Academy of Sciences*, *93*(9), 4431–4436. https://doi.org/10.1073/pnas.93.9.4431

Nern, A., Pfeiffer, B. D., Svoboda, K., & Rubin, G. M. (2011). Multiple new site-specific recombinases for use in manipulating animal genomes. *Proceedings of the National Academy of Sciences*, *108*(34), 14198–14203. https://doi.org/10.1073/pnas.1111704108

Nettleton, E. J., Tito, P., Sunde, M., Bouchard, M., Dobson, C. M., & Robinson, C. V. (2000). Characterization of the oligomeric states of insulin in self-assembly and amyloid fibril formation by mass spectrometry. *Biophysical Journal*, *79*(2), 1053–1065. https://doi.org/10.1016/S0006-3495(00)76359-4

Neuman, S. D., Lee, A. R., Selegue, J. E., Cavanagh, T., & Bashirullah, A. (2021). A novel function for Rab1 and Rab11 during secretory granule maturation. *Journal of Cell Science*, *134*(15). https://doi.org/10.1242/JCS.259037

Ni, J.-Q., Liu, L.-P., Binari, R., Hardy, R., Shim, H.-S., Cavallaro, A., Booker, M., Pfeiffer, B. D., Markstein, M., Wang, H., Villalta, C., Laverty, T. R., Perkins, L. A., & Perrimon, N. (2009). A Drosophila Resource of Transgenic RNAi Lines for Neurogenetics. *Genetics*, *182*(4), 1089–1100. https://doi.org/10.1534/genetics.109.103630

Nie, H., Ju, H., Fan, J., Shi, X., Cheng, Y., Cang, X., Zheng, Z., Duan, X., & Yi, W. (2020). O-GlcNAcylation of PGK1 coordinates glycolysis and TCA cycle to promote tumor growth. *Nature Communications*, *11*(1), 36. https://doi.org/10.1038/s41467-019-13601-8

Nikolova-Karakashian, M. N., & Rozenova, K. A. (2010). Ceramide in Stress Response. In C. Chalfant & M. Del Poeta (Eds.), *Sphingolipids as Signaling and Regulatory Molecules* (pp. 86–108). Springer New York. https://doi.org/10.1007/978-1-4419-6741-1_6

Nishimura, W., Iizuka, T., Hirabayashi, S., Tanaka, N., & Hata, Y. (2000). Localization of BAI-associated protein1/membrane-associated guanylate kinase-1 at adherens junctions in normal rat kidney cells: Polarized targeting mediated by the carboxyl-terminal PDZ domains. *Journal of Cellular Physiology*, *185*(3), 358–365.

https://doi.org/https://doi.org/10.1002/1097-4652(200012)185:3<358::AID-JCP6>3.0.CO;2-#

Norris, A., & Grant, B. D. (2020). Endosomal microdomains: Formation and function. *Current Opinion in Cell Biology*, *65*, 86–95. https://doi.org/https://doi.org/10.1016/j.ceb.2020.02.018

Norris, A., Tammineni, P., Wang, S., Gerdes, J., Murr, A., Kwan, K. Y., Cai, Q., & Grant, B. D. (2017). SNX-1 and RME-8 oppose the assembly of HGRS-1/ESCRT-0 degradative microdomains on endosomes. *Proceedings of the National Academy of Sciences*, *114*(3), E307–E316. https://doi.org/10.1073/pnas.1612730114

Obermüller, S., Calegari, F., King, A., Lindqvist, A., Lundquist, I., Salehi, A., Francolini, M., Rosa, P., Rorsman, P., Huttner, W. B., & Barg, S. (2010). Defective Secretion of Islet Hormones in Chromogranin-B Deficient Mice. *PLOS ONE*, *5*(1), e8936-. https://doi.org/10.1371/journal.pone.0008936

O'Brien, R. J., & Wong, P. C. (2011). Amyloid Precursor Protein Processing and Alzheimer's Disease. *Annual Review of Neuroscience*, *34*(1), 185–204. https://doi.org/10.1146/annurev-neuro-061010-113613

Odorizzi, G., Katzmann, D. J., Babst, M., Audhya, A., & Emr, S. D. (2003). Bro1 is an endosome-associated protein that functions in the MVB pathway in Saccharomyces cerevisiae. *Journal of Cell Science*, *116*(10), 1893–1903. https://doi.org/10.1242/jcs.00395

Ostrowski, M., Carmo, N. B., Krumeich, S., Fanget, I., Raposo, G., Savina, A., Moita, C. F., Schauer, K., Hume, A. N., Freitas, R. P., Goud, B., Benaroch, P., Hacohen, N., Fukuda, M., Desnos, C., Seabra, M. C., Darchen, F., Amigorena, S., Moita, L. F., & Thery, C. (2010). Rab27a and Rab27b control different steps of the exosome secretion pathway. *Nature Cell Biology*, *12*(1), 19–30. https://doi.org/10.1038/ncb2000

O'Sullivan, M. J., & Lindsay, A. J. (2020). The Endosomal Recycling Pathway—At the Crossroads of the Cell. *International Journal of Molecular Sciences*, *21*(17). https://doi.org/10.3390/ijms21176074

Oztan, A., Silvis, M., Weisz, O. A., Bradbury, N. A., Hsu, S.-C., Goldenring, J. R., Yeaman, C., & Apodaca, G. (2007). Exocyst Requirement for Endocytic Traffic Directed Toward the Apical and Basolateral Poles of Polarized MDCK Cells. *Molecular Biology of the Cell*, *18*(10), 3978–3992. https://doi.org/10.1091/mbc.e07-02-0097

Pan, B.-T., & Johnstone, R. M. (1983). Fate of the transferrin receptor during maturation of sheep reticulocytes in vitro: Selective externalization of the receptor. *Cell*, *33*(3), 967–978. https://doi.org/10.1016/0092-8674(83)90040-5

Parchure, A., Tian, M., Stalder, D., Boyer, C. K., Bearrows, S. C., Rohli, K. E., Zhang, J., Rivera-Molina, F., Ramazanov, B. R., Mahata, S. K., Wang, Y., Stephens, S. B., Gershlick, D. C., & von Blume, J. (2022). Liquid–liquid phase separation facilitates the biogenesis of secretory storage granules. *Journal of Cell Biology*, *221*(12), e202206132. https://doi.org/10.1083/jcb.202206132

Park, D. J., Park, J.-E., Lee, S. H., Eliceiri, B. P., Choi, J. S., & Seo, Y. J. (2021). Protective effect of MSC-derived exosomes against cisplatin-induced apoptosis via heat shock protein 70 in auditory explant model. *Nanomedicine: Nanotechnology, Biology and Medicine*, *38*, 102447. https://doi.org/https://doi.org/10.1016/j.nano.2021.102447

Parolini, I., Federici, C., Raggi, C., Lugini, L., Palleschi, S., De Milito, A., Coscia, C., Iessi, E., Logozzi, M., Molinari, A., Colone, M., Tatti, M., Sargiacomo, M., & Fais, S. (2009). Microenvironmental pH Is a Key Factor for Exosome Traffic in Tumor Cells * . *Journal of Biological Chemistry*, *284*(49), 34211–34222. https://doi.org/10.1074/jbc.M109.041152

Paskeh, M. D. A., Entezari, M., Mirzaei, S., Zabolian, A., Saleki, H., Naghdi, M. J., Sabet, S., Khoshbakht, M. A., Hashemi, M., Hushmandi, K., Sethi, G., Zarrabi, A., Kumar, A. P., Tan, S. C., Papadakis, M., Alexiou, A., Islam, M. A., Mostafavi, E., & Ashrafizadeh, M. (2022). Emerging role of exosomes in cancer progression and tumor microenvironment remodeling. *Journal of Hematology & Oncology*, *15*(1), 83. https://doi.org/10.1186/s13045-022-01305-4

Patel, G. K., Khan, M. A., Zubair, H., Srivastava, S. K., Khushman, M., Singh, S., & Singh, A. P. (2019). Comparative analysis of exosome isolation methods using culture supernatant for optimum yield, purity and downstream applications. *Scientific Reports*, *9*(1), 5335. https://doi.org/10.1038/s41598-019-41800-2

Pfitzner, A.-K., Mercier, V., Jiang, X., Moser von Filseck, J., Baum, B., Šarić, A., & Roux, A. (2020). An ESCRT-III Polymerization Sequence Drives Membrane Deformation and Fission. *Cell*, *182*(5), 1140-1155.e18. https://doi.org/10.1016/j.cell.2020.07.021

Pirone, L., Xolalpa, W., Sigurðsson, J. O., Ramirez, J., Pérez, C., González, M., de Sabando, A. R., Elortza, F., Rodriguez, M. S., Mayor, U., Olsen, J. V, Barrio, R., & Sutherland, J. D. (2017). A comprehensive platform for the analysis of ubiquitin-like protein modifications using in vivo biotinylation. *Scientific Reports*, *7*(1), 40756. https://doi.org/10.1038/srep40756

Polanco, J. C., Scicluna, B. J., Hill, A. F., & Götz, J. (2016). Extracellular Vesicles Isolated from the Brains of rTg4510 Mice Seed Tau Protein Aggregation in a Threshold-dependent Manner *. *Journal of Biological Chemistry*, *291*(24), 12445–12466. https://doi.org/10.1074/jbc.M115.709485

Ponnambalam, S., & Baldwin, S. A. (2003). Constitutive protein secretion from the trans - Golgi network to the plasma membrane (Review). *Molecular Membrane Biology*, *20*(2), 129–139. https://doi.org/10.1080/0968768031000084172

Poteryaev, D., Datta, S., Ackema, K., Zerial, M., & Spang, A. (2010). Identification of the Switch in Early-to-Late Endosome Transition. *Cell*, *141*(3), 497–508. https://doi.org/10.1016/j.cell.2010.03.011

Poulain, F. E., & Yost, H. J. (2015). Heparan sulfate proteoglycans: a sugar code for vertebrate development? *Development*, *142*(20), 3456–3467. https://doi.org/10.1242/dev.098178

Pound, L. D., Sarkar, S. A., Benninger, R. K. P., Wang, Y., Suwanichkul, A., Shadoan, M. K., Printz, R. L., Oeser, J. K., Lee, C. E., Piston, D. W., McGuinness, O. P., Hutton, J. C., Powell, D. R., & O'Brien, R. M. (2009). Deletion of the mouse Slc30a8 gene encoding zinc transporter-8 results in impaired insulin secretion. *Biochemical Journal*, *421*(3), 371–376. https://doi.org/10.1042/BJ20090530

Prince, E., Kroeger, B., Gligorov, D., Wilson, C., Eaton, S., Karch, F., Brankatschk, M., & Maeda, R. K. (2019). Rab-mediated trafficking in the secondary cells of Drosophila male accessory glands and its role in fecundity. *Traffic*, *20*(2), 137–151. https://doi.org/https://doi.org/10.1111/tra.12622

Proikas-Cezanne, T., Gaugel, A., Frickey, T., & Nordheim, A. (2006). Rab14 is part of the early endosomal clathrin-coated TGN microdomain. *FEBS Letters*, *580*(22), 5241–5246. https://doi.org/https://doi.org/10.1016/j.febslet.2006.08.053

Pryor, P. R., Mullock, B. M., Bright, N. A., Lindsay, M. R., Gray, S. R., Richardson, S. C. W., Stewart, A., James, D. E., Piper, R. C., & Luzio, J. P. (2004). Combinatorial SNARE complexes with VAMP7 or VAMP8 define different late endocytic fusion events. *EMBO Reports*, *5*(6), 590-595–595. https://doi.org/https://doi.org/10.1038/sj.embor.7400150

Pylypenko, O., Hammich, H., Yu, I. M., & Houdusse, A. (2018). Rab GTPases and their interacting protein partners: Structural insights into Rab functional diversity. In *Small*

GTPases (Vol. 9, Issues 1–2, pp. 22–48). Taylor and Francis Inc. https://doi.org/10.1080/21541248.2017.1336191

Qi, A., Lamont, L., Liu, E., Murray, S. D., Meng, X., & Yang, S. (2023). Essential Protein PHB2 and Its Regulatory Mechanisms in Cancer. *Cells*, *12*(8). https://doi.org/10.3390/cells12081211

Quinn, J. P., Ethier, E. C., Kandigian, S. E., Trombetta, B. A., Arnold, S. E., & Carlyle, B. C. (2021). Characterizing proteoforms of the granin family of neuropeptides in dementia pathophysiology. *Alzheimer's & Dementia*, *17*(S3), e056265. https://doi.org/https://doi.org/10.1002/alz.056265

Quinn, J. P., Ethier, E. C., Novielli, A., Malone, A., Ramirez, C. E., Salloum, L., Trombetta, B. A., Kivisäkk, P., Bremang, M., Selzer, S., Fournier, M., Das, S., Xing, Y., Arnold, S. E., & Carlyle, B. C. (2023). Cerebrospinal Fluid and Brain Proteoforms of the Granin Neuropeptide Family in Alzheimer's Disease. *Journal of the American Society for Mass Spectrometry*, *34*(4), 649–667. https://doi.org/10.1021/jasms.2c00341

Raiborg, C., Bremnes, B., Mehlum, A., Gillooly, D. J., D'Arrigo, A., Stang, E., & Stenmark, H. (2001). FYVE and coiled-coil domains determine the specific localisation of Hrs to early endosomes. *Journal of Cell Science*, *114*(12), 2255–2263. https://doi.org/10.1242/jcs.114.12.2255

Raiborg, C., Wesche, J., Malerød, L., & Stenmark, H. (2006). Flat clathrin coats on endosomes mediate degradative protein sorting by scaffolding Hrs in dynamic microdomains. *Journal of Cell Science*, *119*(12), 2414–2424. https://doi.org/10.1242/jcs.02978

Rajendran, L., Honsho, M., Zahn, T. R., Keller, P., Geiger, K. D., Verkade, P., & Simons, K. (2006). Alzheimer's disease β-amyloid peptides are released in association with

exosomes. *Proceedings of the National Academy of Sciences*, *103*(30), 11172–11177. https://doi.org/10.1073/pnas.0603838103

Rambourg, A., Clermont, Y., & Hermo, L. (1988). Formation of secretion granules in the Golgi apparatus of pancreatic acinar cells of the rat. *American Journal of Anatomy*, *183*(3), 187–199. https://doi.org/https://doi.org/10.1002/aja.1001830302

Rambourg, A., Clermont, Y., Hermo, L., & Chrétien, M. (1989). Formation of secretion granules in the Golgi apparatus of plasma cells in the rat. *American Journal of Anatomy*, *184*(1), 52–61. https://doi.org/https://doi.org/10.1002/aja.1001840106

Redhai, S., Hellberg, J. E. E. U., Wainwright, M., Perera, S. W., Castellanos, F., Kroeger, B., Gandy, C., Leiblich, A., Corrigan, L., Hilton, T., Patel, B., Fan, S. J., Hamdy, F., Goberdhan, D. C. I., & Wilson, C. (2016). Regulation of Dense-Core Granule Replenishment by Autocrine BMP Signalling in Drosophila Secondary Cells. *PLoS Genetics*, *12*(10). https://doi.org/10.1371/journal.pgen.1006366

Reiss, A. B., Ahmed, S., Johnson, M., Saeedullah, U., & De Leon, J. (2023). Exosomes in Cardiovascular Disease: From Mechanism to Therapeutic Target. *Metabolites*, *13*(4). https://doi.org/10.3390/metabo13040479

Reynolds, A. B., Daniel, J., Mccrea, P. D., Wheelock, M. J., Wu, J., & Zhang, Z. (1994). Identification of a New Catenin: the Tyrosine Kinase Substrate p120cas Associates with E-Cadherin Complexes. *Molecular and Cellular Biology*, *14*(12), 8333–8342. https://doi.org/10.1128/mcb.14.12.8333-8342.1994

Rhodes, C. J., Lucas, C. A., Mutkoski, R. L., Orci, L., & Halban, P. A. (1987). Stimulation by ATP of proinsulin to insulin conversion in isolated rat pancreatic islet secretory granules. Association with the ATP-dependent proton pump. *Journal of Biological Chemistry*, *262*(22), 10712–10717. https://doi.org/10.1016/s0021-9258(18)61022-1

Riggs, B., Rothwell, W., Mische, S., Hickson, G. R. X., Matheson, J., Hays, T. S., Gould, G. W., & Sullivan, W. (2003). Actin cytoskeleton remodeling during early Drosophila furrow formation requires recycling endosomal components Nuclear-fallout and Rab11. *Journal of Cell Biology*, *163*(1), 143–154. https://doi.org/10.1083/jcb.200305115

Rizzoli, S. O., Bethani, I., Zwilling, D., Wenzel, D., Siddiqui, T. J., Brandhorst, D., & Jahn, R. (2006). Evidence for Early Endosome-like Fusion of Recently Endocytosed Synaptic Vesicles. *Traffic*, *7*(9), 1163–1176. https://doi.org/https://doi.org/10.1111/j.1600-0854.2006.00466.x

Rodríguez-Ramos, A., González, J. A., & Fanarraga, M. L. (2023). Enhanced Inhibition of Amyloid Formation by Heat Shock Protein 90 Immobilized on Nanoparticles. *ACS Chemical Neuroscience*, *14*(15), 2811–2817. https://doi.org/10.1021/acschemneuro.3c00370

Roher, A. E., Lowenson, J. D., Clarke, S., Woods, A. S., Cotter, R. J., Gowing, E., & Ball, M. J. (1993). beta-Amyloid-(1-42) is a major component of cerebrovascular amyloid deposits: implications for the pathology of Alzheimer disease. *Proceedings of the National Academy of Sciences*, *90*(22), 10836–10840. https://doi.org/10.1073/pnas.90.22.10836

Rohrer, B., Ishii, M., Nicholson, C., Brandon, C., Annamalai, B., & Shah, N. (2019). Exosome-mediated long-range communication in stressed retinal pigment epithelial cell monolayers – focus on up-take mechanisms. *Investigative Ophthalmology & Visual Science*, *60*(9), 1916.

Rojas, R., van Vlijmen, T., Mardones, G. A., Prabhu, Y., Rojas, A. L., Mohammed, S., Heck, A. J. R., Raposo, G., van der Sluijs, P., & Bonifacino, J. S. (2008). Regulation of retromer recruitment to endosomes by sequential action of Rab5 and Rab7. *Journal of Cell Biology*, *183*(3), 513–526. https://doi.org/10.1083/jcb.200804048

Romagnoli, G. G., Zelante, B. B., Toniolo, P. A., Migliori, I. K., & Barbuto, J. A. M. (2015). Dendritic cell-derived exosomes may be a tool for cancer immunotherapy by converting tumor cells into immunogenic targets. *Frontiers in Immunology*, *6*(JAN). https://doi.org/10.3389/fimmu.2014.00692

Roux, K. J., Kim, D. I., Burke, B., & May, D. G. (2018). BioID: A Screen for Protein-Protein Interactions. *Current Protocols in Protein Science*, *91*(1), 19.23.1-19.23.15. https://doi.org/https://doi.org/10.1002/cpps.51

Rowland, A. A., Chitwood, P. J., Phillips, M. J., & Voeltz, G. K. (2014). ER Contact Sites Define the Position and Timing of Endosome Fission. *Cell*, *159*(5), 1027–1041. https://doi.org/10.1016/j.cell.2014.10.023

Russo, A. F. (2017). Overview of Neuropeptides: Awakening the Senses? *Headache: The Journal of Head and Face Pain*, *57*(S2), 37–46. https://doi.org/https://doi.org/10.1111/head.13084

Ryder, P. V, Vistein, R., Gokhale, A., Seaman, M. N., Puthenveedu, M. A., & Faundez, V. (2013). The WASH complex, an endosomal Arp2/3 activator, interacts with the Hermansky–Pudlak syndrome complex BLOC-1 and its cargo phosphatidylinositol-4-kinase type IIα. *Molecular Biology of the Cell*, *24*(14), 2269–2284. https://doi.org/10.1091/mbc.e13-02-0088

Ryu, H.-Y., Ahn, S. H., & Hochstrasser, M. (2020). SUMO and cellular adaptive mechanisms. *Experimental & Molecular Medicine*, *52*(6), 931–939. https://doi.org/10.1038/s12276-020-0457-2

Salton, S., & Lin, W. (2013). The Regulated Secretory Pathway and Human Disease: Insights from Gene Variants and Single Nucleotide Polymorphisms. *Frontiers in Endocrinology*, *4*. https://doi.org/10.3389/fendo.2013.00096

Sánchez-Alegría, K., Flores-León, M., Avila-Muñoz, E., Rodríguez-Corona, N., & Arias, C. (2018). PI3K Signaling in Neurons: A Central Node for the Control of Multiple Functions. *International Journal of Molecular Sciences*, *19*(12). https://doi.org/10.3390/ijms19123725

Sancho-Albero, M., Navascués, N., Mendoza, G., Sebastián, V., Arruebo, M., Martín-Duque, P., & Santamaría, J. (2019). Exosome origin determines cell targeting and the transfer of therapeutic nanoparticles towards target cells. *Journal of Nanobiotechnology*, *17*(1), 16. https://doi.org/10.1186/s12951-018-0437-z

Santarosa, M., & Maestro, R. (2021). The Autophagic Route of E-Cadherin and Cell Adhesion Molecules in Cancer Progression. *Cancers*, *13*(24). https://doi.org/10.3390/cancers13246328

Saraste, J. (2016). Spatial and functional aspects of ER-Golgi Rabs and Tethers. *Frontiers in Cell and Developmental Biology*, *4*(APR). https://doi.org/10.3389/fcell.2016.00028

Saravanan, P. B., Vasu, S., Yoshimatsu, G., Darden, C. M., Wang, X., Gu, J., Lawrence, M. C., & Naziruddin, B. (2019). Differential expression and release of exosomal miRNAs by human islets under inflammatory and hypoxic stress. *Diabetologia*, *62*(10), 1901–1914. https://doi.org/10.1007/s00125-019-4950-x

Sassone, J., Reale, C., Dati, G., Regoni, M., Pellecchia, M. T., & Garavaglia, B. (2021). The Role of VPS35 in the Pathobiology of Parkinson's Disease. In *Cellular and Molecular Neurobiology* (Vol. 41, Issue 2, pp. 199–227). Springer. https://doi.org/10.1007/s10571-020-00849-8

Satoh, T., Nakamura, Y., & Satoh, A. K. (2016). Rab6 functions in polarized transport in Drosophila photoreceptors. In *Fly* (Vol. 10, Issue 3, pp. 123–127). Taylor and Francis Inc. https://doi.org/10.1080/19336934.2016.1182273

Schirmer, C., Lepvrier, E., Duchesne, L., Decaux, O., Thomas, D., Delamarche, C., & Garnier, C. (2016). Hsp90 directly interacts, in vitro, with amyloid structures and modulates their assembly and disassembly. *Biochimica et Biophysica Acta (BBA) - General Subjects*, *1860*(11, Part A), 2598–2609. https://doi.org/https://doi.org/10.1016/j.bbagen.2016.07.033

Schleinitz, A., Pöttgen, L. A., Keren-Kaplan, T., Pu, J., Saftig, P., Bonifacino, J. S., Haas, A., & Jeschke, A. (2023). Consecutive functions of small GTPases guide HOPS-mediated tethering of late endosomes and lysosomes. *Cell Reports*, *42*(1). https://doi.org/10.1016/j.celrep.2022.111969

Schmidt, W. K., & Moore, H. P. (1995). Ionic milieu controls the compartment-specific activation of pro-opiomelanocortin processing in AtT-20 cells. *Molecular Biology of the Cell*, *6*(10), 1271–1285. https://doi.org/10.1091/mbc.6.10.1271

Schulz, L., Ramirez, P., Lemieux, A., Gonzalez, E., Thomson, T., & Frost, B. (2023). Tau-Induced Elevation of the Activity-Regulated Cytoskeleton Associated Protein Arc1 Causally Mediates Neurodegeneration in the Adult Drosophila Brain. *Neuroscience*, *518*, 101–111. https://doi.org/10.1016/j.neuroscience.2022.04.017

Scott, C. C., Vacca, F., & Gruenberg, J. (2014). Endosome maturation, transport and functions. *Seminars in Cell & Developmental Biology*, *31*, 2–10. https://doi.org/https://doi.org/10.1016/j.semcdb.2014.03.034

Seaman, M. N. J. (2021). The Retromer Complex: From Genesis to Revelations. *Trends in Biochemical Sciences*, *46*(7), 608–620. https://doi.org/https://doi.org/10.1016/j.tibs.2020.12.009

Seeler, J.-S., & Dejean, A. (2017). SUMO and the robustness of cancer. *Nature Reviews Cancer*, *17*(3), 184–197. https://doi.org/10.1038/nrc.2016.143

Segev, Nava. (2009). *Trafficking inside cells : pathways, mechanisms, and regulation*. Landes Bioscience.

Seidah, N. G., Sadr, M. S., Chrétien, M., & Mbikay, M. (2013). The Multifaceted Proprotein Convertases: Their Unique, Redundant, Complementary, and Opposite Functions * . *Journal of Biological Chemistry*, *288*(30), 21473–21481. https://doi.org/10.1074/jbc.R113.481549

Sekar, R. B., & Periasamy, A. (2003). Fluorescence resonance energy transfer (FRET) microscopy imaging of live cell protein localizations. *Journal of Cell Biology*, *160*(5), 629–633. https://doi.org/10.1083/jcb.200210140

Shakya, S., Sharma, P., Bhatt, A. M., Jani, R. A., Delevoye, C., & Gangi Setty, S. R. (2018). Rab22A recruits BLOC‐1 and BLOC‐2 to promote the biogenesis of recycling endosomes. *EMBO Reports*, *19*(12), e45918. https://doi.org/https://doi.org/10.15252/embr.201845918

Shelke, G. V., Yin, Y., Jang, S. C., Lässer, C., Wennmalm, S., Hoffmann, H. J., Li, L., Gho, Y. S., Nilsson, J. A., & Lötvall, J. (2019). Endosomal signalling via exosome surface TGFβ-1. *Journal of Extracellular Vesicles*, *8*(1), 1650458. https://doi.org/https://doi.org/10.1080/20013078.2019.1650458

Shennan, K. I., Taylor, N. A., & Docherty, K. (1994). Calcium- and pH-dependent aggregation and membrane association of the precursor of the prohormone convertase PC2. *Journal of Biological Chemistry*, *269*(28), 18646–18650. https://doi.org/https://doi.org/10.1016/S0021-9258(17)32358-X

Shipitsin, M., & Feig, L. A. (2004). RalA but Not RalB Enhances Polarized Delivery of Membrane Proteins to the Basolateral Surface of Epithelial Cells. *Molecular and Cellular Biology*, *24*(13), 5746–5756. https://doi.org/10.1128/MCB.24.13.5746-5756.2004

Shirakawa, R., & Horiuchi, H. (2015). Ral GTPases: crucial mediators of exocytosis and tumourigenesis. *The Journal of Biochemistry*, *157*(5), 285–299. https://doi.org/10.1093/jb/mvv029

Siekevitz, P., & Palade, G. E. (1958a). A Cytochemical Study on the Pancreas of the Guinea Pig : I. Isolation and Enzymatic Activities of Cell Fractions. *The Journal of Biophysical and Biochemical Cytology*, *4*(2), 203–218. https://doi.org/10.1083/jcb.4.2.203

Siekevitz, P., & Palade, G. E. (1958b). A Cytochemical Study on the Pancreas of the Guinea Pig : II. Functional Variations in the Enzymatic Activity of Microsomes. *The Journal of Biophysical and Biochemical Cytology*, *4*(3), 309–318. https://doi.org/10.1083/jcb.4.3.309

Siekevitz, P., & Palade, G. E. (1958c). A Cytochemical Study on the Pancreas of the Guinea Pig : III. In Vivo Incorporation of Leucine-1-C14 into the Proteins of Cell Fractions. *The Journal of Biophysical and Biochemical Cytology*, *4*(5), 557–566. https://doi.org/10.1083/jcb.4.5.557

Simonetti, B., & Cullen, P. J. (2019). Actin-dependent endosomal receptor recycling. *Current Opinion in Cell Biology*, *56*, 22–33. https://doi.org/https://doi.org/10.1016/j.ceb.2018.08.006

Simonetti, B., Danson, C. M., Heesom, K. J., & Cullen, P. J. (2017). Sequence-dependent cargo recognition by SNX-BARs mediates retromer-independent transport of CI-MPR. *Journal of Cell Biology*, *216*(11), 3695–3712. https://doi.org/10.1083/jcb.201703015

Singh, A., Das, K., Banerjee, S., & Sen, P. (2023). Elucidation of the signalling pathways for enhanced exosome release from Mycobacterium-infected macrophages and subsequent induction of differentiation. *Immunology*, *168*(1), 63–82. https://doi.org/https://doi.org/10.1111/imm.13561

Singh, P. (2023). *The physiological and pathological aggregation of transforming growth factor-β-induced and amyloid precursor protein in drosophila secondary cells*.

Singh, P. J., Verma, B., Wells, A., Mendes, C. C., Dunn, D., Chen, Y.-N., Oh, J., Blincowe, L., Wainwright, S. M., Fischer, R., Fan, S.-J., Harris, A. L., Goberdhan, D. C. I., & Wilson, C. (2024). APP and β-amyloid modulate protein aggregation and dissociation from recycling endosomal and exosomal membranes. *BioRxiv*. https://doi.org/10.1101/2024.03.28.586966

Skryabin, G. O., Komelkov, A. V., Savelyeva, E. E., & Tchevkina, E. M. (2020). Lipid Rafts in Exosome Biogenesis. In *Biochemistry (Moscow)* (Vol. 85, Issue 2, pp. 177–191). Pleiades journals. https://doi.org/10.1134/S0006297920020054

Smith, Z. J., Lee, C., Rojalin, T., Carney, R. P., Hazari, S., Knudson, A., Lam, K., Saari, H., Ibañez, E. L., Viitala, T., Laaksonen, T., Yliperttula, M., & Wachsmann-Hogiu, S. (2015). Single exosome study reveals subpopulations distributed among cell lines with variability related to membrane content. *Journal of Extracellular Vesicles*, *4*(1), 28533. https://doi.org/https://doi.org/10.3402/jev.v4.28533

Sönnichsen, B., De Renzis, S., Nielsen, E., Rietdorf, J., & Zerial, M. (2000). Distinct Membrane Domains on Endosomes in the Recycling Pathway Visualized by Multicolor Imaging of Rab4, Rab5, and Rab11. *Journal of Cell Biology*, *149*(4), 901–914. https://doi.org/10.1083/jcb.149.4.901

Stalder, D., & Gershlick, D. C. (2020). Direct trafficking pathways from the Golgi apparatus to the plasma membrane. *Seminars in Cell & Developmental Biology*, *107*, 112–125. https://doi.org/10.1016/j.semcdb.2020.04.001

Stefani, C., Miricescu, D., Stanescu-Spinu, I.-I., Nica, R. I., Greabu, M., Totan, A. R., & Jinga, M. (2021). Growth Factors, PI3K/AKT/mTOR and MAPK Signaling Pathways in Colorectal

Cancer Pathogenesis: Where Are We Now? *International Journal of Molecular Sciences*, *22*(19). https://doi.org/10.3390/ijms221910260

Stuffers, S., Sem Wegner, C., Stenmark, H., & Brech, A. (2009). Multivesicular Endosome Biogenesis in the Absence of ESCRTs. *Traffic*, *10*(7), 925–937. https://doi.org/https://doi.org/10.1111/j.1600-0854.2009.00920.x

Sturchio, A., Dwivedi, A. K., Young, C. B., Malm, T., Marsili, L., Sharma, J. S., Mahajan, A., Hill, E. J., Andaloussi, S. E. L., Poston, K. L., Manfredsson, F. P., Schneider, L. S., Ezzat, K., & Espay, A. J. (2021). High cerebrospinal amyloid-β 42 is associated with normal cognition in individuals with brain amyloidosis. *EClinicalMedicine*, *38*. https://doi.org/10.1016/j.eclinm.2021.100988

Subra, C., Grand, D., Laulagnier, K., Stella, A., Lambeau, G., Paillasse, M., De Medina, P., Monsarrat, B., Perret, B., Silvente-Poirot, S., Poirot, M., & Record, M. (2010). Exosomes account for vesicle-mediated transcellular transport of activatable phospholipases and prostaglandins [S]. *Journal of Lipid Research*, *51*(8), 2105–2120. https://doi.org/10.1194/jlr.M003657

Sugawara, K., Shibasaki, T., Mizoguchi, A., Saito, T., & Seino, S. (2009a). Rab11 and its effector Rip11 participate in regulation of insulin granule exocytosis. *Genes to Cells*, *14*(4), 445–456. https://doi.org/10.1111/j.1365-2443.2009.01285.x

Sugawara, K., Shibasaki, T., Mizoguchi, A., Saito, T., & Seino, S. (2009b). Rab11 and its effector Rip11 participate in regulation of insulin granule exocytosis. *Genes to Cells*, *14*(4), 445–456. https://doi.org/https://doi.org/10.1111/j.1365-2443.2009.01285.x

Sullivan, C. P., Jay, A. G., Stack, E. C., Pakaluk, M., Wadlinger, E., Fine, R. E., Wells, J. M., & Morin, P. J. (2011). Retromer disruption promotes amyloidogenic APP processing.

Neurobiology of Disease, *43*(2), 338–345. https://doi.org/https://doi.org/10.1016/j.nbd.2011.04.002

Sun, Z., & Brodsky, J. L. (2019). Protein quality control in the secretory pathway. *Journal of Cell Biology*, *218*(10), 3171–3187. https://doi.org/10.1083/jcb.201906047

Sun-wada, G. H., Toyomura, T., Murata, Y., Yamamoto, A., Futai, M., & Wada, Y. (2006). The a3 isoform of V-ATPase regulates insulin secretion from pancreatic β-cells. *Journal of Cell Science*, *119*(21), 4531–4540. https://doi.org/10.1242/jcs.03234

Svensson, G., Awad, W., Håkansson, M., Mani, K., & Logan, D. T. (2012). Crystal Structure of N-Glycosylated Human Glypican-1 Core Protein: STRUCTURE OF TWO LOOPS EVOLUTIONARILY CONSERVED IN VERTEBRATE GLYPICAN-1 *. *Journal of Biological Chemistry*, *287*(17), 14040–14051. https://doi.org/10.1074/jbc.M111.322487

Swanson, M. J., Lewis, K. N., Carpenter, R., Whetzel, A., & Bae, N. S. (2023). The human RAP1 and GFAPε proteins increase γ-secretase activity in a yeast model system. *G3 Genes|Genomes|Genetics*, *13*(8), jkad057. https://doi.org/10.1093/g3journal/jkad057

Szenci, G., Csizmadia, T., & Juhász, G. (2023). The role of crinophagy in quality control of the regulated secretory pathway. *Journal of Cell Science*, *136*(8), jcs260741. https://doi.org/10.1242/jcs.260741

Tai, Y.-L., Chen, K.-C., Hsieh, J.-T., & Shen, T.-L. (2018). Exosomes in cancer development and clinical applications. *Cancer Science*, *109*(8), 2364–2374. https://doi.org/https://doi.org/10.1111/cas.13697

Takahashi, S., Kubo, K., Waguri, S., Yabashi, A., Shin, H.-W., Katoh, Y., & Nakayama, K. (2012). Rab11 regulates exocytosis of recycling vesicles at the plasma membrane. *Journal of Cell Science*, *125*(17), 4049–4057. https://doi.org/10.1242/jcs.102913

Tan, S. S., Yin, Y., Lee, T., Lai, R. C., Yeo, R. W. Y., Zhang, B., Choo, A., & Lim, S. K. (2013). Therapeutic MSC exosomes are derived from lipid raft microdomains in the plasma membrane. *Journal of Extracellular Vesicles*, *2*(1), 22614. https://doi.org/10.3402/jev.v2i0.22614

Tang, M. K. S., Yue, P. Y. K., Ip, P. P., Huang, R.-L., Lai, H.-C., Cheung, A. N. Y., Tse, K. Y., Ngan, H. Y. S., & Wong, A. S. T. (2018). Soluble E-cadherin promotes tumor angiogenesis and localizes to exosome surface. *Nature Communications*, *9*(1), 2270. https://doi.org/10.1038/s41467-018-04695-7

Tang, X., Chang, C., Guo, J., Lincoln, V., Liang, C., Chen, M., Woodley, D. T., & Li, W. (2019). Tumour-Secreted Hsp90α on External Surface of Exosomes Mediates Tumour - Stromal Cell Communication via Autocrine and Paracrine Mechanisms. *Scientific Reports*, *9*(1), 15108. https://doi.org/10.1038/s41598-019-51704-w

Tanguy, E., Carmon, O., Wang, Q., Jeandel, L., Chasserot-Golaz, S., Montero-Hadjadje, M., & Vitale, N. (2016). Lipids implicated in the journey of a secretory granule: from biogenesis to fusion. *Journal of Neurochemistry*, *137*(6), 904–912. https://doi.org/https://doi.org/10.1111/jnc.13577

Tanguy, E., Wolf, A., Wang, Q., Chasserot-Golaz, S., Ory, S., Gasman, S., & Vitale, N. (2022). Phospholipase D1-generated phosphatidic acid modulates secretory granule trafficking from biogenesis to compensatory endocytosis in neuroendocrine cells. *Advances in Biological Regulation*, *83*, 100844. https://doi.org/https://doi.org/10.1016/j.jbior.2021.100844

Taupenot, L., Harper, K. L., Mahapatra, N. R., Parmer, R. J., Mahata, S. K., & O'Connor, D. T. (2002). Identification of a novel sorting determinant for the regulated pathway in the secretory protein chromogranin A. *Journal of Cell Science*, *115*(24), 4827–4841. https://doi.org/10.1242/jcs.00140

Tauro, B. J., Greening, D. W., Mathias, R. A., Mathivanan, S., Ji, H., & Simpson, R. J. (2013). Two Distinct Populations of Exosomes Are Released from LIM1863 Colon Carcinoma Cell-derived Organoids * . *Molecular & Cellular Proteomics*, *12*(3), 587–598. https://doi.org/10.1074/mcp.M112.021303

Tebo, A. G., & Gautier, A. (2019). A split fluorescent reporter with rapid and reversible complementation. *Nature Communications*, *10*(1), 2822. https://doi.org/10.1038/s41467-019-10855-0

Tejeda-Guzmán, C., Rosas-Arellano, A., Kroll, T., Webb, S. M., Barajas-Aceves, M., Osorio, B., & Missirlis, F. (2018). Biogenesis of zinc storage granules in Drosophila melanogaster. *Journal of Experimental Biology*, *221*(6). https://doi.org/10.1242/jeb.168419

Thomas, L. L., Highland, C. M., & Fromme, J. C. (2021). Arf1 orchestrates Rab GTPase conversion at the trans-Golgi network. *Molecular Biology of the Cell*, *32*(11), 1104–1120. https://doi.org/10.1091/mbc.E20-10-0664

Thorens, B. (2015). GLUT2, glucose sensing and glucose homeostasis. *Diabetologia*, *58*(2), 221–232. https://doi.org/10.1007/s00125-014-3451-1

Tolwinski, N. S. (2017). Introduction: Drosophila—A Model System for Developmental Biology. *Journal of Developmental Biology*, *5*(3). https://doi.org/10.3390/jdb5030009

Tomas, A., Vaughan, S. O., Burgoyne, T., Sorkin, A., Hartley, J. A., Hochhauser, D., & Futter, C. E. (2015). WASH and Tsg101/ALIX-dependent diversion of stress-internalized EGFR from the canonical endocytic pathway. *Nature Communications*, *6*(1), 7324. https://doi.org/10.1038/ncomms8324

Tompkins, L. S., Nullmeyer, K. D., Murphy, S. M., Weber, C. S., & Lynch, R. M. (2002a). Regulation of secretory granule pH in insulin-secreting cells. *American Journal of*

Physiology-Cell Physiology, *283*(2), C429–C437. https://doi.org/10.1152/ajpcell.01066.2000

Tompkins, L. S., Nullmeyer, K. D., Murphy, S. M., Weber, C. S., & Lynch, R. M. (2002b). *Regulation of secretory granule pH in insulin-secreting cells*. https://doi.org/10.1152/ajpcell

Tooze, S. A. (1998). Biogenesis of secretory granules in the trans-Golgi network of neuroendocrine and endocrine cells. *Biochimica et Biophysica Acta (BBA) - Molecular Cell Research*, *1404*(1), 231–244. https://doi.org/https://doi.org/10.1016/S0167-4889(98)00059-7

Tooze, S. A., & Huttner, W. B. (1990). Cell-Free Protein Sorting to the Regulated and Constitutive Secretory Pathways. In *Cell* (Vol. 60).

Tozluoğlu, M., Karaca, E., Nussinov, R., & Haliloğlu, T. (2010). A Mechanistic View of the Role of E3 in Sumoylation. *PLOS Computational Biology*, *6*(8), e1000913-. https://doi.org/10.1371/journal.pcbi.1000913

Trajkovic, K., Hsu, C., Chiantia, S., Rajendran, L., Wenzel, D., Wieland, F., Schwille, P., Brügger, B., & Simons, M. (2008). Ceramide Triggers Budding of Exosome Vesicles into Multivesicular Endosomes. *Science*, *319*(5867), 1244–1247. https://doi.org/10.1126/science.1153124

Tremel, S., Ohashi, Y., Morado, D. R., Bertram, J., Perisic, O., Brandt, L. T. L., von Wrisberg, M.-K., Chen, Z. A., Maslen, S. L., Kovtun, O., Skehel, M., Rappsilber, J., Lang, K., Munro, S., Briggs, J. A. G., & Williams, R. L. (2021). Structural basis for VPS34 kinase activation by Rab1 and Rab5 on membranes. *Nature Communications*, *12*(1), 1564. https://doi.org/10.1038/s41467-021-21695-2

Tsang, H. T. H., Connell, J. W., Brown, S. E., Thompson, A., Reid, E., & Sanderson, C. M. (2006). A systematic analysis of human CHMP protein interactions: Additional MIT domain-containing proteins bind to multiple components of the human ESCRT III complex. *Genomics*, *88*(3), 333–346. https://doi.org/https://doi.org/10.1016/j.ygeno.2006.04.003

Tu, Y., & Seaman, M. N. J. (2021). Navigating the Controversies of Retromer-Mediated Endosomal Protein Sorting. In *Frontiers in Cell and Developmental Biology* (Vol. 9). Frontiers Media S.A. https://doi.org/10.3389/fcell.2021.658741

Valadi, H., Ekström, K., Bossios, A., Sjöstrand, M., Lee, J. J., & Lötvall, J. O. (2007). Exosome-mediated transfer of mRNAs and microRNAs is a novel mechanism of genetic exchange between cells. *Nature Cell Biology*, *9*(6), 654–659. https://doi.org/10.1038/ncb1596

van Weering, J. R. T., Verkade, P., & Cullen, P. J. (2010). SNX–BAR proteins in phosphoinositide-mediated, tubular-based endosomal sorting. *Seminars in Cell & Developmental Biology*, *21*(4), 371–380. https://doi.org/https://doi.org/10.1016/j.semcdb.2009.11.009

van Niel, G., Bergam, P., Di Cicco, A., Hurbain, I., Lo Cicero, A., Dingli, F., Palmulli, R., Fort, C., Potier, M. C., Schurgers, L. J., Loew, D., Levy, D., & Raposo, G. (2015). Apolipoprotein E Regulates Amyloid Formation within Endosomes of Pigment Cells. *Cell Reports*, *13*(1), 43–51. https://doi.org/10.1016/j.celrep.2015.08.057

van Niel, G., Charrin, S., Simoes, S., Romao, M., Rochin, L., Saftig, P., Marks, M. S., Rubinstein, E., & Raposo, G. (2011). The Tetraspanin CD63 Regulates ESCRT-Independent and -Dependent Endosomal Sorting during Melanogenesis. *Developmental Cell*, *21*(4), 708–721. https://doi.org/10.1016/j.devcel.2011.08.019

Vazquez-Martinez, R., & Gasman, S. (2014). The regulated secretory pathway in neuroendocrine cells. In *Frontiers in Endocrinology* (Vol. 5, Issue APR). Frontiers Research Foundation. https://doi.org/10.3389/fendo.2014.00048

Venko, K., & Žerovnik, E. (2023). Protein Condensates and Protein Aggregates: In Vitro, in the Cell, and In Silico. *Frontiers in Bioscience-Landmark*, *28*(8), 183.

Villarroya-Beltri, C., Gutiérrez-Vázquez, C., Sánchez-Cabo, F., Pérez-Hernández, D., Vázquez, J., Martin-Cofreces, N., Martinez-Herrera, D. J., Pascual-Montano, A., Mittelbrunn, M., & Sánchez-Madrid, F. (2013). Sumoylated hnRNPA2B1 controls the sorting of miRNAs into exosomes through binding to specific motifs. *Nature Communications*, *4*(1), 2980. https://doi.org/10.1038/ncomms3980

Viñas, J. L., Spence, M., Gutsol, A., Knoll, W., Burger, D., Zimpelmann, J., Allan, D. S., & Burns, K. D. (2018). Receptor-Ligand Interaction Mediates Targeting of Endothelial Colony Forming Cell-derived Exosomes to the Kidney after Ischemic Injury. *Scientific Reports*, *8*(1), 16320. https://doi.org/10.1038/s41598-018-34557-7

Wang, H., Lallemang, M., Hermann, B., Wallin, C., Loch, R., Blanc, A., Balzer, B. N., Hugel, T., & Luo, J. (2021). ATP Impedes the Inhibitory Effect of Hsp90 on Aβ40 Fibrillation. *Journal of Molecular Biology*, *433*(2), 166717. https://doi.org/https://doi.org/10.1016/j.jmb.2020.11.016

Wang, Q., & Lu, Q. (2017). Plasma membrane-derived extracellular microvesicles mediate non-canonical intercellular NOTCH signaling. *Nature Communications*, *8*(1), 709. https://doi.org/10.1038/s41467-017-00767-2

Wang, Y., Thiele1, C., & Huttner, W. B. (2000). Cholesterol is Required for the Formation of Regulated and Constitutive Secretory Vesicles from the trans-Golgi Network. *Traffic*, *1*(12), 952–962. https://doi.org/https://doi.org/10.1034/j.1600-0854.2000.011205.x

Wei, D., Zhan, W., Gao, Y., Huang, L., Gong, R., Wang, W., Zhang, R., Wu, Y., Gao, S., & Kang, T. (2021). RAB31 marks and controls an ESCRT-independent exosome pathway. *Cell Research*, *31*(2), 157–177. https://doi.org/10.1038/s41422-020-00409-1

Wei, Y., Chiang, W.-C., Sumpter Jr., R., Mishra, P., & Levine, B. (2017). Prohibitin 2 Is an Inner Mitochondrial Membrane Mitophagy Receptor. *Cell*, *168*(1), 224-238.e10. https://doi.org/10.1016/j.cell.2016.11.042

Weigert, R., Yeung, A. C., Li, J., & Donaldson, J. G. (2004). Rab22a Regulates the Recycling of Membrane Proteins Internalized Independently of Clathrin. *Molecular Biology of the Cell*, *15*(8), 3758–3770. https://doi.org/10.1091/mbc.e04-04-0342

Wells, A., Mendes, C. C., Castellanos, F., Mountain, P., Wright, T., Wainwright, S. M., Stefana, M. I., Harris, A. L., Goberdhan, D. C. I., & Wilson, C. (2023). A Rab6 to Rab11 transition is required for dense-core granule and exosome biogenesis in Drosophila secondary cells. *PLOS Genetics*, *19*(10), e1010979-. https://doi.org/10.1371/journal.pgen.1010979

Wells, A., Yates, C., & Shepard, C. R. (2008). E-cadherin as an indicator of mesenchymal to epithelial reverting transitions during the metastatic seeding of disseminated carcinomas. *Clinical & Experimental Metastasis*, *25*(6), 621–628. https://doi.org/10.1007/s10585-008-9167-1

Wells, C., Brennan, S., Keon, M., & Ooi, L. (2021). The role of amyloid oligomers in neurodegenerative pathologies. *International Journal of Biological Macromolecules*, *181*, 582–604. https://doi.org/https://doi.org/10.1016/j.ijbiomac.2021.03.113

Welsh, J. A., Goberdhan, D. C. I., O'Driscoll, L., Buzas, E. I., Blenkiron, C., Bussolati, B., Cai, H., Di Vizio, D., Driedonks, T. A. P., Erdbrügger, U., Falcon-Perez, J. M., Fu, Q.-L., Hill, A. F., Lenassi, M., Lim, S. K., Mahoney, M. G., Mohanty, S., Möller, A., Nieuwland, R., … Witwer, K. W. (2024). Minimal information for studies of extracellular vesicles

(MISEV2023): From basic to advanced approaches. *Journal of Extracellular Vesicles*, *13*(2), e12404. https://doi.org/https://doi.org/10.1002/jev2.12404

Wen G, Pang H, Wu X, Jiang E, Zhang X, & Zhan X. (2021). Proteomic characterization of secretory granules in dopaminergic neurons indicates chromogranin/secretogranin-mediated protein processing impairment in Parkinson's disease. *Aging*, *13*(16), 20335–20358.

Wen, Z., Mai, Z., Zhu, X., Wu, T., Chen, Y., Geng, D., & Wang, J. (2020). Mesenchymal stem cell-derived exosomes ameliorate cardiomyocyte apoptosis in hypoxic conditions through microRNA144 by targeting the PTEN/AKT pathway. *Stem Cell Research & Therapy*, *11*(1), 36. https://doi.org/10.1186/s13287-020-1563-8

White, J., Johannes, L., Mallard, F., Girod, A., Grill, S., Reinsch, S., Keller, P., Tzschaschel, B., Echard, A., Goud, B., & Stelzer, E. H. K. (1999). Rab6 Coordinates a Novel Golgi to ER Retrograde Transport Pathway in Live Cells 7. In *The Journal of Cell Biology* (Vol. 147, Issue 4). http://www.jcb.org

Willms, E., Johansson, H. J., Mäger, I., Lee, Y., Blomberg, K. E. M., Sadik, M., Alaarg, A., Smith, C. I. E., Lehtiö, J., EL Andaloussi, S., Wood, M. J. A., & Vader, P. (2016). Cells release subpopulations of exosomes with distinct molecular and biological properties. *Scientific Reports*, *6*(1), 22519. https://doi.org/10.1038/srep22519

Wilson, C., Leiblich, A., Goberdhan, D. C. I., & Hamdy, F. (2017). Chapter Eleven - The Drosophila Accessory Gland as a Model for Prostate Cancer and Other Pathologies. In L. Pick (Ed.), *Current Topics in Developmental Biology* (Vol. 121, pp. 339–375). Academic Press. https://doi.org/https://doi.org/10.1016/bs.ctdb.2016.06.001

Winkler, H., & Westhead, E. (1980). Th molecular organization of adrenal chromaffin granules. *Neuroscience*, *5*(11), 1803–1823. https://doi.org/https://doi.org/10.1016/0306-4522(80)90031-7

Wolfner, M. F. (1997). Tokens of love: Functions and regulation of drosophila male accessory gland products. *Insect Biochemistry and Molecular Biology*, *27*(3), 179–192. https://doi.org/https://doi.org/10.1016/S0965-1748(96)00084-7

Wörthmüller, J., & Rüegg, C. (2021). MAGI1, a Scaffold Protein with Tumor Suppressive and Vascular Functions. *Cells*, *10*(6). https://doi.org/10.3390/cells10061494

Wu, B., & Guo, W. (2015). The Exocyst at a Glance. *Journal of Cell Science*, *128*(16), 2957–2964. https://doi.org/10.1242/jcs.156398

Wu, J., Petralia, R. S., Kurushima, H., Patel, H., Jung, M., Volk, L., Chowdhury, S., Shepherd, J. D., Dehoff, M., Li, Y., Kuhl, D., Huganir, R. L., Price, D. L., Scannevin, R., Troncoso, J. C., Wong, P. C., & Worley, P. F. (2011). Arc/Arg3.1 Regulates an Endosomal Pathway Essential for Activity-Dependent β-Amyloid Generation. *Cell*, *147*(3), 615–628. https://doi.org/10.1016/j.cell.2011.09.036

Wu, M. M., Grabe, M., Adams, S., Tsien, R. Y., Moore, H.-P. H., & Machen, T. E. (2001). Mechanisms of pH Regulation in the Regulated Secretory Pathway *. *Journal of Biological Chemistry*, *276*(35), 33027–33035. https://doi.org/10.1074/jbc.M103917200

Wu, S., Mehta, S. Q., Pichaud, F., Bellen, H. J., & Quiocho, F. A. (2005). Sec15 interacts with Rab11 via a novel domain and affects Rab11 localization in vivo. *Nature Structural & Molecular Biology*, *12*(10), 879–885. https://doi.org/10.1038/nsmb987

Wunderley, L., Zhang, L., Yarwood, R., Qin, W., Lowe, M., & Woodman, P. (2021). Endosomal recycling tubule scission and integrin recycling involve the membrane curvature-

supporting protein LITAF. *Journal of Cell Science*, *134*(15), jcs258549. https://doi.org/10.1242/jcs.258549

Xiao, T., Zhang, W., Jiao, B., Pan, C.-Z., Liu, X., & Shen, L. (2017). The role of exosomes in the pathogenesis of Alzheimer' disease. *Translational Neurodegeneration*, *6*(1), 3. https://doi.org/10.1186/s40035-017-0072-x

Xie, S., Zhang, Q., & Jiang, L. (2022). Current Knowledge on Exosome Biogenesis, Cargo-Sorting Mechanism and Therapeutic Implications. *Membranes*, *12*(5). https://doi.org/10.3390/membranes12050498

Xu, H., Jia, Z., Ma, K., Zhang, J., Dai, C., Yao, Z., Deng, W., Su, J., Wang, R., & Chen, X. (2020). Protective effect of BMSCs-derived exosomes mediated by BDNF on TBI via miR-216a-5p. *Medical Science Monitor*, *26*, 0. https://doi.org/https://dx.doi.org/10.12659/MSM.920855

Xu, J., Zhang, L., Ye, Y., Shan, Y., Wan, C., Wang, J., Pei, D., Shu, X., & Liu, J. (2017). SNX16 Regulates the Recycling of E-Cadherin through a Unique Mechanism of Coordinated Membrane and Cargo Binding. *Structure*, *25*(8), 1251-1263.e5. https://doi.org/https://doi.org/10.1016/j.str.2017.06.015

Xu, R.-G., Wang, X., Shen, D., Sun, J., Qiao, H.-H., Wang, F., Liu, L.-P., & Ni, J.-Q. (2019). Perspectives on gene expression regulation techniques in Drosophila. *Journal of Genetics and Genomics*, *46*(4), 213–220. https://doi.org/https://doi.org/10.1016/j.jgg.2019.03.006

Yan, C., & Theodorescu, D. (2018). RAL GTPases: Biology and Potential as Therapeutic Targets in Cancer. *Pharmacological Reviews*, *70*(1), 1. https://doi.org/10.1124/pr.117.014415

Yang, X., Zhang, Y., Zhang, Y., Zhang, S., Qiu, L., Zhuang, Z., Wei, M., Deng, X., Wang, Z., & Han, J. (2021). The Key Role of Exosomes on the Pre-metastatic Niche Formation in

Tumors. In *Frontiers in Molecular Biosciences* (Vol. 8). Frontiers Media S.A. https://doi.org/10.3389/fmolb.2021.703640

Yoon, J. H., Ashktorab, H., Smoot, D. T., Nam, S. W., Hur, H., & Park, W. S. (2020). Uptake and tumor-suppressive pathways of exosome-associated GKN1 protein in gastric epithelial cells. *Gastric Cancer*, *23*(5), 848–862. https://doi.org/10.1007/s10120-020-01068-2

Yu, J., Feng, H., Sang, Q., Li, F., Chen, M., Yu, B., Xu, Z., Pan, T., Wu, X., Hou, J., Zhu, Z., Yan, C., Su, L., Li, J., & Liu, B. (2023). VPS35 promotes cell proliferation via EGFR recycling and enhances EGFR inhibitors response in gastric cancer. *EBioMedicine*, *89*. https://doi.org/10.1016/j.ebiom.2023.104451

Yuan, X., Qian, N., Ling, S., Li, Y., Sun, W., Li, J., Du, R., Zhong, G., Liu, C., Yu, G., Cao, D., Liu, Z., Wang, Y., Qi, Z., Yao, Y., Wang, F., Liu, J., Hao, S., Jin, X., … Li, Y. (2021). Breast cancer exosomes contribute to pre-metastatic niche formation and promote bone metastasis of tumor cells. *Theranostics*, *11*(3), 1429–1445. https://doi.org/10.7150/thno.45351

Zhang, C., Dhanvantari, S., Lou, H., & Loh, Y. P. (2003). Sorting of carboxypeptidase E to the regulated secretory pathway requires interaction of its transmembrane domain with lipid rafts. *The Biochemical Journal*, *369 Pt 3*, 453–460. https://api.semanticscholar.org/CorpusID:9343287

Zhang, J., Pavlova, N. N., & Thompson, C. B. (2017). Cancer cell metabolism: the essential role of the nonessential amino acid, glutamine. *The EMBO Journal*, *36*(10), 1302-1315–1315. https://doi.org/https://doi.org/10.15252/embj.201696151

Zhang, X., Li, Y., Xu, H., & Zhang, Y. W. (2014). The γ-secretase complex: From structure to function. In *Frontiers in Cellular Neuroscience* (Vol. 8, Issue DEC). Frontiers Media S.A. https://doi.org/10.3389/fncel.2014.00427

Zhang, X.-M., Ellis, S., Sriratana, A., Mitchell, C. A., & Rowe, T. (2004). Sec15 Is an Effector for the Rab11 GTPase in Mammalian Cells *. *Journal of Biological Chemistry*, *279*(41), 43027–43034. https://doi.org/10.1074/jbc.M402264200

Zhang, Y.-L., Wang, R.-C., Cheng, K., Ring, B. Z., & Su, L. (2017). Roles of Rap1 signaling in tumor cell migration and invasion. *Cancer Biology & Medicine*, *14*(1), 90–99. https://doi.org/10.20892/j.issn.2095-3941.2016.0086

Zhang, Z., Zou, Y., Song, C., Cao, K., Cai, K., Chen, S., Wu, Y., Geng, D., Sun, G., Zhang, N., Zhang, X., Zhang, Y., Sun, Y., & Zhang, Y. (2023). Advances in the study of exosomes in cardiovascular diseases. *Journal of Advanced Research*. https://doi.org/https://doi.org/10.1016/j.jare.2023.12.014

Zheng, H., Guan, S., Wang, X., Zhao, J., Gao, M., & Zhang, X. (2020). Deconstruction of Heterogeneity of Size-Dependent Exosome Subpopulations from Human Urine by Profiling N-Glycoproteomics and Phosphoproteomics Simultaneously. *Analytical Chemistry*, *92*(13), 9239–9246. https://doi.org/10.1021/acs.analchem.0c01572

Zheng, H., & Koo, E. H. (2011). Biology and pathophysiology of the amyloid precursor protein. *Molecular Neurodegeneration*, *6*(1), 27. https://doi.org/10.1186/1750-1326-6-27

Zheng, X., Liu, J., Li, X., Tian, R., Shang, K., Dong, X., & Cao, B. (2021). Angiogenesis is promoted by exosomal DPP4 derived from 5-fluorouracil-resistant colon cancer cells. *Cancer Letters*, *497*, 190–201. https://doi.org/https://doi.org/10.1016/j.canlet.2020.10.009

Zheng, Y., Tu, C., Zhang, J., & Wang, J. (2019). Inhibition of multiple myeloma-derived exosomes uptake suppresses the functional response in bone marrow stromal cell. *International Journal of Oncology*, *54*(3), 1061–1070. https://doi.org/10.3892/ijo.2019.4685

Zhenlan, Y., Yunsheng, Q., Xiaofang, L., Jieliang, C., Jiahui, D., Lu, B., Fang, S., Bisheng, S., Jia, L., Lu, P., Jianhua, L., & Zhenghong, Y. (2018). Exosomes Exploit the Virus Entry Machinery and Pathway To Transmit Alpha Interferon-Induced Antiviral Activity. *Journal of Virology*, *92*(24), 10.1128/jvi.01578-18. https://doi.org/10.1128/jvi.01578-18

Zhou, Q., Qi, F., Zhou, C., Ji, J., Jiang, J., Wang, C., Zhao, Q., Jin, Y., Wu, J., Cai, Q., Tian, H., & Zhang, J. (2023). VPS35 promotes gastric cancer progression through integrin/FAK/SRC signalling-mediated IL-6/STAT3 pathway activation in a YAP-dependent manner. *Oncogene*. https://doi.org/10.1038/s41388-023-02885-2

Zhou, Z., Ai, H., Li, K., Yao, X., Zhu, W., Liu, L., Yu, C., Song, Z., Bao, Y., Huang, Y., Wu, Y., Zheng, L., Sun, Y., Wang, G., Ma, K., Sun, L., & Li, Y. (2018). Prohibitin 2 localizes in nucleolus to regulate ribosomal RNA transcription and facilitate cell proliferation in RD cells. *Scientific Reports*, *8*(1), 1479. https://doi.org/10.1038/s41598-018-19917-7

Zitvogel, L., Regnault, A., Lozier, A., Wolfers, J., Flament, C., Tenza, D., Ricciardi-Castagnoli, P., Raposo, G., & Amigorena, S. (1998). Eradication of established murine tumors using a novel cell-free vaccine: dendritic cell derived exosomes. *Nature Medicine*, *4*(5), 594–600. https://doi.org/10.1038/nm0598-594

Zou, J., Peng, H., & Liu, Y. (2021). The Roles of Exosomes in Immunoregulation and Autoimmune Thyroid Diseases. In *Frontiers in Immunology* (Vol. 12). Frontiers Media S.A. https://doi.org/10.3389/fimmu.2021.757674

Zuehlke, A. D., Beebe, K., Neckers, L., & Prince, T. (2015). Regulation and function of the human HSP90AA1 gene. *Gene*, *570*(1), 8–16. https://doi.org/https://doi.org/10.1016/j.gene.2015.06.018

Zulkefli, K. L., Houghton, F. J., Gosavi, P., & Gleeson, P. A. (2019). A role for Rab11 in the homeostasis of the endosome-lysosomal pathway. *Experimental Cell Research*, *380*(1), 55–68. https://doi.org/10.1016/j.yexcr.2019.04.010